CRYSTALLIZATION AND THERMO-VISCOELASTIC MODELLING OF POLYMER COMPOSITES

by

Kamyar Gordnian

B.Sc. (Mechanical Engineering), Sharif University of Technology, 1999

M.Sc. (Mechanical Engineering), Sharif University of Technology, 2002

A THESIS SUBMITTED IN PARTIAL FULFILLMENT OF

THE REQUIREMENTS FOR THE DEGREE OF

DOCTOR OF PHILOSOPHY

in

THE FACULTY OF GRADUATE AND POSTDOCTORAL STUDIES

(Materials Engineering)

THE UNIVERSITY OF BRITISH COLUMBIA

(Vancouver)

October 2017

Abstract

Process models of composite materials are useful tools for understanding the effect of process parameters and variables on the final part and reducing manufacturing risks and costs. Sub-model approach for process modelling has been developed and used for processing of thermoset composites since the early 1980s. In this approach analysis is performed in different sub-models such as thermochemical, flow, void and stress, and the analysis results from one sub-model are sequentially transferred to another sub-model, until the analysis is complete. In recent years there has been growing interest in using high performance thermoplastics such as PEEK and PEKK in aircraft structures.

During processing of thermoplastic materials, the material undergoes melting and crystallization, based on the temperature cycle. Therefore a major component of the thermochemical/thermophysical sub-model for process modelling of thermoplastics is the crystallization kinetics/melt kinetics model. Most of the crystallization kinetics models in the literature are valid for constant temperatures or cooling at constant cooling rates. The number of melt kinetics models are very limited and their application is restricted to small heating rates. As a material point in the part may undergo complex temperature cycles, having a rate-type crystallization/melt kinetics model which is independent of the temperature cycle is desired.

Another problem in processing of composites is development of residual stresses and shape distortions in the final part. The stresses and distortions are analyzed in the stress sub-model using the constitutive model for mechanical response. Different constitutive models are available in the literature including thermo-elastic, CHILE and viscoelastic. Most thermoplastic materials such as

PEEK are viscoelastic, however their unrelaxed values of moduli are temperature dependent, or their behaviour is ‘thermo-rheologically complex’.

In this thesis the crystallization and melt behaviour of PEEK carbon fibre composites is investigated using different DSC experiments. A rate type crystallization kinetics model is developed for prediction of degree of crystallinity during crystallization process. A concept of ‘master melt curve’ is introduced and is used along with the crystallization kinetics model for prediction of crystallinity change during an arbitrary process.

Thermo-viscoelastic behaviour of the material is studied using DMA experiments. A thermo-viscoelastic (TVE) constitutive model is developed and is generalized to three dimensional cases for analyzing the stress and deformation response of the material. Some case studies are analyzed and validity of both crystallization/melt kinetics and TVE models are investigated.

Lay Summary

Planes and cars must work in demanding environments; needing to be lightweight and strong. Traditionally, the only materials which can survive under these conditions have been metals, like aluminum. Newer materials called ‘fibre reinforced polymers’ use strong fibres and glue to offer comparable strength and lighter weight. This glue is rigid at room temperature but runny, like honey, when very hot. When heating, the transition between hard and soft is complex and insufficiently understood.

A prohibitively expensive strategy for working within this complexity is to make many parts and testing and breaking them to see which condition made the strongest part. A better strategy is to use computers to create virtual parts and see which condition results in the best part. The difficulty, and goal of this thesis, is to give the computer the right set of mathematics and properties so that the virtual parts behave like real world parts.

Preface

All experiments, explained in Chapter 3 and Chapter 4 of this thesis were designed and performed by Kamyar Gordnian at the Composites Research Network lab at The University of British Columbia, Vancouver. All experimental results were analyzed by Kamyar Gordnian under the supervision of Dr. Anoush Poursartip. Crystallization and melt kinetics model in Chapter 3 were developed by Kamyar Gordnian, under supervision of Dr. Anoush Poursartip. The thermo-viscoelastic model in Chapter 4 was developed by Kamyar Gordnian, under supervision of Dr. Anoush Poursartip and Dr. Reza Vaziri. Both crystallization/melt kinetics models and thermo-viscoelastic model were implemented in process modelling packages RAVEN and COMPRO CCA by Convergent Manufacturing Technologies. Figure 5-1, Figure 5-2, Figure 5-3, Figure 5-4, Figure 5-5, data for Figure 5-6, data for Figure 5-21, experimental data for Figure 5-25, experimental data for Figure 5-26, data for Table 5-1 and data for Table 5-2 were provided by a previous M.A.Sc. student, Mr. Gabriel Fortin. The experiments for this case study were performed by Mr. Gabriel Fortin at the Composites Research Network lab at The University of British Columbia, Vancouver. The experimental work for case study 2 (AFP) in Chapter 5 was performed at the Aerospace Manufacturing Technologies Centre, National Research Council Canada, Montreal, and data was provided by Dr. Ali Yousefpour. All simulation work for the case studies in Chapter 5 was conducted by Kamyar Gordnian.

A version of Chapter 3 was presented at the 20th International Conference on Composite Materials, Copenhagen, 2015. A paper was published in the conference proceedings. **Gordnian, K.** and Poursartip, A. "A rate-type crystallization kinetics model for process modelling of PEEK

matrix composites," in *20th International Conference on Composites Materials*, Copenhagen, 2015. All parts of the paper were written by Kamyar Gordnian under supervision of Dr. Anoush Poursartip.

A version of Chapter 3 was presented at the SAMPE Conference, Seattle, 2017. A paper was published in the conference proceedings. **Gordnian, K.**, Vaziri, R. and Poursartip, A. "Crystallization and melt kinetics for process modelling of PEEK matrix composites," in *SAMPE Conference*, Seattle, 2017. All parts of the paper were written by Kamyar Gordnian under supervision of Dr. Anoush Poursartip and Dr. Reza Vaziri.

Table of Contents

List of Tables

List of Figures

List of Symbols

X_{vc}	Volume fraction of crystallinity
X_{∞}	Equilibrium (final) volume fraction of crystallinity
k	Kinetics constant
n	Avrami exponent
a	Cooling rate (Ozawa model)
$\chi_C(T)$	Cooling rate function (Ozawa model)
m	Ozawa exponent
X_f	Degree of melting
X_{vci}	Initial degree of crystallinity
K_0	Pre-exponential factor (Arrhenius equation)
E_a	Activation energy (Arrhenius equation)
R	Universal gas constant (Arrhenius equation)
C_p	Heat Capacity
$E(T)$	Temperature dependent modulus
$\epsilon^T(T)$	Thermal expansion/shrinkage strain
$\Delta\theta$	Spring-in angle
θ	Original angle
CTE_R	Radial coefficient of thermal expansion
CTE_θ	Circumferential coefficient of thermal expansion
α	Degree of cure
$E(T,\alpha)$	Instantaneous modulus of the material

$D(t)$	Creep compliance
$E(t)$	Relaxation modulus
τ	Relaxation time
ξ	Reduced time
a_T	Horizontal shift factor
$D_I(T)$	Initial value of creep compliance
a_G	Vertical shift factor for creep compliance
$\frac{dH}{dt}$	Heat flow rate
X_{mc}	Mass fraction crystallinity
H_f^0	Theoretical heat of fusion of 100 % crystallized material
X_{mr}	Mass fraction of the reinforcing phase
ρ_c	Density of the crystalline phase
ρ_a	Density of the amorphous phase
X	Volume fraction crystallinity (or crystallinity)
T_m^0	Equilibrium melting temperature
$\frac{dX}{dt}$	Crystallization rate
$k(T)$	Temperature dependence of crystallization rate
$f(X)$	Crystallinity dependence of crystallization rate
T_g	Glass transition temperature
k_0	Pre-exponential factor for temperature dependence of crystallization rate

$-\frac{E_g(X)}{R}$	Model parameter for temperature dependence of crystallization rate
$-\frac{E_m(X)}{R}$	Model parameter for temperature dependence of crystallization rate
a_g	Model constant for temperature dependence of crystallization rate
b_g	Model constant for temperature dependence of crystallization rate
c_g	Model constant for temperature dependence of crystallization rate
a_m	Model constant for temperature dependence of crystallization rate
b_m	Model constant for temperature dependence of crystallization rate
c_m	Model constant for temperature dependence of crystallization rate
t_i	Induction time for isothermal crystallization
t_m	Model constant for induction time model
c	Model constant for induction time model
t_I	Induction time for non-isothermal crystallization
X_{max}	Maximum degree of crystallinity
ΔX_c	Increment in degree of crystallinity due to crystallization
ΔX_m	Increment in degree of crystallinity due to melting
ΔX	Total increment in degree of crystallinity
$\dot{T}$	Heating rate
E_2	Modulus in transverse direction
E^u	Unrelaxed modulus
a_F	Vertical shift factor for relaxation modulus
E^N	Normalized modulus

T_{ref}	Reference temperature for master curve
E_e	Relaxed modulus
E_i	Prony constants
τ_i	Relaxation times
q_i	States variables
α	Coefficient of thermal expansion
β	Magnitude of thermal stress due to a unit change in temperature in a constrained body
α^{cs}	Coefficient of cure/crystallization expansion
γ	Stress due to a unit change in degree of cure/crystallinity in a constrained body
P	Constant force applied to the beam sample
L	Beam length
b	Beam width
h	Beam cross section height
δ	Mid-beam deflection
I	Second moment of inertia for beam cross section

List of Abbreviations

PEEK	Poly ether ether ketone
PEKK	Poly ether ketone ketone
CHILE	Cure Hardening Instantaneously Linear Elastic
TVE	Thermo-viscoelastic
DMA	Dynamic Mechanical Analysis
DSC	Differential Scanning Calorimetry
GMM	Generalized Maxwell Model
GKM	Generalized Kelvin Model
DF	Differential form
1D	One dimensional
3D	Three dimensional
TSM	Thermo-rheologically simple material
TCM	Thermo-rheologically complex material
TCM-1	Thermo-rheologically complex material, class 1
TCM-2	Thermo-rheologically complex material, class 2
UMAT	User material subroutine
CTE	Coefficient of thermal expansion
TTT	Time-Temperature-Transformation
AFP	Automatic fibre placement
WAXS	Wide Angle X-ray Scattering

Acknowledgements

I would like to acknowledge my supervisors, Dr. Anoush Poursartip and Dr. Reza Vaziri for their help, insight and guidance during the course of my PhD.

Special thanks to past and present members of UBC Composites Group and Composites Research Network for their friendship and help. Especially I would like to thank Dr. Navid Zobeiry, Dr. Alireza Forghani, Dr. Mehdi Haghshenas, Dr. Leila Farhang, Dr. Sardar Malek, Mr. Roger Bennett, Ms. Suzana Topic, Mr. Gabriel Fortin, Dr. Christophe Mobuchon, Dr. Casey Keulen, Dr. Mina Shahbazi, Dr. Sina Amini Niaki, Mr. Andrew Stewart, Ms. Chao Li, Ms. Janna Fabris, Mr. Marty Roy, Mr. Kyle Farnand and Dr. Sanjukta Chatterjee. I also would like to appreciate all the help from Dr. Anthony Floyd, the late Corey Lynam and Mr. Alastair McKee of Convergent Manufacturing Technologies and Dr. Ali Yousefpour of National Research Council Canada.

Special thanks to my friends Ms. Maryam Zamani, Dr. Houshin Nejati, Mr. Amir Mahmoudi and Dr. Shayesteh Haghdan for their kindness and support.

Last but not least, I would like thank my mother Mahin, my father Mansour, my brother Keyvan and my sisters Katayoun and Shahrzad for their love and affection.

Dedication

To my parents.

Chapter 1: Introduction and Background

1.1 Process modelling of composite materials

Polymeric composite materials are generally categorized into thermoset and thermoplastic composites. Thermoplastic composites have fast processing cycles, can be formed/reformed by application of heat and pressure and are resistant to environmental conditions. Their common applications include bridges, railroad ties and automotive parts. Most composite materials used in the aerospace industry are thermoset composites, however, thermoplastic composites have been used for aircraft interior structures such as pressure bulkheads. Other aerospace applications of thermoplastic composites are the undercarriage door of the Fokker 50 and the fixed wing leading edges of the Airbus A340 and A380. In recent years, there has been a growing interest to produce primary aircraft structures, such as fuselage panels, from thermoplastic composites.

How well the processed part meets the design conditions, dimensional fidelity, is an important issue in the processing of composite materials. Processing of composites involves complex physical phenomena such as heat transfer, resin cure or crystallization, resin flow and stress development. For both thermoset and thermoplastic composites, the cured or crystallized component has different dimensions at room temperature from the tool it was processed on. The main drivers for these deviations are differences between thermal expansion coefficients of the tool and part, anisotropic thermal expansion (and contraction) and cure/crystallization shrinkage of composite part, tool-part interaction, and non-uniform temperature and cure/crystallization distributions in the composite part. A non-uniform distribution of temperature and degree of cure/crystallization leads to inhomogeneous mechanical properties in the part which in turn results

in residual stresses and dimensional changes. Residual stresses can further cause cracks and failure in the product.

It is always desirable to have control on dimensions and residual stresses of the product during the process. Unsuccessful dimensional control leads to problems during assembly, especially for complex geometries and large components, which in turn leads to extra cost and time. Dimensional deviations can be controlled by controlling each of the drivers. Another approach is to change the tool geometry so that the final product after the dimensional deviations meets the designed conditions.

The traditional approach for managing these issues was making a tool, processing the part with some pre-assumed process parameters (based on experience), measuring the dimensional deviations of the part after the tool removal at room temperature and then modifying the tool and process parameters and repeating this (trial and error) to achieve the desired product. The main disadvantage of this approach is that one cannot understand the important parameters that control the deformations and therefore it is not possible to ensure that the optimum process conditions are achieved. On the other hand, if the product is large size, it is not possible (cost-wise and time-wise) to do the trial and error process with the real scale part and therefore a small scale prototype is made. The problem with this small scale prototype methodology is the uncertainty concerning valid representation of the final product and process conditions.

According to the aforementioned discussions it is highly advantageous to have process modelling packages to establish the required process parameters virtually. Process models help us understand qualitatively and quantitatively the effects of the process variables and parameters on the dimensional changes and residual stresses of the final product. Therefore the number of trial and

error tests will be reduced significantly, optimum process conditions are ensured and consequently production risks and costs are minimized.

Loos and Springer [1] introduced a sub-model approach for process modelling of thermoset composites. Their analysis consists of thermochemical, flow, void and stress sub-models. Each of these sub-models calculates some of the process state variables such as temperature, degree of cure and viscosity, pressure and resin flow, void size and residual stresses. The analysis results are sequentially passed from one sub-model to another, until the analysis is complete.

The core component of the thermochemical sub-model for thermoset composites is the cure kinetics model. The energy equation (heat transfer equation), is coupled with the cure kinetics model, as the heat source, and is solved within the thermochemical sub-model and the degree of cure history and temperature history during the process is predicted. The thermochemical sub-model can be used as a user material subroutine with a commercial finite element code for prediction of temperature and degree of cure distribution and history, throughout the composite part, during the process.

This sub-model approach for process modelling can be used for processing of thermoplastic composites as well [2]. For thermoplastic composites, the main component of the thermochemical/thermophysical module is the crystallization kinetics/melt kinetics model. These models are used for heat transfer analysis and prediction of temperature and degree of crystallinity history, throughout the thermoplastic composite part, during the process.

Mechanical response constitutive models are used in the stress sub-model for prediction of process distortions and residual stresses. Different generations of constitutive models have been used for process modelling of composite materials. These models will be reviewed in Chapter 2.

The focus of this research is on the further development of the available process modelling approach for both thermoplastics and thermoset composites. The scope and research objectives are explained at the end of Chapter 2.

Chapter 2: Literature Review and Research Objectives

As explained in Chapter 1, in the sub-model approach for process modelling, different sub-models such as thermochemical, flow, void formation and stress exist and the results from one sub-model are sequentially passed to the next sub-model, until the process simulation is complete.

For thermoset composites, the main component of the thermochemical sub-model is the cure kinetics model. For thermoplastic composites, chemical reactions do not occur in the material during the process. Therefore, it is more relevant to use the name thermo-physical for this sub-model. The main components of the thermo-physical sub-model for thermoplastics composites are the crystallization kinetics and the melt kinetics models.

In the stress sub-model, stress and strain components are related by means of the mechanical constitutive model. Different mechanical constitutive models have been used for process modelling of composites.

In this chapter we review crystallization and melting of polymers. Some of the available models are also introduced and reviewed. The constitutive models for mechanical response used for process modelling are also briefly reviewed in this chapter.

2.1 Crystallization kinetics

Polymer crystallization has been a subject of interest to polymer physicists for many years. Many polymers, when cooled down from molten state, form a semi-crystalline spherulitic microstructure. In this section the morphology of semi-crystalline polymers and also overall crystallization kinetics theories are briefly reviewed.

2.1.1 Semi-crystalline polymers

In some polymers, molecular chains can pack together and form crystalline structures. Experimental results show that polymers are only partially crystallized and crystalline and amorphous regions coexist in the material. For example, the measured density of the material is intermediate between the density of the crystal and that of the amorphous phase. The first proposed model for explaining the semi-crystalline structure was the ‘fringed-micelle’ model [3], as shown schematically in Figure 2-1.

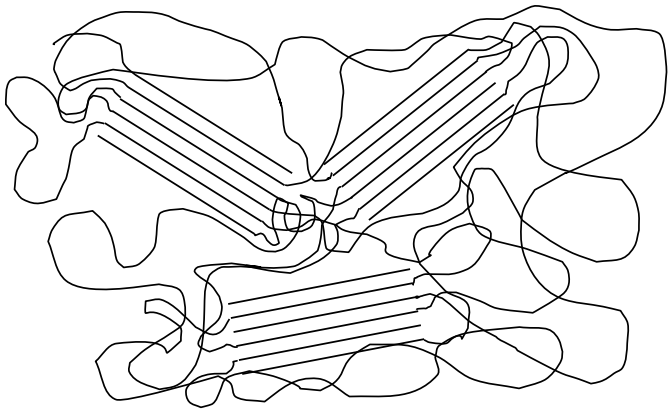

Figure 2-1 Fringed-micelle model for semi-crystalline polymers

In Figure 2-1, the regions which are schematically shown as parallel lines are the crystalline regions. As shown in Figure 2-1, one molecular chain can pass through several crystalline and amorphous regions.

As the fringed-micelle model failed in explaining the very thin platelet form of polymer single crystals, the ‘chain-folding’ model was introduced by Keller [4]. In the chain-folding model as shown schematically in Figure 2-2, a single molecular chain enters and exits the same crystal many times by folding regularly on the crystal base surface and it is normal to the crystal surface. Such a crystalline structure was termed chain-folded lamellar crystal.

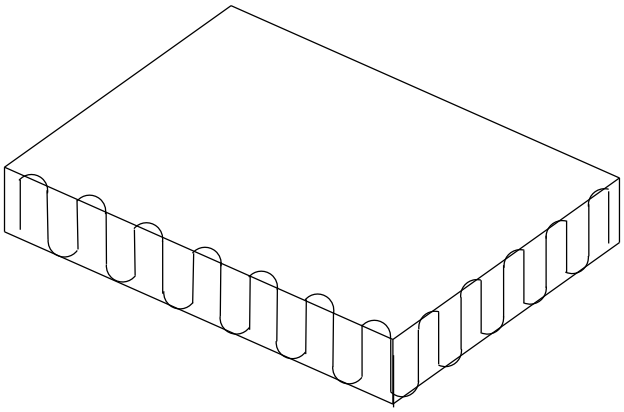

Figure 2-2 Schematic of chain-folded lamellar structure

The existence of lamellar structure was also reported by Palmer [5] with a less regular chain folding format. Lamellar structures are parts of larger crystalline structures, known as the spherulites. Arrays of lamellar structures act as the radii of each spherulite. A schematic of the spherulite is shown in Figure 2-3.

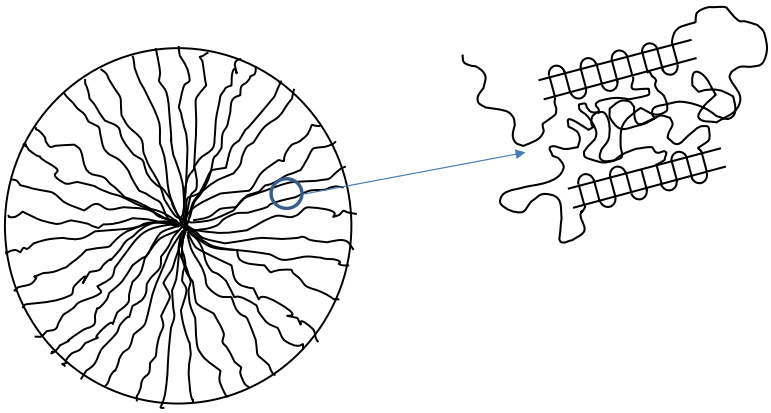

Figure 2-3 Schematic of spherulite

During the crystallization process under isothermal conditions, the radii of the spherulites increase with time. Finally the spherulites impinge on one another and form spherulites boundaries. Amorphous regions exist in the intermediate spaces between lamellar structures.

2.1.2 Crystallization kinetics models

The crystallization kinetics of polymers is typically studied as isothermal crystallization or non-isothermal crystallization separately.

Isothermal crystallization kinetics of semi-crystalline polymers is generally investigated using Avrami [6]-[8] and Evans' [9] models. Although Avrami's model is based on the concept of the so-called 'extended volume' and Evans' model is derived from probability theory, both approaches are identical.

According to Avrami

$$X_{vc} = X_{\infty}\left[1 - e^{-kt^{n}}\right] \qquad \textbf{(2-1)}$$

In Equation (2-1), X_{vc} is the volume fraction of crystallinity, X_{∞} is the equilibrium (final) volume fraction of crystallinity, k is the kinetics constant, n is the Avrami exponent and t is the crystallization time. Equation (2-1) is also known as Johnston-Mehl-Avrami-Kolmogorov

(JMAK) and has been used for studying isothermal crystallization and recrystallization of metals [10], [11]. This model can be expressed in differential form as

$$\frac{d(X_{vc}/X_{\infty})}{dt} = nk^{1/n}(1 - X_{vc}/X_{\infty})[\ln(1/(1 - X_{vc}/X_{\infty}))]^{(n-1)/n} \quad \textbf{(2-2)}$$

Most crystallization kinetics models for non-isothermal crystallization are extensions of Avrami's or Evans' model [12]. As an example, Ozawa [13] proposed a model for non-isothermal crystallization at constant cooling rates based on Evans' model as

$$X_{vc} = X_{\infty}\left[1 - e^{-\frac{\chi_C(T)}{a^m}}\right] \quad \textbf{(2-3)}$$

where a is the cooling rate, $\chi_C(T)$ is the cooling rate function and m is Ozawa exponent. Ozawa showed that Equation (2-3) can be used to predict the degree of crystallinity of poly ethylene terephthalate, PET, in constant cooling rate experiments. Ozawa's model needs the values of crystallinity for different cooling rates at each target temperature. Therefore it is not possible to cover a wide range of cooling rates and temperatures [12]. Moreover it is restricted to constant cooling rate conditions and is therefore not suitable for process modelling.

A generalization of Avrami equation was proposed by Nakamura *et al* [14] as:

$$X_{vc} = X_{\infty}\left[1 - e^{-\left(\int_0^t K(T)dt\right)^n}\right] \quad \textbf{(2-4)}$$

Nakamura's model is derived from Avrami's model for non-isothermal conditions. According to the authors [14], this model is valid within a temperature range where the ratio of the secondary nucleation growth rate to the frequency of activation of primary nuclei is constant (isokinetic assumption). An equivalent of Nakamura's model was also presented by Billon *et al* [15].

Differential forms of kinetics models are more useful for process modelling, as the material may undergo arbitrary temperature cycles. A differential form of Nakamura's model was presented by Patel and Spruiell [12] as:

$$\frac{d(X_{vc}/X_{\infty})}{dt} = nK(T)(1 - X_{vc}/X_{\infty})[\ln(1/(1 - X_{vc}/X_{\infty}))]^{(n-1)/n} \quad \textbf{(2-5)}$$

Equation (2-5) is equivalent to the differential for of Avrami (Equation (2-2)). The integral and differential forms of Nakamura's model predict the crystallization, identically.

Kamal and Chu [16] proposed an empirical integral Avrami expression to represent the non-isothermal primary crystallization:

$$X_{vc} = X_{\infty}\left[1 - e^{-\int_0^t K(T)nt^{n-1}dt}\right] \quad \textbf{(2-6)}$$

Similarly, a differential form of Equation (2-6) was presented by Patel and Spruiell [12]:

$$\frac{d(X_{vc}/X_{\infty})}{dt} = nK(T)(1 - X_{vc}/X_{\infty})t^{n-1} \quad \textbf{(2-7)}$$

Equation (2-7) depends explicitly on residence time which is difficult to keep track of in a process and makes this model unsuitable for process modelling.

Dietz [17] argued that neither Nakamura's nor Kamal's model accounted for the effects of secondary crystallization and introduced a modified differential crystallization kinetics model:

$$\frac{d(X_{vc}/X_{\infty})}{dt} = nK(T)(1 - X_{vc}/X_{\infty})t^{n-1}e^{-\alpha\left[\frac{X_{vc}/X_{\infty}}{1-X_{vc}/X_{\infty}}\right]} \qquad \textbf{(2-8)}$$

As mentioned by Patel and Spruiell [12], Dietz mistakenly considered Equation (2-8) as a modification of Nakamura's model, however, the model is in fact a modification of the differential form of Kamal's model, Equation (2-7). Patel and Spruiell argue that although the Dietz model improves Kamal's model for secondary crystallization, it introduces an additional parameter α which makes characterization more difficult.

Both the Nakamura model and the Kamal model reduce to Avrami's model under isothermal condition. As shown by Patel and Spruiell [12] both models in their integral form over-predict the non-isothermal crystallization data. However, Nakamura's predictions are more accurate. The cause of over-prediction of crystallinity in these models is not accounting for the induction time for nucleation [12], [18].

The integral form of Kamal's model, like its differential form is explicitly dependent on the residence time, t, which makes it improper for process modelling.

Velisaris and Seferis [19] proposed a model consisting of two separate Avrami type crystallization processes, in parallel, for modelling the primary and secondary crystallizations of PEEK and APC-2 PEEK composites. This model is based on the integral Avrami expression of Kamal and Chu, Equation (2-6). Recently, Bessard *et al* [20] introduced a similar dual mechanism model by combining two differential forms of the Nakamura model, Equation (2-5), instead.

Cebe [21] reexamined and revised the Velisaris and Seferis model for APC-2 PEEK. Fitting the data for non-isothermal cooling rates of $1, 5, \text{and } 10\ ℃/\text{min}$, Cebe obtained different values of parameters for different cooling rates. Hence, this model is of little practical significance in process modelling [12].

As mentioned, differential forms of kinetics models are more useful for process modelling, as the material may undergo arbitrary temperature cycles. In all crystallization kinetics models, reviewed in this chapter, some specific functional form is assumed for crystallization rate. As discussed, none of these forms are valid for the complete range of crystallization regimes. Therefore, fitting any of these models to experimental data will introduce some error in prediction of crystallinity. A more practical approach is avoiding these unwanted errors by not assuming any specific functional forms. This approach which was introduced by Vyazovkin [126] is the basis of crystallization kinetics modelling in this work.

2.2 Melting of polymers

2.2.1 Factors affecting the melting behaviour

The melting behaviour of polymers is affected by a number of phenomena including recrystallization and thickening of the lamellae [22]. Crystals formed from solution or melt are usually metastable [23]. During crystallization chain folded narrow strips or lamellae are formed on surfaces of growing crystals. The thickness of a lamella is determined by crystallization conditions, temperature and supercooling [23]. According to Jaffe and Wunderlich [23], the crystal grows in the form of folded chains up to the point that it is unstable relative to the extended chain crystal of the same weight. At that point the crystal thickens to a more stable crystal.

When a crystalline material is heated, the metastable crystalline regions melt which is followed by formation of crystals from the newly melted material. This phenomenon is known as recrystallization. As will be explained in the next section, a double peak behaviour is observed in heat flow curves of PEEK during a melting experiment. This behaviour is explained by some researchers as the result of continuous melting and recrystallization of the crystalline structure [24], [25]. This phenomenon is explained in detail in section 2.2.2.

Another possible phenomenon upon heating is reorganization and thickening of crystalline lamellae at a temperature which is very close to the melting point and the resulting crystals usually have a higher melting temperature.

2.2.2 Melting behaviour of PEEK

Melting behaviour of PEEK has been extensively studied in the literature. Blundell and Osborn [26] explored the morphology and related properties including crystallinity, crystallization and melting behaviour, lamellar thickness and spherulitic structure of PEEK utilizing differential scanning calorimetry (DSC), wide-angle X-ray diffraction and small-angle X-ray scattering techniques. They prepared isothermally crystallized samples of PEEK at $200\,℃$, $230\,℃$, $270\,℃$ (cold crystallization), $310\,℃$ and $320\,℃$ (melt crystallization). All samples were heated up at $20\,℃/\mathrm{min}$ in a DSC. In all cases a double peak behaviour is observed in the DSC thermograms. The peak at lower temperature (usually smaller) occurs about $10\,℃$ above the isothermal crystallization temperature. The peak at higher temperature (usually larger) is observed in the vicinity of $335\,℃$. Blundell and Osborn [26] associate the lower temperature peak with melting of the crystalline region formed during the previous isothermal crystallization. They believe the polymer goes through continuous melting and recrystallization upon heating above the lower peak temperature. There is a competition between these processes until the material reaches a temperature at which the net melting rate experiences a maximum and the higher temperature peak is observed.

In a later study [27], Blundell examined the double peak melting endotherms of isothermally crystallized PEEK in terms of two schools of thought: (i) two peaks are due to melting of two separate populations of crystals morphologies; (ii) they are related to continuous melting and recrystallization of a single crystal morphology. Argument (i) is supported by researchers like Cebe and Hong [24] and Cheng, Cao and Wunderlich [25]. They argue that the higher temperature peak is due to melting of main crystals formed during isothermal crystallization and the lower

temperature peak is related to less stable crystals grown in the intermediate spaces of main crystals. Blundell [27] conducted experiments on four PEEK samples. All samples were isothermally crystallized at 210 ℃ in a hot press for 30 min. Three of the samples were post annealed for 2 min at 250 ℃, 275 ℃ and 300 ℃. The short annealing time was chosen to avoid thickening of the crystals. All samples were heated in a DSC at 20 ℃/min and 80 ℃/min. Experimental results show that post annealing essentially affects the lower temperature peak and the higher temperature peak remains unchanged. With increasing the heating rate, the position of the lower temperature peak is raised and the position of the higher temperature peak is lowered. Also crystallinity and overall crystal perfection is increased as the temperature is increased above the isothermal crystallization temperature. Blundell argues that all these observations are in agreement with hypothesis (ii) which involves continuous recrystallization of just one type of crystalline morphology. The lower temperature peak is explained as the point where the original crystals become unstable and melting and the recrystallization process starts. If the heating experiment stops at this point, the crystal population are more stable compared to the original one. If the material is heated again, the lower temperature peak occurs at a higher temperature compared to the original one. This phenomenon was observed in the post annealed samples. The higher temperature peak is described as the point where the resultant of rates of melting and recrystallization reaches a maximum. Also since the recrystallization is mostly controlled by molecular characteristics rather than crystalline population it is not affected by crystallization history.

Argument (ii) has also been suggested by Lee and Porter [28]. In their experiments they report an increase in the heat of fusion and peak temperature of the lower melting peak and a decrease in the

heat of fusion and peak temperature of the higher temperature peak with increasing heating rate. They clarify that as the heating rate is increased, the amount of crystalline region that has time to recrystallize is decreased; which results in a smaller higher temperature melting peak and a larger lower temperature melting peak. The decrease in the temperature at which the higher temperature melting peak occurs is explained due to the shorter reorganization times.

Ivanov *et al* [29] reported two types of reorganization behaviour upon reheating cold crystallized PEEK specimens. While the temperature is lower than $T_g + \sim 50$, due to low mobility of amorphous regions, all reorganizations are lamellar scale which results in a slight increase of the crystal thickness. Increasing the temperature, causes larger scale reorganizations which consists of melting and recrystallization of whole lamellae, resulting in more stable and thicker crystals with lower state of free energy.

2.2.3 Melting kinetics models

Unlike crystallization kinetics, melting kinetics models, capable of quantitatively predicting the amount of melting, are not as widely studied in the literature. To the best knowledge of the author, the only melting kinetics model is the one introduced by Maffezzoli *et al* [30]. In their paper about induction welding of PEEK/Carbon fibre composites [30], they defined a degree of melting, X_f, as

$$X_f = (X_{vc} - X_{vci})/X_{vci} \quad \textbf{(2-9)}$$

where X_{vc} is the degree of crystallinity (crystallinity volume fraction) and X_{vci} is the initial degree of crystallinity. They adopted a simple n^{th}- order kinetic model for melting as

$$dX_f/dt = K(T)\left(1 - X_f\right)^n \quad \textbf{(2-10)}$$

with $K(T)$ given by an Arrhenius expression

$$K(T) = K_0 e^{-E_a/RT} \quad \textbf{(2-11)}$$

In Equations (2-10) and (2-11), n is the kinetics order, K_0 is the pre-exponential factor, T is the temperature, E_a is the activation energy of the melting process and R is the universal gas constant (8.314 J/K.mol).

The model given by Equations (2-10) and (2-11) has been extensively used by researchers for both process simulation of thermoplastic composites and bonding simulation of thermoplastics, and key works are described next.

Jacobsen *et al* [31] presented a transient two-dimensional anisotropic heat transfer analysis for resistance welding of thermoplastic composites. They considered three mechanisms for internal generation or absorption of heat in the heat equation. These include the resistance of the heating element, the heat absorbed during melting and the heat generated during crystallization. Melting heat is assumed to be proportional to the melting rate which is calculated using Equation(2-10).

Ageorges et al [32] incorporated Maffezzoli's melt model [30] coupled with a crystallization kinetics model [13], [19], [33] into a three-dimensional transient heat transfer/consolidation model for resistance welding of APC-2 laminate/PEEK film. In their analysis, they assume the onset and completion temperatures of crystal melting are constant at $320\ ℃$ and $385\ ℃$ respectively. They conclude that the effect of latent heat of crystallization and melting on the heat transfer during resistance welding is negligible, as a small quantity of the material is subjected to phase transformation.

Nicodeau [34] examined the applicability of Maffezzoli's model [30] for different conditions and realized that the model is not valid for all cases (for example $40\ ℃/\mathrm{min}$). They concluded that the melt model is difficult to use.

Mantell and Springer [2] introduced a manufacturing process model for thermoplastic composites. This model consists of three sub-models; thermo-chemical, consolidation and bonding, stress and strain. The energy equation in the thermo-chemical sub-model has two unknowns, namely temperature and degree of crystallinity. They incorporated Maffezzoli's model [30], combined with a crystallization kinetics model [19], in the thermo-chemical sub-model. This additional expression completes the formulation of the problem. The sub-model adopts the crystallization kinetics model during cooling ($dT/dt \leq 0$) and uses the melt kinetics model during heating ($dT/dt > 0$). Mantell and Springer [35] later used the same approach for process modelling of filament winding. Maffezzoli's melt model [30] was also adopted via a similar approach by Sarrazin and Springer [36] to assess the influence of processing parameters on quality of parts made by tape laying process.

Sonmez and Hahn [37] employed Maffezzoli's [30] melt model coupled with a crystallization kinetics model [38]-[40] for analyzing the crystallization behaviour of thermoplastic composites (carbon fibre reinforced PEEK) during the tape placement process.

Tierney and Gillespie [41] developed an experimental setup for rapid heating and cooling of composite laminates. They applied Maffezzoli's model [30] and a crystallization kinetics model [19] for prediction of the final degree of crystallinity under very high heating and cooling rates and concluded that the model predictions are in good agreement with their experimental measurements. As mentioned, the model predictions and experimental results are compared for the final degree of crystallinity and not during the process.

2.3 Mechanical constitutive models for process modelling

2.3.1 Linear elastic models

Hahn and Pagano [42] assumed linear elastic behaviour in their analysis. They considered a total stress-strain-temperature formulation for determination of the curing stresses in boron/epoxy composite laminates. The considered constitutive equation in unidirectional form was

$$\epsilon = \frac{1}{E(T)}\sigma + \epsilon^{T}(T) \qquad \textbf{(2-12)}$$

where $E(T)$ is the temperature dependent modulus and $\epsilon^T(T)$ is the thermal expansion/shrinkage strain. Similar material behaviour was used in the works of Loos and Springer [1] and Nelson and Cairns [43]. Nelson and Cairns created a simple closed-form solution for the change in the original angle, hereafter referred to as 'spring-in', of a curved composite part subjected to a change of temperature as

$$\Delta\theta = \theta \frac{(CTE_\theta - CTE_R)}{1 + CTE_R \Delta T} \Delta T \qquad \textbf{(2-13)}$$

In Equation(2-13), $\Delta\theta$ is the spring-in, θ is the original angle, ΔT is the temperature change, and CTE_R and CTE_θ are the radial and circumferential coefficients of thermal expansion, respectively.

Elastic models provide some general and qualitative insight about the process, however, they are not accurate quantitatively.

2.3.2 Chemical hardening models

The effects of chemical hardening on mechanical properties of isotropic thermoset materials was studied by Levitsky and Shaffer [44]-[46]. Considering these effects, Cure Hardening Instantaneously Linear Elastic constitutive models (CHILE) were used by Bogetti and Gillespie [47], Lange *et al* [48], Johnston *et al* [49], [50], Fernlund *et al* [51] and Antonucci *et al* [52] in their works (The term CHILE was introduced by Johnston *et al* [49]). CHILE models consider the cure and temperature dependent elastic modulus and assume a linear elastic relation for the stress

increment in terms of the strain increment at each instant of the process. Mathematically, a CHILE constitutive model in the uni-axial form is expressed as

$$\Delta\sigma = E(T, \alpha)\Delta\epsilon \qquad \textbf{(2-14)}$$

where $E(T, \alpha)$ is the instantaneous modulus of the material at the temperature T and the degree of cure α.

2.3.3 Viscoelastic models

Polymer materials are known in general to show time dependent or viscoelastic mechanical behaviour. Although CHILE models can represent the behaviour of thermosets during curing, they are not valid when the modulus is decreasing, such as during post-curing after tool removal. Viscoelastic models are then essential as they consider the relaxation phenomenon in the material. Some authors like Weitsman and Harper [53]-[55], Yeoh *et al* [56], Wang *et al* [57] and Plazek and Choy [58] have considered that the history dependent mechanical behaviour of the material is only a function of temperature. Adolf and Martin [59] and later White and Hahn [60], [61] took into account the change in the microstructure of the material and therefore considered the time dependent mechanical properties as a function of degree of cure and temperature. Since then a significant number of viscoelastic based process modelling work for composite materials have been reported in the literature. As some important references we can mention the works of Kim

and White [62]-[64], Zhu [65], Svanberg and Holmberg [66], [67], Clifford *et al* [68] and Zobeiry *et al* [69], [70].

Some researchers consider nonlinear viscoelastic constitutive models for analysis of materials. The Schapery single integral model [71] is one of the most famous examples which has been widely used in the literature [72]-[77]. Most of the available nonlinear viscoelastic models do not consider the change in microstructure of materials. Also they need a significant computational effort for implementation. Therefore linear viscoelastic models are often being used for process modelling of composites.

Almost all recent works in viscoelastic modelling of polymers use the linear stress-strain relationship in hereditary integral form. The hereditary integral method was introduced by Boltzmann in 1874 and is based on Boltzmann Superposition Principle [78]. This principle simply considers the state of stress and strain as functions of all events over the history of the material and expresses the stress as an integral over the history of strain and vice versa. The uniaxial strain-stress relation in the hereditary integral form is written as

$$\epsilon(t) = \int_0^t D(t-\tau)\frac{d\sigma(\tau)}{d\tau}d\tau \qquad \textbf{(2-15)}$$

In Equation (2-15), $D(t)$ is the creep compliance. Similarly the stress-strain relation is expressed as

$$\sigma(t) = \int_0^t E(t-\tau)\frac{d\epsilon(\tau)}{d\tau}d\tau \qquad \textbf{(2-16)}$$

where $E(t)$ is the relaxation modulus. Although the hereditary integral constitutive relation rigorously models the physical behaviour of the material and the elegant idea behind that should be appreciated, it is not very effective in process modelling of composites. The numerical integration schemes either need to recalculate the time integral from time zero to the current time at each instant of the process [60], [61], [79], [80] or at least need to store the stresses for the last two time steps [65], [81], [82]. In all cases the time integrations are very time consuming and their complex formulations make their implementation in finite element codes very difficult.

Years before Boltzmann's article on viscoelasticity, in 1867, James Clark Maxwell in the introductory part of his gas dynamics paper [83] stated that the viscoelastic behaviour of the materials obeys the first order differential equation (Maxwell's notation is different)

$$\frac{d\sigma}{dt} = E\frac{d\epsilon}{dt} - \frac{\sigma}{\tau} \qquad \textbf{(2-17)}$$

In Equation (2-17), σ is the stress, ϵ is the strain, E is the spring stiffness and τ is the relaxation time, such that the dashpot constant is $\eta = E\tau$. A different first order differential equation was proposed in 1874 by Meyer [84] as (Meyer's equation was three dimensional and his notation was different.)

$$\sigma = E\epsilon + \eta\frac{d\epsilon}{dt} \quad \textbf{(2-18)}$$

The differential equation in Equation (2-18) is usually attributed to Voigt and Kelvin in the literature [78]. The above differential equations can be associated to a spring and a dashpot connected in series (Equation (2-17)) or in parallel (Equation (2-18)). The combination of a spring and a dashpot in series and parallel are referred to as a Maxwell element and a Kelvin element, respectively. The differential equations in Equations (2-17) and (2-18) relate the stress and strain in a one dimensional (1D) viscoelastic body and therefore they can be interpreted as constitutive models in differential form (DF). By combining *N* Maxwell elements in parallel or *N* Kelvin elements in series we obtain constitutive equations of higher order that can model the behaviour of a material more precisely. These models are called 'Generalized Maxwell Model' (GMM) or Maxwell chain and 'Generalized Kelvin Model' (GKM) or Kelvin chain. The DF form of the constitutive equations has a much simpler form compared to the hereditary integral form and specifically is not history dependent. Therefore the analysis can be performed much faster and with less computational effort. There are a few works in the literature that use DF for viscoelastic analysis of materials. As some references we can mention the works of Zienkiewicz *et al* [85], Bazant *et al* [86]-[90], Carpenter *et al* [91], Jurkiewiez *et al* [92], [93], Idesman *et al* [94], [95] and Mesquita and Coda [96]-[104]. According to Bazant [90] another advantage of the DF is that it allows a much simpler formulation of thermodynamics. There are also a limited number of works that use the DF approach for process modelling of composites such as the works of Kokan *et al*

[105], Xia and Ellyin [106], Wiersma *et al* [107], Chen and Ellyin [108], Ellyin and Xia [109] and Zobeiry *et al* [69].

The majority of the process modelling works available in the literature are related to thermoset composites. The first manufacturing process model for thermoplastic composites was presented by Lee and Springer [110]. This model, which is similar to the sub-model approach of Loos and Springer for thermoset composites [1], consists of three modules, named as "impregnation", "consolidation" and "crystallinity". In the "impregnation" sub-model the degree of impregnation as a function of time is determined and the time required for complete impregnation is calculated. The "consolidation" sub-model consists of models for determining the effects of processing variables such as temperature, pressure and time on intimate contact of adjacent plies and bonding at ply interface, called autohesion. Finally, in the crystallization sub-model, by using the non-isothermal crystallization kinetics model of Ozawa [13] and solving the coupled heat transfer-crystallization problem, the degree of crystallinity and temperature as a function of position and time are determined. Ozawa's model [13] relates the degree of crystallinity to cooling rate and temperature which are both processing variables. Then the material properties are related directly to degree of crystallinity using the empirical models presented by Talbott *et al* [111]. In the work of Talbott *et al* [111] Young's modulus and shear modulus of PEEK polymer are empirically (using curve fitting) stated as second order function and linear function of degree of crystallinity, respectively. The manufacturing process model of Lee and Springer [110] does not predict the residual stresses and distortions of the final product and only predicts its mechanical properties.

A model for prediction of in-plane residual stresses in semi-crystalline thermoplastic composites was presented by Chapman *et al* [112]. This model consists of Thermal History, Mechanical

Properties and Stress Analysis modules. In the thermal history module the coupled heat transfer-crystallization kinetics problem is solved. The mechanical property module is divided into a linear elastic property section and a viscoelastic section. Using the micromechanics methodology of Ogale and McCullough [113], material properties are evaluated as functions of time, temperature and crystallinity in the linear elastic section. The volume shrinkage due to both crystallization and temperature change is also calculated. In the viscoelastic section the effect of degree of crystallinity is neglected and the properties are given for different times and temperatures. Finally in the stress analysis module, the in-plane stresses are evaluated using the incremental form of the classical laminated plate theory.

A plane-strain linear elastic finite element model with temperature and crystallinity dependent material properties was developed by Li *et al* [114] for predicting residual stresses in cross section of thick thermoplastic composites. Trende *et al* [115] used the temperature and crystallinity dependent material properties in a commercial finite element code and performed the residual stress analysis for compression moulded thermoplastic composites with both isotropic viscoelastic and transversely isotropic elastic material models. An anisotropic thermo-viscoelastic material model was introduced by Sunderland *et al* [116] for prediction of the process induced stresses. Similar thermo-viscoelastic formulations and finite element analyses were presented by Kim *et al* [117], Sonmez *et al* [118] and Clifford *et al* [68]. Sonmez *et al* [118] performed their analysis for the tape placement process. Similar to thermoset composites, almost all viscoelastic models for analysis of thermoplastic composites use the constitutive equations in integral form.

Schwarzl and Staverman [119] divided the materials with linear viscoelastic behaviour into two general groups (Class A and Class B) regarding their response to change of temperature. In the

first group (Class A), which is termed “thermo-rheologically simple” a change of temperature is equivalent to a shift in the logarithm of time. Considering this, the effects of time and temperature together will be reduced to one parameter, called “reduced time” or “pseudo time” by defining a “shift factor” or “shift function”. Therefore the stresses, strains and the material properties in the constitutive relations, in general, will be functions of position and this reduced time [120]. The reduced time ξ was presented by Morland and Lee [120] as

$$\xi = \int_0^t \frac{d\tau}{a_T[T(\tau)]} \qquad \textbf{(2-19)}$$

In Equation (2-19), a_T is the shift factor which is a function of time and temperature. Using the notion of reduced time, as described here, is sometimes referred to as “Time-Temperature Superposition”. As mentioned previously, Adolf and Martin [59] and also White and Hahn [60], [61] took into account the change in the microstructure. The shift factor that they are using is a function of time, temperature and degree of cure. Reducing the effect of time, temperature and degree of cure to one parameter is referred to as “Time-Temperature-Cure superposition”. All viscoelastic formulations and process models for both thermoset and thermoplastic composites that have been addressed so far assume thermo-rheologically simple material behaviour. In the differential form of viscoelastic constitutive equations, assuming temperature dependent (or degree of cure and temperature dependent) relaxation times (or equivalently the viscosities of the dashpots) is the equivalent of assuming thermo-rheologically simple material behaviour as explained by Zobeiry [69].

The materials that do not obey thermo-rheologically simple behaviour are termed "Thermo-rheologically Complex" by Schapery [121]. Schapery [121] introduces two classes of thermo-rheologically complex materials named TCM-1 and TCM-2. He defines TCM-1 as a composite material consisting of two or more thermo-rheologically simple phases with different shift factors. He also defines TCM-2 as a material whose uni-axial behaviour (e.g. a bar subjected to uniaxial stress σ_x) is governed by the equation

$$\epsilon_{x\sigma} = D_I \sigma_x + \int_0^t \Delta D(\xi - \xi') \frac{d}{dt'} \left(\frac{\sigma_x}{a_G} \right) dt' \qquad \textbf{(2-20)}$$

In Equation (2-20), ξ is defined as in Equation (2-19), $D_I = D_I(T)$ is the initial value of creep compliance, $\epsilon_{x\sigma}$ is the strain due to stress (or mechanical strain) and a_G is shown to be a vertical shift factor. If Equation (2-20) is applied to an isothermal creep test, the creep compliance D_T will be calculated as

$$D_T = \frac{\epsilon_{x\sigma}}{\sigma_x} = D_I(T) + \frac{\Delta D(\xi)}{a_G(T)} \qquad \textbf{(2-21)}$$

where $\xi = t/a_T$. Equation (2-21) can be rewritten as $\log(D_T - D_I) = \log \Delta D - \log a_G$. Also we have $\log \xi = \log \mathrm{t} - \log a_T$. Furthermore we assume that for an arbitrary reference temperature, $a_T = a_G = 1$. From Equation (2-21) we have $\Delta D(t) = D_T(t, T_R) - D_I(T_R)$. Then we see that a plot of $\log(D_T - D_I)$ versus $\log \mathrm{t}$ at a temperature T can be obtained from the plot of the same at the reference temperature T_R by a rigid horizontal and vertical shifting of the magnitude $\log a_T$

and $\log a_G$ respectively. As a special case of Equation (2-20), we assume $D_I(T) = \frac{D_I(T_R)}{a_G(T)}$. Then from Equation (2-21) the creep compliance will be obtained as

$$D_T = \frac{D_I(T_R) + \Delta D(\xi)}{a_G(T)} = \frac{D(\xi)}{a_G(T)} \qquad \textbf{(2-22)}$$

Then the constitutive equation in Equation (2-20) reduces to

$$\epsilon_{x\sigma} = \int_0^t D(\xi - \xi') \frac{d}{dt'} \left(\frac{\sigma_x}{a_G}\right) dt' \qquad \textbf{(2-23)}$$

Also we can obtain the inverse of this equation as

$$\sigma_x = a_G \int_0^t E(\xi - \xi') \frac{d\epsilon_{x\sigma}}{dt'} dt' \qquad \textbf{(2-24)}$$

and the relaxation modulus will be $E_T = a_G(T)E(\xi)$. In this special case, plots of $\log D_T$ and $\log E_T$ versus $\log \mathrm{t}$ at a temperature T can be obtained from the plot of the same at the reference temperature T_R by a rigid horizontal and vertical shifting of the magnitude $\log a_T$ and $\log a_G$. Zobeiry [122] showed that assuming a temperature dependent spring in a Maxwell element leads to an equivalent to this special case of TCM-2. Harper and Weitsman [123] demonstrated a characterization method for a more general form of the integral constitutive equation of Schapery. This more general form of the constitutive equation was later used by Hashin *et al* [124] for

determination of the thermo-viscoelastic properties of unidirectional fibre composites. Sadkin and Aboudi [125] presented a similar work by using a different form of micromechanics.

As addressed by Schapery [121], based on limited experimental data available in the literature, the constitutive equations of thermo-rheologically simple behaviour work very well for amorphous polymers at temperatures above T_g (the glass transition temperature). For semi-crystalline polymers and also for amorphous polymers near and below their T_g, the constitutive equations of a TCM should be used. Schwarzl and Staverman [119] explain that the assumption of thermo-rheologically simple (TSM) behaviour means that at different temperatures, the same sequence of molecular processes take place in the material however with different speeds. On the other hand, for thermo-rheologically complex (TCM) materials, as a result of change in the temperature of the experiment not only the speed but also the sequence of molecular events changes. They conclude that if a special structure cannot be achieved in a TSM at a specific temperature, it cannot happen at any other temperature. In other words, if heat treatment changes the structure of a material, this material cannot be categorized as TSM. As a result of this discussion we may argue that materials like fully cured thermoset polymers and rubbers can be considered as TSM (at temperatures higher than T_g according to Schapery) however uncured thermosets during the curing process and also semi-crystalline thermoplastic polymers during heating up (melting) and also cooling down (crystallizing) should be treated as TCM.

Although processing of polymeric composite materials (thermosets and thermoplastics) involves changes in the material structure, all available viscoelastic based process modelling works (e.g. [60], [61]) assume thermo-rheologically simple behaviour and use a horizontal shift factor which is temperature and degree of cure (or degree of crystallinity) dependent. As explained previously

based on discussions by Schwarzl and Staverman [119] this is not a physically correct assumption. For thermoset composites, a significant amount of residual stresses develop during the curing process. Also for thermoplastic composites, the polymer crystallizes during cooling down from melt. Therefore for studying the residual stresses during the processing of both thermoset and thermoplastic composites more sophisticated constitutive models that assume thermo-rheologically complex behaviour are required. Although such constitutive equations are available (e.g. [121], [124], [125]), they are all in integral form which as explained previously are not efficient enough to be used in process modelling. There is a noticeable lack of process models for composites that consider thermo-rheologically complex behaviour and analyze the stress and deformation using the differential form of thermo-viscoelastic constitutive equations. Finally, the availability of a more sophisticated constitutive model enables us to evaluate the simpler models such as viscoelastic [69], [122] and CHILE [49], [50] and use them with confidence within their validity bounds.

2.4 Scope and research objectives

Based on the discussions in section 2.1.2, most of the crystallization kinetics work available in the literature studies the isothermal and non-isothermal crystallization as two separate processes. Also, almost all models do not consider the induction time prior to crystallization which results in overpredictions of the degree of crystallinity. Also, as explained in section 2.2.3, the only available melt kinetics model [30] is not valid for all heating rate cases [34].

During processing, such as compression moulding, thermoforming and AFP, thermoplastic composite parts may experience arbitrary and complex temperature cycles and the available kinetics models have little practical application. A differential form crystallization kinetics/melt kinetics model, along with an induction time model for prediction of the onset of crystallization is desirable.

As discussed in sections 2.3.2 and 2.3.3, processing of composite materials involves concurrent changes in the molecular structure (chemical/physical hardening) and relaxation of residual stresses. Therefore, a more sophisticated (thermo-viscoelastic) model is required for simulating the development and relaxation of the residual stresses during the process and predicting their effects on the final part distortions and strength.

Based on these discussions, the objectives of this research are as follows:

1. Designing and performing characterization experiments for studying both isothermal and non-isothermal crystallization kinetics of AS4/PEEK composites.
2. Designing and performing characterization experiments for studying melt kinetics of AS4/PEEK composites.
3. Developing a differential form crystallization kinetics/melt kinetics model for AS4/PEEK, along with an induction time model, capable of predicting the crystallinity changes during an arbitrary temperature cycle.
4. Designing and performing characterization experiments for thermo-viscoelastic behaviour of different composite materials. These experiments should capture the relaxation behaviour of the material as well as the temperature dependence of mechanical behaviour when unrelaxed.

5. Developing a thermo-viscoelastic constitutive model in differential form. This model should be capable of capturing the thermo-rheologically complex behaviour and consider the temperature dependence of the mechanical response of the material when unrelaxed.
6. Integration of the developed crystallization model, melt kinetics model and the thermo-viscoelastic model into commercially available process modelling package to predict the residual stresses and shape distortions in composites. As well, analyzing several case studies to validate the model's capabilities is warranted.

Chapter 3: Crystallization Kinetics/Melt Kinetics of AS4/PEEK Composites; Experiments and Model Development

In this chapter, DSC experiments and their results are presented for studying the crystallization and melt behaviour of AS4/PEEK. Melting behaviour is further investigated using complementary annealing experiments. Experimental results are analyzed and dependence of the crystallization rate on temperature and degree of crystallinity is investigated. A crystallization kinetics model in differential form is presented for prediction of degree of crystallinity during the process. The rate of crystallization is a function of temperature and degree of crystallinity. No model is considered for crystallinity dependence and the model-free approach introduced by Vyazovkin [126] is adopted. A simple empirical model and the concept of additivity from phase transitions of metals is used for estimation of induction time.

A concept of 'master melt curve' is introduced and is used along with the crystallization kinetics model for prediction of crystallinity changes during melting of the material. Model predictions are compared with experimental results for different temperature cycles.

3.1 Crystallization kinetics experiments, materials and methodologies

The material used for crystallization and melt kinetics characterization is TenCate Cetex® TC1200 PEEK AS4 [127] unidirectional tape (Figure 3-1), which is briefly referred to as AS4/PEEK for

the rest of this document. TenCate Cetex® TC1200 PEEK is a semi-crystalline poly-ether-ether-ketone thermoplastic composite with a very low void content (< 1%).

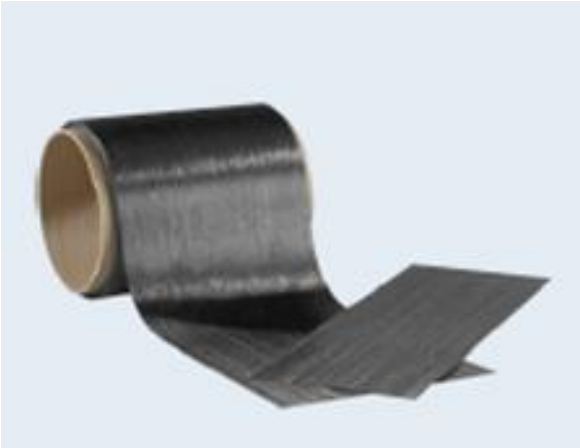

Figure 3-1 AS4/PEEK unidirectional tape (Courtesy Fortin [128])

Figure 3-2 TA Instruments DSC Discovery machine

It has a resin content of 34 % by weight and 59 % of fibre by volume. The glass transition temperature, T_g, for this material is 143 ℃ and the equilibrium melt temperature, T_m^0, is 343 ℃ [127].

The characterization technique used for crystallization and melt kinetics is Differential Scanning Calorimetry, DSC. A TA Instruments DSC Discovery machine, shown in Figure 3-2, was employed for conducting the experiments. The DSC machine has a monthly calibration schedule. However, the calibration was performed prior to each set of experiments. The calibration procedure is briefly explained in section 3.1.1.

3.1.1 Calibration of DSC

The DSC machine operates based on Tzero® technology. In the Tzero® technology, a thermocouple is added between the sample and reference sensors. The heat flow between the sample and this thermocouple, is related to the temperature difference between this thermocouple and the sample sensor, using two parameters, termed sample resistance and capacitance. Similarly a resistance and capacitance is defined for reference. The total heat flow between the sample and the reference is determined using these four parameters.

The first step in the DSC calibration is determination of these four constants. This calibration step is termed Tzero® calibration. The Tzero® calibration consists of two experiments: a temperature ramp of an empty cell and a temperature ramp with two sapphire disks, mounted directly on the sample and reference sensors. After these two experiments, the differences between the sample and reference resistance and capacitance values are considered and adjusted by the software.

The next step in the calibration is cell constant and temperature calibration. This step is performed using one or two traceable metal samples such as indium, lead and zinc. These standard metals have known reference melting endotherms and melting temperatures. Cell constant is the ratio of the measured and theoretical heat of fusion. The difference between the theoretical and measured melting temperature is calculated and adjusted by the software. After performing these two calibration steps, the machine is ready for starting the experiments.

3.1.2 Isothermal DSC experiments

Isothermal DSC tests were conducted for studying the crystallization behaviour of the material at different temperatures. Samples of approximately 5 milligrams were prepared in Tzero® hermetic DSC pans. Samples were heated in the DSC to 380 ℃ and held for 10 minutes. They were cooled down at 60 ℃/min to temperatures between 305 ℃ to 325 ℃, followed by an isothermal hold at each temperature until the crystallization was complete.

3.1.3 Non-isothermal DSC experiments

Non-isothermal DSC tests were performed for investigation of crystallization behaviour of the material, whilst heated above the glass transition temperature and cooled from the molten state. Samples of approximately 5 milligrams were prepared from AS4/PEEK tape, similar to isothermal tests. Samples were heated at heating rates between 1 ℃/min to 10 ℃/min to 380 ℃. Subsequent to an isothermal hold of 10 minutes, samples were cooled at cooling rates between 1 ℃/min to 10 ℃/min to room temperature.

3.1.4 Raw data and general interpretations

DSC test results are usually given as plots of heat flow rate as a function of time or temperature. Normalized heat flow rate results for isothermal tests at nine different temperatures are shown in Figure 3-3.

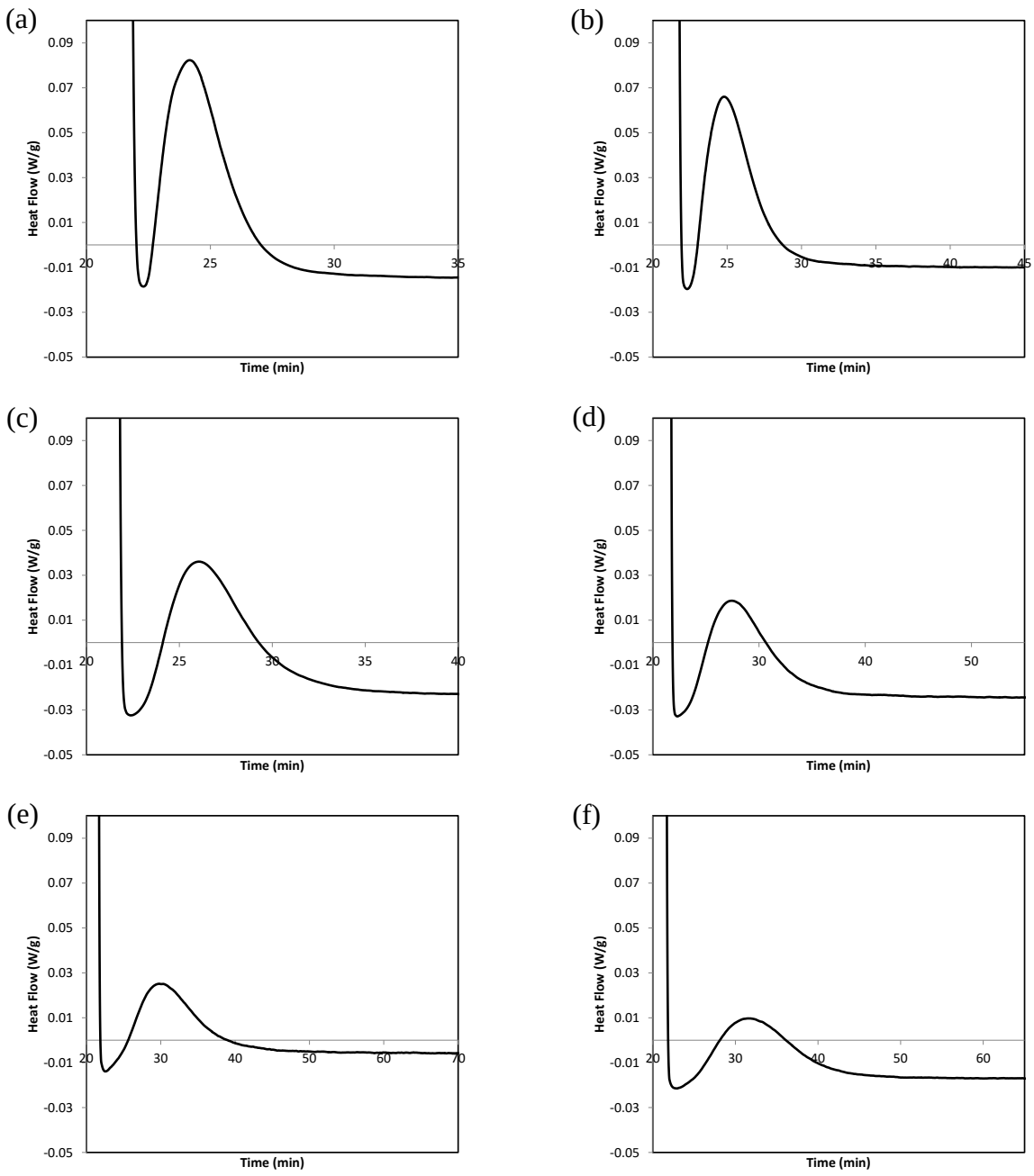
(a)
(b)
(c)
(d)
(e)
(f)
Heat Flow (W/g)
Time (min)
0.09
0.07
0.05
0.03
0.01
-0.01
-0.03
-0.05
20
25
30
35
40
45
50
60
70

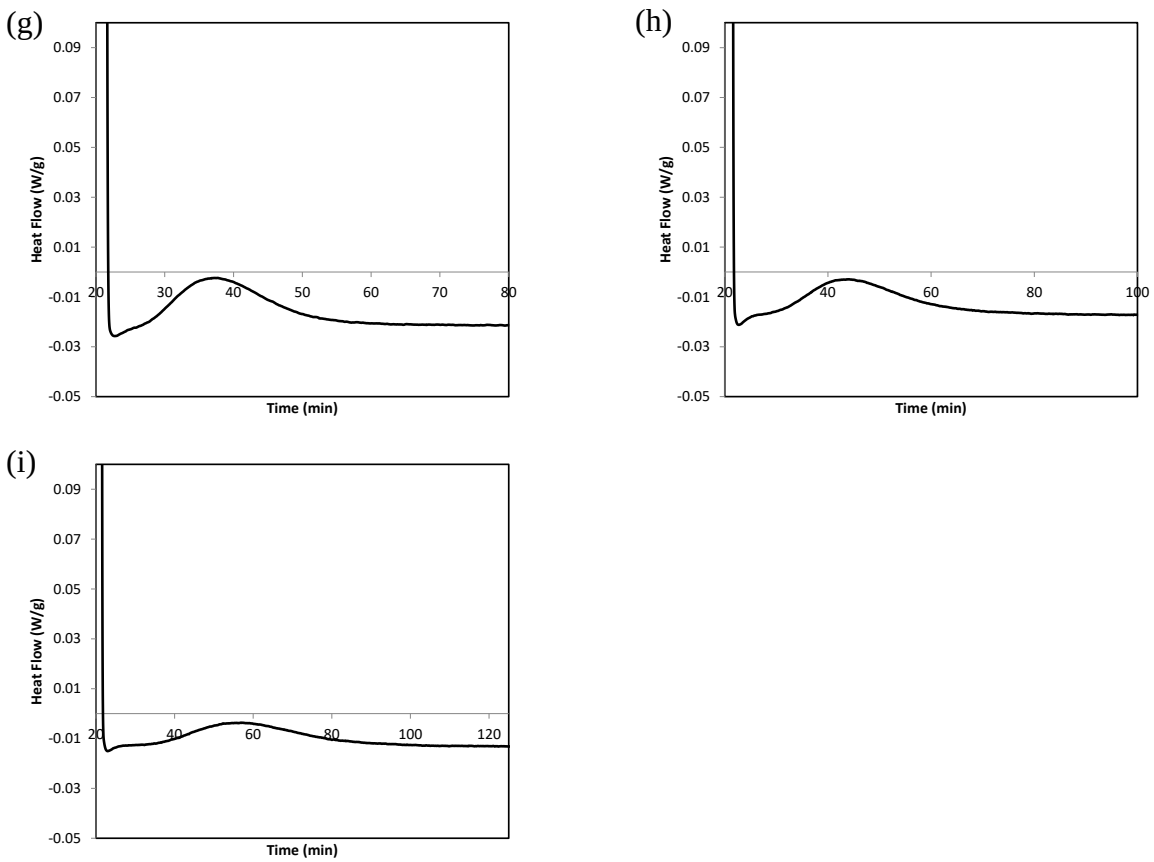

Figure 3-3 Normalized heat flow rate for isothermal crystallization at (a) 305 ℃, (b) 307 ℃, (c) 310 ℃, (d) 312 ℃, (e) 315 ℃, (f) 317 ℃, (g) 320 ℃, (h) 322 ℃, (i) 325 ℃

In Figure 3-3, it is seen that the heat flow drops very rapidly during the initial cooling to the target temperature. During the isothermal hold, an exothermic peak is observed in the heat flow diagram which is due to the latent heat, released by the material as a result of crystallization. For low target temperatures, such as 305 ℃ and 307 ℃, this exothermic peak is sharp and occurs over a short period. As the target temperature is increased, peaks occur gradually over longer time periods. Normalized heat flow rate values versus temperature for non-isothermal experiments on the samples made of the as-received material at ten different heating rates are given in Figure 3-4.

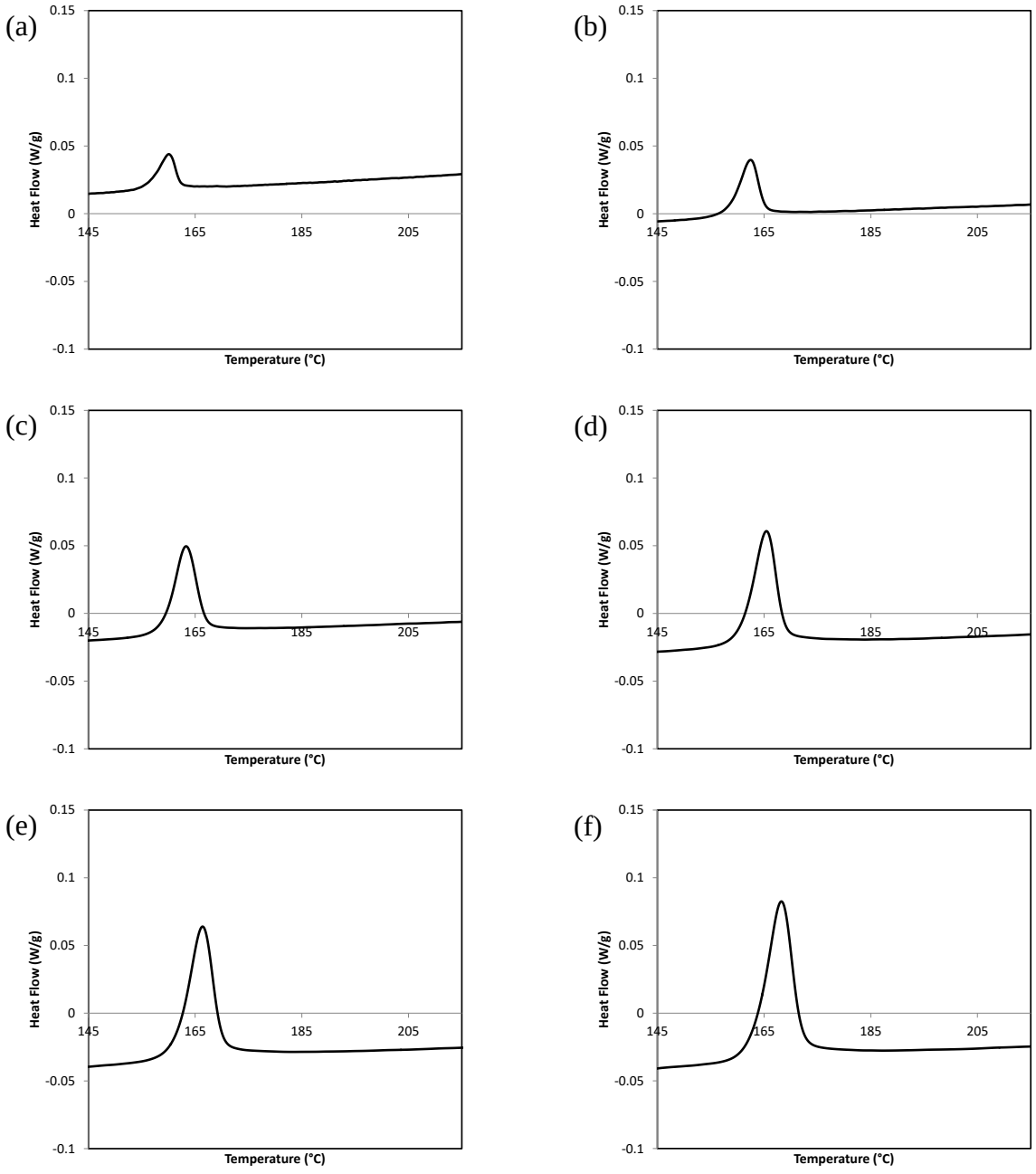
(a)
(b)
(c)
(d)
(e)
(f)
Heat Flow (W/g)
Temperature (°C)
0.15
0.1
0.05
0
-0.05
-0.1
145
165
185
205

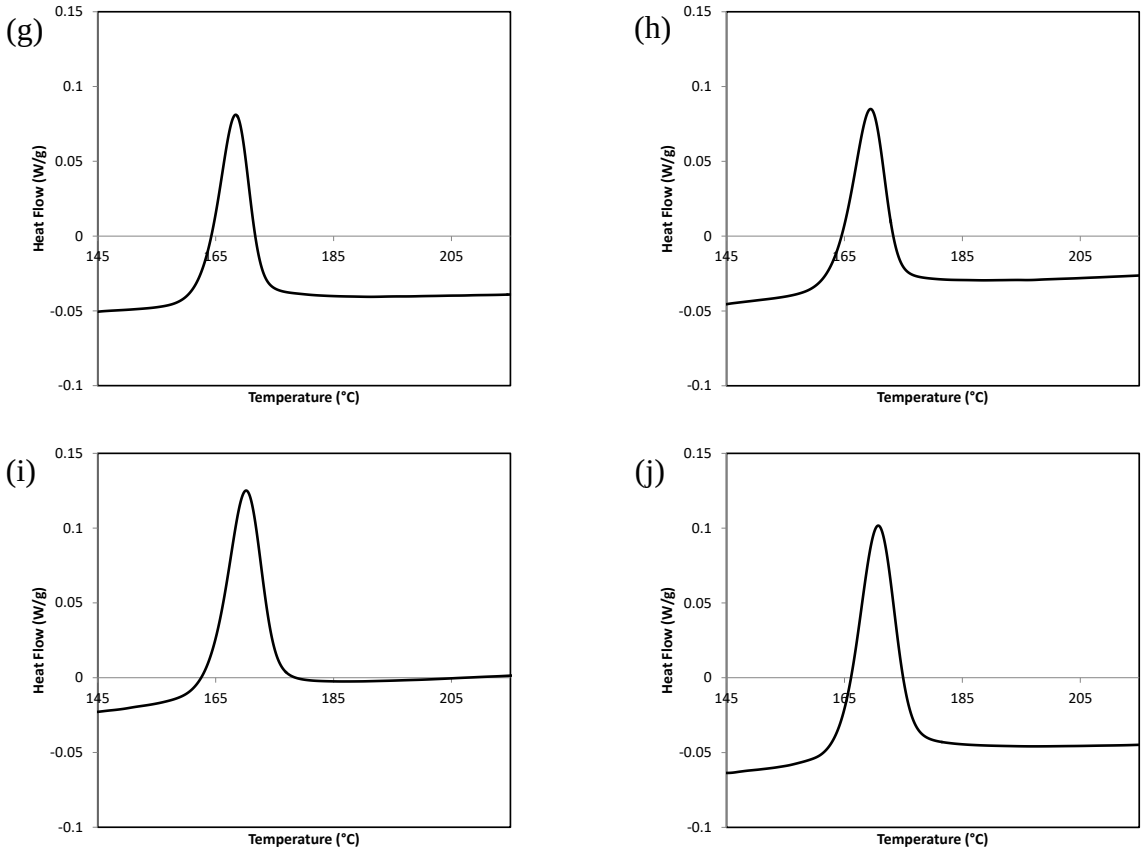

Figure 3-4 Normalized heat flow rate from non-isothermal heating of the as-received material at (a) 1 ℃/min, (b) 2 ℃/min, (c) 3 ℃/min, (d) 4 ℃/min, (e) 5 ℃/min, (f) 6 ℃/min, (g) 7 ℃/min, (h) 8 ℃/min, (i) 9 ℃/min, (j) 10 ℃/min

It is recognized from Figure 3-4 that the as-received material crystallizes when heated above the glass transition temperature ($T_g = 143$ ℃). This phenomenon is known as 'cold crystallization'. It is also realized that at higher heating rates, cold crystallization starts and ends at higher temperatures.

Normalized heat flow rate results versus temperature for non-isothermal experiments on the samples cooled from the molten state at ten different heating rates are demonstrated in Figure 3-5.

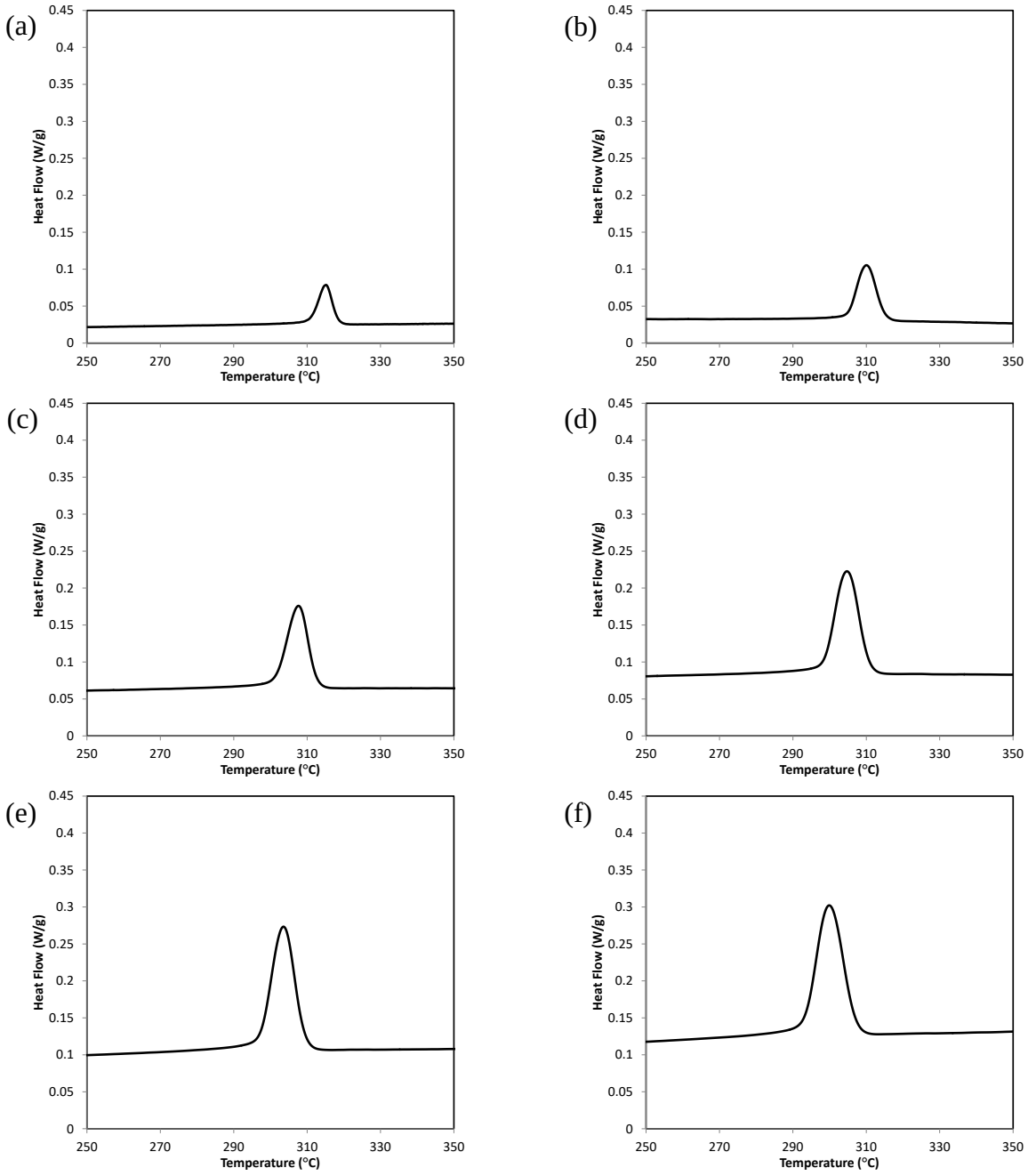
(a)
(b)
(c)
(d)
(e)
(f)
Heat Flow (W/g)
Temperature (°C)
0.45
0.4
0.35
0.3
0.25
0.2
0.15
0.1
0.05
0
250
270
290
310
330
350

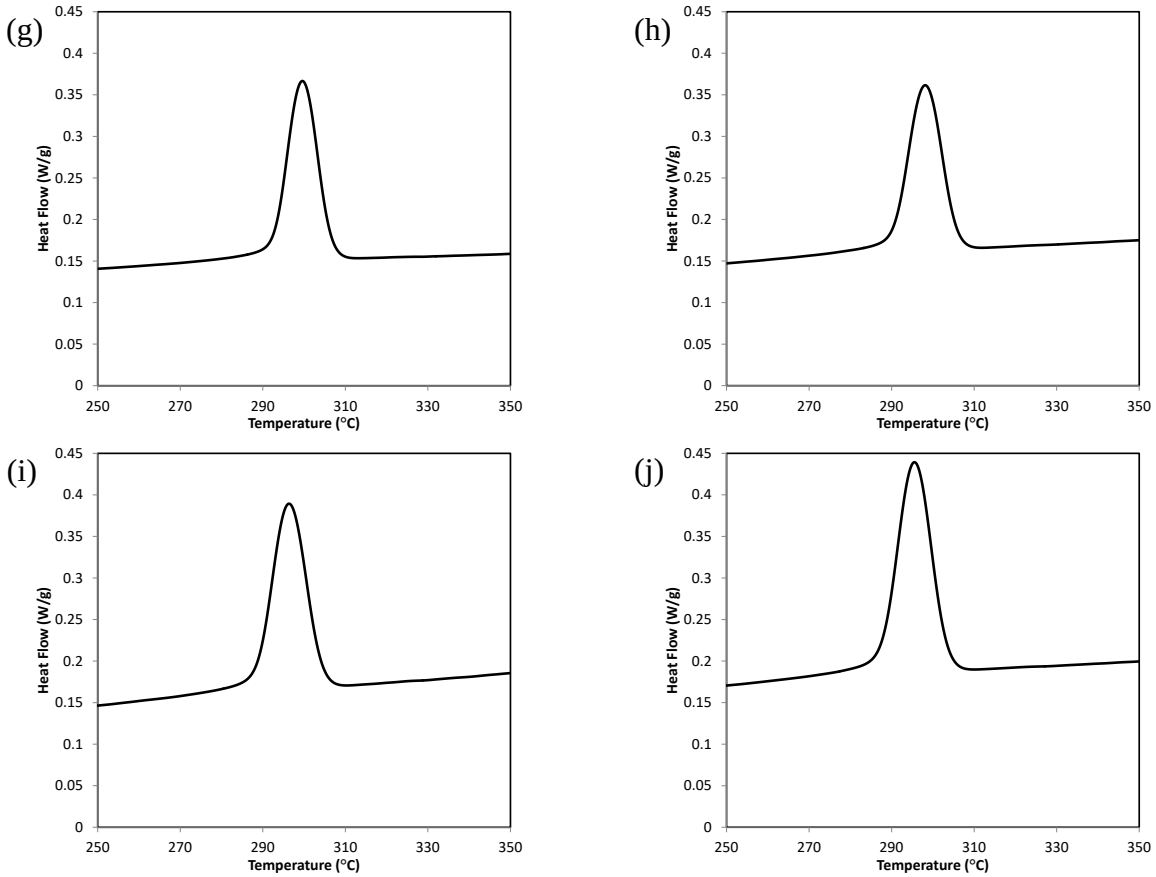

Figure 3-5 Normalized heat flow from non-isothermal cooling of samples from molten state at (a) 1 ℃/min, (b) 2 ℃/min, (c) 3 ℃/min, (d) 4 ℃/min, (e) 5 ℃/min, (f) 6 ℃/min, (g) 7 ℃/min, (h) 8 ℃/min, (i) 9 ℃/min, (j) 10 ℃/min

Figure 3-5 shows that the material crystallizes whilst continuously cooled from the molten state. With increasing cooling rate, the onset and completion of crystallization occur at lower temperatures. Furthermore, the maximum heat flow rate value, which is proportional to the maximum crystallization rate, is higher for higher cooling rates.

3.1.5 Baseline selection

The part of the heat flow rate curve, where no transition in the sample is occurring, is called the 'baseline'. When a reaction or transition associated with heat, such as melting or crystallization, happens, a 'peak' appears in the heat flow rate signal. A peak deviates from the baseline at the temperature where the transition or reaction starts and after going through a maximum/minimum, merges back into the baseline at the temperature where the transition ends [129]. The curve that connects the baselines before and behind the transition, in the peak region, is known as the 'interpolated baseline'. This is a virtual line which would have been recorded if all heat capacity, C_p, changes and also changes of heat transfer had happened without any transitions occurring [129]. It is important to construct the interpolated baseline (hereafter referred to as baseline) as the area between the heat flow rate curve and this curve is needed for calculation of the latent heat of reaction due to transition.

For the isothermal test results shown in Figure 3-3, the baselines behind the transition are all straight lines, however, little information can be obtained for the shape of the baselines before the transition. For these cases we extrapolate the straight part on the right side of the curve (behind the transition) and consider it as the baseline. As explained, extrapolation of the straight baseline is due to lack of knowledge regarding the shape of the baseline before the transition. This is a source of uncertainty in crystallization calculations.

In non-isothermal cases, both for cold crystallization and melt crystallization, the baselines before and behind the transition are both straight lines, however, they are not aligned with each other. In

these cases we have used the procedure explained in [129] to construct sigmoidal baselines. These baselines are used in the next section for calculation of degree of crystallinity.

3.1.6 Calculation of degree of crystallinity

When the baseline is constructed for all isothermal and non-isothermal cases, the next step is calculation of the enthalpy of crystallization at any time during the crystallization. This is achieved via calculation of the area between the heat flow rate peak and the constructed baseline, from the onset of crystallization to the current time.

$$\Delta H(t) = \int_{t_1}^{t} \frac{dH}{dt} dt \qquad \textbf{(3-1)}$$

In Equation (3-1), $\frac{dH}{dt}$ is the heat flow rate, t_1 is the time at the onset of crystallization and t is the current time. Using the enthalpy of crystallization values obtained from Equation (3-1), mass fraction crystallinity is calculated as

$$X_{mc}(t) = \frac{\Delta H(t)}{(1 - X_{mr}) H_f^0} \qquad \textbf{(3-2)}$$

where $X_{mc}(t)$ is mass fraction crystallinity, H_f^0 is the theoretical heat of fusion of 100 % crystallized material and X_{mr} is mass fraction of the reinforcing phase. The value of H_f^0 for PEEK

is 130 J/g [19]. The theoretical heat of fusion, H_f^0, is determined using the indirect methods, such as comparison of the DSC and wide angle X-ray scattering (WAXS) results and extrapolation [130]. The volume fraction crystallinity (hereafter referred to as degree of crystallinity or crystallinity) is obtained as

$$X_{vc}(t) = \frac{X_{mc}(t)}{X_{mc}(t) + \frac{\rho_c}{\rho_a}\left(1 - X_{mc}(t)\right)} \qquad \textbf{(3-3)}$$

In Equation (3-3), ρ_c and ρ_a are the densities of the crystalline phase and the amorphous phase, respectively. For PEEK material, typical values of ρ_c and ρ_a are reported [19] as 1.40 g/cm^3 and 1.26 g/cm^3, respectively. Since these density values are temperature dependent, using these nominal values is another source of uncertainty in crystallinity calculations. X_{vc} which is the volume fraction crystallinity (or crystallinity) will be denoted by X hereafter in this thesis.

Figure 3-6 shows the crystallinity vs time for nine isothermal DSC experiments. The constructed baselines are also shown in the plots.

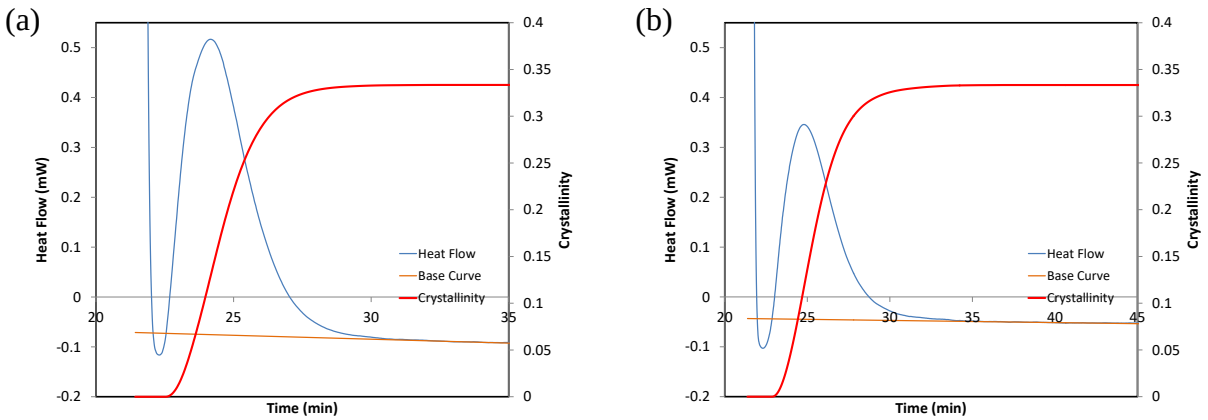

(c)

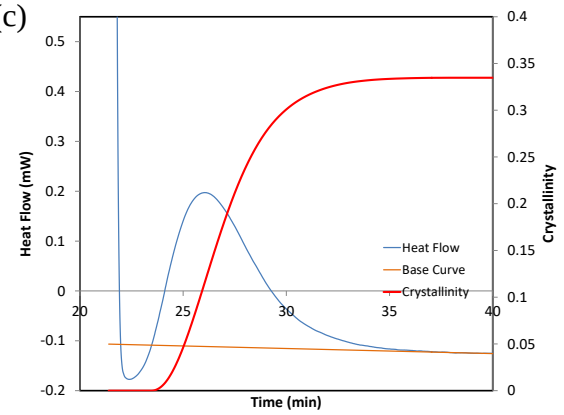
Heat Flow (mW)
Crystallinity
Time (min)
Heat Flow
Base Curve
Crystallinity

(d)

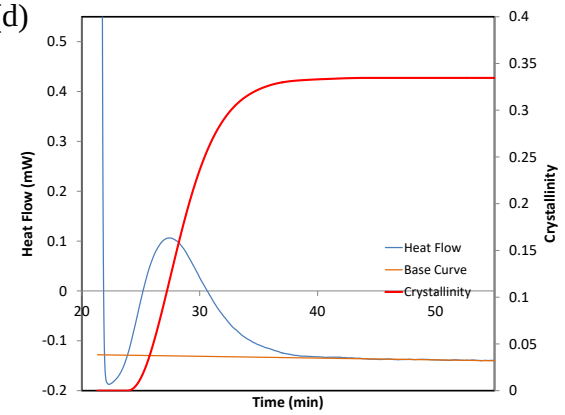
Heat Flow (mW)
Crystallinity
Time (min)
Heat Flow
Base Curve
Crystallinity

(e)

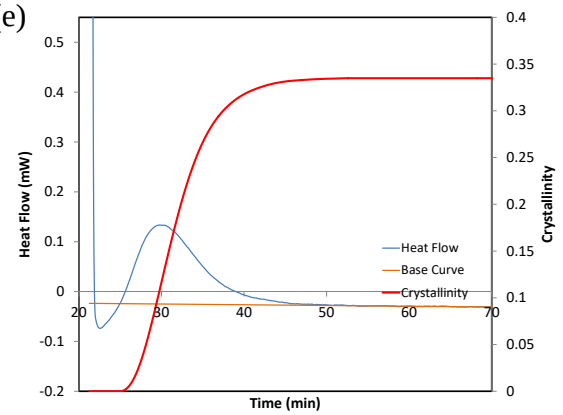
Heat Flow (mW)
Crystallinity
Time (min)
Heat Flow
Base Curve
Crystallinity

(f)

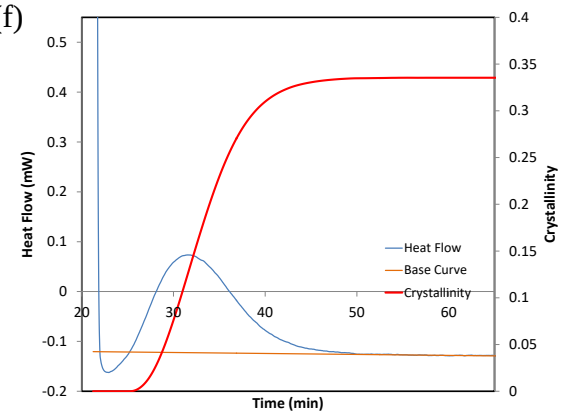
Heat Flow (mW)
Crystallinity
Time (min)
Heat Flow
Base Curve
Crystallinity

(g)

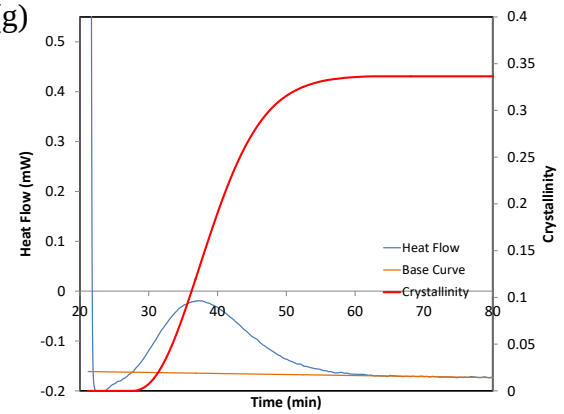
Heat Flow (mW)
Crystallinity
Time (min)
Heat Flow
Base Curve
Crystallinity

(h)

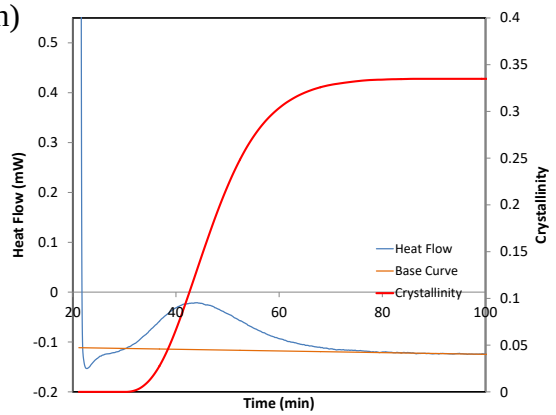
Heat Flow (mW)
Crystallinity
Time (min)
Heat Flow
Base Curve
Crystallinity

(i)

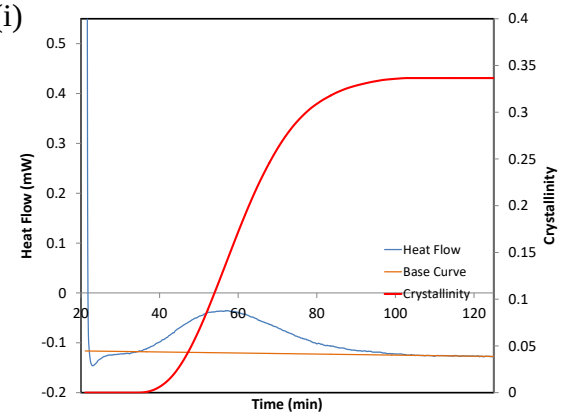

Figure 3-6 Variation of crystallinity with time for isothermal DSC experiments at (a) 305 ℃, (b) 307 ℃, (c) 310 ℃, (d) 312 ℃, (e) 315 ℃, (f) 317 ℃, (g) 320 ℃, (h) 322 ℃, (i) 325 ℃

The time origin has been arbitrarily chosen as the time where the sample temperature is 343 ℃ (T_m^0, the equilibrium melting temperature for PEEK). Variation of crystallinity with time for different isothermal cases are compared in Figure 3-7.

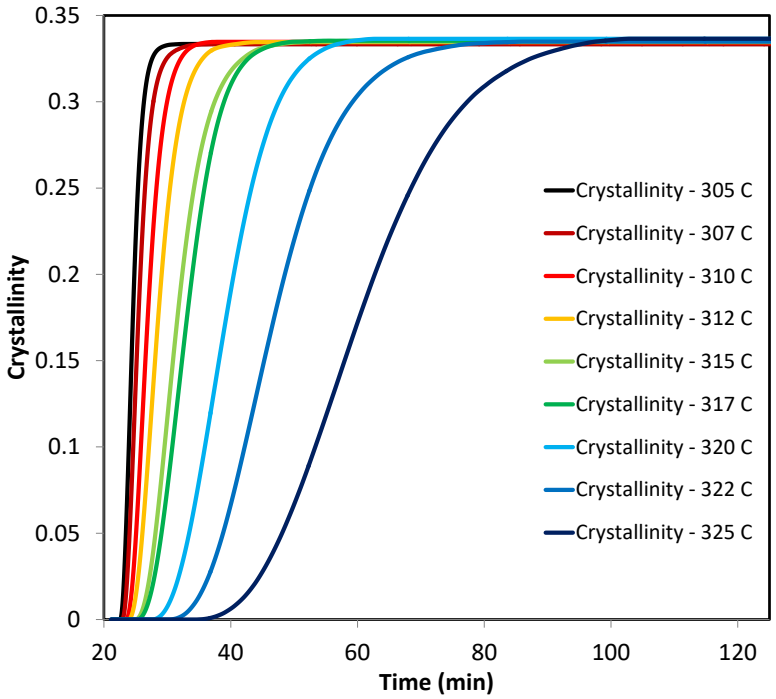

Figure 3-7 Isothermal crystallinity growth at different temperatures

Results in Figure 3-7 show that for all temperatures in the investigated temperature range, the maximum degree of crystallinity is approximately 0.34. For all cases, an induction time or incubation period exists prior to the crystallization growth. This induction time is higher for higher crystallization temperatures.

The crystallinity growth versus time for cold crystallization at different heating rates and melt crystallization for different cooling rates are given in Figure 3-8 and Figure 3-9, respectively.

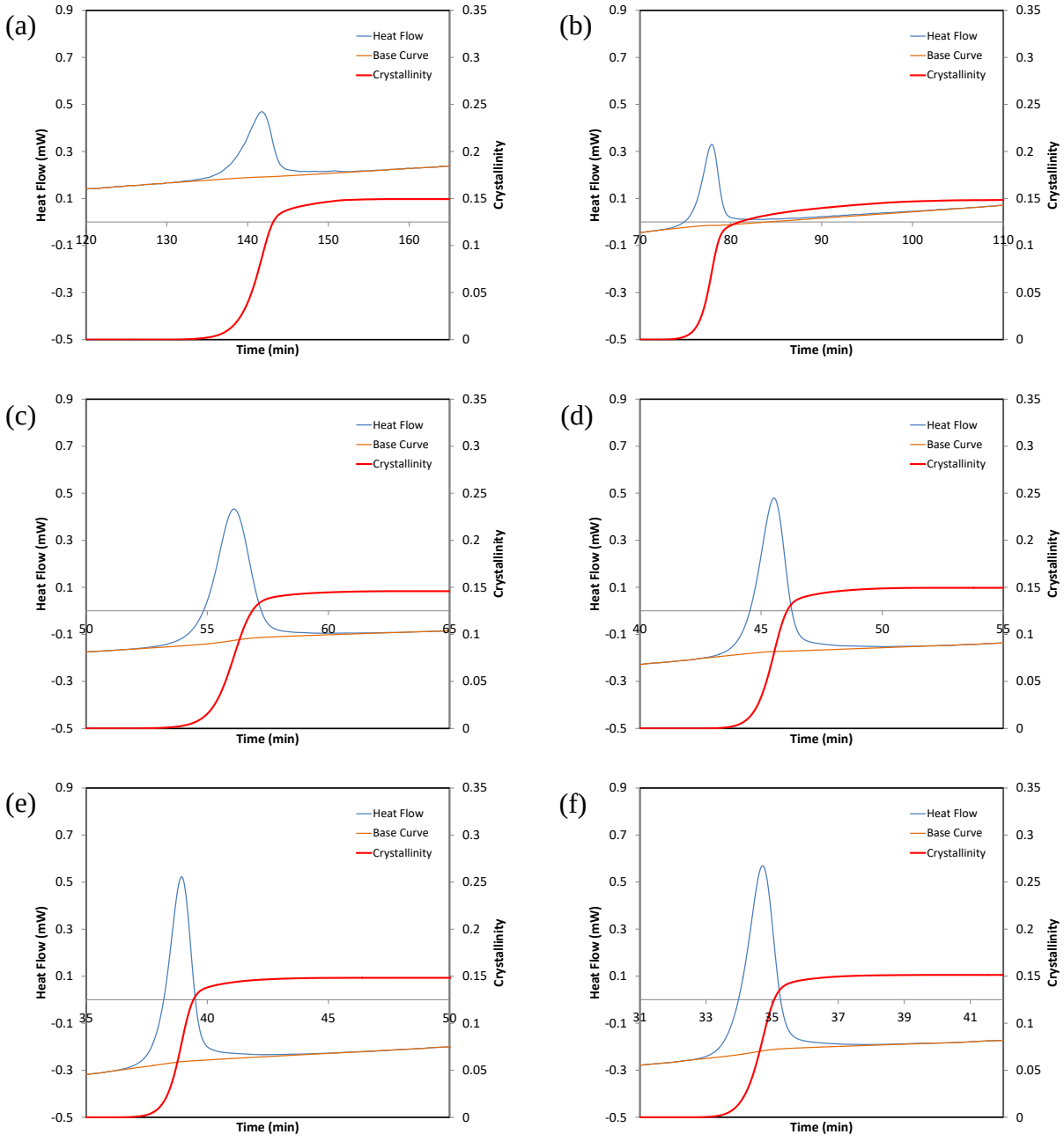
(a)
Heat Flow
Base Curve
Crystallinity
Heat Flow (mW)
Crystallinity
Time (min)
(b)
Heat Flow
Base Curve
Crystallinity
Heat Flow (mW)
Crystallinity
Time (min)
(c)
Heat Flow
Base Curve
Crystallinity
Heat Flow (mW)
Crystallinity
Time (min)
(d)
Heat Flow
Base Curve
Crystallinity
Heat Flow (mW)
Crystallinity
Time (min)
(e)
Heat Flow
Base Curve
Crystallinity
Heat Flow (mW)
Crystallinity
Time (min)
(f)
Heat Flow
Base Curve
Crystallinity
Heat Flow (mW)
Crystallinity
Time (min)

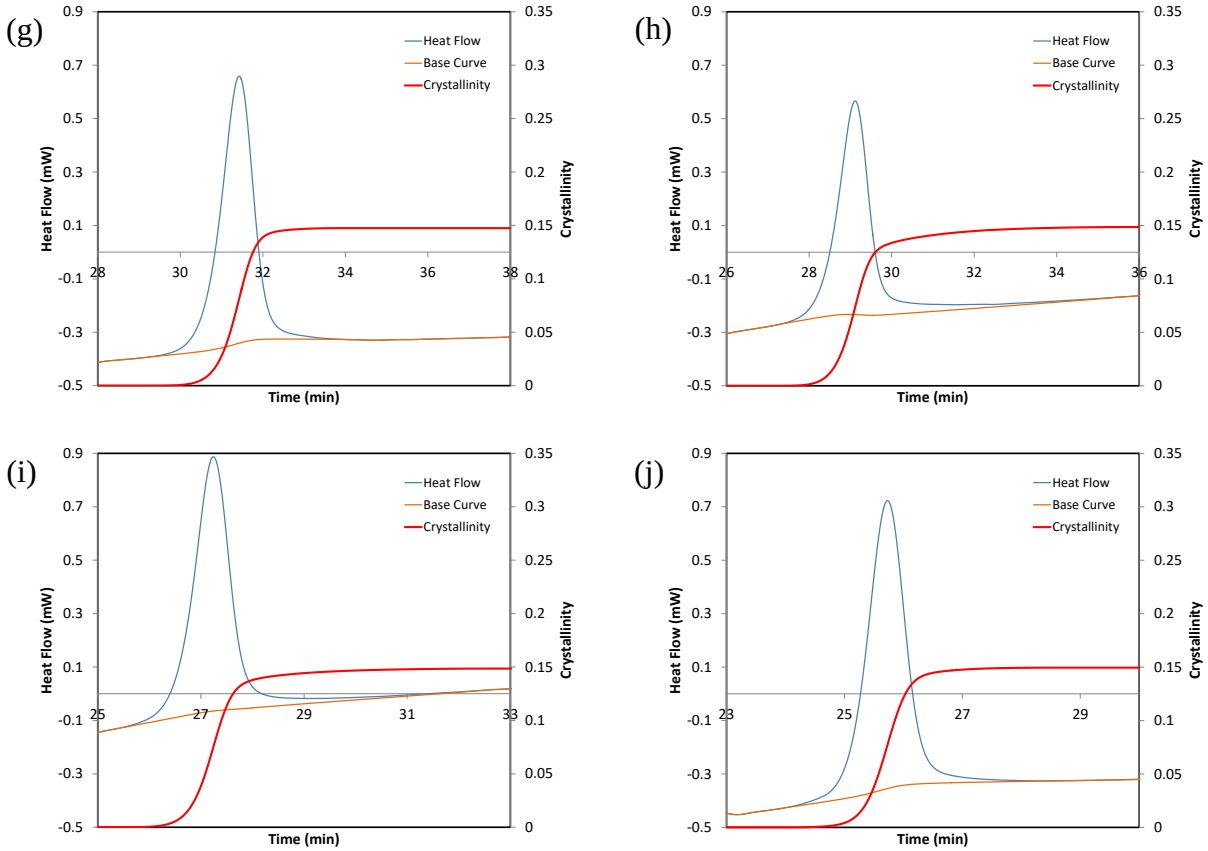

Figure 3-8 Cold crystallization of the as-received material whilst heating at (a) 1 ℃/min, (b) 2 ℃/min, (c) 3 ℃/min, (d) 4 ℃/min, (e) 5 ℃/min, (f) 6 ℃/min, (g) 7 ℃/min, (h) 8 ℃/min, (i) 9 ℃/min, (j) 10 ℃/min

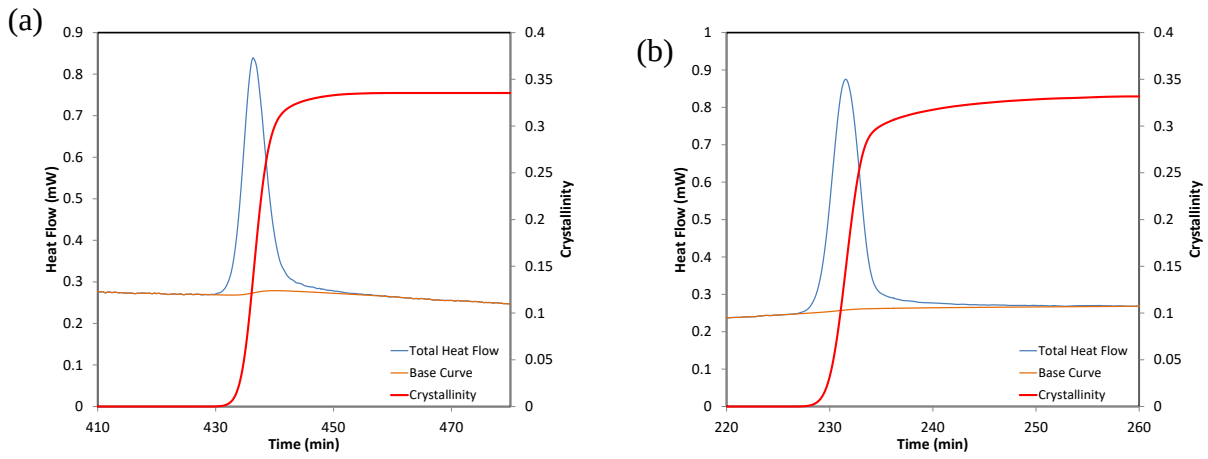

(c)

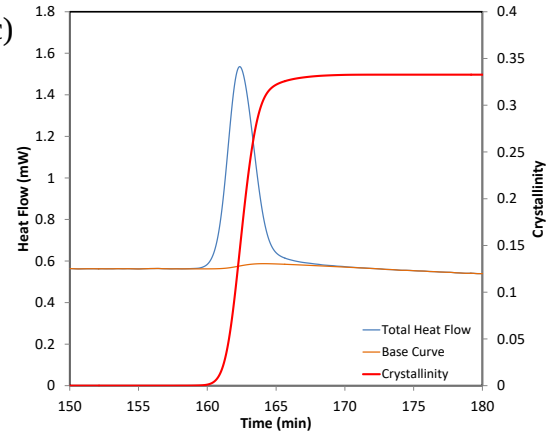
Heat Flow (mW)
Crystallinity
Time (min)
Total Heat Flow
Base Curve
Crystallinity

(d)

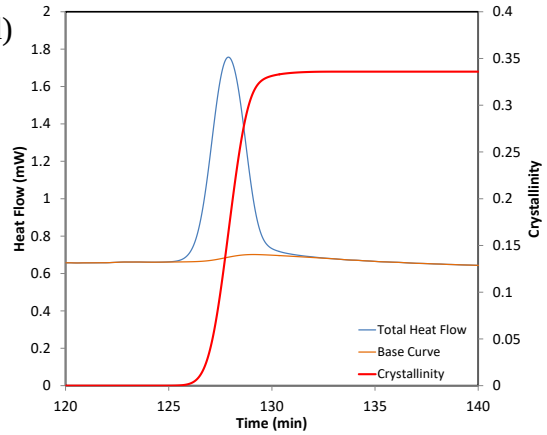
Heat Flow (mW)
Crystallinity
Time (min)
Total Heat Flow
Base Curve
Crystallinity

(e)

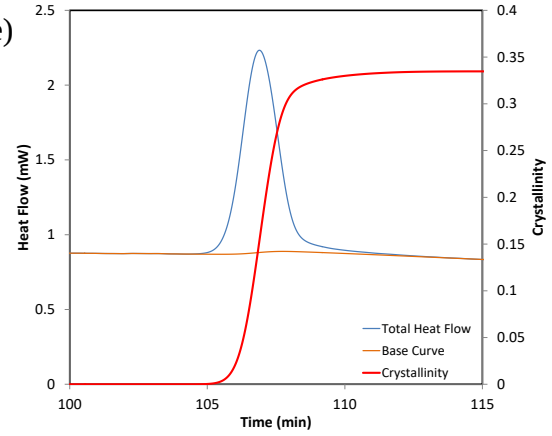
Heat Flow (mW)
Crystallinity
Time (min)
Total Heat Flow
Base Curve
Crystallinity

(f)

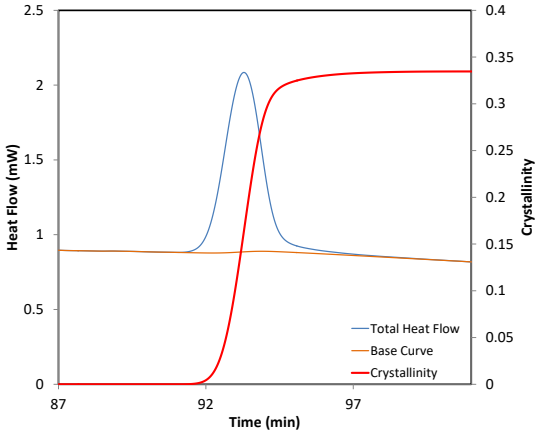
Heat Flow (mW)
Crystallinity
Time (min)
Total Heat Flow
Base Curve
Crystallinity

(g)

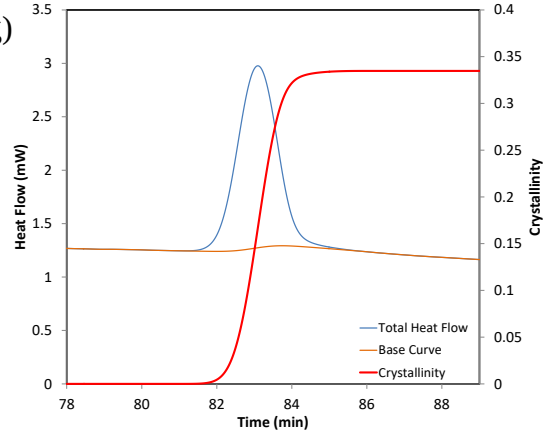
Heat Flow (mW)
Crystallinity
Time (min)
Total Heat Flow
Base Curve
Crystallinity

(h)

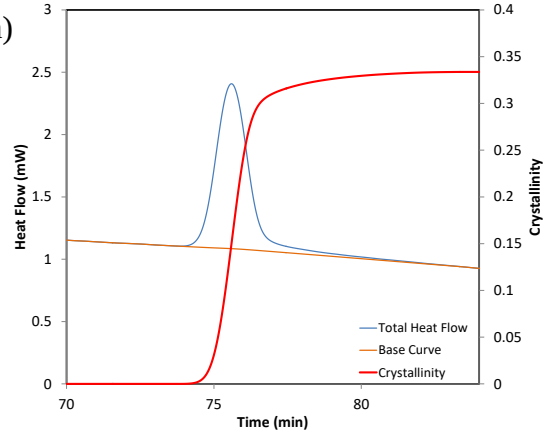
Heat Flow (mW)
Crystallinity
Time (min)
Total Heat Flow
Base Curve
Crystallinity

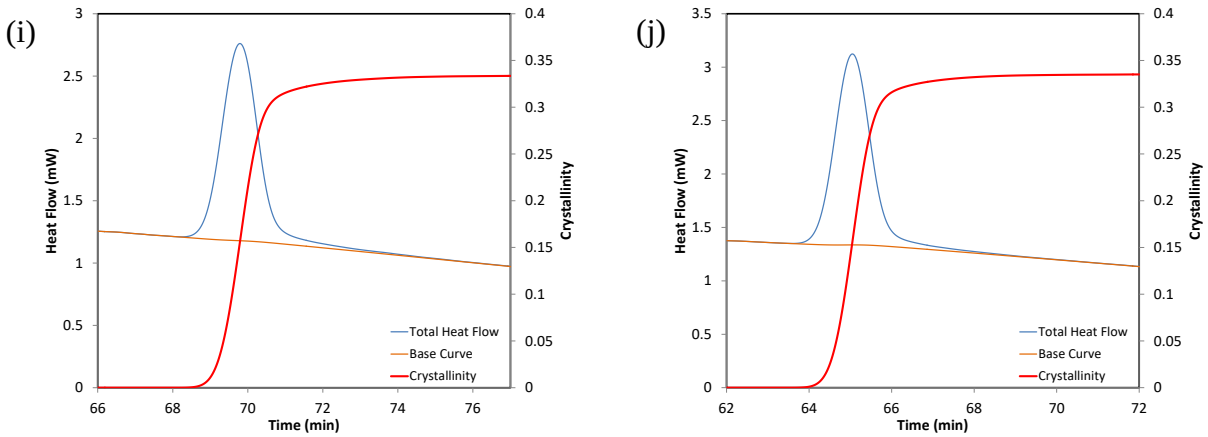

Figure 3-9 Melt crystallization of the material whilst cooling at (a) 1 ℃/min, (b) 2 ℃/min, (c) 3 ℃/min, (d) 4 ℃/min, (e) 5 ℃/min, (f) 6 ℃/min, (g) 7 ℃/min, (h) 8 ℃/min, (i) 9 ℃/min, (j) 10 ℃/min

Similar to the isothermal cases, the time origin for melt crystallization is set where the material temperature reaches $T_m^0 = 343$ ℃. Moreover, in the investigated cooling rate range, the maximum crystallinity for all melt crystallized samples is 0.34. Variation of crystallinity with temperature for different cooling rates are compared in Figure 3-10.

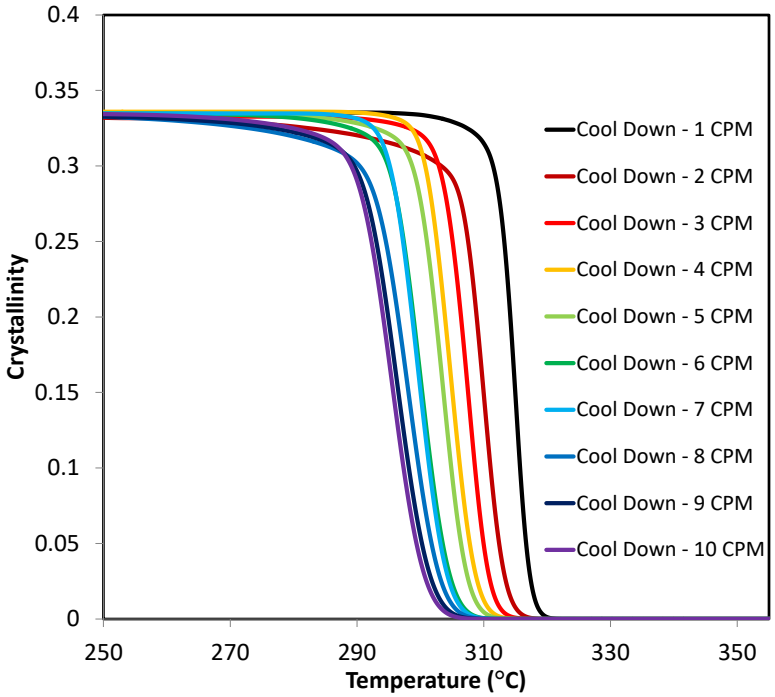

Figure 3-10 Variation of crystallinity with temperature at different cooling rates

From Figure 3-10 it is easily seen that at higher cooling rates, the crystallization starts at lower temperatures.

3.2 Crystallization kinetics analysis and modelling

In this section the kinetics of crystallization is investigated. The aim of kinetics investigations is to find a functional relationship which may be used to quantitatively predict the crystallinity for a temperature cycle. Since a material point during a process may undergo an arbitrary temperature

profile, path independence of the models is very important and therefore, differential form or rate-type kinetics models are more desirable. A general rate-type model is written as

$$\frac{dX}{dt} = g(X,T) \qquad \textbf{(3-4)}$$

Initially, we assume that the right-hand side of Equation (3-4) is separable. This equation is rewritten as

$$\frac{dX}{dt} = k(T)f(X) \qquad \textbf{(3-5)}$$

In this section, we reduce the experimental data from the isothermal and non-isothermal DSC experiments to obtain a functional form of Equation (3-5).

3.2.1 Crystallization rate iso-conversionals

To investigate the functional form of the crystallization rate, we start by studying the temperature dependence, $k(T)$. To do this, we extract plots of $\ln\left(\frac{dX}{dt}\right)$ versus temperature for different degrees of crystallinity from all the experimental data. At each degree of crystallinity, plots from isothermal crystallization, non-isothermal cold crystallization and non-isothermal melt

crystallization data are overlaid on the same graph. These graphs are often called 'iso-conversionals'. The iso-conversionals for some specific degrees of crystallinity are given in Figure 3-11.

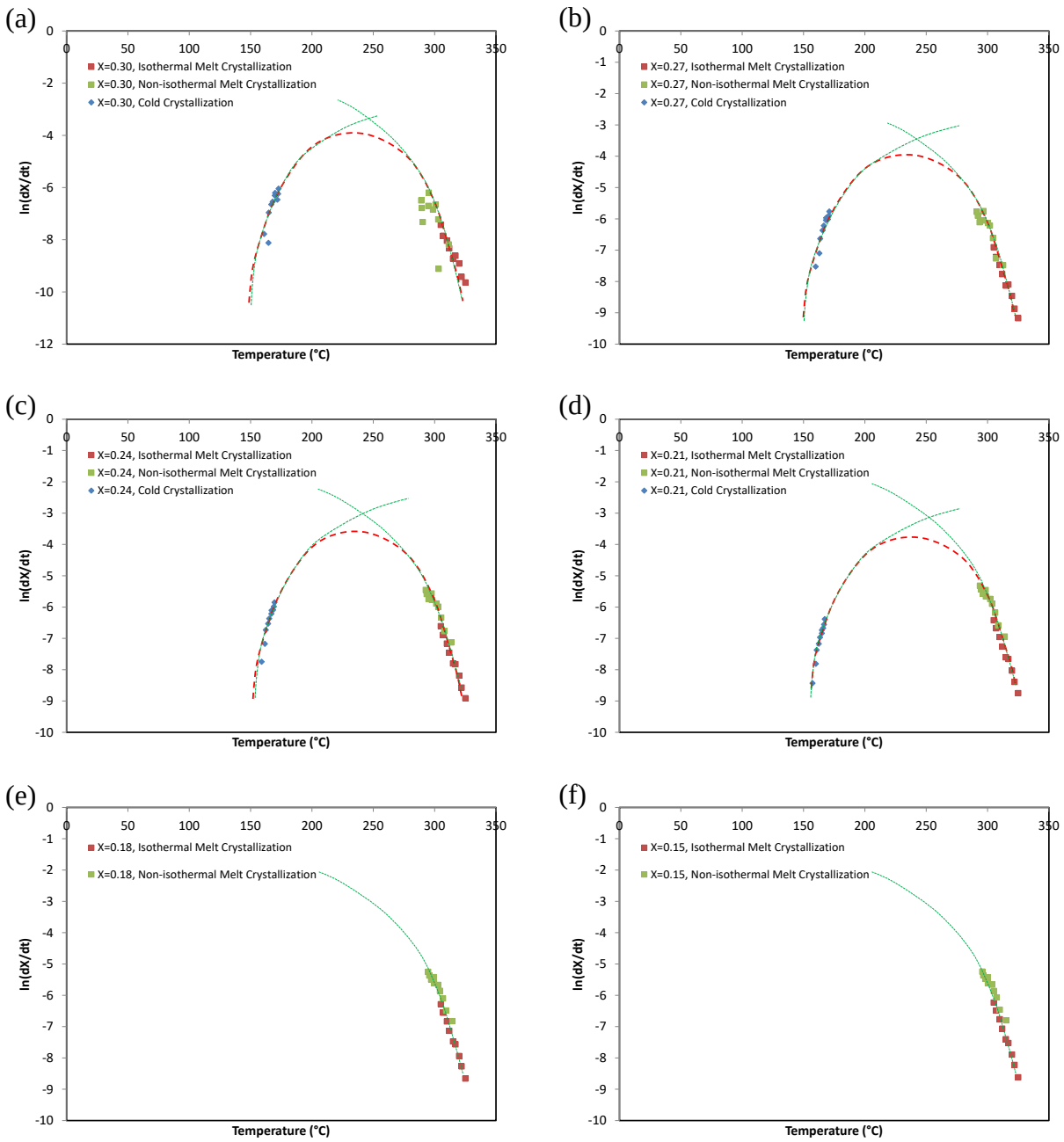

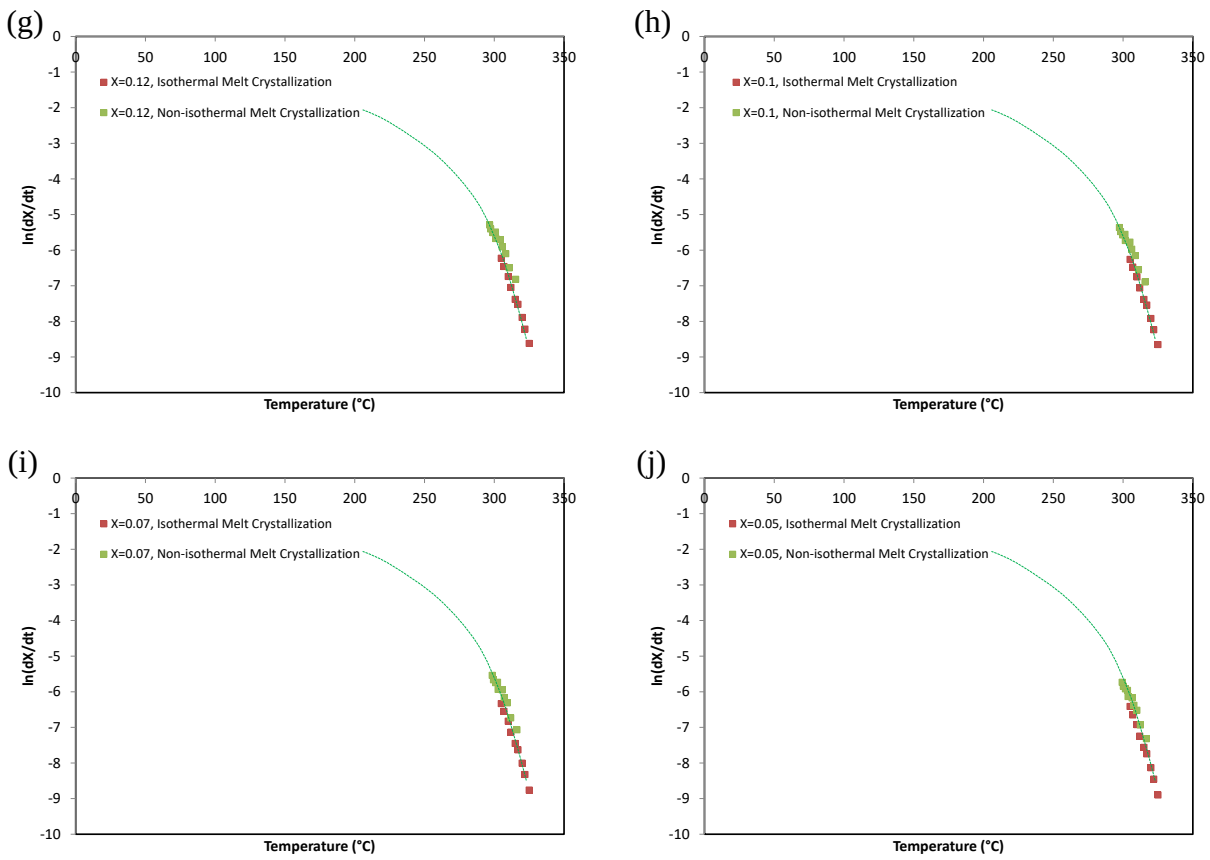

Figure 3-11 Iso-conversionals overlaid from isothermal crystallization, non-isothermal cold crystallization and non-isothermal melt crystallization at (a) X=0.3, (b) X=0.27, (c) X=0.24, (d) X=0.21, (e) X=0.18, (f) X=0.15, (g) X=0.12, (h) X=0.1, (i) X=0.07, (j) X=0.05

Degree of crystallinity in the as-received material is 0.18. Therefore, in Figure 3-11, for degrees of crystallinity less than 0.18, there is no cold crystallization and only the data from isothermal melt crystallization and non-isothermal melt crystallization are overlaid. From these plots it is concluded that there is no significant difference between isothermal and non-isothermal melt crystallization mechanisms. A green dotted curve is sketched through the isothermal and non-isothermal melt crystallization data on each graph to show that these data points are falling on the

same curve. For degrees of crystallinity more than 0.18, in addition to the data from isothermal melt crystallization and non-isothermal melt crystallization, there are data points from non-isothermal cold crystallization on the left side of the graph. A dotted green curve is sketched through the cold crystallization data.

3.2.2 Crystallization rate temperature dependence

From the right side of plots in Figure 3-11, it is concluded that with decreasing temperature, or increasing degree of undercooling, $T_m^0 - T$, the crystallization rate increases. The data on the left side of the graphs are extracted from the cold crystallization experiments. From these results it is implied that by increasing the temperature, farther from the glass transition temperature, the rate of cold crystallization increases. Given that the same mechanism that drives the cold crystallization must slow down the melt crystallization (mobility/lack of mobility of molecular chains), it is concluded that approaching the glass transition temperature, or decreasing $T - T_g$, decreases the crystallization rate. Based on the discussion given above, it is assumed that the crystallization rate has a temperature dependence of the form [131]

$$k(T) = k_0 e^{-\frac{E_g}{R(T-T_g)}} e^{-\frac{E_m}{R(T_m^0-T)}} \quad \textbf{(3-6)}$$

Equation (3-6), which is schematically shown as a dashed red 'horse shoe' form curve on each graph, indicates that as the temperature is changed, there are two competing mechanisms that affect

the rate of crystallization. These horse shoe form curves are similar to C-shape curves in Time-Temperature-Transformation (TTT) diagrams [132].

In Equation (3-6), k_0 is the pre-exponential factor and $-\frac{E_g}{R}$ and $-\frac{E_m}{R}$ are model constants. Using Equation (3-6), Equation (3-5) may be rewritten as

$$\ln\left(\frac{dX}{dt}\right) = \ln\left(k_0 f(X)\right) - \frac{E_g}{R\left(T - T_g\right)} - \frac{E_m}{R(T_m^0 - T)} \qquad \textbf{(3-7)}$$

Fitting Equation (3-7) to the iso-conversionals, $-\frac{E_g}{R}$, $-\frac{E_m}{R}$ and $k_0 f(X)$ may be found. Different methods can be used for the fitting procedure. Here, first a constant value has been assumed for $-\frac{E_g}{R}$. Then at each degree of crystallinity, tables of $\ln\left(\frac{dX}{dt}\right) + \frac{E_g}{R(T-T_g)}$ versus $\frac{1}{(T_m^0-T)}$ are generated and $-\frac{E_m}{R}$ and $\ln\left(k_0 f(X)\right)$ are estimated as the slope and the intercept in a linear regression analysis. Next, based on the goodness of this linear regression, the assumed value of $-\frac{E_g}{R}$ is modified and the procedure is repeated until a good fit is obtained. The final best fit values are shown in Figure 3-12 to Figure 3-14.

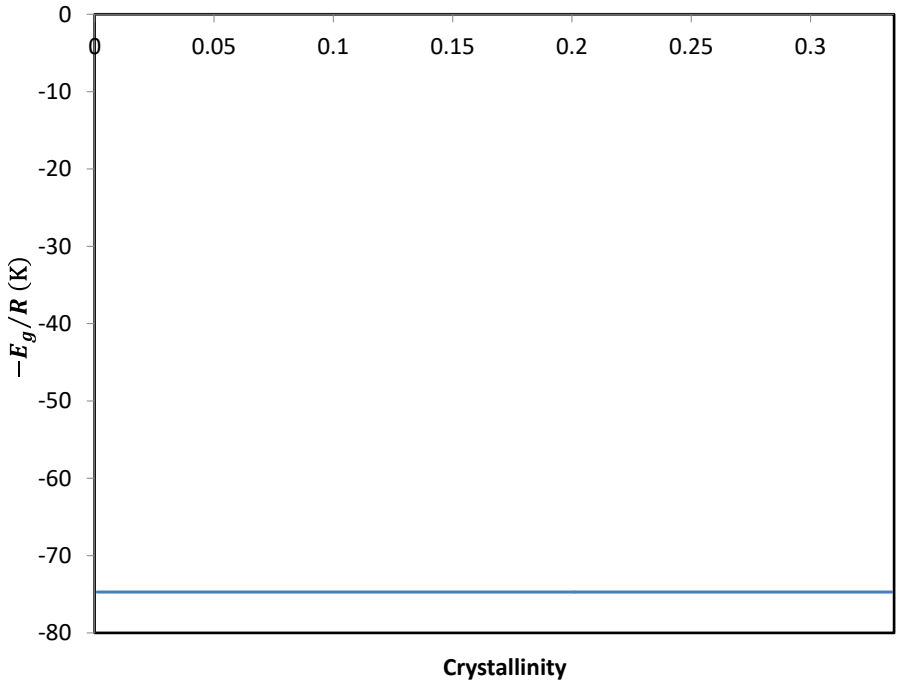

Figure 3-12 A constant value is assumed for $-\frac{E_g}{R}$ and modified by trial and error

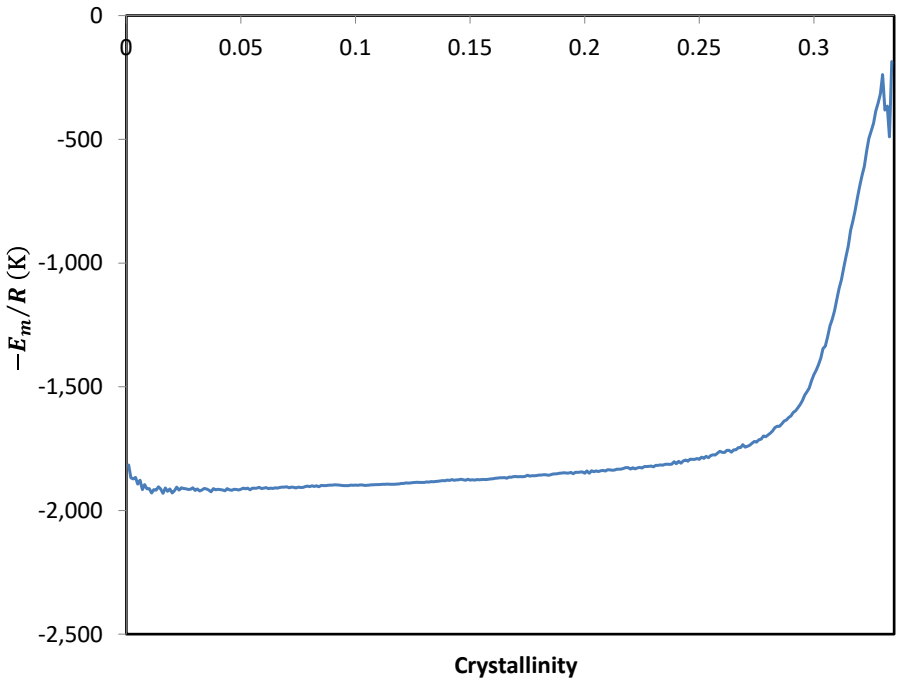

Figure 3-13 Values of $-\frac{E_m}{R}$ obtained from best fit

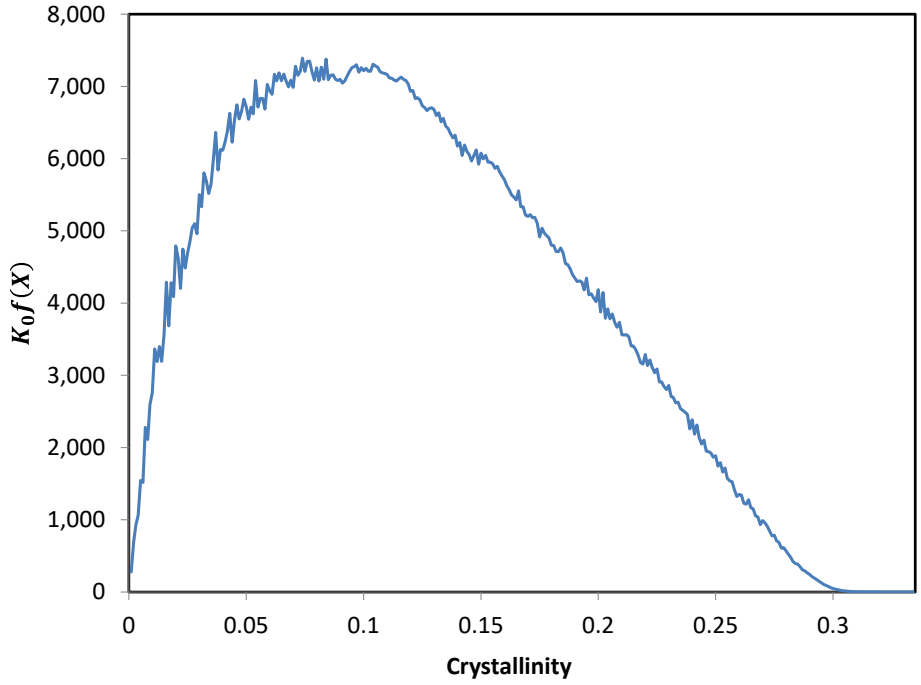

Figure 3-14 Values of $k_0 f(X)$ obtained from best fit

From Figure 3-13 it is recognized that $-\frac{E_m}{R}$ does not have a constant value and is crystallinity dependent. Considering this, Equations (3-6) and (3-5) are revised as

$$\frac{dX}{dt} = k_0 f(X) e^{-\frac{E_g(X)}{R(a_g T_g + b_g T + c_g)}} e^{-\frac{E_m(X)}{R(a_m T_m^0 + b_m T + c_m)}} \quad \textbf{(3-8)}$$

The constants $a_g, b_g, c_g, a_m, b_m,$ and c_m are considered for improving the quality of the predictions. The common approach in process modelling is finding a functional form for $f(X)$.

However, since the crystallinity dependence is observed in $-\frac{E_m}{R}$, it is more practical to provide the values of $k_0 f(X)$, $-\frac{E_m}{R}$ and $-\frac{E_g}{R}$, given in Figure 3-12 to Figure 3-14, as look-up data for different values of crystallinity. The constants $a_g, b_g, c_g, a_m, b_m,$ and c_m are given in Table 3-1.

Table 3-1 Parameters for Equation (3-8), obtained from best fit

a_g	b_g	c_g	a_m	b_m	c_m
-1	1	0	1.07	-1	50

This modelling approach is a 'semi model-free' method, similar to the approach introduced by Vyazovkin [126]. Equation (3-8) along with the look-up data can be used for prediction of the crystallization rate for an arbitrary temperature and X combination.

3.2.3 Induction time

The results in Figure 3-6 and Figure 3-9 indicate that an induction time or incubation period exists prior to the crystallization growth. Prediction of the induction time is significant in crystallization modelling in that it determines the time where the Equation (3-8) becomes active. From Figure 3-6 and Figure 3-9, it is seen that in isothermal crystallization, the induction time is higher for

higher temperatures. Also in non-isothermal melt crystallization, the induction time decreases by increasing the cooling rate.

Godovsky [133] suggested a simple empirical model for induction time in isothermal crystallization as

$$t_i = t_m(T_m^0 - T)^{-c} \quad \textbf{(3-9)}$$

In Equation (3-9), t_i is the isothermal induction time and t_m and c are empirical model fitting parameters. Fitting this model to measured induction times from isothermal DSC experiments, results in the fitting parameters as given in Table 3-2.

Table 3-2 Fitting parameters for Equation (3-9)

$\boldsymbol{t_m}$	$\boldsymbol{c}$
$\mathbf{1.20 \times 10^6}$	3.99

The measured induction time values and the predicted values using Equation (3-9) and the parameters in Table 3-2 are compared in Figure 3-15. In the experiments, the induction time is arbitrarily considered as the time where $X = 0.001$, a small but measurable value.

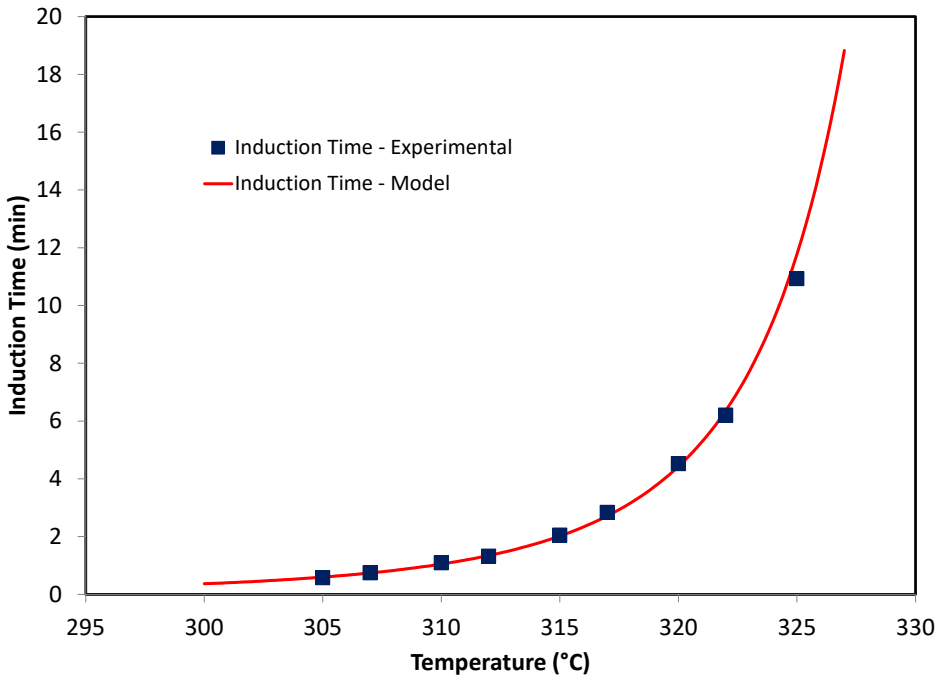

Figure 3-15 Induction time values for isothermal DSC experiments, measured and model predicted

Figure 3-15 shows that the model predictions are in good agreement with the measured values.

The concept of 'additivity', from the phase transitions of metals, is adopted here for prediction of the induction time during non-isothermal conditions. According to Christian [132], the principle of additivity states that "the total time required to reach a specific amount of transformation, X_a, is obtained by summing the fractions of time taken to reach this stage isothermally, until the sum reaches a value of one.". Assuming $X_a = 0.001$ (the crystallinity value used for measuring the induction time in both isothermal and non-isothermal experiments), additivity can be used for prediction of induction time. This may be expressed mathematically as

$$\int_0^{t_I} dt/t_i(T) = 1 \qquad \textbf{(3-10)}$$

where $t_i(T)$ is the induction time for isothermal transformation at the temperature T and the upper limit of the integral, t_I, is the induction time for non-isothermal transformation.

Using Equation (3-10) along with Equation (3-9) (and the fitting parameters given in Table 3-2), the induction time for an arbitrary non-isothermal condition can be estimated. In Figure 3-16, the model predictions are compared with the experimental measurements for non-isothermal melt crystallization experiments. The predicted values are in good agreement with experimental measurements.

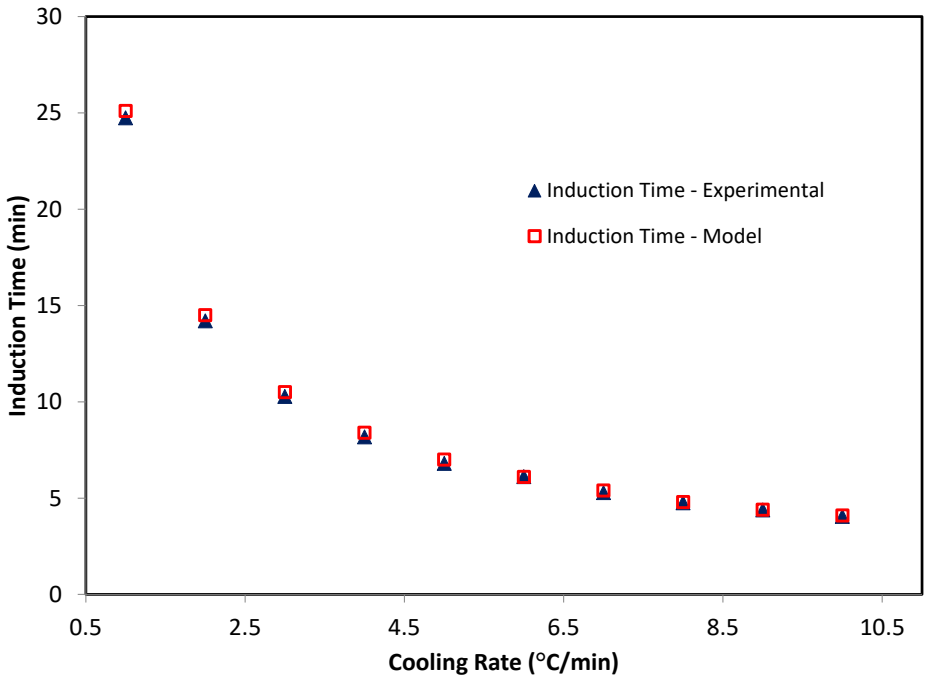

Figure 3-16 Induction times for non-isothermal cool down DSC tests, model predictions and experimental measurements

3.2.4 Summary and goodness of the model

In this section, the rate-type model of Equation (3-8) together with the fitting parameters given in Table 3-2 is used for prediction of crystallinity for a given temperature cycle. Moreover, Equations of (3-9) and (3-10) are used for prediction of the time for the onset of crystallization. It should be addressed that the induction time needs to be taken into account only in situations where the material is fully amorphous, or crystallinity is less than a threshold value, $X_0 = 0.001$. A pseudo-code of the calculation procedure is summarized here. Note that in these equations, a

superscript n is for the value of the variable at the end of the current time step and a superscript $n-1$ is for the value of the variable at the end of the previous time step.

Step 1- Check the value of crystallinity, X.

- If $X < X_0$, then

  - Set $X = X_0$

  - Calculate the induction time, t_I, using the Equations (3-9) and (3-10)

  - Update the time step as $t^n = t^{n-1} + t_I$

  - Go to Step 1

- If $X \geq X_0$, then

  - Update the time step as $t^n = t^{n-1} + \Delta t^n$

  - Calculate the crystallization rate using Equation (3-11)

$$\left(\frac{dX}{dt}\right)^n = k_0 f(X^{n-1}) e^{-\frac{E_g(X^{n-1})}{R(a_g T_g + b_g T^{n-1} + c_g)}} e^{-\frac{E_m(X^{n-1})}{R(a_m T_m^0 + b_m T^{n-1} + c_m)}} \quad \textbf{(3-11)}$$

  - Update the crystallinity value as

$$X^n = X^{n-1} + \Delta t^n \left(\frac{dX}{dt}\right)^n \quad \textbf{(3-12)}$$

Step 2- Go to Step 1

Using the procedure explained above, the values of crystallinity can be predicted for any arbitrary temperature cycle. In Figure 3-17, predicted values of crystallinity for nine isothermal cases are compared with experimental results. From the plots it is evident that the model predictions are in good agreement with the experimental results for both the induction time and the crystallinity growth.

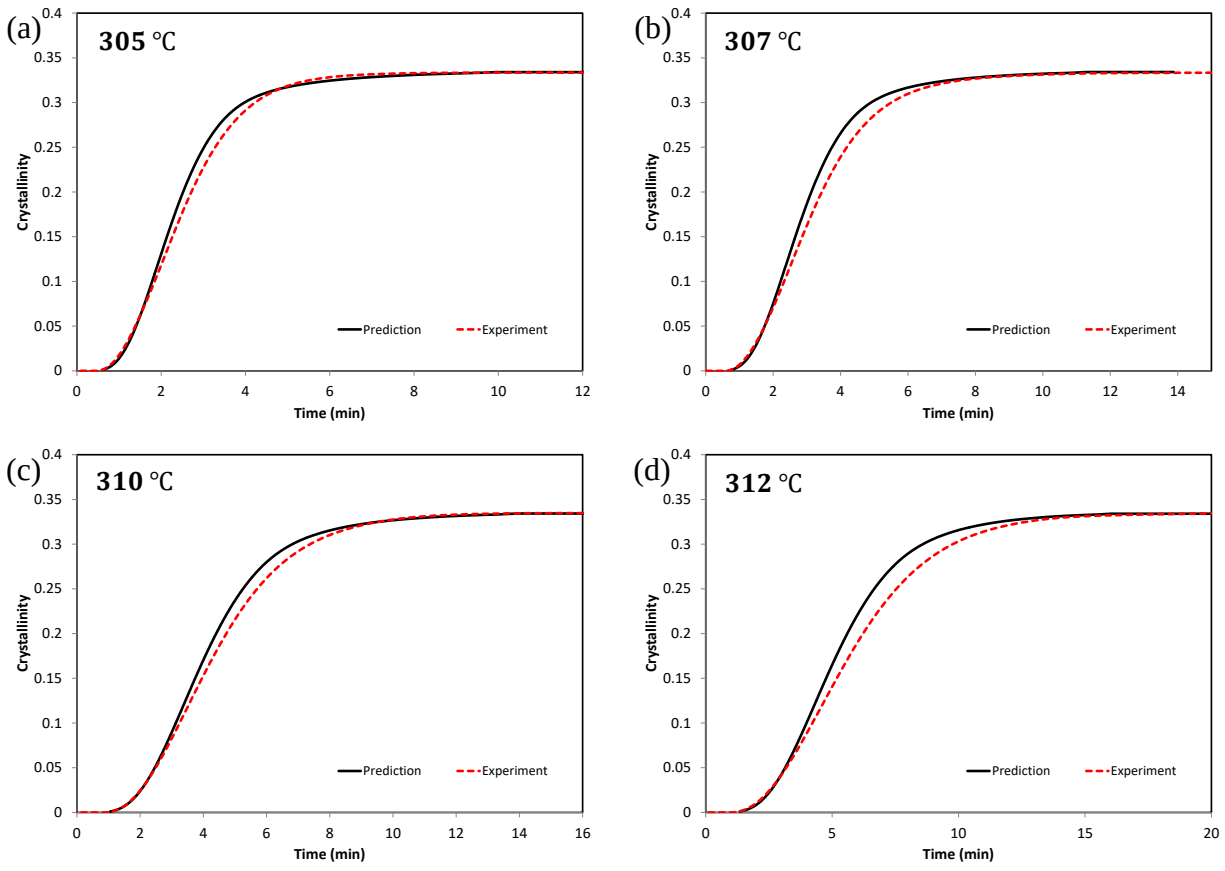

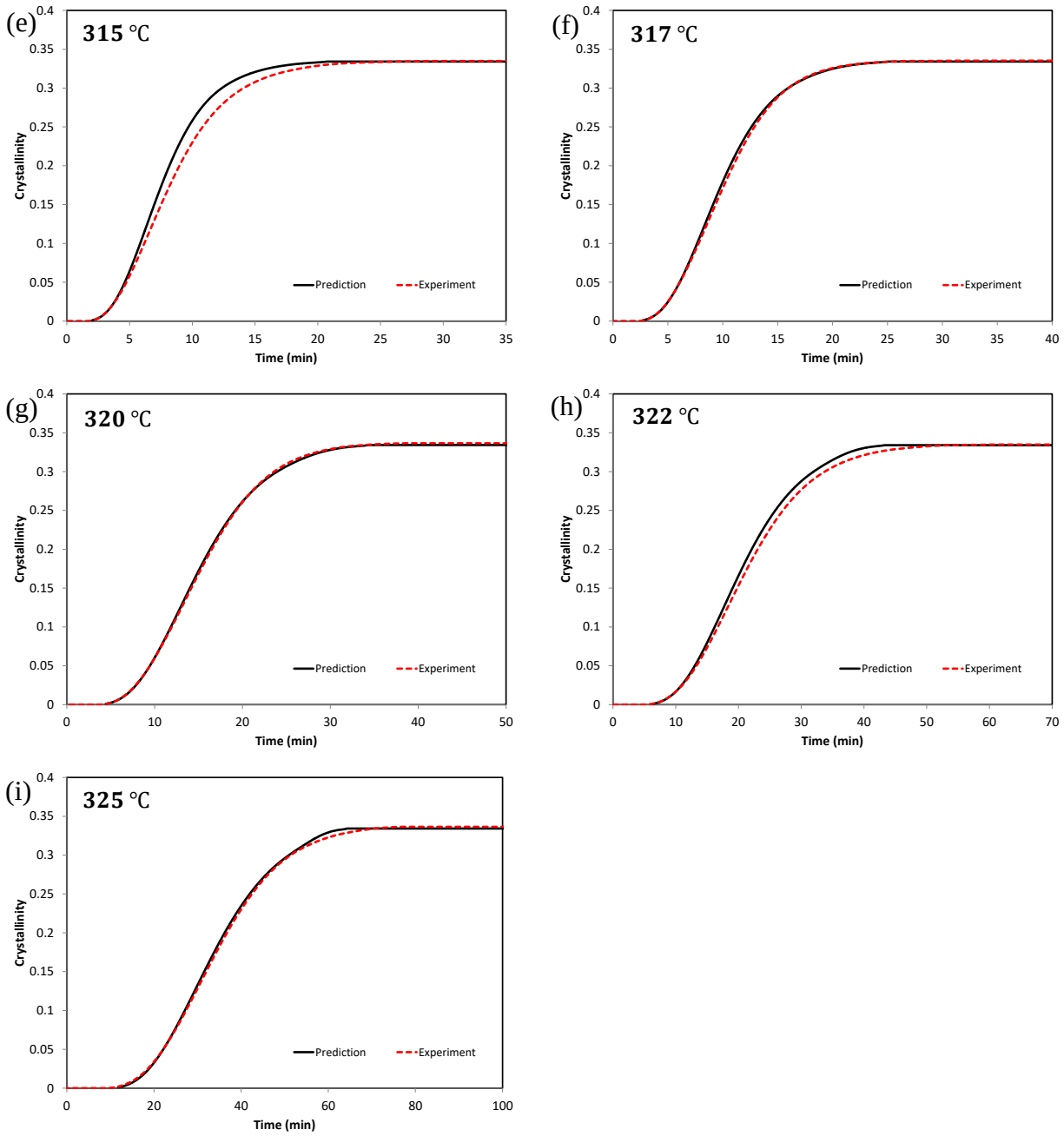

Figure 3-17 Variation of crystallinity with time for isothermal DSC experiments at (a) 305 ℃, (b) 307 ℃, (c) 310 ℃, (d) 312 ℃, (e) 315 ℃, (f) 317 ℃, (g) 320 ℃, (h) 322 ℃, (i) 325 ℃, model predictions and experimental results

A summary of model predictions for isothermal crystallization at different temperatures is shown in Figure 3-18.

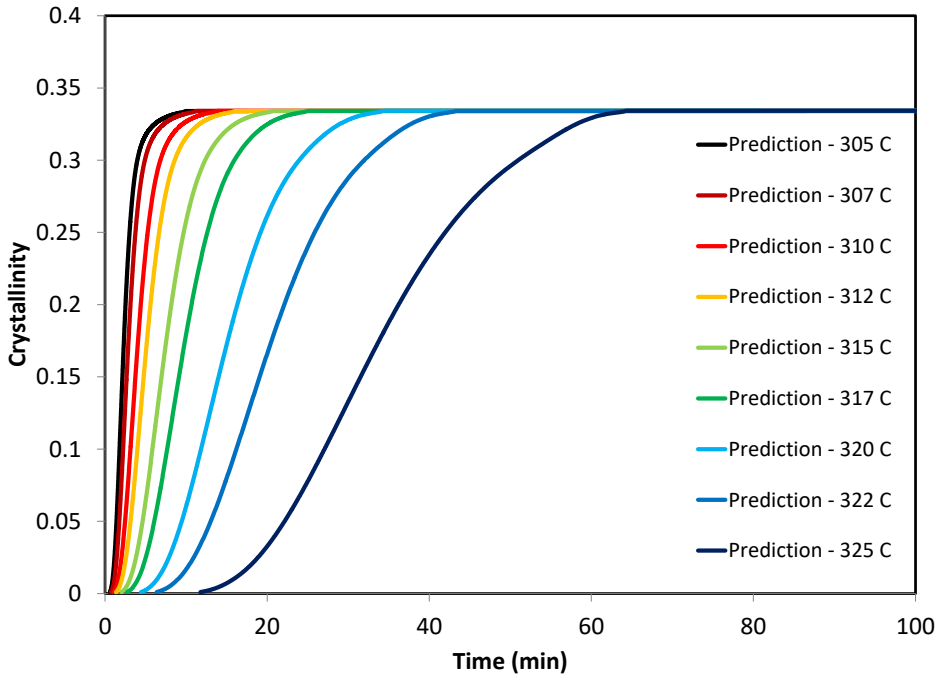

Figure 3-18 Model predictions for isothermal crystallizations at different temperatures

Predicted values of crystallinity versus temperature are compared with experimental results for ten non-isothermal melt crystallization tests in Figure 3-19.

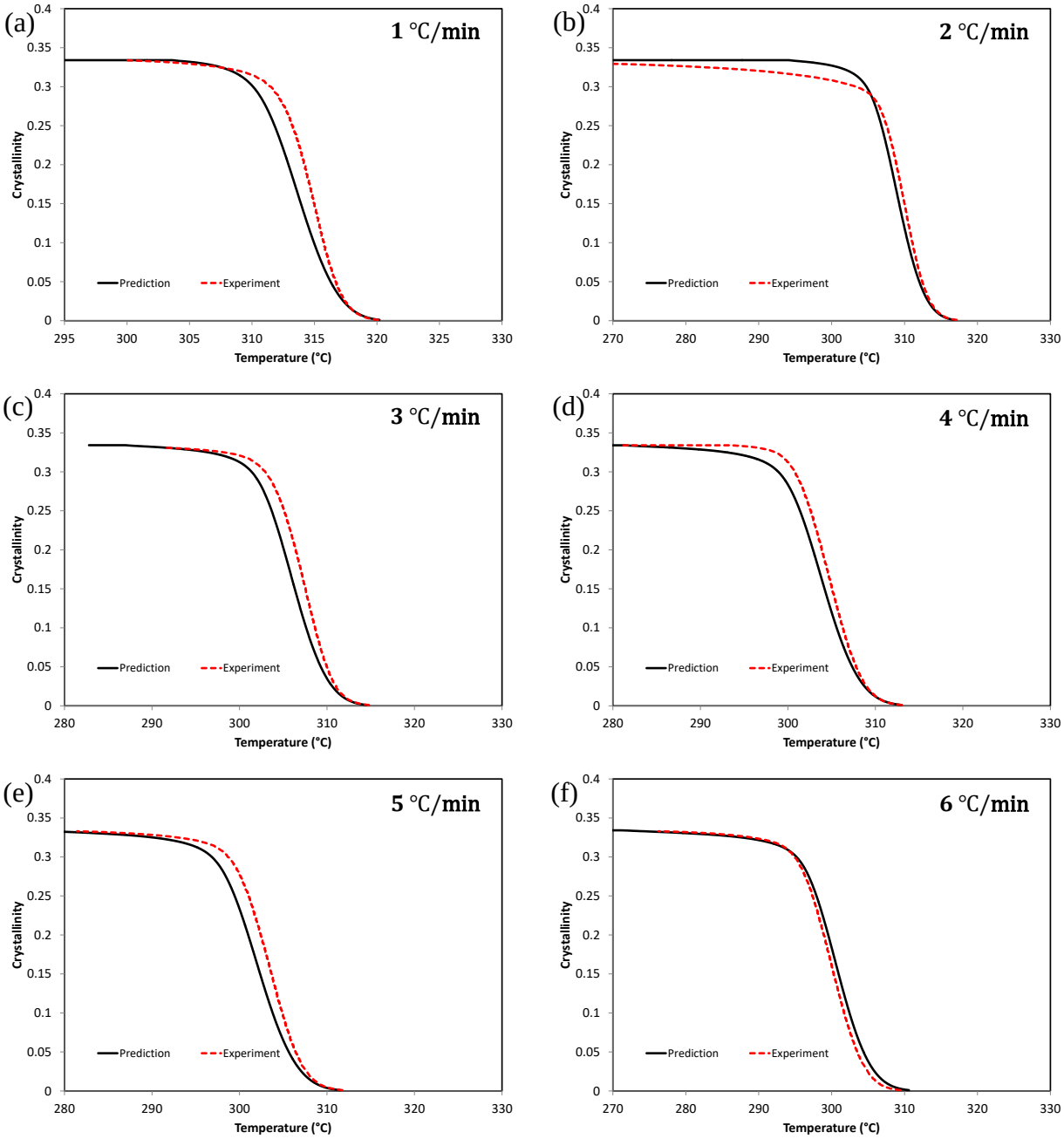
(a)
1 ℃/min
Crystallinity
Temperature (°C)
Prediction
Experiment
(b)
2 ℃/min
Crystallinity
Temperature (°C)
Prediction
Experiment
(c)
3 ℃/min
Crystallinity
Temperature (°C)
Prediction
Experiment
(d)
4 ℃/min
Crystallinity
Temperature (°C)
Prediction
Experiment
(e)
5 ℃/min
Crystallinity
Temperature (°C)
Prediction
Experiment
(f)
6 ℃/min
Crystallinity
Temperature (°C)
Prediction
Experiment

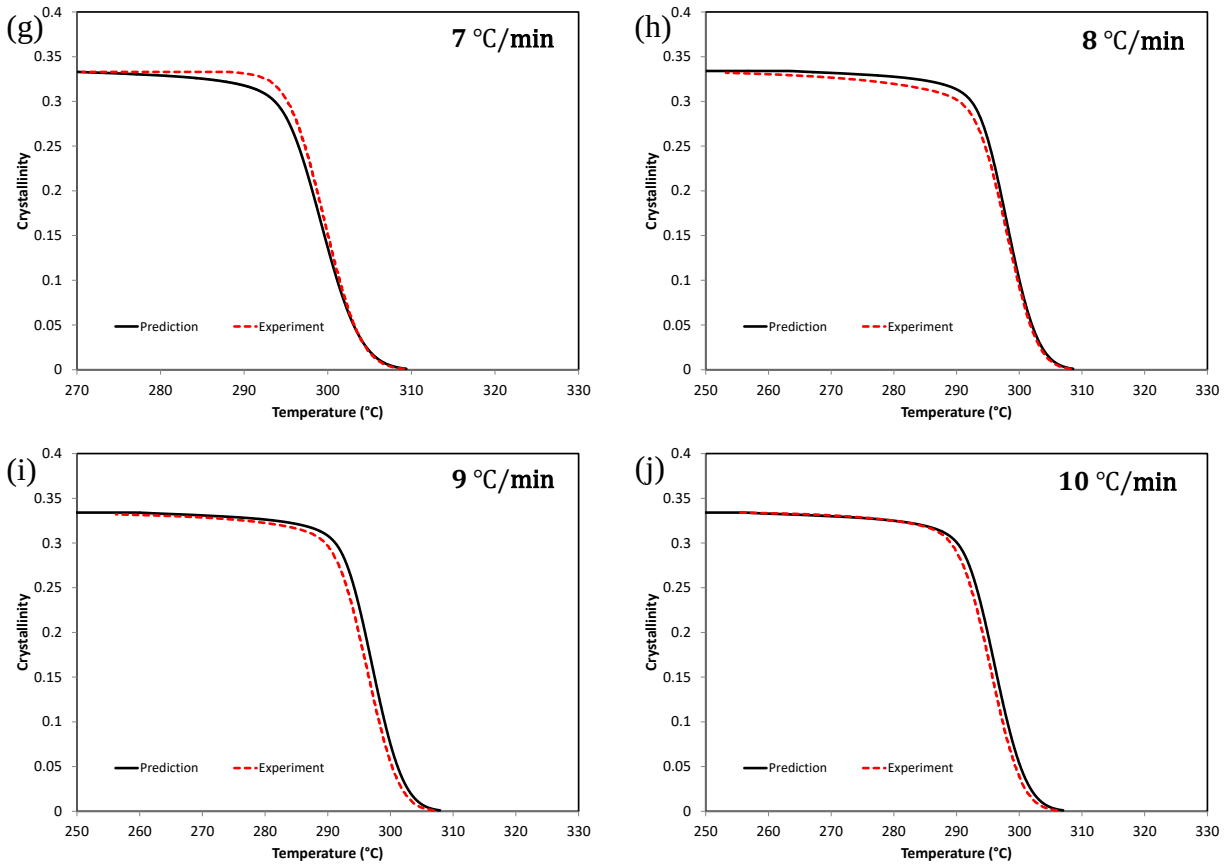

Figure 3-19 Variation of crystallinity with temperature for crystallization of the material whilst cooling at (a) 1 ℃/min, (b) 2 ℃/min, (c) 3 ℃/min, (d) 4 ℃/min, (e) 5 ℃/min, (f) 6 ℃/min, (g) 7 ℃/min, (h) 8 ℃/min, (i) 9 ℃/min, (j) 10 ℃/min, model predictions and experimental results

The results in Figure 3-19 indicate that the model predictions are in good agreement with the experimental results in both the onset temperature and growth. Model predictions for the ten cooling rates are compared in Figure 3-20.

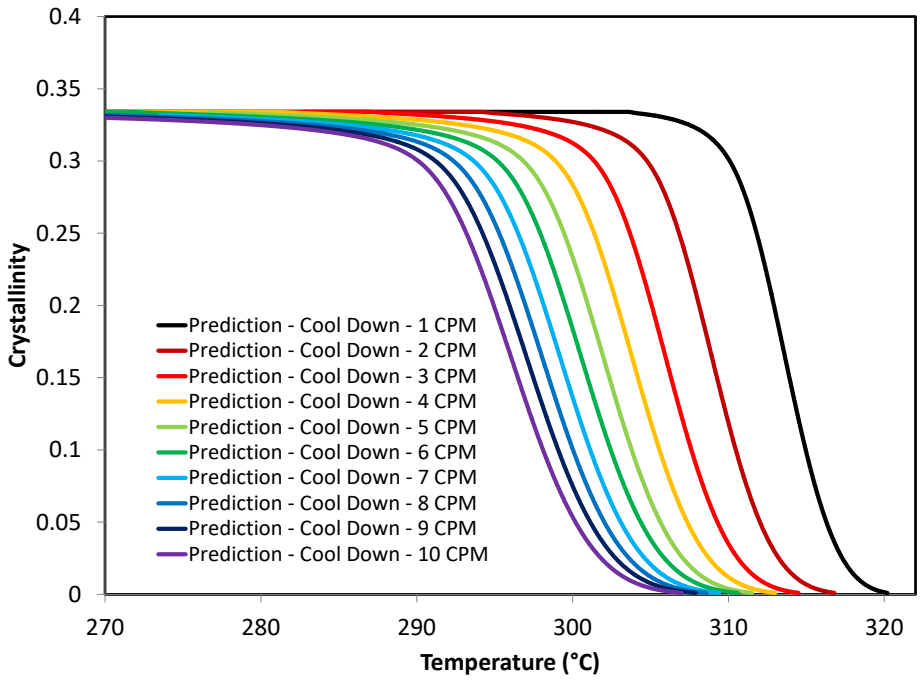

Figure 3-20 Model predicted crystallinity versus temperature for melt crystallization at different cooling rates

3.2.5 Process maps

Process maps are tools for visualization of conversion behaviour over a wide range of temperature and degree of conversion [134]. Having the crystallization kinetics model, process maps can be generated as constant time contours or constant cooling rate contours in the crystallinity-temperature space. Constant time contour graphs are shown in Figure 3-21. The contours illustrate the crystallization data for time between 1 min (inner contour) and 900 min (outer contour). A general overview of these contours show that for short time periods, such as 1 min, the material is never fully crystalline regardless of temperature. This process map can be used for designing processing cycles, such as the time required at each temperature for full

crystallization. A few data points on these graphs are shown in Figure 3-22. From this graph it is easily seen that if a sample is rapidly cooled from the molten state to 295 ℃, the crystallinity in the material is about 20 % after 1 min. On the other hand, if the sample is cooled to 324 ℃, it takes 30 min for the material to become 20% crtstalline. Process maps can also be generated as contours of constant cooling rates. The cooling rates on this map vary between 1 ℃/min and 9000 ℃/min. Looking into these graphs, it is seen that for a cooling rate of 1 ℃/min the material is 20% crystalline at 313 ℃. If the material is cooled down at 200 ℃/min, it is 25% crystalline at 256 ℃. If the cooling rate is increased to 9000 ℃/min, based on the process map, the maximum degree of crystallinity is 7%.

Similar to the constant time contours, constant cooling rate contours can be used for designing processing cycles.

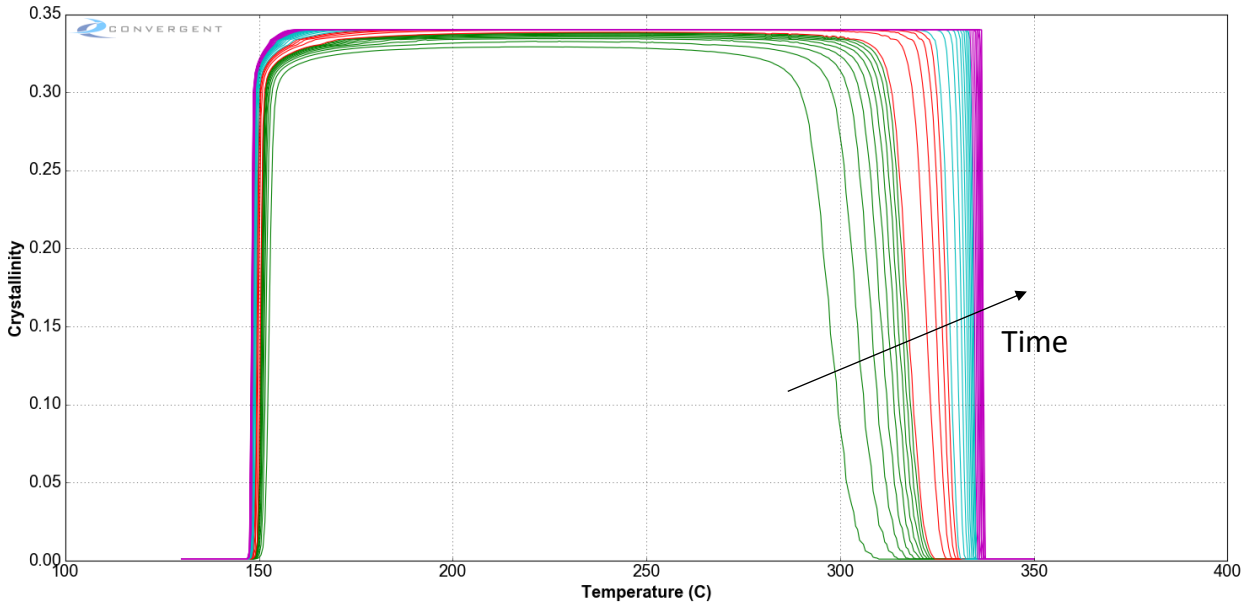

Figure 3-21 Process map, constant time contours for AS4/PEEK

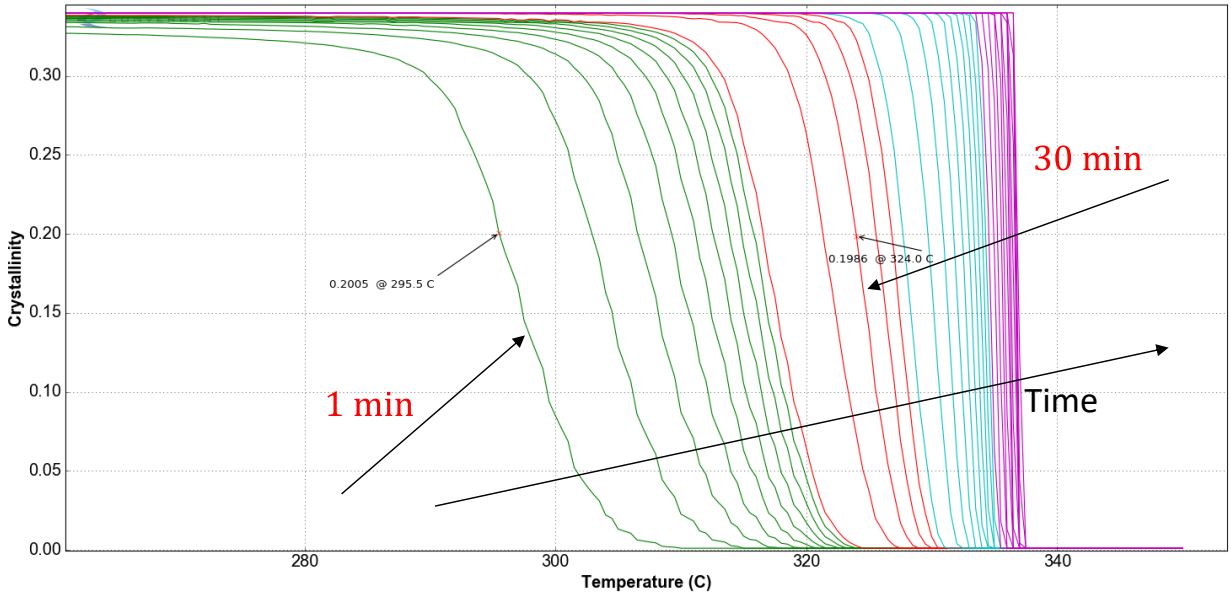

Figure 3-22 Process map, constant time contours for AS4/PEEK

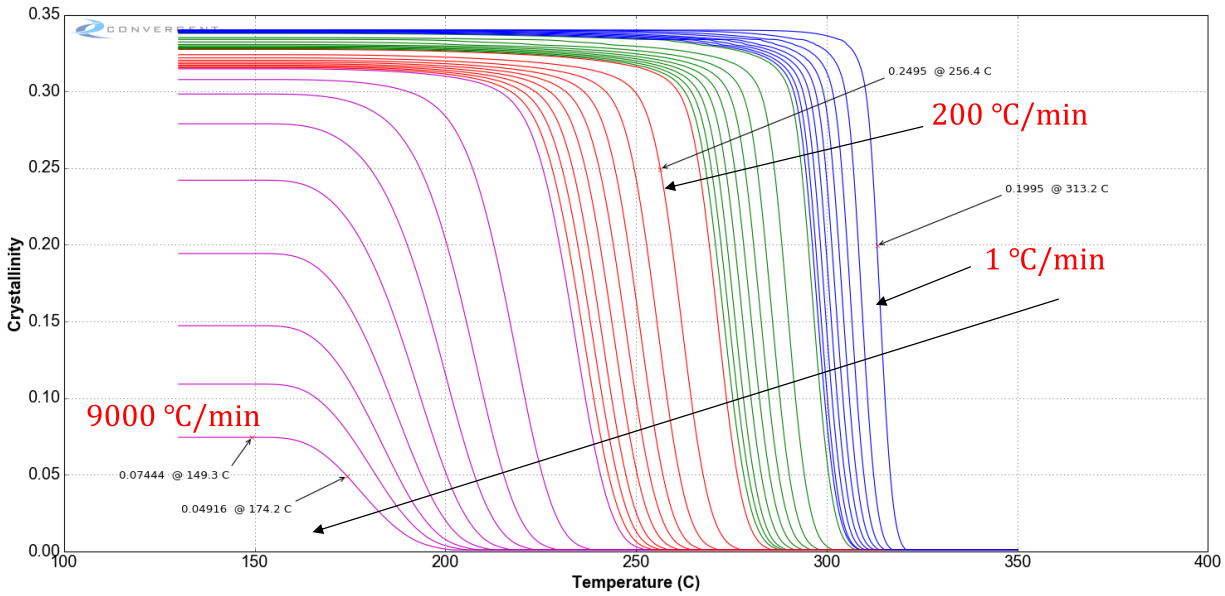

Figure 3-23 Process map, constant cooling rate contours for AS4/PEEK

3.3 Melt kinetics experiments

Similar to crystallization kinetics, the DSC was used for studying the melting kinetics of AS4/PEEK. Ten samples of approximately 5 milligrams were prepared in Tzero® hermetic DSC pans. To ensure all samples have identical conditions prior to melting, they were heated to 380 °C. After an isothermal soak of 10 minutes, they were cooled to room temperature at 10 °C/min. At this stage, the samples were heated at heating rates between 1 °C/min to 10 °C/min to 380 °C.

3.3.1 Raw data and general interpretations

The normalized heat flow rate results for melting tests at ten different heating rates are shown in Figure 3-24.

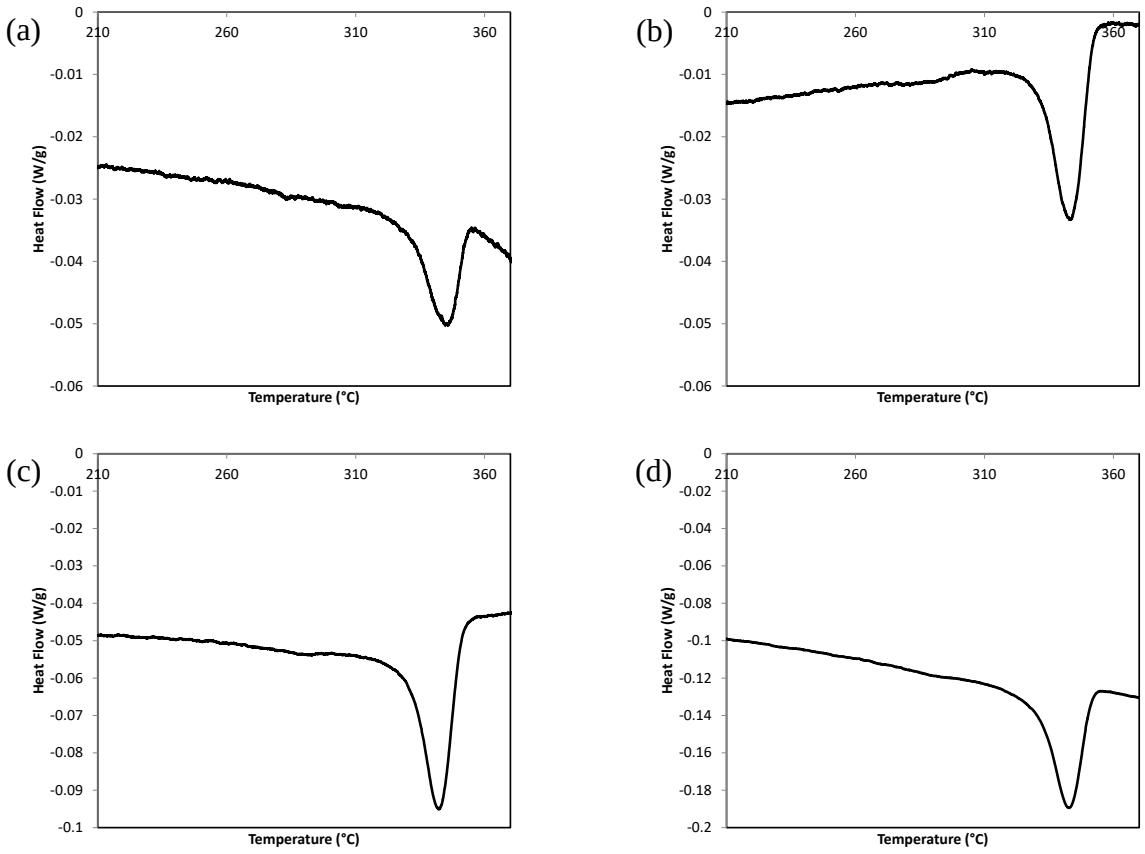

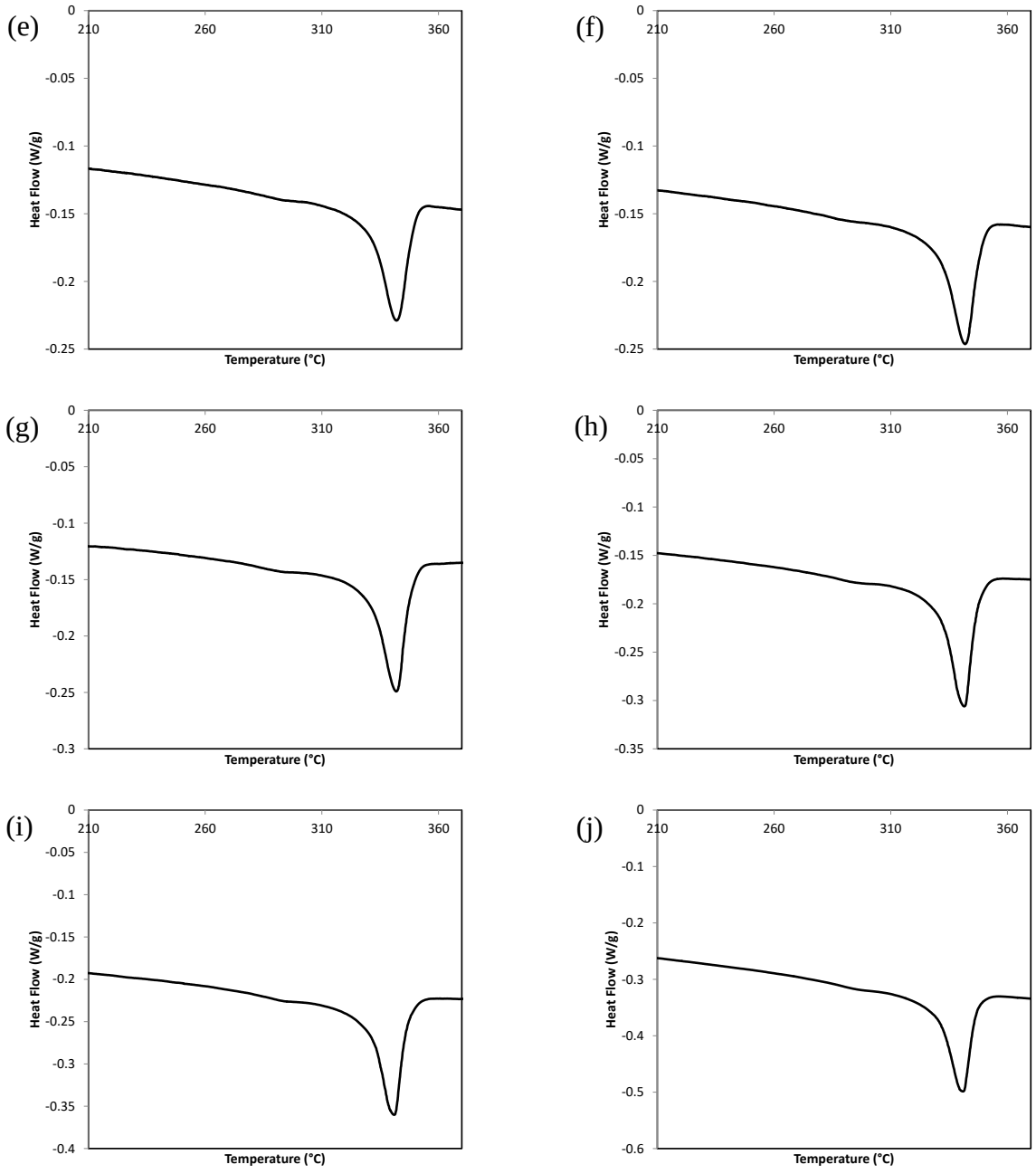

Figure 3-24 Normalized heat flow of the material whilst heating at (a) 1 ℃/min, (b) 2 ℃/min, (c) 3 ℃/min, (d) 4 ℃/min, (e) 5 ℃/min, (f) 6 ℃/min, (g) 7 ℃/min, (h) 8 ℃/min, (i) 9 ℃/min, (j) 10 ℃/min

From the plots in Figure 3-24, it is recognized that for all cases, in the investigated heating rate range, two melting peaks exist in the heat flow curve. This double-peak behaviour in melting of PEEK has been addressed in the literature as discussed in section 2.2.2. This will be investigated in detail, later in this chapter.

Similar to non-isothermal crystallization cases, it is realized from Figure 3-24 that the baselines before and behind the transition are both straight lines, however, they are not aligned with each other. Using the procedure explained in [129], sigmoidal baselines are constructed. Finally, Equations (3-1) to (3-3) are used and the degree of crystallinity at each time during melting is calculated. The results for variation of crystallinity with temperature along with the sigmoidal baselines are shown in Figure 3-25.

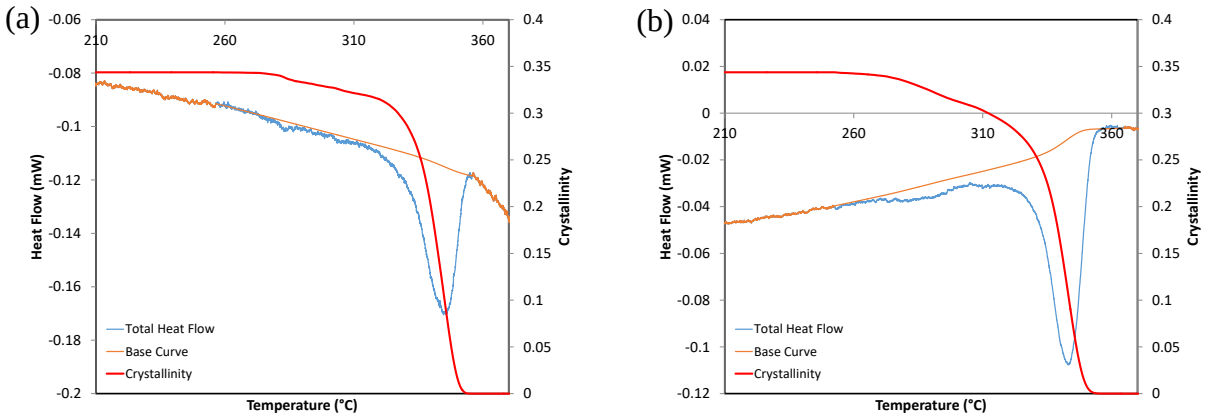

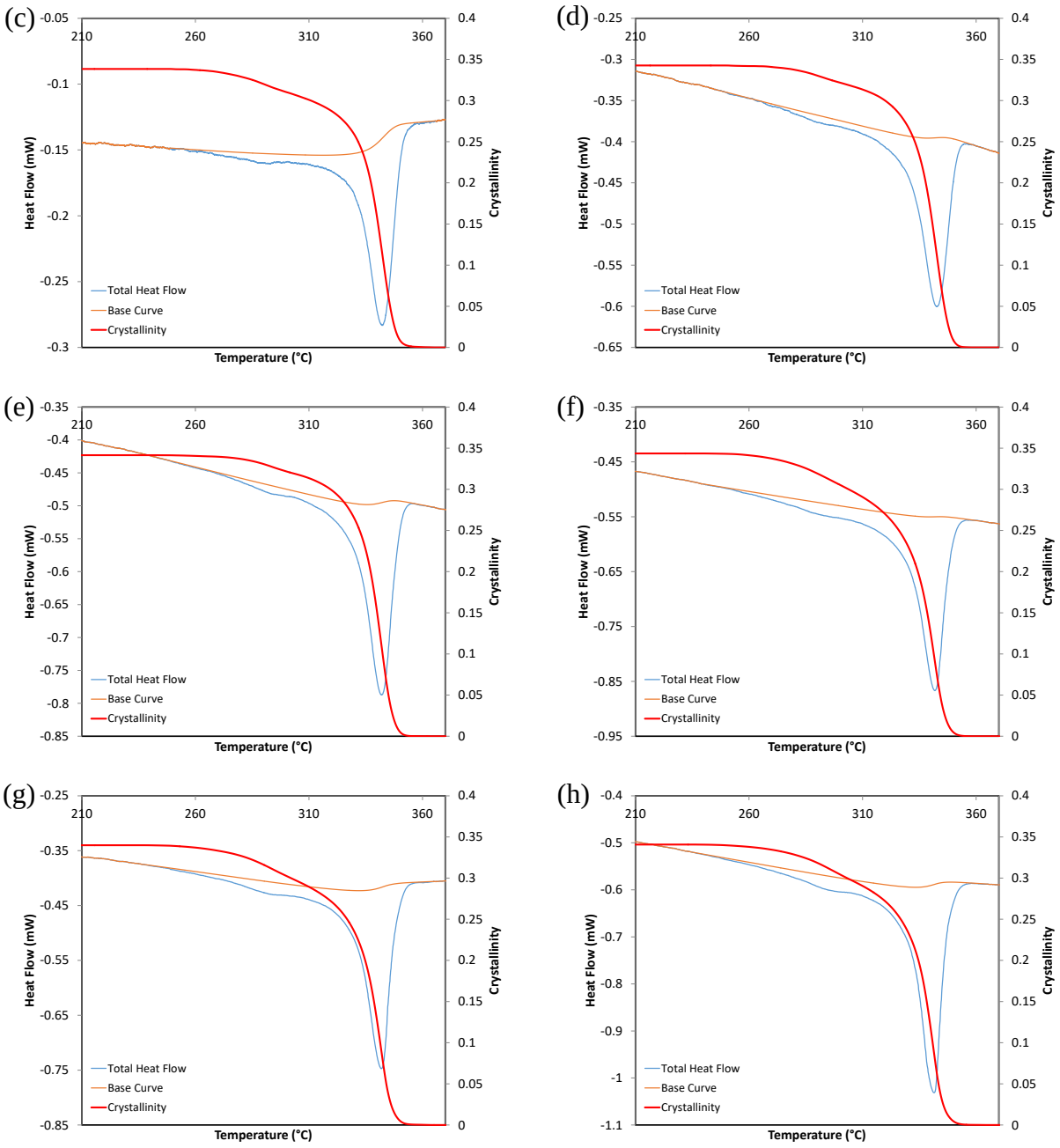
(c)
(d)
(e)
(f)
(g)
(h)
Heat Flow (mW)
Crystallinity
Temperature (°C)
Total Heat Flow
Base Curve
Crystallinity

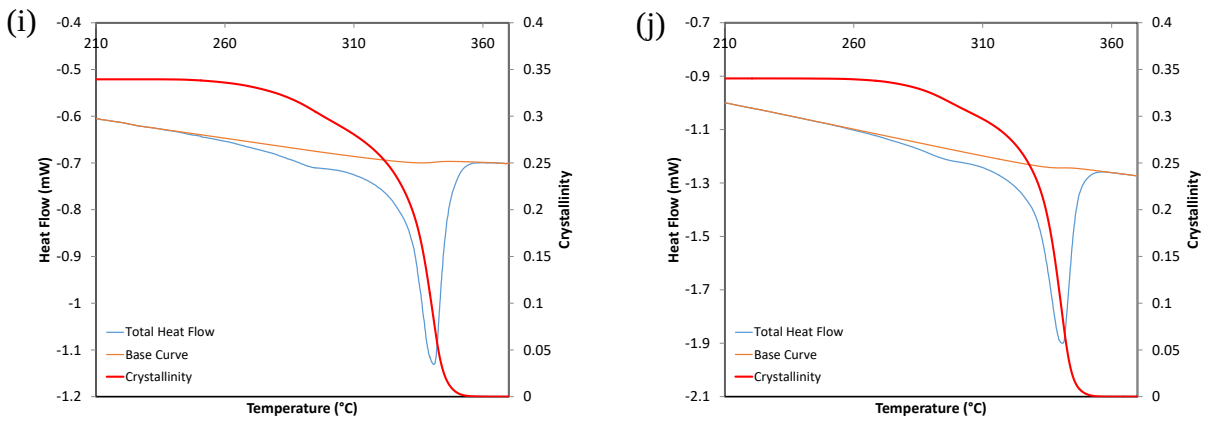

Figure 3-25 Variation of the crystallinity whilst melting at (a) 1 ℃/min, (b) 2 ℃/min, (c) 3 ℃/min, (d) 4 ℃/min, (e) 5 ℃/min, (f) 6 ℃/min, (g) 7 ℃/min, (h) 8 ℃/min, (i) 9 ℃/min, (j) 10 ℃/min

Variations of crystallinity with temperature and melting rate with temperature for ten different heating rates are compared in Figure 3-26 and Figure 3-27, respectively.

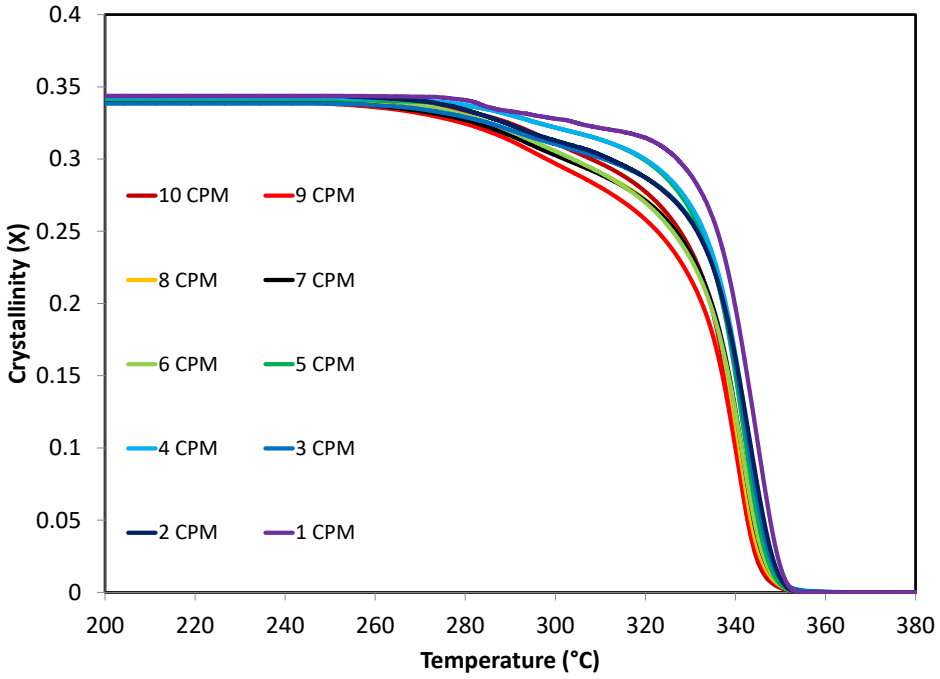

Figure 3-26 Variation of crystallinity with temperature for melting at different heating rates

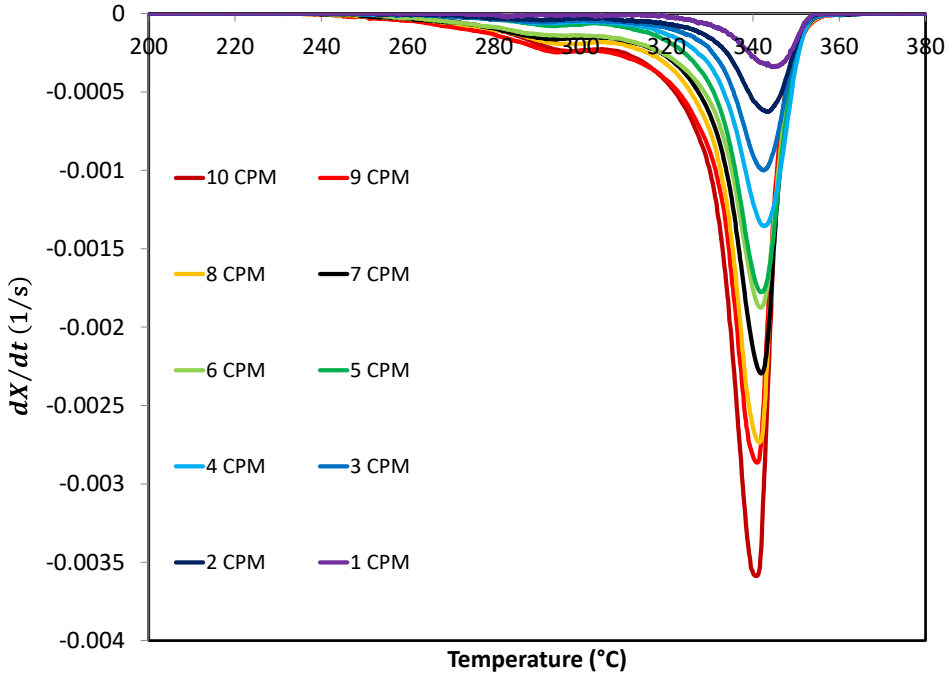

Figure 3-27 Variation of melting rate with temperature for melting at different heating rates

It is seen from Figure 3-26 and Figure 3-27 that the maximum melting rate increases by increasing the heating rate. The maximum melting rate and also the completion of melting for all heating rates occur approximately at the same temperature.

In Figure 3-28, crystallinity versus temperature for melting at different heating rates and melt crystallization at different cooling rates are compared. The results for melting rates and crystallization rates are also compared in Figure 3-29.

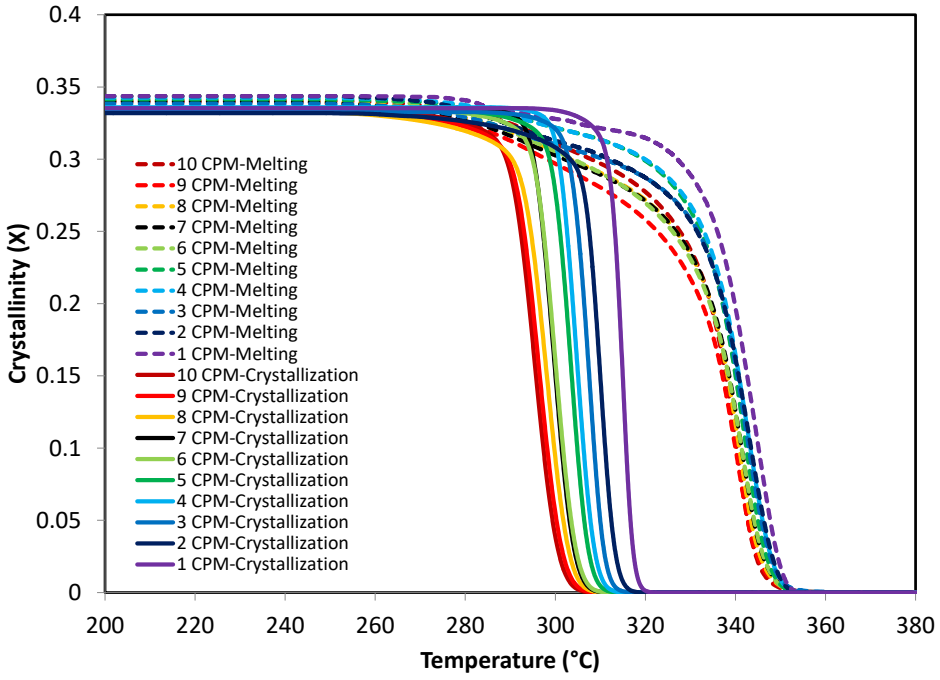

Figure 3-28 Variation of crystallization with temperature for crystallization at different cooling rates and melting at different heating rates

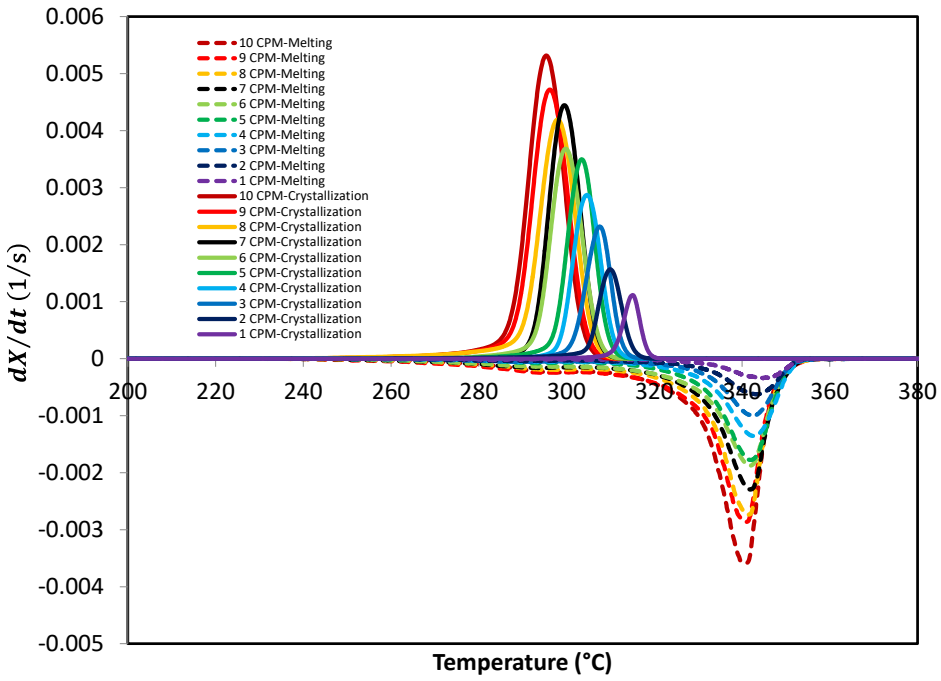

Figure 3-29 Variation of crystallization rate and melting rate with temperature for crystallization at different cooling rates and melting at different heating rates

In contrast to melting, from Figure 3-29 it is recognized that in melt crystallization, the temperature where the maximum crystallization rate occurs decreases with increasing cooling rate. Also compared to crystallization, melting occurs over a wider temperature range.

To get some insight into the double-peak melting behaviour of the material, some annealing experiments were performed which are presented in the following sections.

3.3.2 Annealing experiments

To have a clear understanding of the double-peak behaviour of the material in melting, the initial conditions of the samples, before melting, was varied. This is accomplished by annealing of the samples at different temperatures for different times.

3.3.2.1 Experiments with different annealing times

Eight samples of approximately 5 milligram were prepared in Tzero® hermetic DSC pans. Samples were heated to 380 ℃ and after an isothermal soak of 10 minutes, they were cooled to room temperature at 10 ℃/min. Next, all samples were heated at 10 ℃/min to 320 ℃. At this stage, eight samples were kept isothermal for 1 minute, 2 minutes, 3 minutes, 4 minutes, 5 minutes, 10 minutes, 1 hour, and 10 hours. Finally, they were heated at 10 ℃/min to 380 ℃.

Normalized heat flow curves for heating at 10 ℃/min subsequent to the isothermal holds for different time periods are shown in Figure 3-30.

(a)

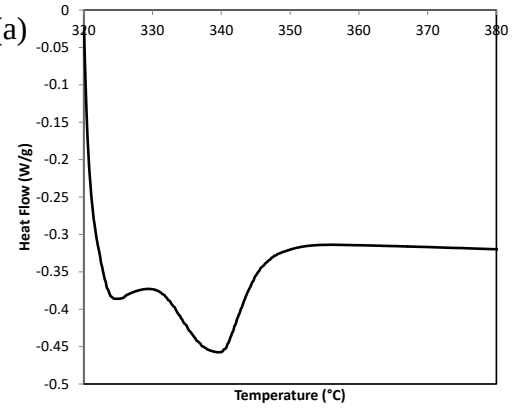

(b)

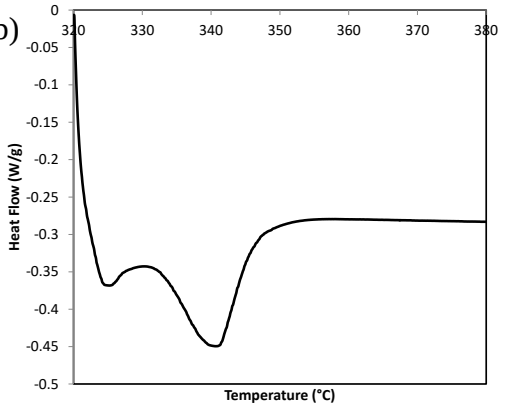

(c)

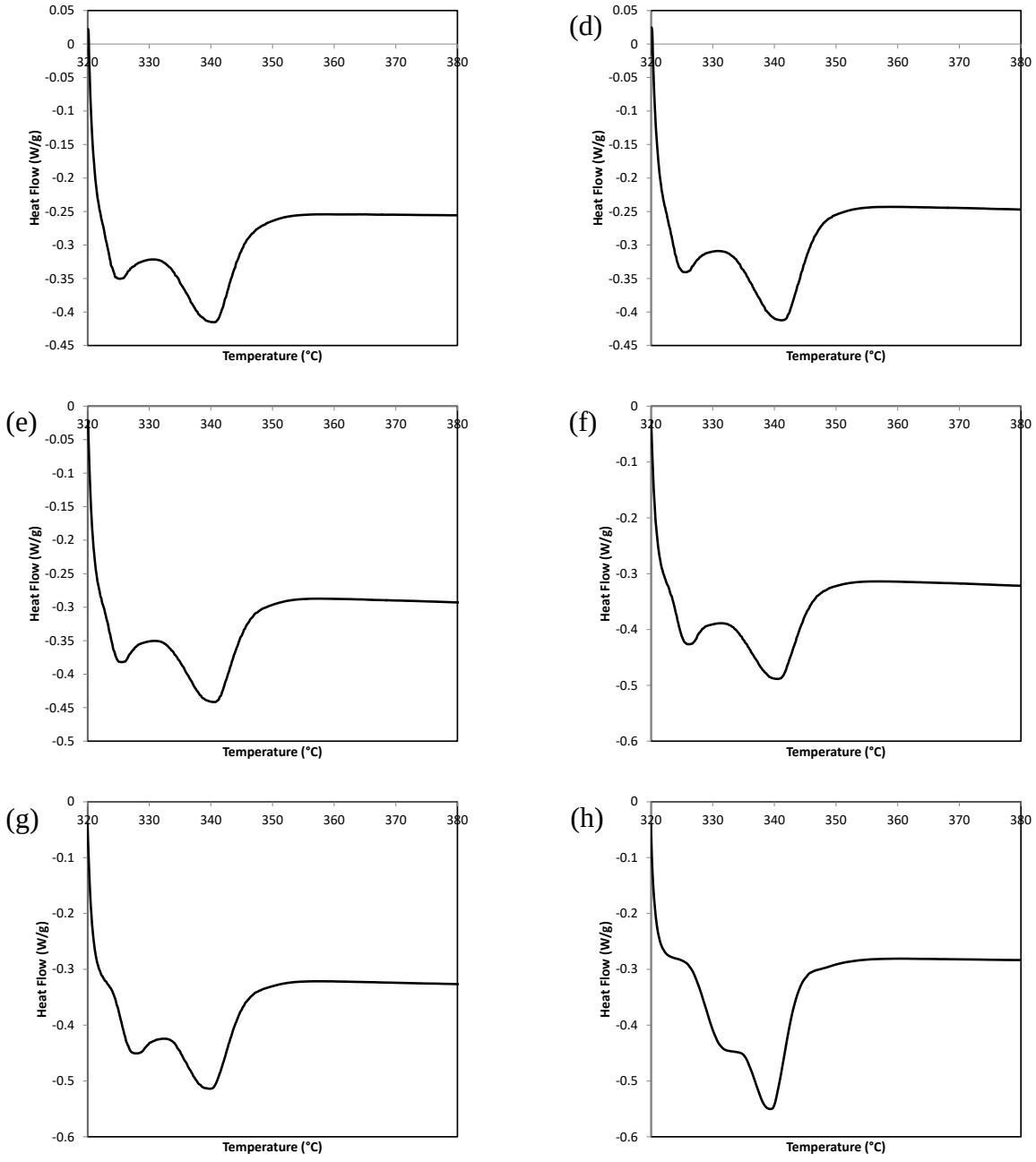

Figure 3-30 Normalized heat flow for heating at 10 ℃/min subsequent to heat up at 10 ℃/min from room temperature to 320 ℃ and then isothermal hold for (a) 1 min, (b) 2 min, (c) 3 min, (d) 4 min, (e) 5 min, (f) 10 min, (g) 1 hour, (h) 10 hour

The double-peak behaviour is noticed in all plots in Figure 3-30. Using sigmoidal baselines, crystallinity is calculated for these annealing and melting experiments as presented in Figure 3-31.

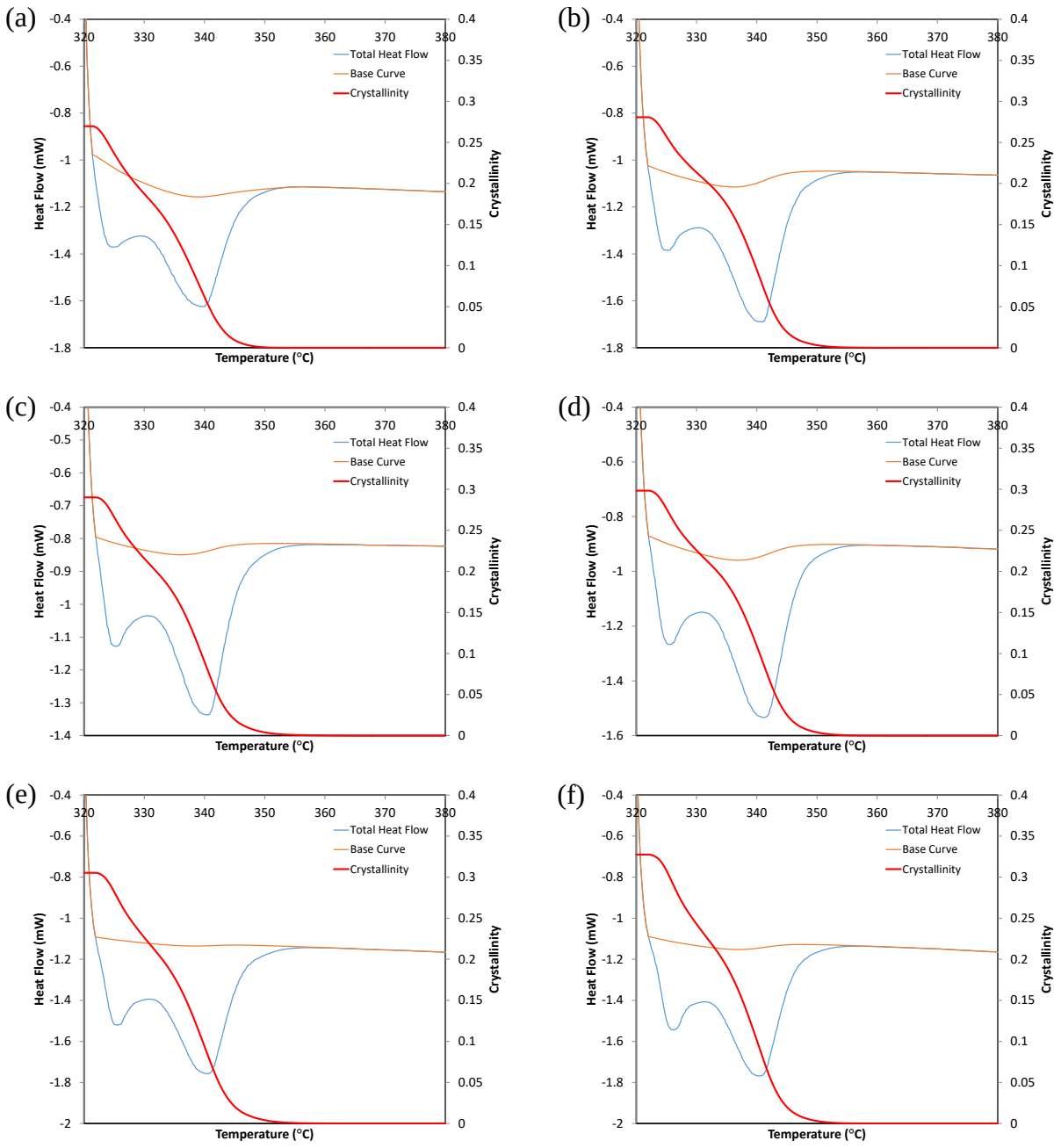

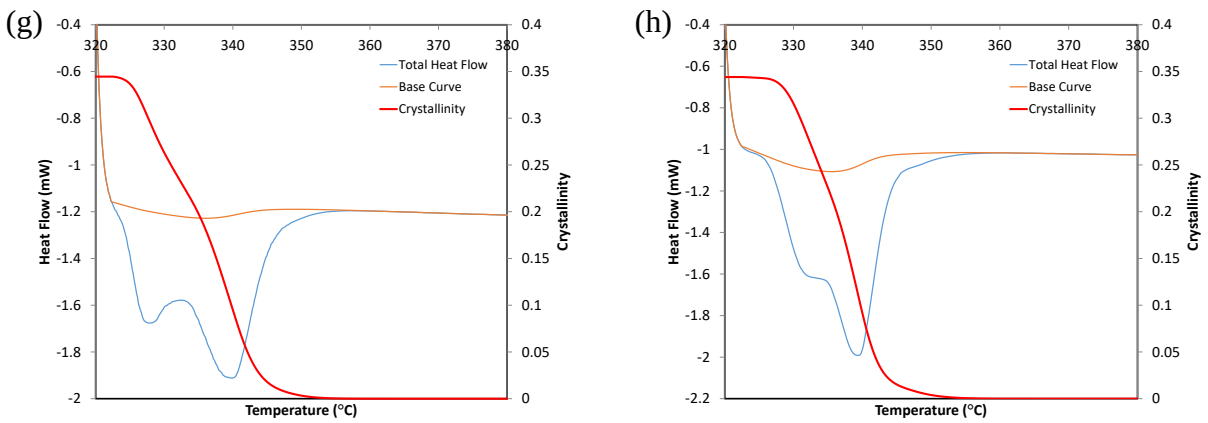

Figure 3-31 Variation of crystallinity for heating at 10 ℃/min subsequent to heating at 10 ℃/min from room temperature to 320 ℃ and then isothermal hold for (a) 1 min, (b) 2 min, (c) 3 min, (d) 4 min, (e) 5 min, (f) 10 min, (g) 1 hour, (h) 10 hour

Variation of melting rate and crystallinity for these eight annealing cases and the case of continuous heating at 10 ℃/min from room temperature to 380 ℃ are compared in Figure 3-32 and Figure 3-33.

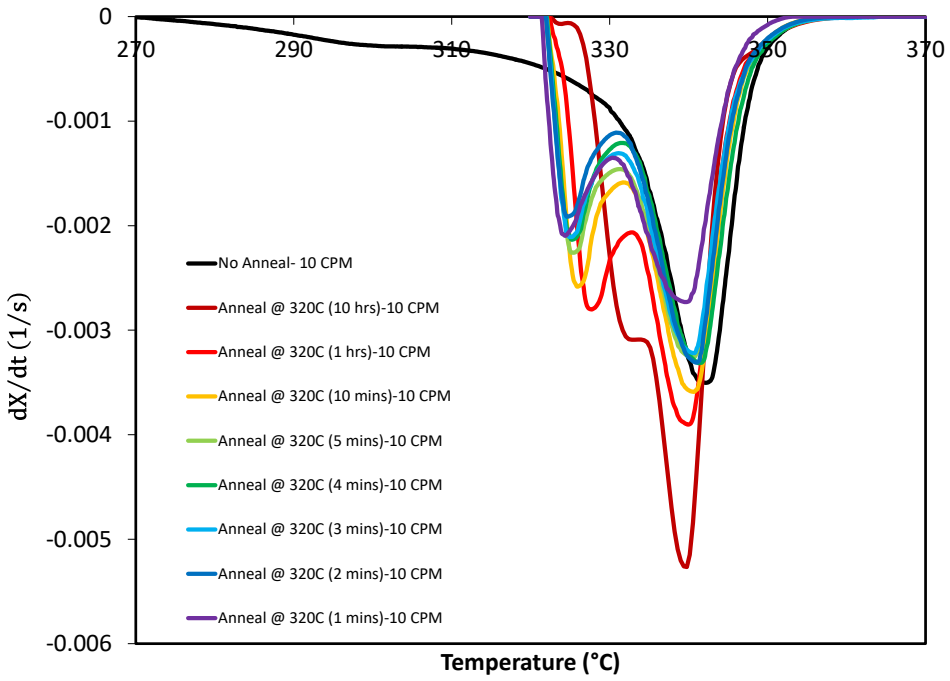

Figure 3-32 Variation of melting rate for heating at 10 ℃/min subsequent to heating at 10 ℃/min from room temperature to 320 ℃ and then isothermal hold for different annealing times and also continuous heating at 10 ℃/min

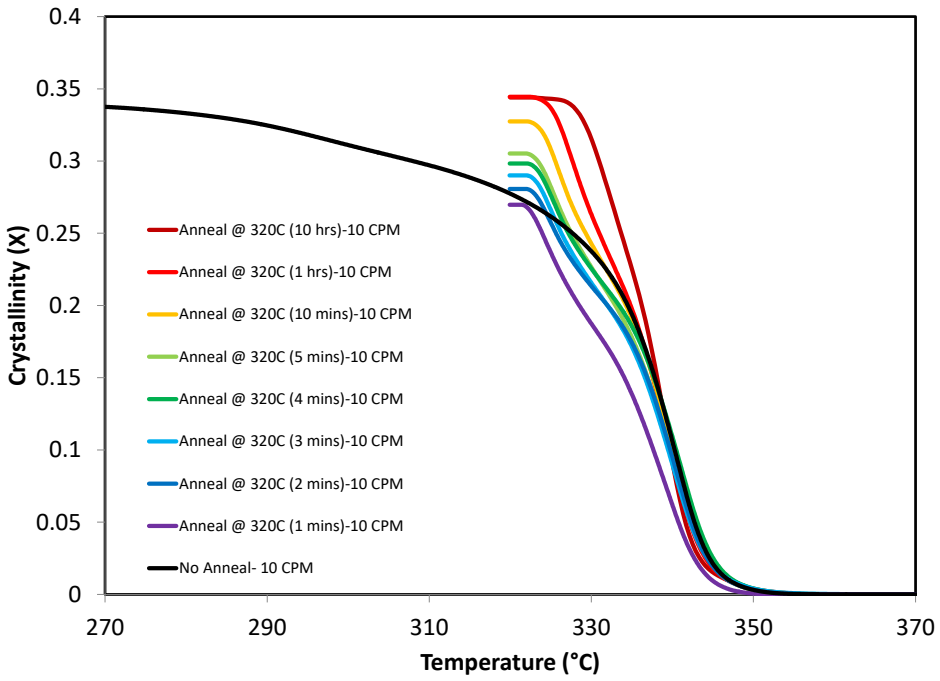

Figure 3-33 Variation of crystallinity for heating at 10 ℃/min subsequent to heating at 10 ℃/min from room temperature to 320 ℃ and then isothermal hold for different annealing times and also continuous heating at 10 ℃/min

It is clear from Figure 3-32 that the peak at higher temperature (hereafter referred to as the second peak) for all cases occurs approximately at the same temperature. In a different manner, the peak at the lower temperature (hereafter referred to as the first peak) shifts toward higher temperatures when the annealing time is increased. This indicates that the melting onset temperature is increased with increasing annealing time.

3.3.2.2 Experiments at different annealing temperatures

Samples of approximately 5 milligrams were prepared in Tzero® hermetic DSC pans. Samples were heated to 380 ℃ and after an isothermal soak of 10 minutes, they were cooled to room temperature at 10 ℃/min. They were heated at 10 ℃/min to 300 ℃, 310 ℃, 320 ℃ and 330 ℃. At this stage, samples were kept isothermal for 10 hours and then were heated at 10 ℃/min to 380 ℃.

Normalized heat flow curves for heating at 10 ℃/min subsequent to the isothermal holds for different time periods are shown in Figure 3-34.

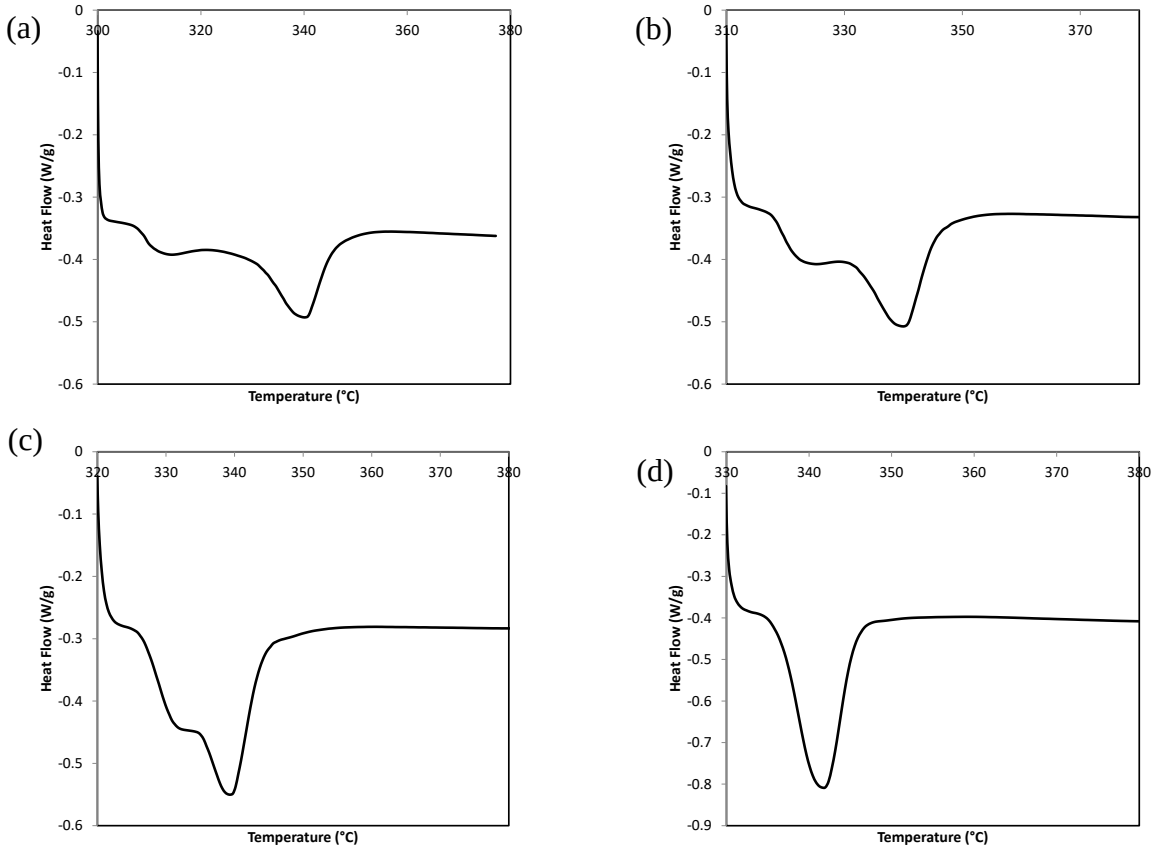

Figure 3-34 Normalized heat flow for heating at 10 ℃/min subsequent to heat up at 10 ℃/min from room temperature and then isothermal hold at (a) 300 ℃, (b) 310 ℃, (c) 320 ℃, (d) 330 ℃

Using the procedures explained in previous sections, sigmoidal baselines were constructed and crystallinities were calculated as displayed in Figure 3-35.

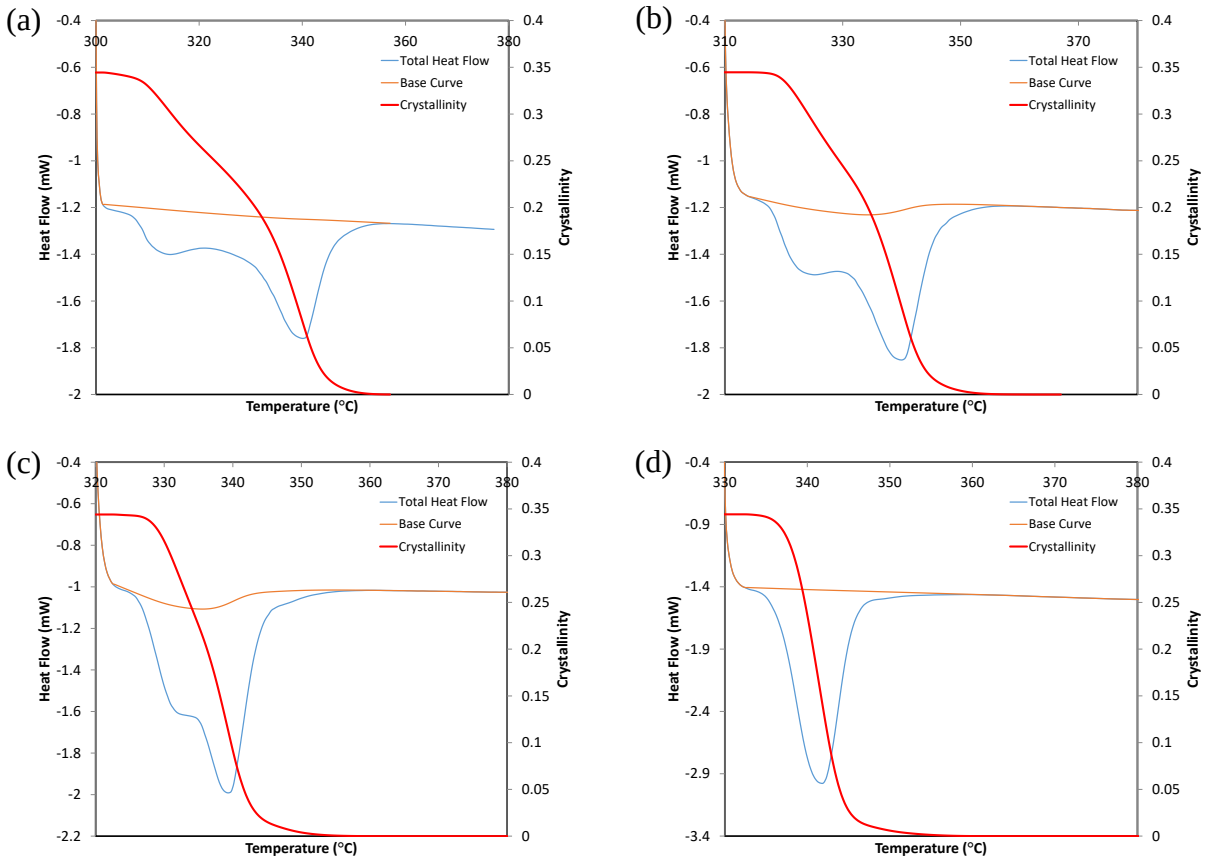

Figure 3-35 Variation of crystallinity for heating at 10 ℃/min subsequent to heat up at 10 ℃/min from room temperature and then isothermal hold at (a) 300 ℃, (b) 310 ℃, (c) 320 ℃, (d) 330 ℃

Variation of melting rate and crystallinity with temperature for the four annealing temperatures are displayed in Figure 3-36 and Figure 3-37.

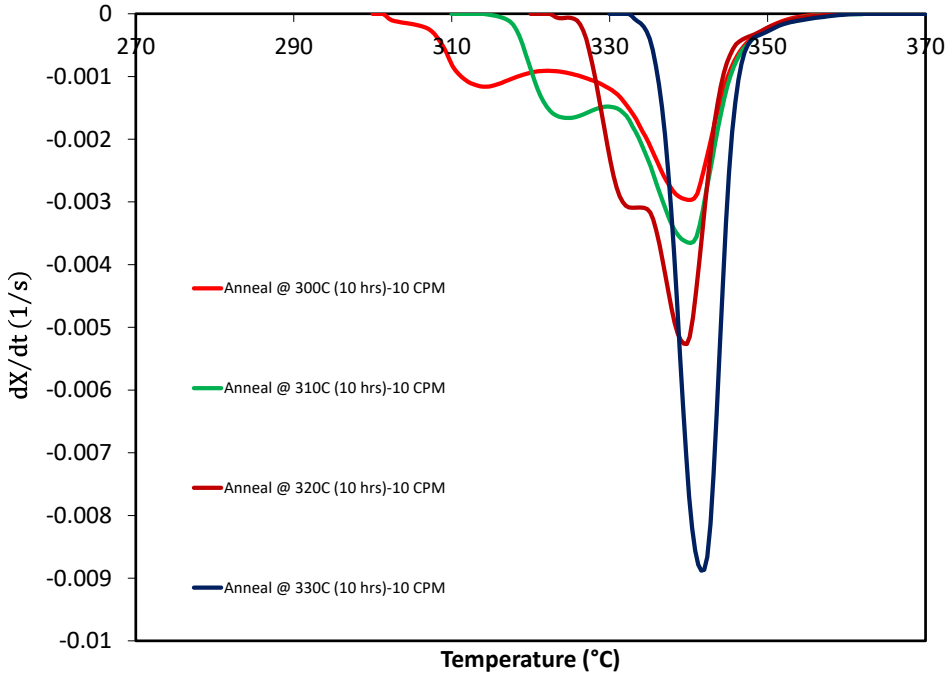

Figure 3-36 Variation of melting rate for heating at 10 ℃/min after heating from room temperature and annealing for 10 hours at different temperatures

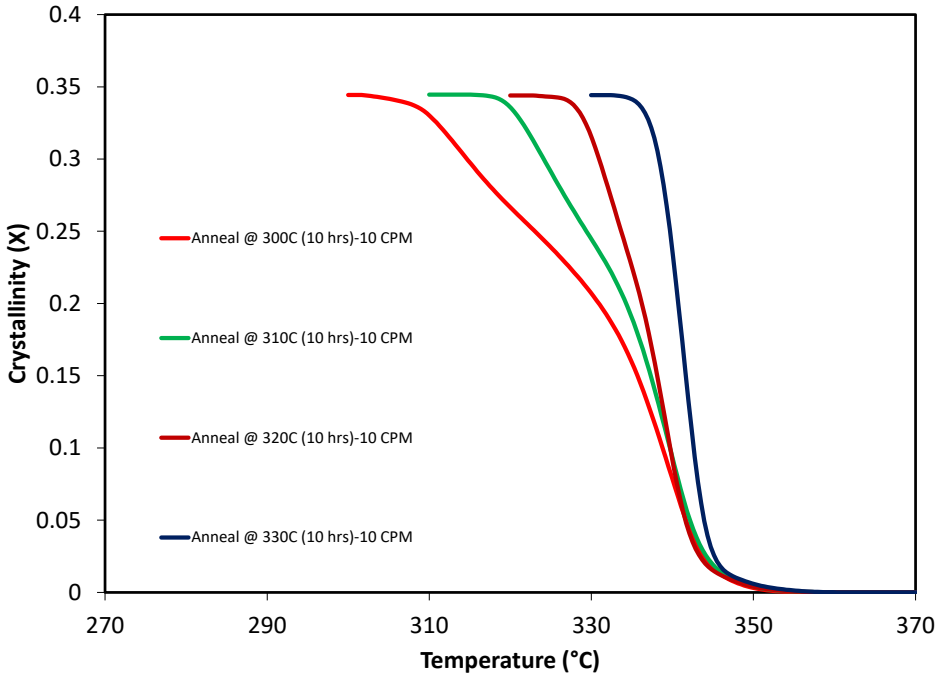

Figure 3-37 Variation of crystallinity for heating at 10 ℃/min after heating from room temperature and annealing for 10 hours at different temperatures

It is clear from Figure 3-36 that the second peak temperature is approximately the same for all annealing temperatures. The first peak shifts to higher temperatures with increasing annealing temperature. For the case of annealing at 330 ℃, the first peak merges into the second peak.

3.3.2.3 Annealing experiments subsequent to cooling from melt to different temperatures

In the previous section, crystallized samples were heated from room temperature to different temperatures and were annealed for 10 hours prior to melting. In these series of experiments,

samples were heated to 380 ℃, followed by an isothermal hold of 10 minutes. Subsequently, they were cooled at 10 ℃/min to 300 ℃, 310 ℃, 320 ℃ and 330 ℃ and kept isothermal for 10 hours. Finally, the samples were heated at 10 ℃/min to 380 ℃. Normalized heat flow curves of the final melting for four samples are shown in Figure 3-38.

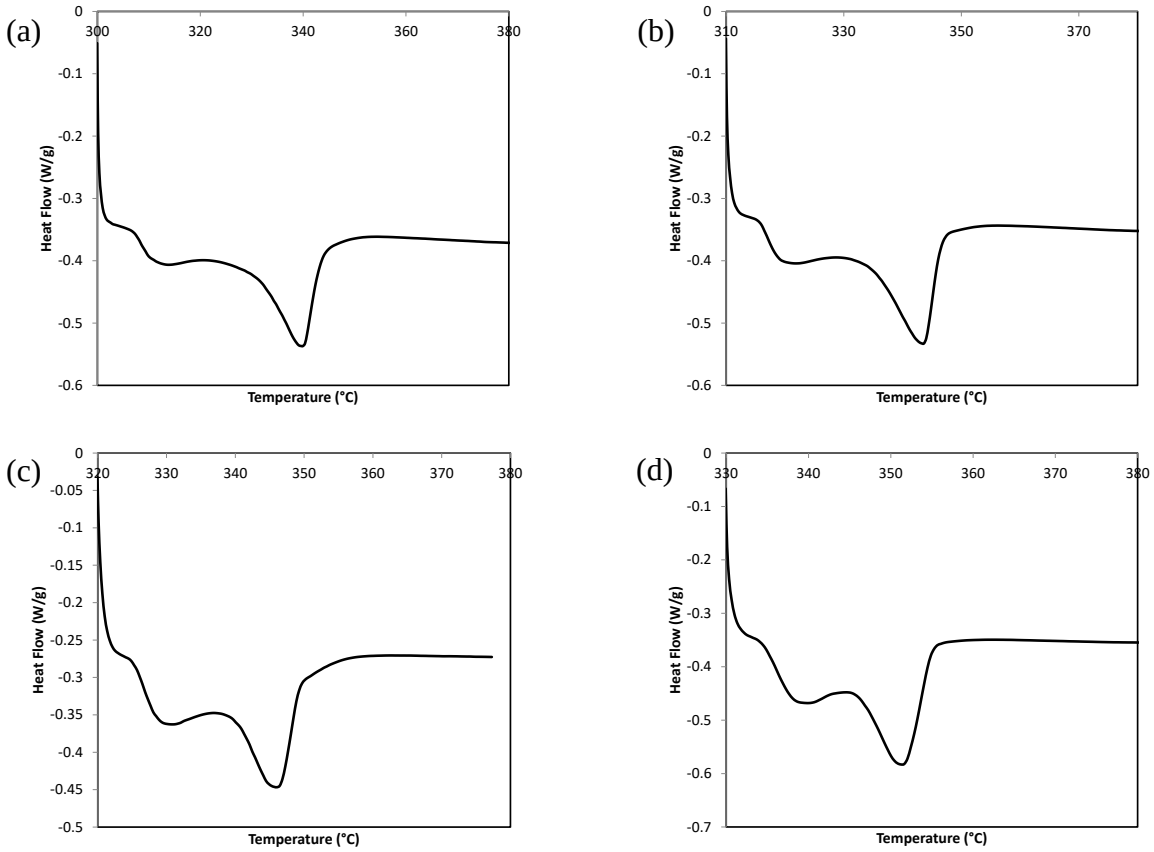

Figure 3-38 Normalized heat flow for heating at 10 ℃/min subsequent to cooling at 10 ℃/min from 380 ℃ and then isothermal hold at (a) 300 ℃, (b) 310 ℃, (c) 320 ℃, (d) 330 ℃

Sigmoidal baselines and variation of crystallinity for these tests are displayed in Figure 3-39.

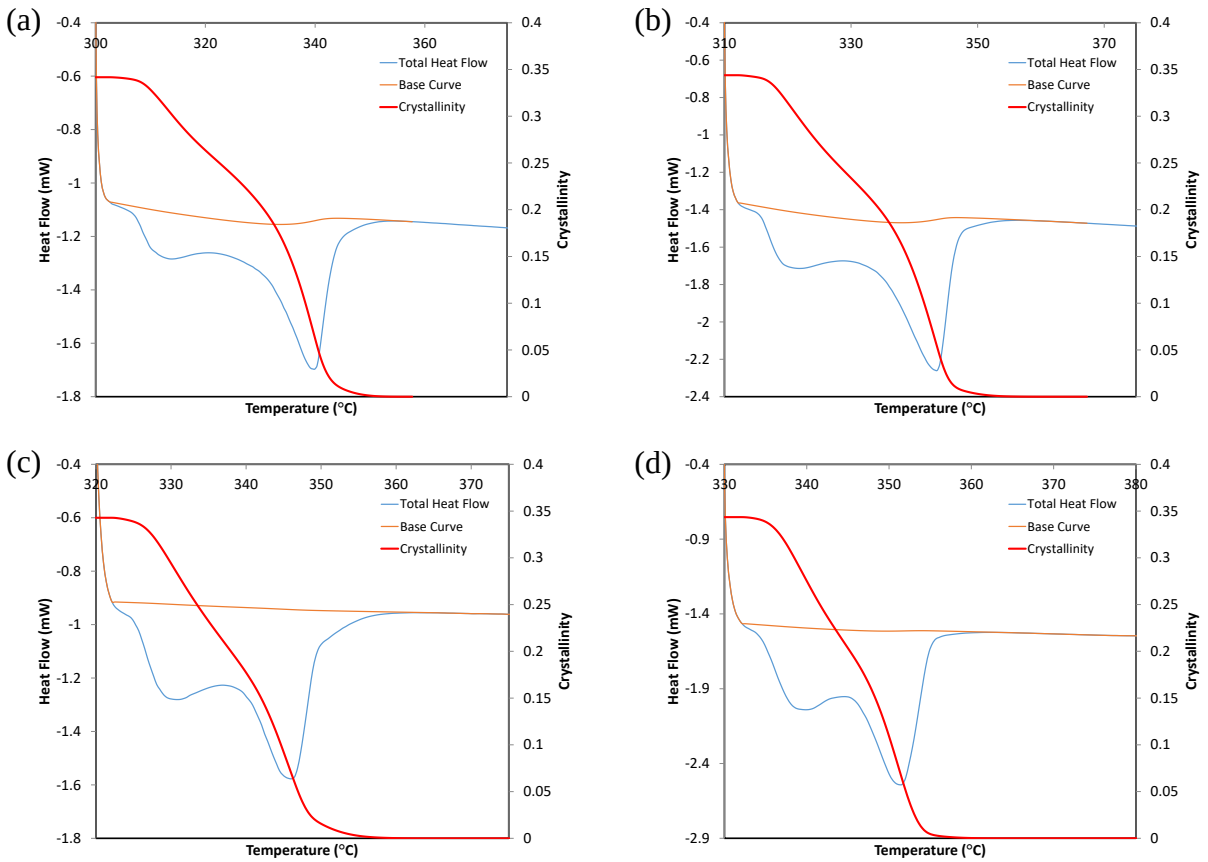

Figure 3-39 Variation of crystallinity for heating at 10 ℃/min subsequent to cooling at 10 ℃/min from 380 ℃ and then isothermal hold at (a) 300 ℃, (b) 310 ℃, (c) 320 ℃, (d) 330 ℃

Meting rate and crystallinity for the four melting cases are compared in Figure 3-40 and Figure 3-41.

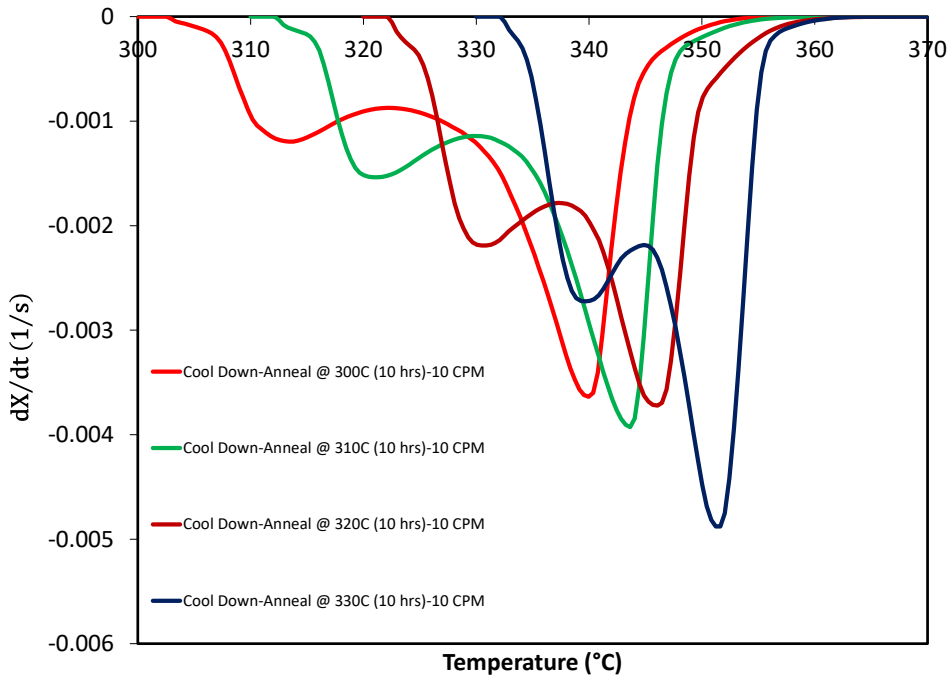

Figure 3-40 Variation of melting rate for heating at 10 ℃/min after cooling from 380 ℃ and annealing for 10 hours at different temperatures

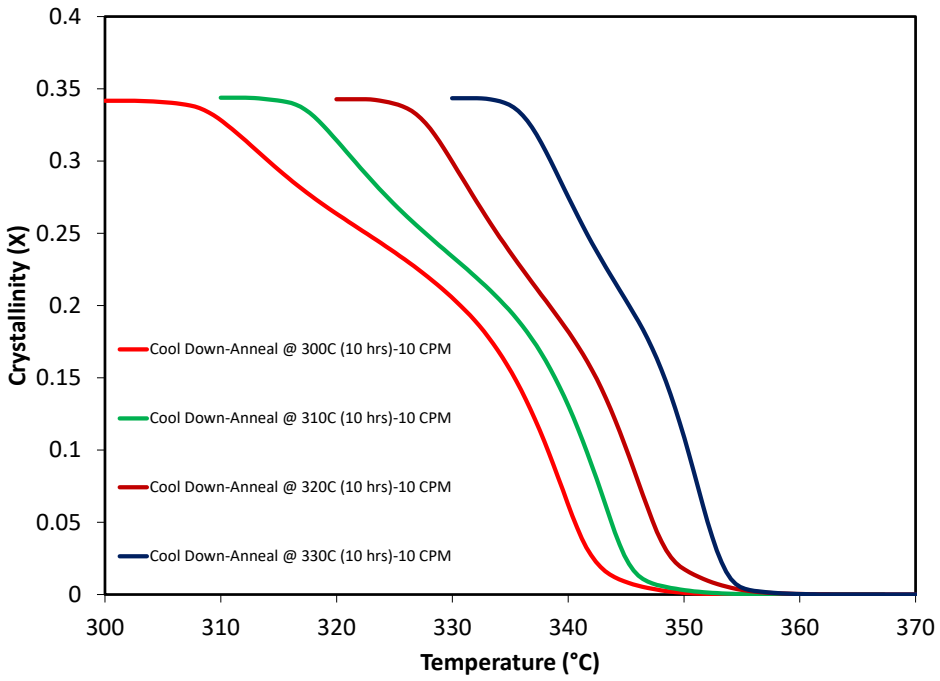

Figure 3-41 Variation of crystallinity for heating at 10 ℃/min after cooling from 380 ℃ and annealing for 10 hours at different temperatures

In contrast to the experiments explained in the previous section, from Figure 3-40 it is evident that the second peak temperatures are shifting to higher temperatures with increasing annealing temperature. The same behaviour is detected for first peak temperatures.

Melting rate behaviour for cases of heating from room temperature and annealing for 10 hours against cooling from 380 ℃ and annealing for 10 hours at four different temperatures are compared in Figure 3-42.

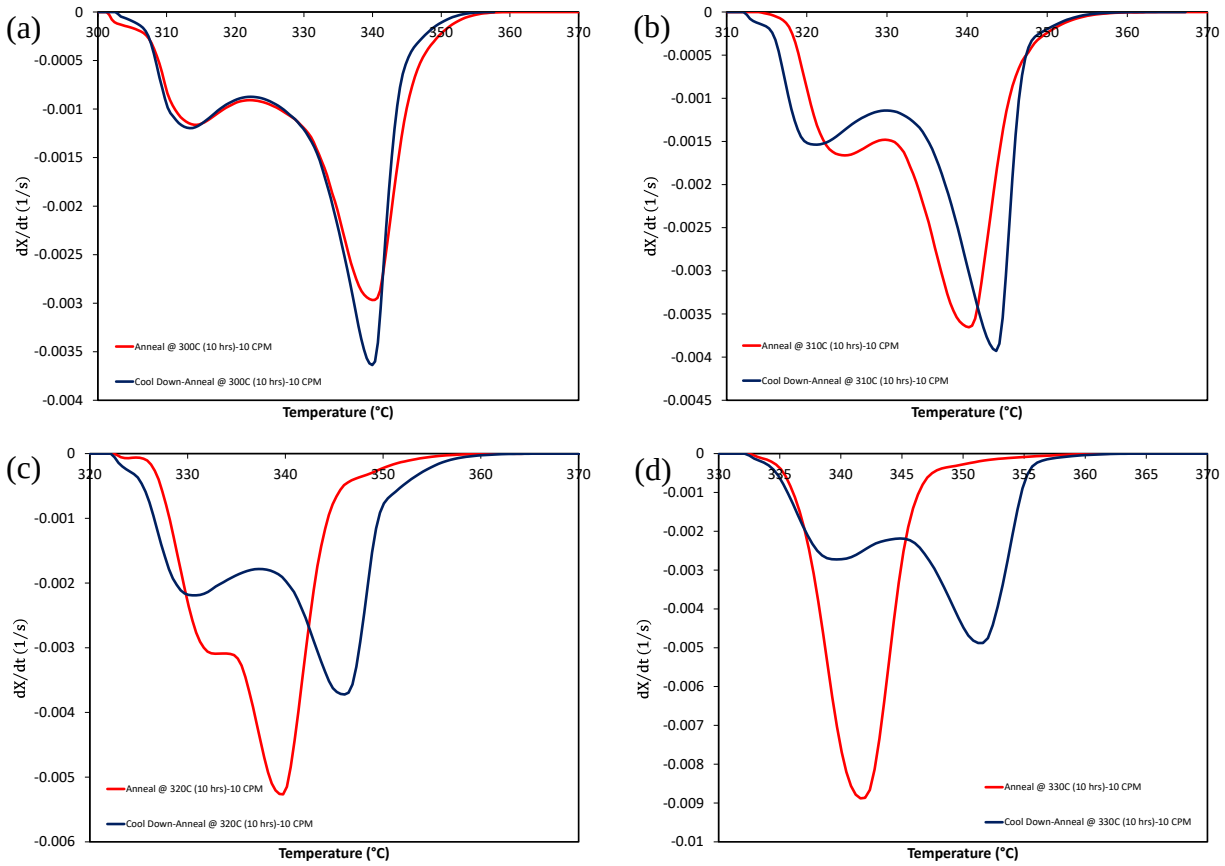

Figure 3-42 Melting rate for heating from room temperature and annealing for 10 hours compared with cooling from 380 ℃ and annealing for 10 hours at (a) 300 ℃, (b) 310 ℃, (c) 320 ℃, (d) 330 ℃

From Figure 3-42 it is noted that for annealing at 300 ℃, the first peak temperature and the second peak temperature is the same for both experiments. For higher annealing temperatures, the second melting peak of the cooling-annealing-melting experiments shifts towards higher temperatures whereas for heating-annealing-melting experiments, the second peak temperature is approximately constant.

3.3.2.4 Double-peak melting behaviour

In section 2.2.2, the double-peak behaviour of PEEK during melting was discussed. It was explained that there are generally two schools of thought: (i) the two peaks are due to melting of two separate populations of crystal morphologies; (ii) they are related to continuous melting and recrystallization of a single crystal morphology. Supporters of argument (i) [24], [25] argue that the higher temperature peak is due to melting of the main crystals and the lower temperature peak is related to less stable crystals grown in the intermediate spaces of main crystals.

On the other hand, according to followers of hypothesis (ii) [27], [28], the lower temperature peak is explained as the point where the original crystals become unstable and the melting and recrystallization process starts. The higher temperature peak is described as the point where the resultant of rates of melting and recrystallization reaches a maximum.

Inspecting Figure 3-32 based on the argument (i), it is concluded that with increasing annealing time, the main crystals melt approximately at the same temperature but the crystals grown in the intermediate spaces melt at higher temperatures. In other words, for the samples crystallized in similar conditions, increasing the annealing time at a fixed temperature improves the quality of the less stable crystals, however, the main crystals remain intact. If the same results are examined according to argument (ii), it is inferred that increasing the annealing time at a fixed temperature shifts the onset of melting and recrystallization of crystals to higher temperatures. From this observation it is implied that crystals in the samples with higher annealing times are of higher quality.

Corresponding to argument (i), similar conclusions may be drawn from Figure 3-36. With a constant annealing time, increasing the annealing temperature results in higher melting temperatures for the less stable crystals, however, the main crystals are not affected. Similarly, using hypothesis (ii), it is evident that with equal annealing times, higher annealing temperatures cause shifting of the onset of melting and recrystallization to higher temperatures. This indicates that annealing at higher temperatures creates higher quality crystals. From these two sets of annealing experiments, it is concluded that increasing the annealing time or annealing temperature has similar effects on the subsequent melting behaviour of material.

The explanation of the results from Figure 3-42 using argument (i) is as follows. When annealing at 300 ℃, both the less stable crystals and the main crystals show similar melting behaviour for heating-annealing-melting and cooling-annealing-melting experiments. For the other three annealing temperatures, in cooling-annealing-melting experiments, the less stable crystals melt at lower temperatures, whereas the main crystals melt at higher temperatures. This indicates that the main crystals are of higher quality in cooling-annealing-melting experiments compared to heating-annealing-melting experiments. The quality of the main crystals is improving with increasing annealing temperature. With a similar explanation, the quality of the less stable crystals is diminishing when the annealing temperature is increasing. This may be explained, as with the cooling-annealing-melting experiments, as the crystals are actually formed from melt and subsequently their quality is improving during the annealing process. For higher hold temperatures, the lamellar thickness of the crystalline structure is higher and hence the main crystals are of higher quality.

If argument (ii) is invoked, the results in Figure 3-42 indicate that the crystals in the cooling-annealing-melting experiments start to melt and recrystallize at lower temperatures compared to those in heating-annealing-melting experiments, however, the recrystallization process results in crystals that melt at higher temperatures.

Based on the discussions giving in this section, argument (ii) is adopted for the rest of this chapter, recognizing the fact that the recrystallized structure after annealing has crystals of higher quality.

3.4 Melt kinetics modelling

In this section the kinetics of melting is investigated. Revisiting Figure 3-26 and Figure 3-27, it is shown that increasing the heating rate results in increasing apparent or net melting rate, which is the resultant of melting and recrystallization rate. This can be explained by invoking argument (ii) from section 3.3.2.4. When the heating rate is increased, the time available to the material for recrystallization decreases, which shows itself in higher net melting rate.

The arguments given above are used for melt kinetics modelling. It is assumed that an original underlying melting profile, where no recrystallization occurs, exists for the material. This pure melt profile is referred to as the ‘master melt curve’. The details of the model and the results are explained in the following sections.

3.4.1 Prediction of the crystallinity

From discussions in the previous section, it is inferred that as the heating rate approaches infinity, the melt curve gets close to the master melt curve. Since reaching high heating rates is not possible using DSC, the results from one of the non-isothermal melting experiments, presented in section 3.3.1, are used. The crystallization kinetics model, developed in section 3.2, is then used for subtracting the recrystallization amount at each time step to obtain the pure melt increment, which is the melting increment corresponding to the master melt curve. Here the results from melting at 7 ℃/min are used and using the crystallization kinetics model and subtracting the recrystallized amount at each time step, the pure melting curve is obtained as shown in Figure 3-43.

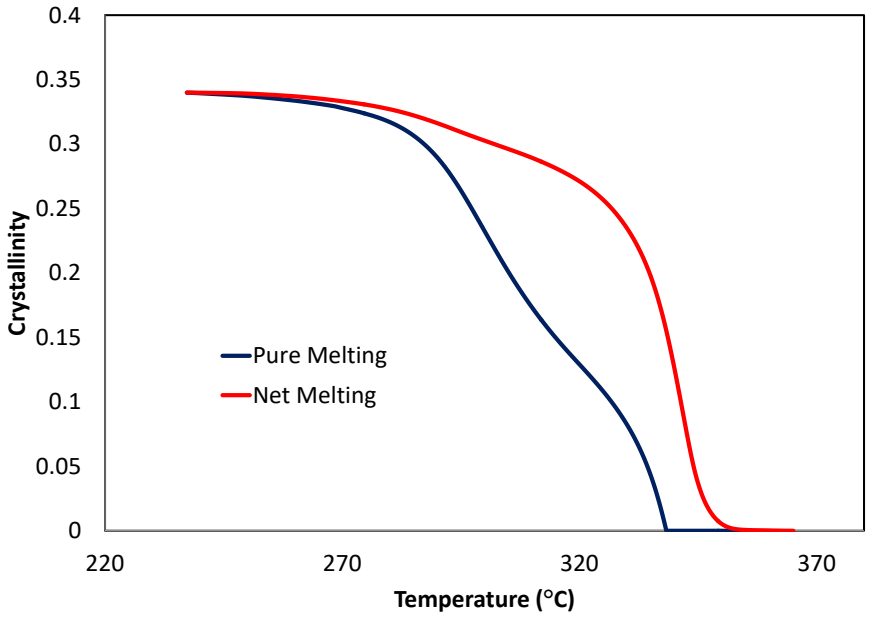

Figure 3-43 Pure melting and net melting curves for heat up at 7 ℃/min

Having the melting increment, corresponding to the master melt curve, the crystallization kinetics model is then used for calculation of the recrystallization increment during each time step in an arbitrary temperature cycle and therefore the actual degree of crystallinity is updated. Let's define $\left(\frac{dX}{dt}\right)_{\text{master}}$ as rate of crystallization (negative in melting) in the master melt curve. Given that it is taken from the results of heating at $7\ ℃/\text{min}$, $\left(\frac{dX}{dt}\right)_{\text{master}}$ can be rewritten as:

$$\left(\frac{dX}{dt}\right)_{\text{master}} = \left(\frac{dX}{dT}\right)_{\text{master}} .(7\ ℃/\text{min}) \qquad \textbf{(3-13)}$$

This way, the time effects related to the $7\ ℃/\text{min}$ curve are removed and $\left(\frac{dX}{dT}\right)_{\text{master}}$ can be considered as a true master curve as shown in Figure 3-44.

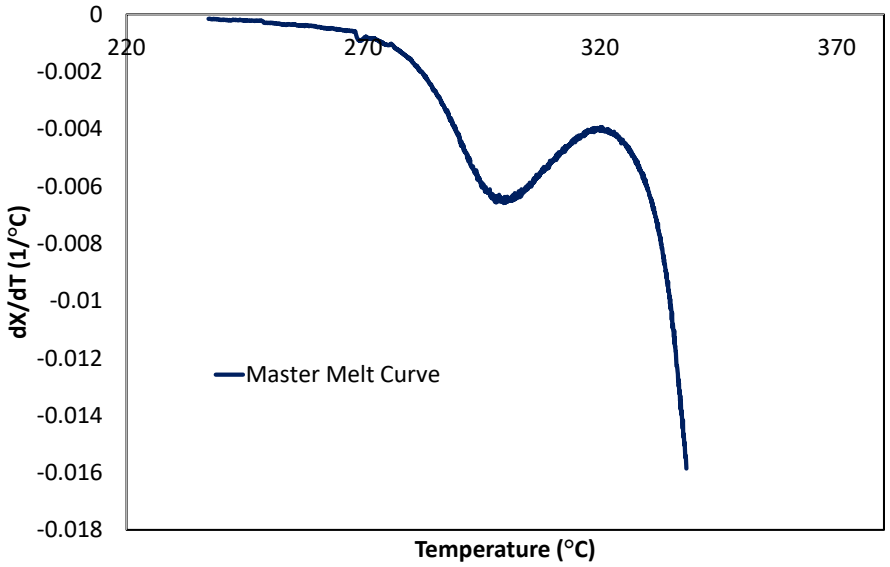

Figure 3-44 Master melt curve

Defining Δt: time increment in the current time step, ΔT: temperature increment in the current time step, X_{max}: maximum degree of crystallinity, $\frac{dX_c}{dt}$: crystallization rate, ΔX_c: increment in degree of crystallinity due to crystallization, ΔX_m: increment in degree of crystallinity due to melting, ΔX: total increment in degree of crystallinity, X^n: degree of crystallinity at the end of current time step, X^{n-1}: degree of crystallinity at the end of previous time step, $\dot{T}$: heating rate, degree of crystallinity may be predicted, based on the applied temperature profile as

$$\Delta X_c = \begin{cases} \frac{dX_c}{dt}\Delta t & X < X_{max} \\ 0 & X = X_{max} \end{cases},$$

$$\Delta X_m = \begin{cases} \left(\frac{dX}{dT}\right)_{\text{master}} \Delta T & \dot{T} > 0 \\ 0 & \dot{T} \leq 0 \end{cases}, \qquad \textbf{(3-14)}$$

$$\Delta X = \Delta X_c + \Delta X_m,$$

$$X^n = X^{n-1} + \Delta X$$

Using Equation (3-14), for any arbitrary temperature history, at a temperature T, the master melt curve gives the corresponding X value and identifies the melt behaviour if the material is heated from that T and X.

In the next section the predictions using the Equations (3-14) are compared with the experimental results.

3.4.2 Comparison of model predictions and experimental results

In this section, the model presented in the previous section is used for prediction of crystallinity for different melting experiments. Model predictions are compared with experimental results for ten different heating rates in Figure 3-45.

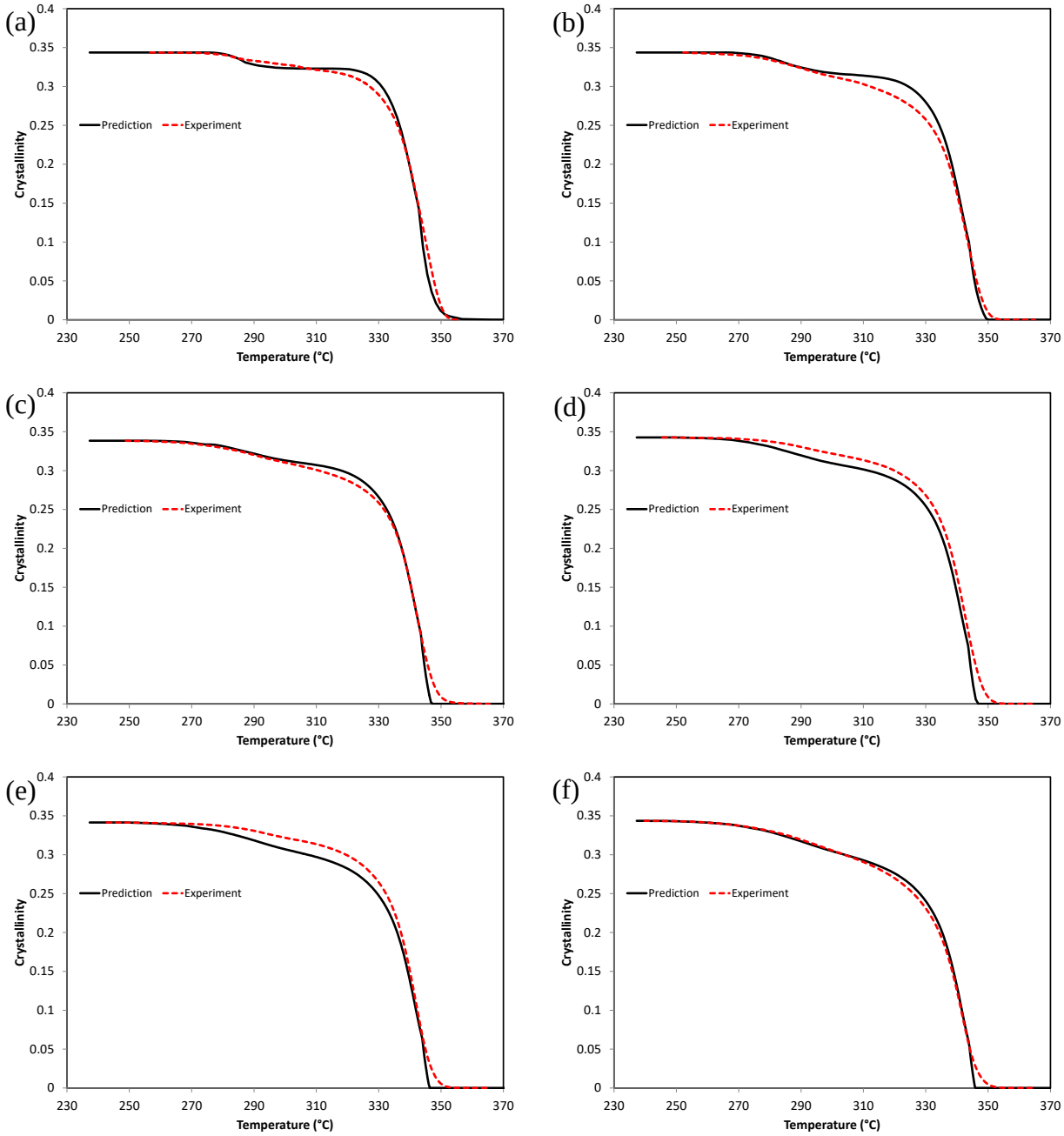
(a)
(b)
(c)
(d)
(e)
(f)
Prediction
Experiment
Crystallinity
Temperature (°C)
0
0.05
0.1
0.15
0.2
0.25
0.3
0.35
0.4
230
250
270
290
310
330
350
370

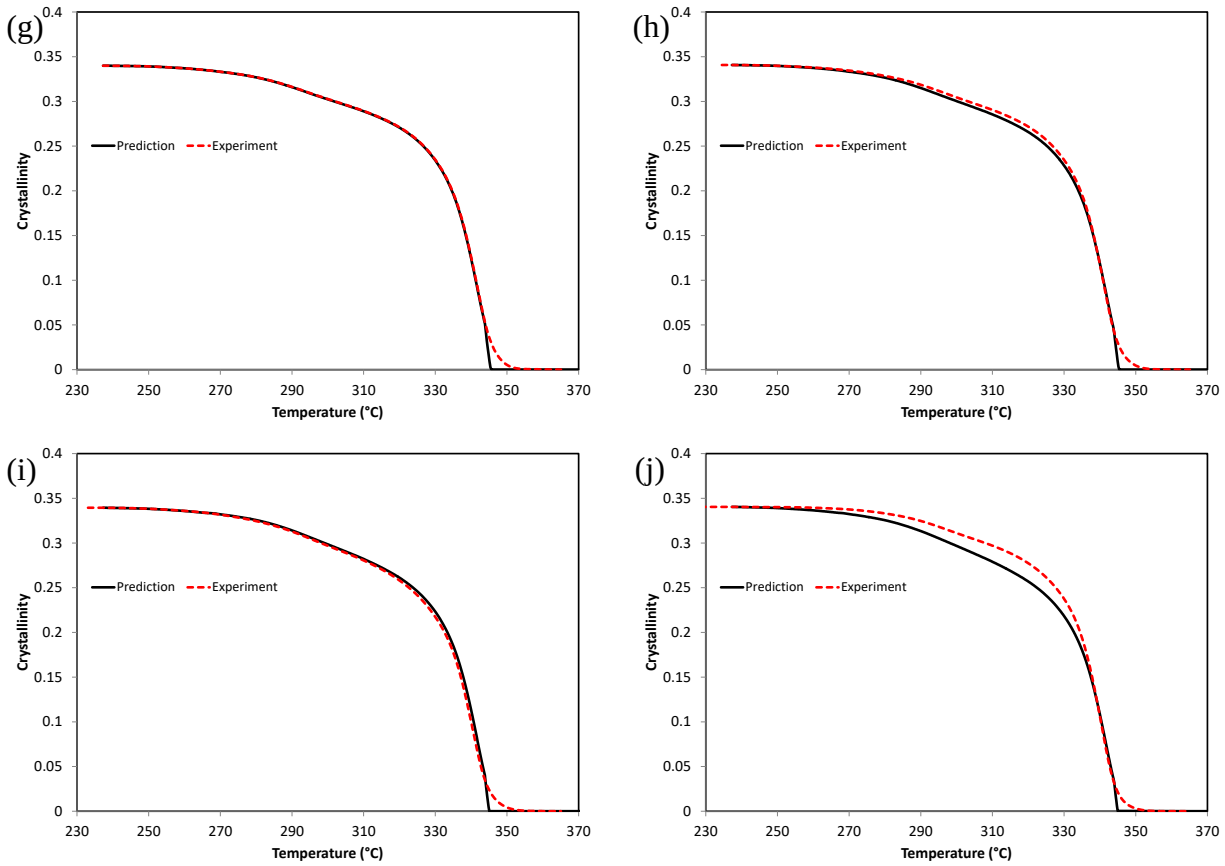

Figure 3-45 Variation of the crystallinity whilst melting at (a) 1 ℃/min, (b) 2 ℃/min, (c) 3 ℃/min, (d) 4 ℃/min, (e) 5 ℃/min, (f) 6 ℃/min, (g) 7 ℃/min, (h) 8 ℃/min, (i) 9 ℃/min, (j) 10 ℃/min, model predictions and experimental results

It is evident from Figure 3-45 that predicted results and experimental data are in good agreement. Model predictions for different heating rates are shown in Figure 3-46. The model is run for some higher heating rates including 100 ℃/min, 1000 ℃/min, 10000 ℃/min. It is seen that with increasing heating rate, the melt curves asymptotically approach one curve which is in fact the master curve.

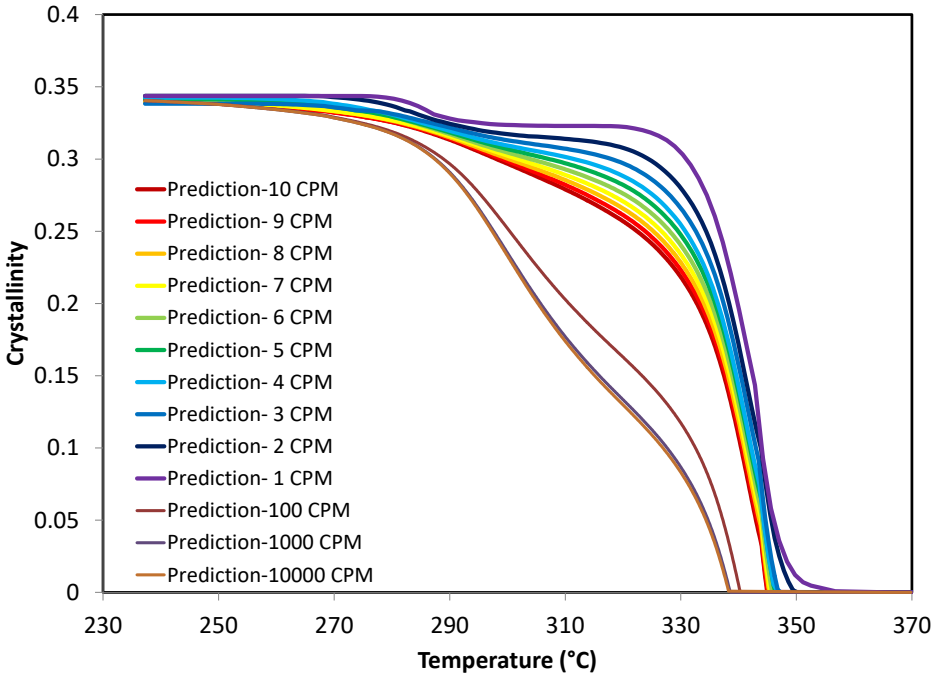

Figure 3-46 Model predicted crystallinity for different heating rates

Predicted results for melting of the material after annealing at 320 ℃ with different hold times are compared with experimental data in Figure 3-47.

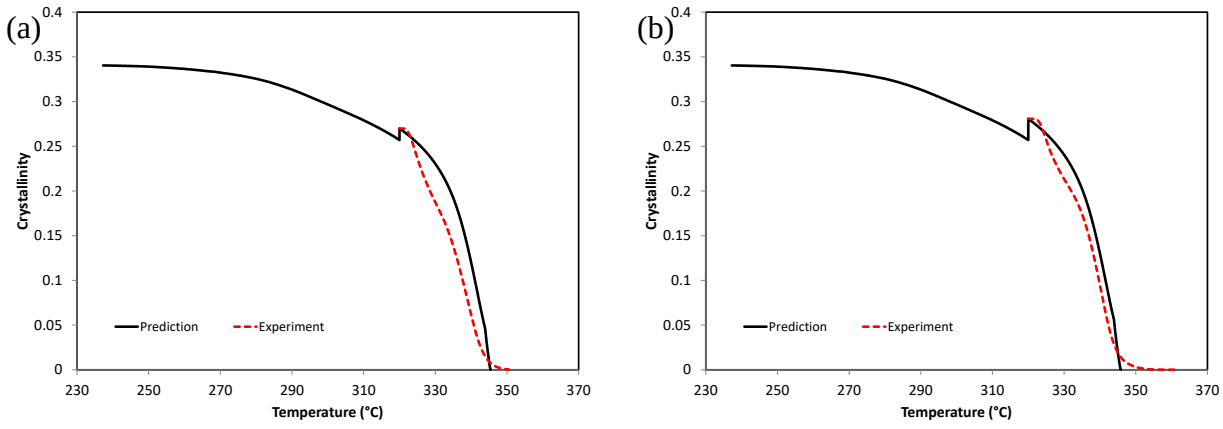

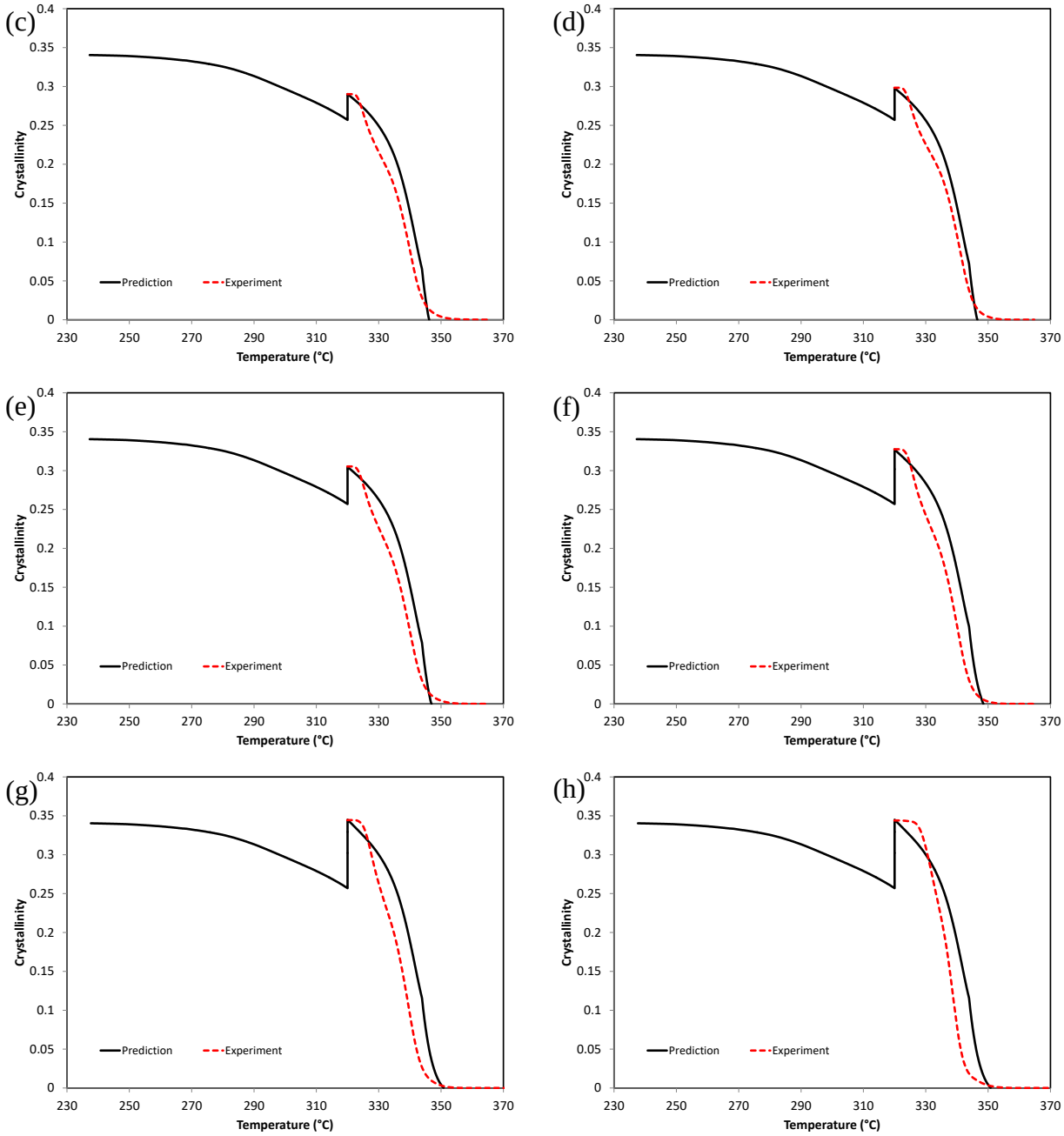

Figure 3-47 Variation of crystallinity for heating at 10 ℃/min subsequent to heating at 10 ℃/min from room temperature to 320 ℃ and then isothermal hold for (a) 1 min, (b) 2 min, (c) 3 min, (d) 4 min, (e) 5 min, (f) 10 min, (g) 1 hour, (h) 10 hour, model predictions and experimental results

The results in Figure 3-47 indicate that the model predictions are in reasonable agreement with the experimental results. The predicted results for different annealing times at 320 ℃ are compared in Figure 3-48.

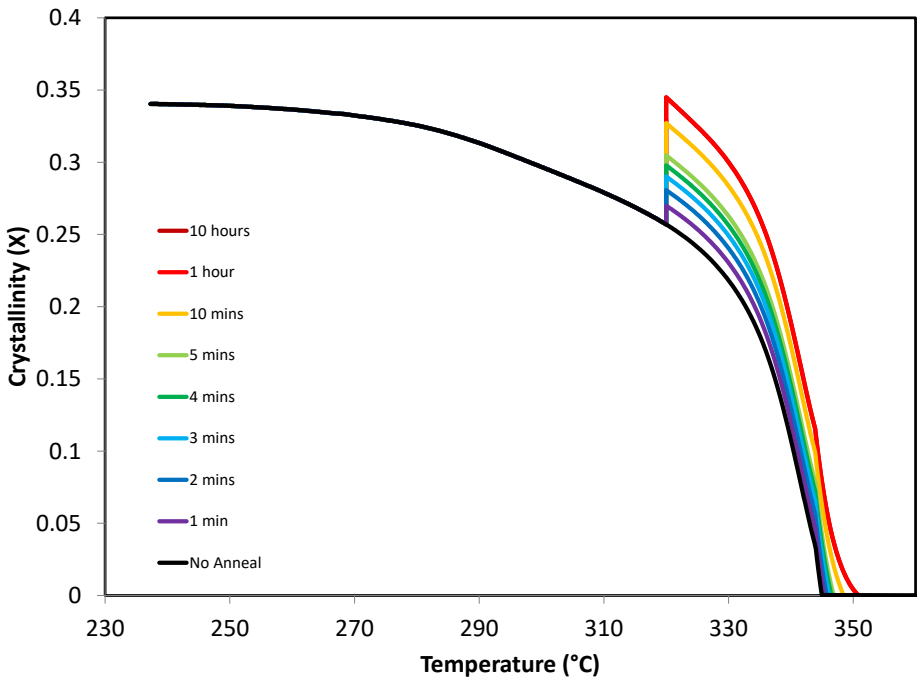

Figure 3-48 Variation of crystallinity for heating at 10 ℃/min subsequent to heating at 10 ℃/min from room temperature to 320 ℃ and then isothermal hold for different annealing times

From Figure 3-48, it is recognized that increasing the annealing time at a constant temperature results in increasing the degree of crystallinity. When the crystallinity reaches its maximum, the model does not predict any extra changes for the rest of the annealing time. This may be concluded considering that in Figure 3-48, the results for 1 hour and 10 hour annealing time are the same.

Predicted results for melting of the material after annealing for 10 hours at different temperatures are compared with experimental data in Figure 3-49.

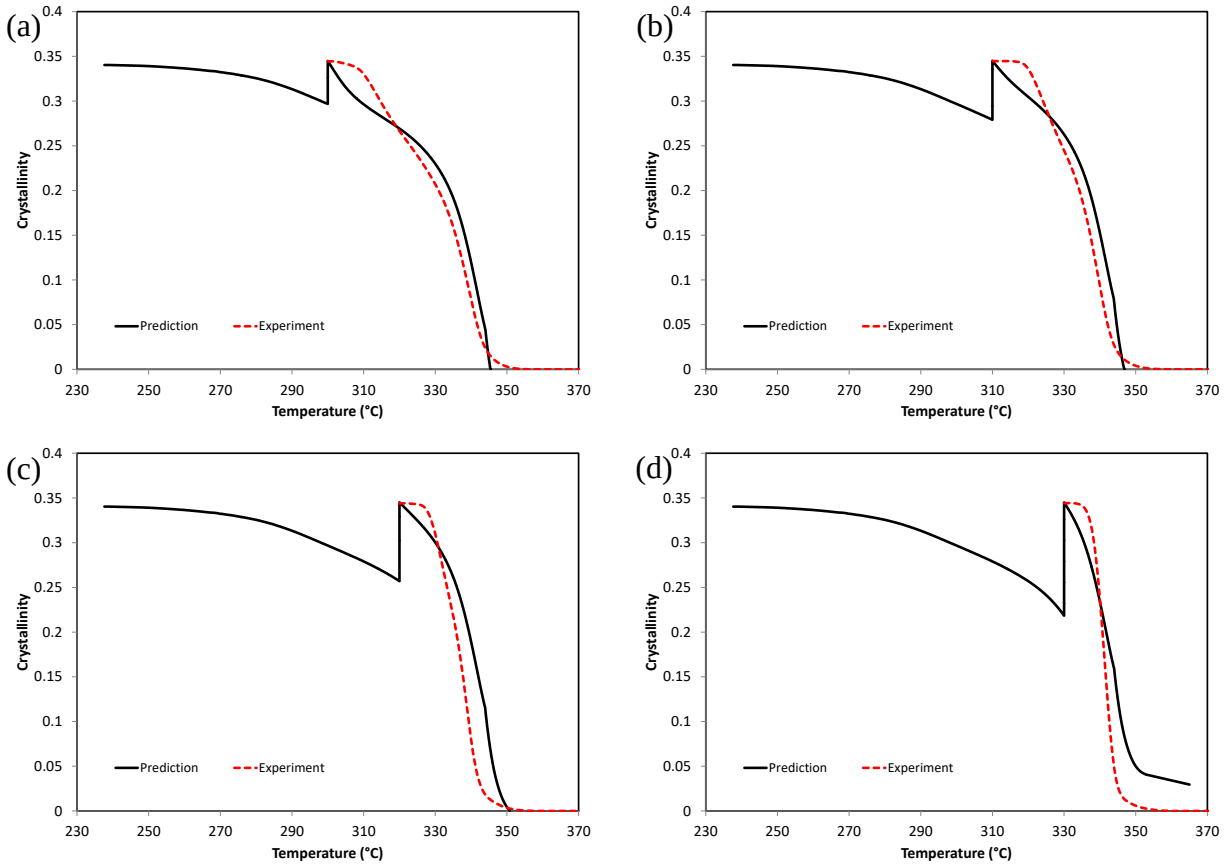

Figure 3-49 Variation of crystallinity for heating at 10 ℃/min subsequent to heating at 10 ℃/min from room temperature and then isothermal hold at (a) 300 ℃, (b) 310 ℃, (c) 320 ℃, (d) 330 ℃, model predictions and experimental results

Model predicted results and experimental data for cooling-annealing-melting experiments are compared in Figure 3-50.

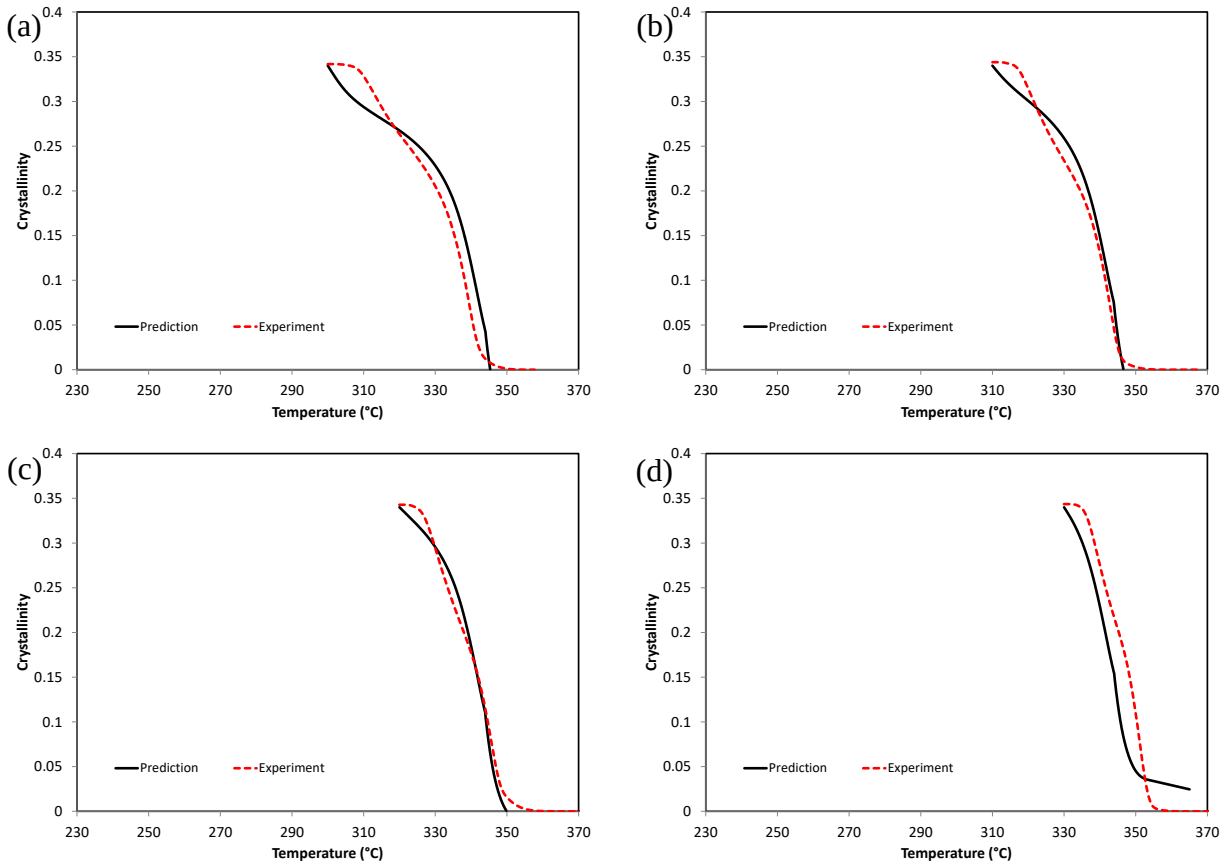

Figure 3-50 Variation of crystallinity for heating at 10 ℃/min subsequent to cooling at 10 ℃/min from 380 ℃ and then isothermal hold at (a) 300 ℃, (b) 310 ℃, (c) 320 ℃, (d) 330 ℃, model predictions and experimental results

The results from both Figure 3-49 and Figure 3-50 indicate that model predictions are acceptable.

In summary, the 'master melt curve' concept introduced in this chapter, along with the presented crystallization kinetics model, can be used for prediction of changes in the degree of crystallinity during the processing of the material with an arbitrary temperature cycle. Model predictions were compared with the experimental measurements for different scenarios and they are in good agreement.

Chapter 4: Thermo-Viscoelastic Behaviour; Experiments and Model Development

In this chapter, stress relaxation experiments and their results are presented for AS4/PEEK, neat PEEK, fully cured AS4/8552 and fully cured neat 8552 resin. Temperature dependency of the unrelaxed values of the moduli is concluded from the experimental results. A 'vertical shift factor' is introduced and the master curves of the relaxation moduli are generated. Prony series are fitted to the master curves.

Thermo-elastic behaviour of the polymer in the glassy regime is studied using some load control tests on fully cured 8552 resin.

The integral form constitutive model of Schapery is introduced for creep of thermo-rheologically complex materials. The integral is transformed to the differential form and it is shown that it has a Kelvin-type mechanical analogue. A stress relaxation-type equivalent of Schapery's integral is proposed based on nonlinear models of Schapery, derived from thermodynamics. The integral is converted to the differential form which has a Maxwell-type mechanical analogue. The constitutive relations are modified based on the experimental results for the behaviour of material in glassy regime. The equations are generalized to three dimensional form for isotropic, transversely-isotropic and orthotropic cases. Time integration of equations is carried out and the final equations are derived for implementation as a finite element user material (UMAT).

4.1 Stress relaxation experiments

Thermo-viscoelastic characterization was performed via stress relaxation experiments, using a TA instrument Q800 DMA machine (Figure 4-1), with 3-Point bending and dual cantilever clamps.

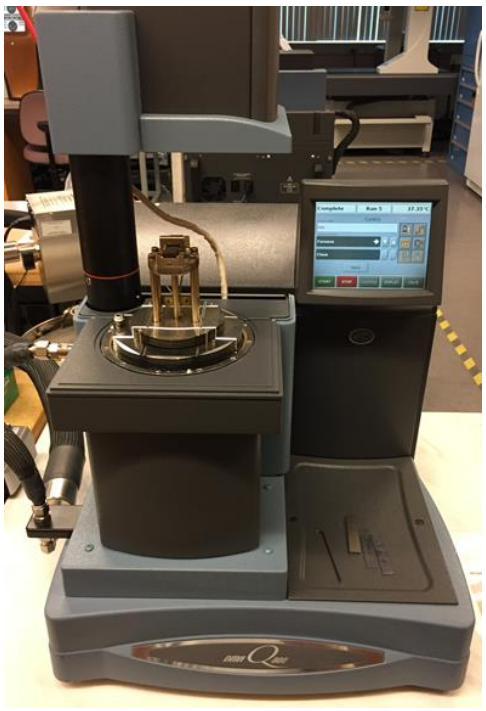

Figure 4-1 TA Instruments Q800 DMA machine

4.1.1 Materials

Stress relaxation experiments were conducted on specimens made of four different materials.

4.1.1.1 TenCate Cetex® TC1200 PEEK AS4

AS4/PEEK, introduced in section 3.1, was used for making unidirectional laminated panels. The panel was made of 16 layers of the unidirectional tape. Processing was performed in a picture frame tool assembly using a Wabash hydraulic hot press [128]. The material was heated in an oven, close to the hot press, to 390 ℃ and then consolidated for 6 min in the hot press while the temperature of the platens were held constant at 290 ℃. Finally the part was removed from the press and naturally cooled to room temperature. Beam samples were cut from the plate such that the fibres are in transverse direction.

4.1.1.2 Victrex® PEEK 150P

Victrex® PEEK 150P [135] powder is used for making DMA beam samples. To the best knowledge of the author [136], this is the same PEEK material used in AS4/PEEK. The samples were manufactured using an in house developed mini autoclave by Convergent Manufacturing Technologies. Material was heated to 390 ℃, under a pressure of 100 psi (pressurized nitrogen) and then cooled at 3 ℃/min to 20 ℃. This material is referred to as neat PEEK for the rest of this document.

4.1.1.3 Hexcel HexPly® 8552/AS4

Hexcel HexPly® 8552/AS4 prepreg was used for making fully cured panels. This material is referred to as AS4/8552 for the rest of this document. 12 layers of prepreg were used for making

the unidirectional panels. The panel was cured in an autoclave with the following temperature cycle: Heating at 2℃/min to 180 ℃, hold for 2 hour and cooling at 3 ℃/min to 20 ℃. Finally it was post-cured by heating at 0.5 ℃/min to 220 ℃ and holding isothermal for 30 min. DMA beam samples were cut from the panel such that the fibres were in the transverse direction.

4.1.1.4 Hexcel 8552 resin film

Hexcel 8552 resin film was used for making DMA beam samples. The curing process was conducted in the in house made mini autoclave by Convergent Manufacturing Technologies. The employed cure cycle was as follows: heating at 5 ℃/min to 110 ℃, isothermal hold for 100 min, heating at 0.5 ℃/min to 220 ℃, and isothermal hold for 60 min. This material is referred to as fully cured 8552 resin for the rest of this document.

One example of DMA samples from each material is shown in Figure 4-2.

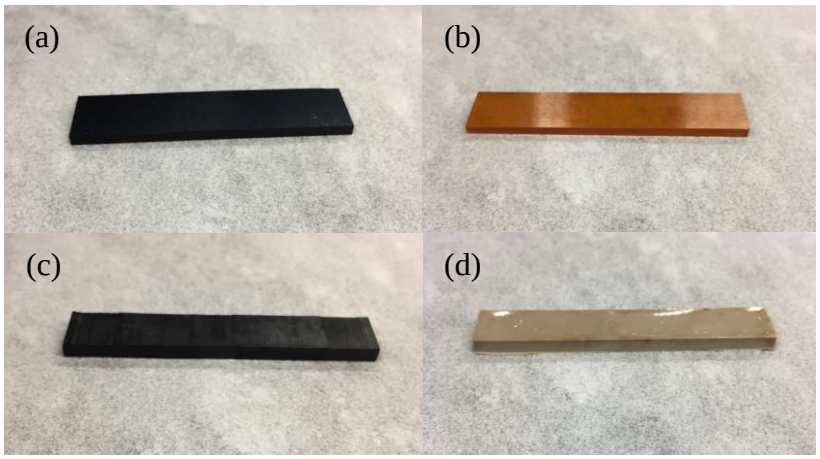

Figure 4-2 DMA specimens made of (a) AS4/8552 (b) 8552 neat resin (c) AS4/PEEK (d) neat PEEK

4.1.2 Methodology

Beam samples of rectangular cross section were tested in 3-point bending or dual cantilever clamps, as shown in Figure 4-3.

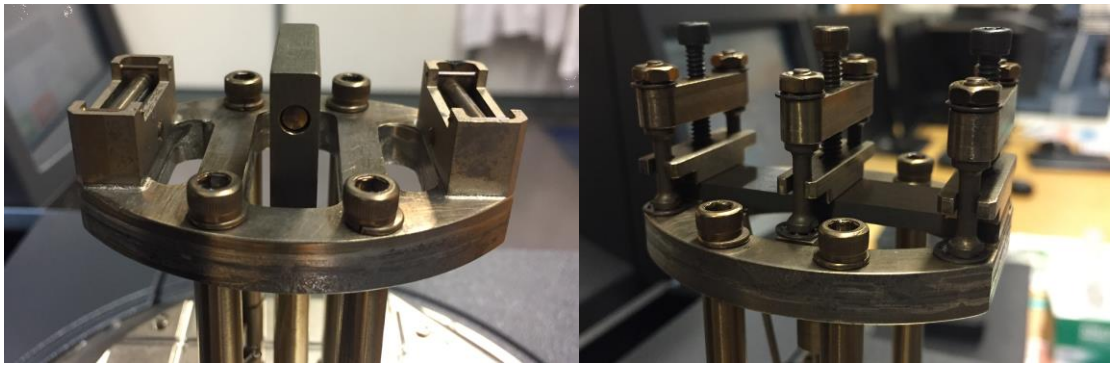

Figure 4-3 DMA clamps: 3-Point bending (left), Dual cantilever (right)

All composite samples were unidirectional and were tested in the transverse direction. Samples dimensions and clamps are given in Table 4-1.

Table 4-1 DMA samples dimensions and clamps

Material	Sample	Length (mm)	Width (mm)	Thickness (mm)	Clamp
AS4/PEEK	A	35	11.62	3.12	Dual cantilever
AS4/PEEK	B	35	11.25	3.09	Dual cantilever
AS4/PEEK	C	35	11.52	3.10	Dual cantilever
PEEK	A	35	9.94	3.04	Dual cantilever
PEEK	B	35	9.80	3.04	Dual cantilever
AS4/8552	A	50	12.32	2.29	3-point bending
AS4/8552	B	50	13.21	2.30	3-point bending
AS4/8552	C	50	12.54	2.30	3-point bending
8552	A	50	12.63	2.87	3-point bending
8552	B	50	12.63	2.90	3-point bending

In each stress relaxation experiment, the sample was equilibrated at each temperature followed by an isothermal hold for 5 minute. A constant deflection was applied to the beam for 10 minute and the force required for keeping this deflection was recorded by the machine. Next the sample was equilibrated at another temperature and the mentioned steps were repeated. This procedure

continued until the complete desired temperature range was covered. Using the force and deflection data and sample dimensions, the modulus of the material was calculated using beam theory. The calculated modulus for the composite samples is the transverse modulus, E_2.

4.1.3 Raw data and general interpretations

4.1.3.1 Test results for AS4/PEEK

Three AS4/PEEK samples, as given in Table 4-1, were tested. For sample A, the temperature was changed from 30 ℃ to 340 ℃. The temperature range for samples B and C was between -50 ℃ to 340 ℃. The relaxation moduli versus time at different temperatures are given in Figure 4-4, Figure 4-5, and Figure 4-6 for samples A, B and C, respectively. According to the melting rate curves in Figure 3-27, the material melts at temperatures higher than approximately 250 ℃. Therefore, any relaxation data for temperatures higher than 250 ℃ should be interpreted carefully.

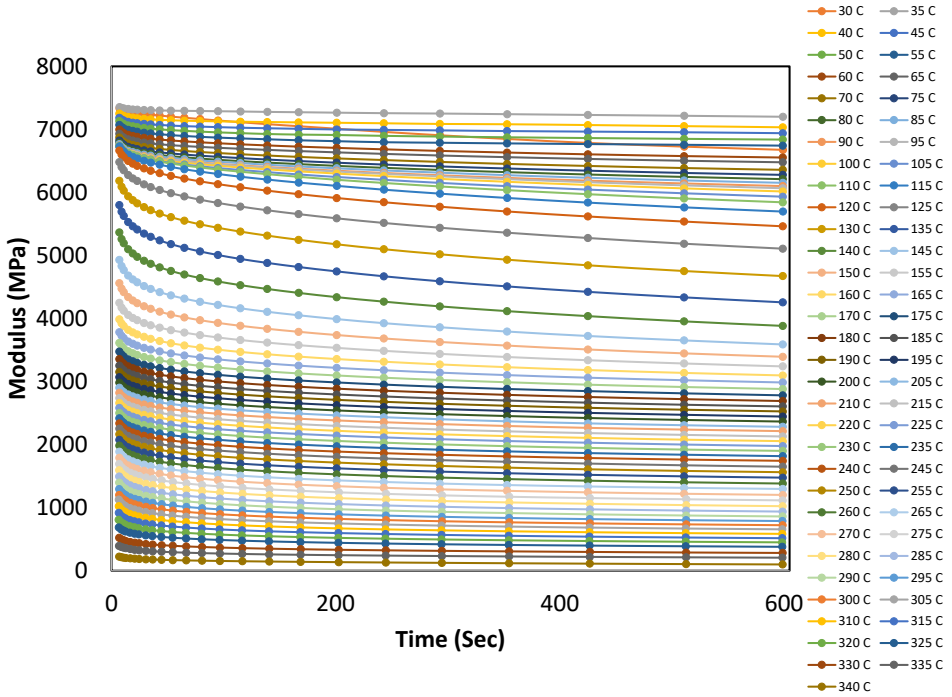

Figure 4-4 Relaxation moduli, $E_2(t)$, for AS4/PEEK-Sample A at different temperatures

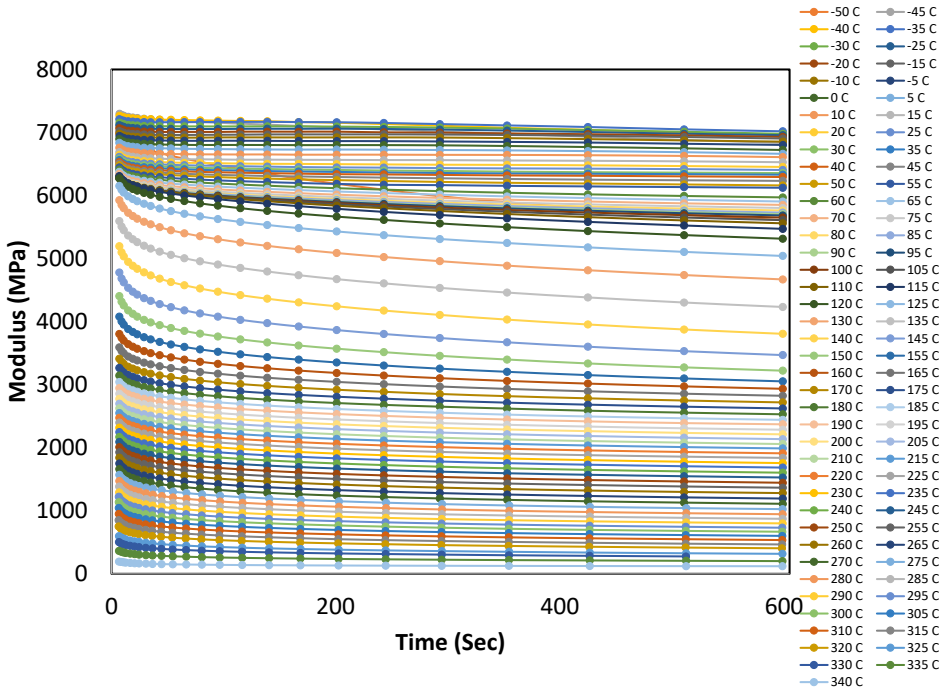

Figure 4-5 Relaxation moduli, $E_2(t)$, for AS4/PEEK-Sample B at different temperatures

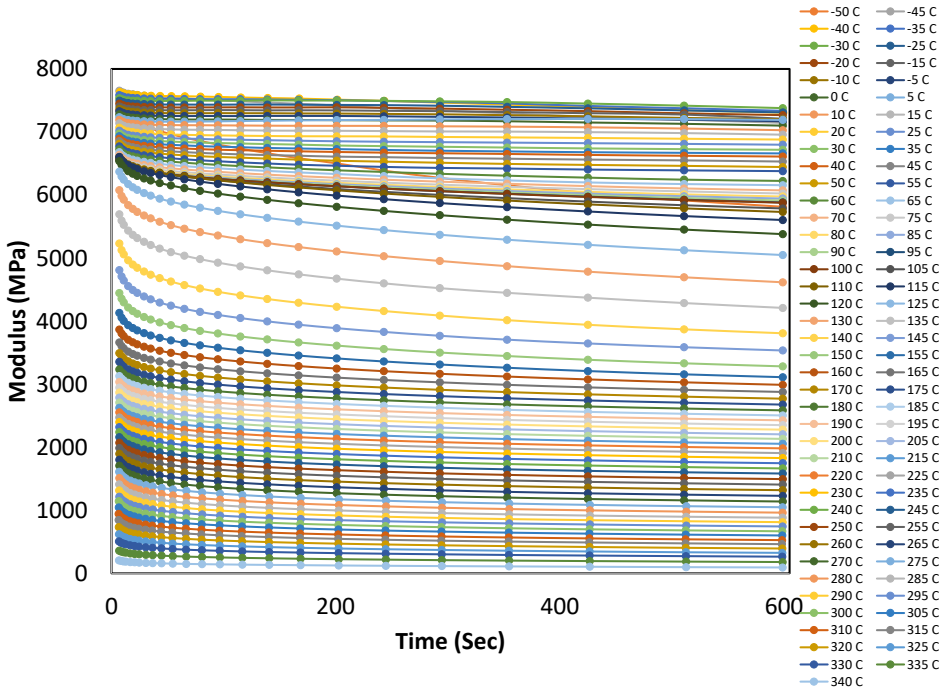

Figure 4-6 Relaxation moduli, $E_2(t)$, for AS4/PEEK-Sample C at different temperatures

From test results it is concluded that at all temperatures, the modulus values decrease gradually. The decline of the modulus is lower at very low temperatures as well as very high temperatures.

4.1.3.2 Test results for neat PEEK

Variations of relaxation moduli with time at different temperatures for neat PEEK specimens are displayed in Figure 4-7 and Figure 4-8. Temperature range for samples A and B is between 30 ℃ and 290 ℃, and −100 ℃ and 300 ℃, respectively. For neat PEEK, temperatures higher than

300 ℃ are not applicable as the material flows and the beam specimen loses its shape. In contrast, for AS4/PEEK, presence of fibres inhibits flowing of the resin and higher temperatures are valid, accordingly.

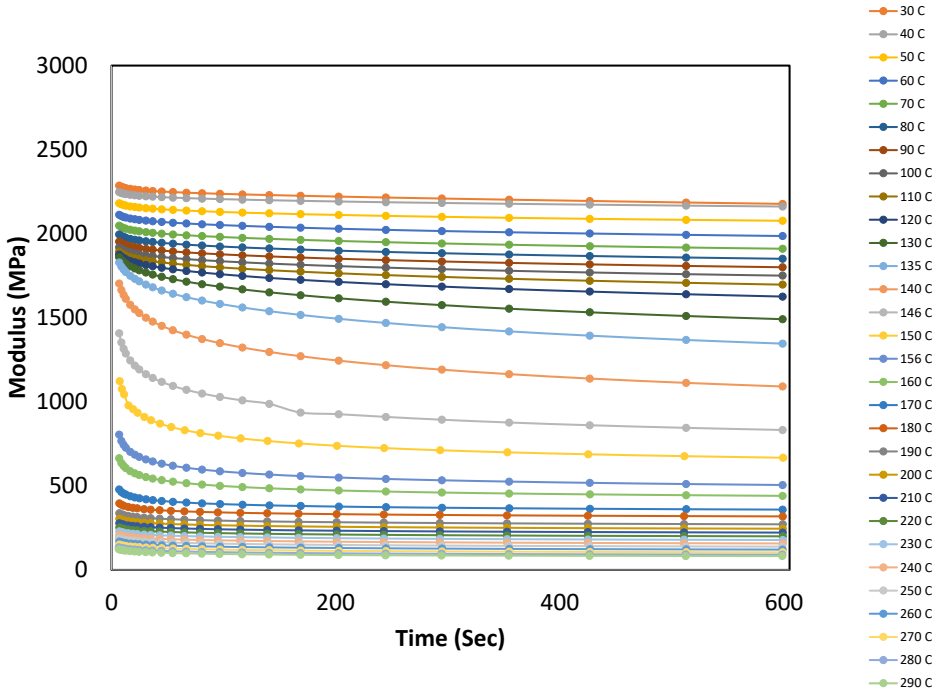

Figure 4-7 Relaxation moduli, $E(t)$, for PEEK-Sample A at different temperatures

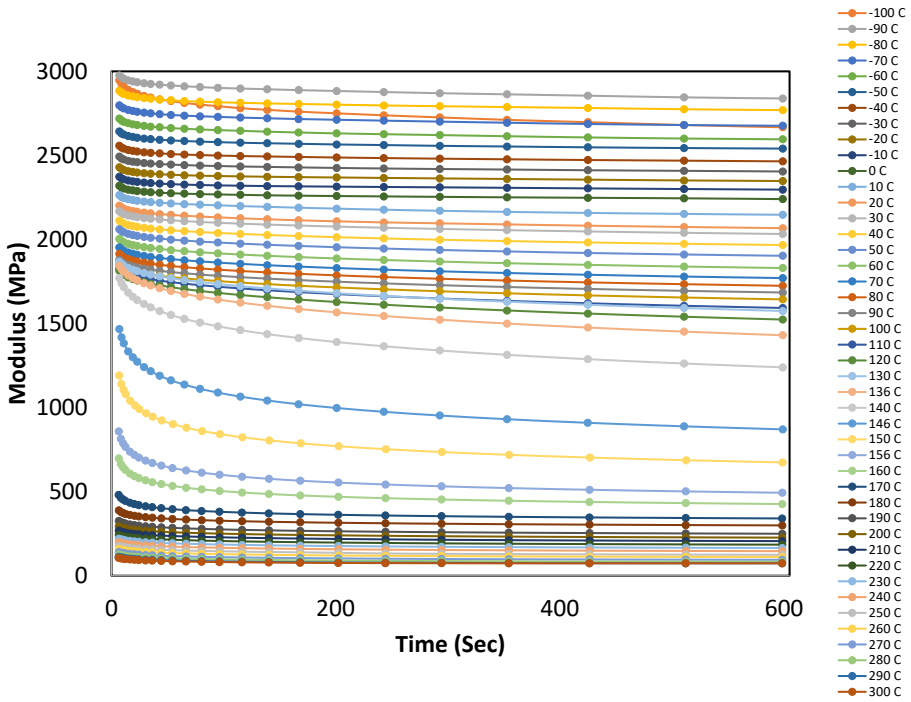

Figure 4-8 Relaxation moduli, $E(t)$, for PEEK-Sample B at different temperatures

4.1.3.3 Test results for fully cured AS4/8552

Relaxation moduli for three different fully cured AS4/8552 samples at different temperatures are shown in Figure 4-9, Figure 4-10, and Figure 4-11.

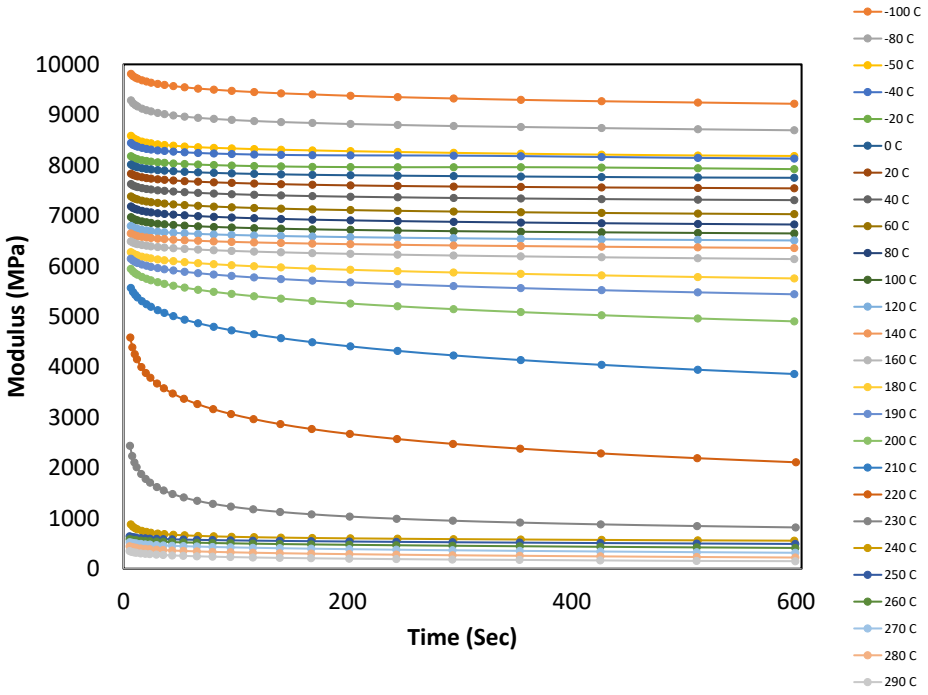

Figure 4-9 Relaxation moduli, $E_2(t)$, for AS4/8552-Sample A at different temperatures

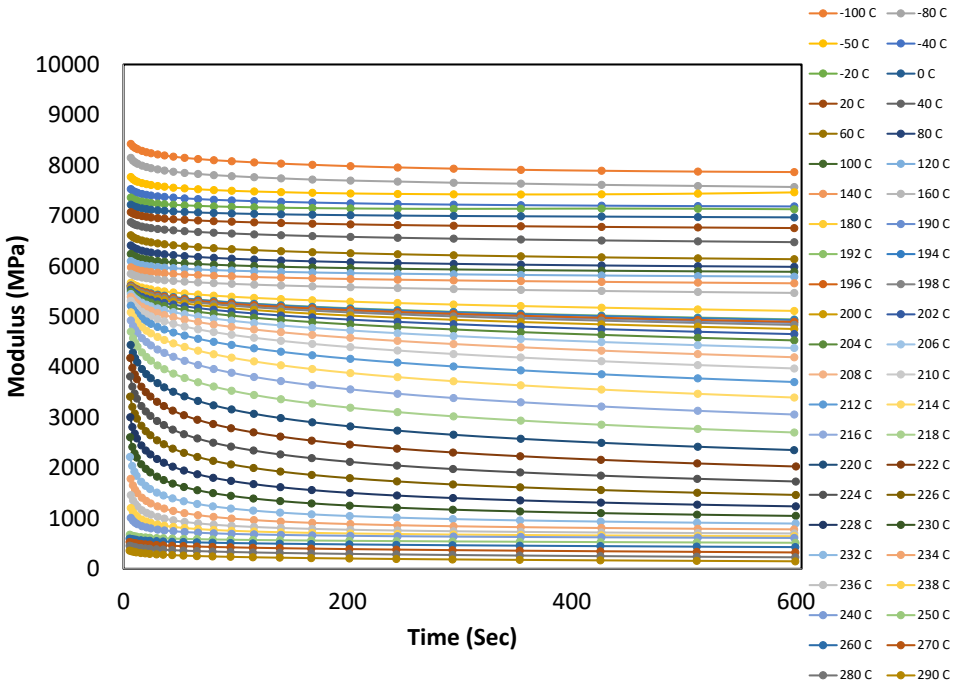

Figure 4-10 Relaxation moduli, $E_2(t)$, for AS4/8552-Sample B at different temperatures

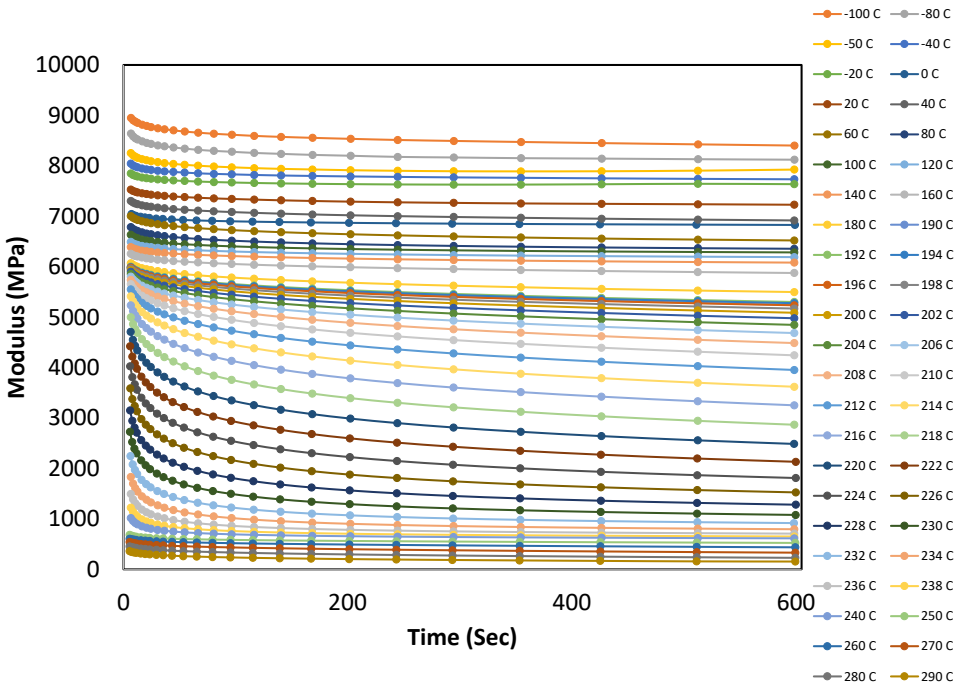

Figure 4-11 Relaxation moduli, $E_2(t)$, for AS4/8552-Sample C at different temperatures

For all three samples the temperature was varied between -100 ℃ and 290 ℃. For test results at temperatures above 250 ℃, the material might be degraded.

4.1.3.4 Test results for fully cured 8552 resin

The relaxation modulus test results for fully cured 8552 resin samples are illustrated in Figure 4-12 and Figure 4-13.

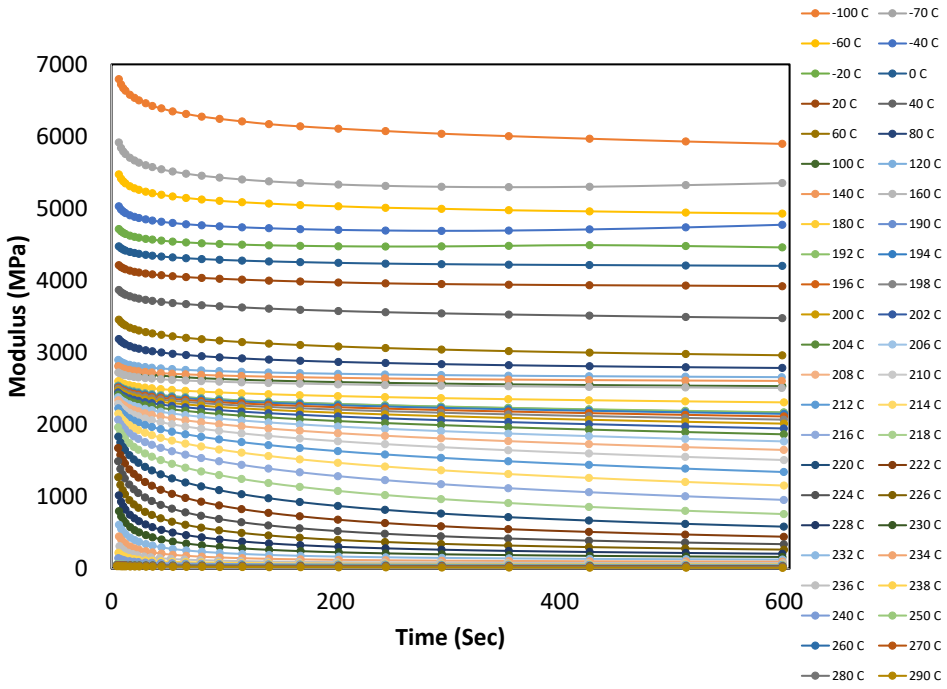

Figure 4-12 Relaxation moduli, $E(t)$, for 8552-Sample A at different temperatures

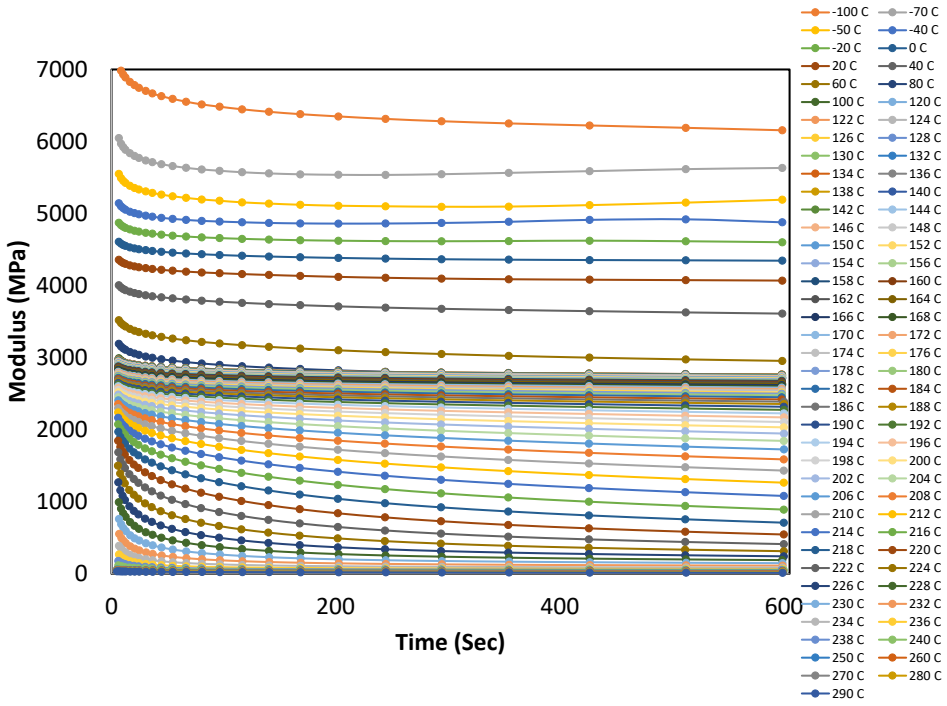

Figure 4-13 Relaxation moduli, $E(t)$, for 8552-Sample B at different temperatures

Similar to AS4/8552 samples, the temperature was varied between -100 ℃ and 290 ℃.

4.1.4 Generating the master curves

According to Schwarzl and Staverman [119], if the change of temperature for a linear viscoelastic material is equivalent to a shift of logarithmic time scale, the material is called 'thermo-rheologically simple'. For such a material, the relaxation moduli data at different temperatures are plotted versus $\log t$. A reference temperature is chosen and moduli curves for other temperatures are shifted horizontally such that one smooth curve is created. The resulting curve is the so-called 'master curve' at that reference temperature. The procedure of generating the master curves using horizontal shifting in the $\log t$ space is referred to as 'time-temperature superposition' [137].

At the molecular level, thermo-rheologically simple behaviour implies that at different temperatures, the same sequence of molecular events occurs with different speeds [119]. Another interpretation of thermo-rheologically simple behaviour is that all relaxation times of the material are affected by the temperature in the same way [137]. One important feature of thermo-rheologically simple materials is that the initial and long-term values of the moduli, hereafter referred to as unrelaxed and relaxed moduli are independent of temperature [138].

In this section, applicability of time-temperature superposition is examined for all AS4/PEEK, PEEK, fully cured AS4/8552 and fully cured 8552 samples and a procedure is proposed for generation of the master-curves.

4.1.4.1 Master curves for AS4/PEEK

In this section, the procedure of generating the master curve for transverse modulus, E_2, of AS4/PEEK-sample C is explained. The variation of relaxation modulus at different temperatures for AS4/PEEK-sample C are displayed in Figure 4-14, in logarithmic-logarithmic scale.

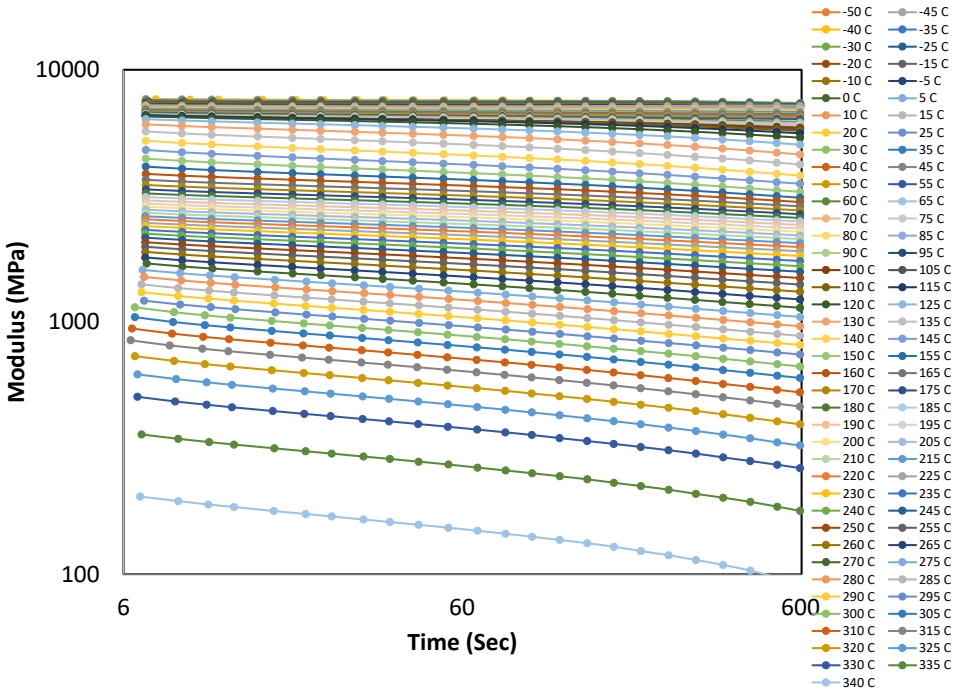

Figure 4-14 Relaxation moduli, $E_2(t)$, for AS4/PEEK-Sample C at different temperatures, in logarithmic-logarithmic scale

For investigating the temperature dependence of unrelaxed modulus, the first data point from the relaxation experiments at different temperatures is extracted and the results are plotted against

temperature in Figure 4-15. The first data point at each temperature is collected at 6.98 seconds, subsequent to application of the deflection. Such a graph is called the 'isochronous curve' at 6.98 second, $E_2(t = 6.98\ \text{s})$.

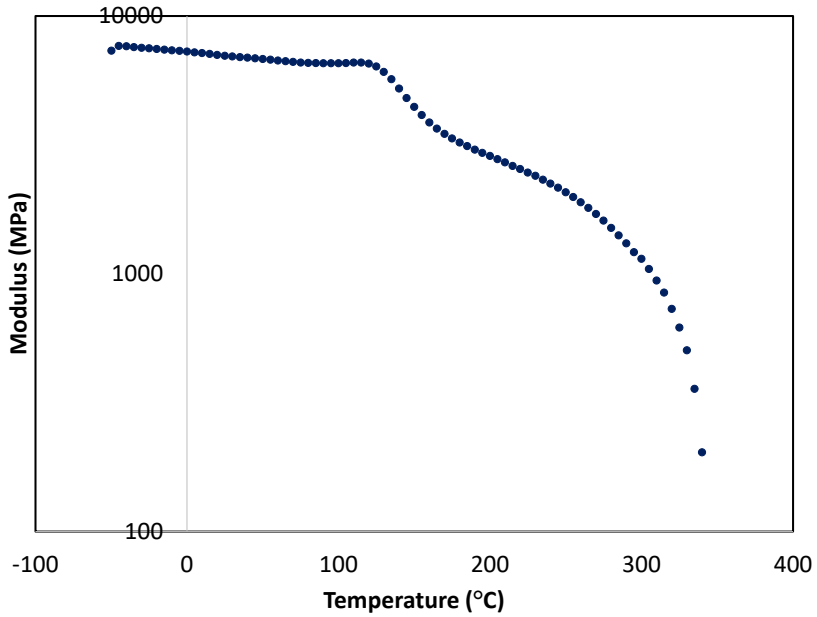

Figure 4-15 Isochronous moduli at 6.98 s, $E_2(6.98\ \text{s})$, for AS4/PEEK-Sample C

As mentioned, the plot in Figure 4-15 is created using the first data points collected in each relaxation test. For temperatures less than 120 ℃, which is near T_g, these modulus values may be considered as the unrelaxed moduli. For temperatures higher than 120 ℃, a significant decline is realized in the modulus. At these high temperatures, the material relaxes at a high speed and the machine is not capable of recording the unrelaxed moduli. Therefore, we extrapolate the unrelaxed modulus at 120 ℃ for higher temperatures and consider it as the unrelaxed modulus for those

temperatures. It is seen later that this approach results in a smooth master curve. The unrelaxed modulus, $E_2^u(T)$, is shown in Figure 4-16.

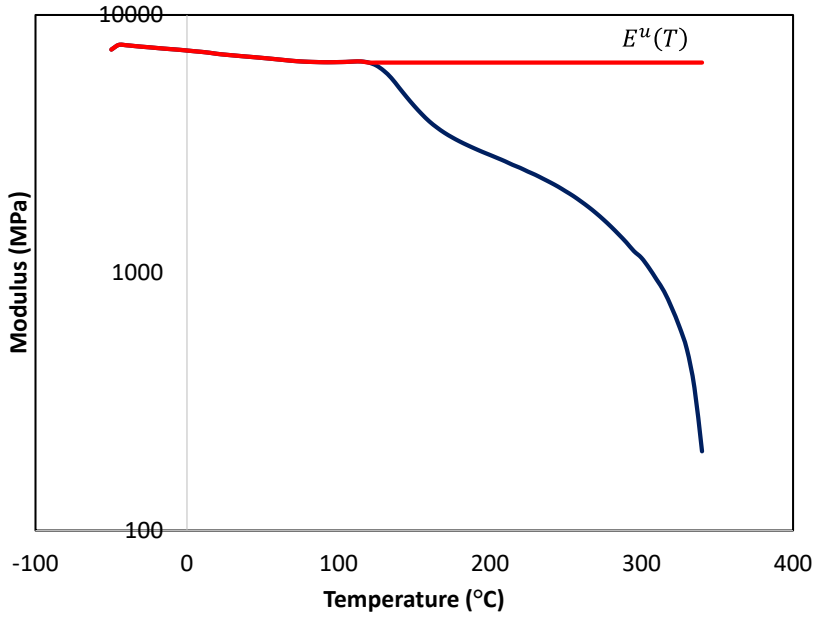

Figure 4-16 Isochronous moduli at 6.98 s and unrelaxed modulus, $E_2^u(T)$, for AS4/PEEK-Sample C

As explained, the unrelaxed modulus of the material is temperature dependent which implies the material behaviour is not thermo-rheologically simple. Such a material behaviour was termed 'thermo-rheologically complex' behaviour by Schapery [121].

The first step in generating the master curve is picking a reference temperature, T_{ref}. Here, T_{ref} is selected as 140 ℃. Since the simple shifting of the curves in logarithmic time space is not sufficient for generating the master curves, a so-called 'vertical shift factor' is defined for normalizing the modulus values, prior to horizontal shifting, as

$$a_F(T) = \frac{E^u(T)}{E^u(T_{ref})} \qquad \textbf{(4-1)}$$

The relaxation modulus values at each temperature, $E(t,T)$, are normalized as

$$E^N(t,T) = \frac{E(t,T)}{a_F(T)} \qquad \textbf{(4-2)}$$

The normalized values of modulus, obtained using Equation (4-2), are displayed in Figure 4-17.

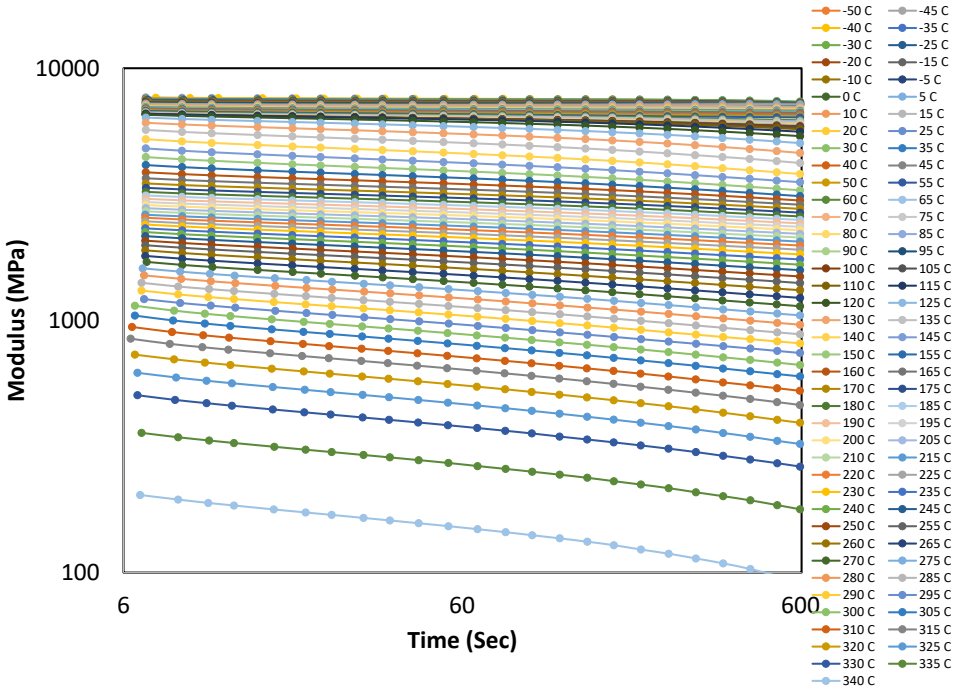

Figure 4-17 Normalized relaxation moduli, E_2^N, for AS4/PEEK-Sample C at different temperatures, in logarithmic-logarithmic scale

Next, these normalized moduli are horizontally shifted in the logarithmic time space and the master curve is generated which is shown in Figure 4-18.

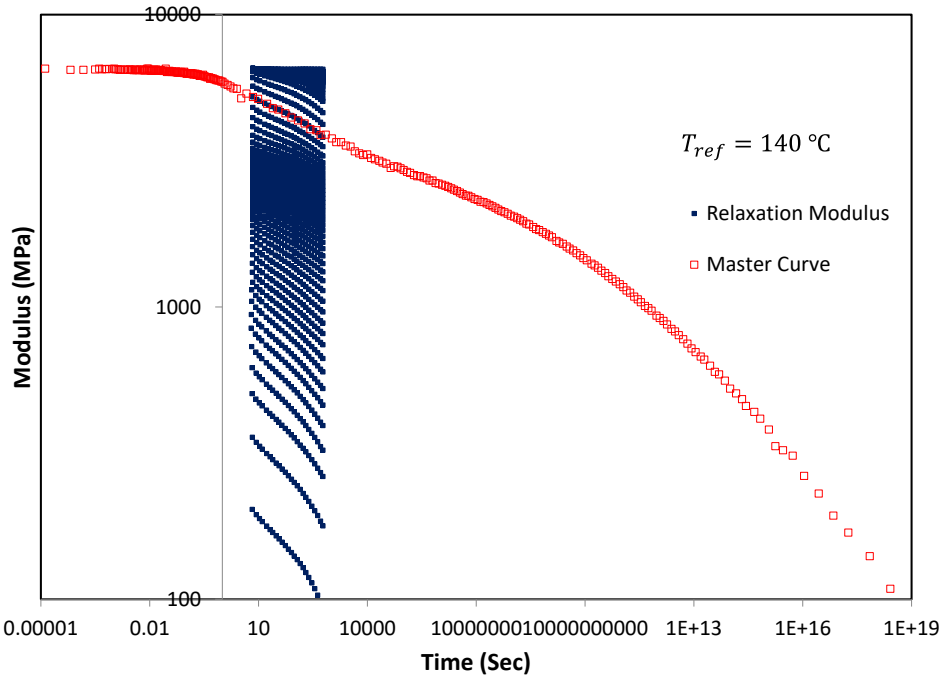

Figure 4-18 Master curve of relaxation modulus, $E_2(t)$, for AS4/PEEK-Sample C at T_{ref} = 140 ℃

The generated master curve in Figure 4-18 is smooth which confirms that the proposed procedure is satisfactory. It is evident from the graph that the results corresponding to temperatures higher than the reference temperature are horizontally shifted to the right, and the results related to temperatures lower than the reference temperature and shifted to the left. The extent of horizontal shifting in the logarithmic time space at each temperature is $\log a_T(T)$ where $a_T(T)$ is defined as

the ‘horizontal shift factor’. The horizontal and vertical shift factors used for generating the master curve in Figure 4-18 are displayed in Figure 4-19 and Figure 4-20.

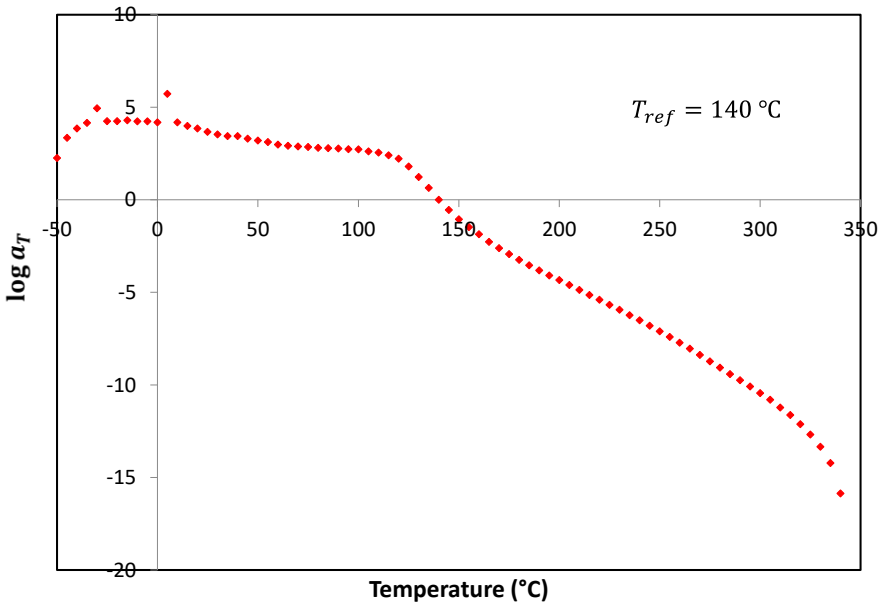

Figure 4-19 Horizontal shift factor of relaxation modulus, $E_2(t)$, for AS4/PEEK-Sample C at $T_{ref} = 140$ ℃

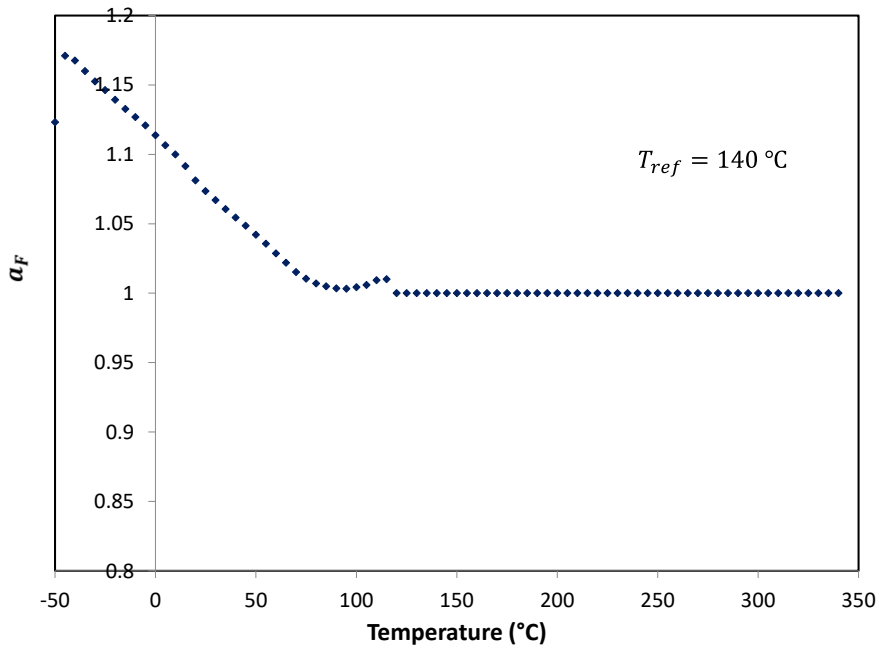

Figure 4-20 Vertical shift factor of relaxation modulus, $E_2(t)$, for AS4/PEEK-Sample C at $T_{ref} = 140$ ℃

Following the same procedure, master curves are generated for samples A and B. The master curves for three samples A, B and C are compared in Figure 4-21.

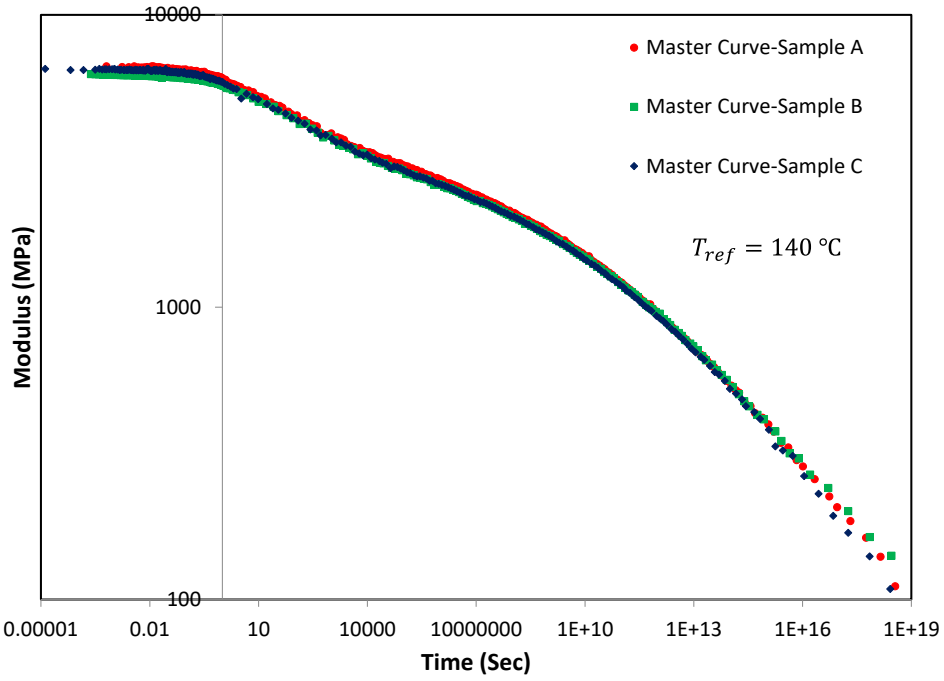

Figure 4-21 Master curves of relaxation modulus, $E_2(t)$, for AS4/PEEK samples at $T_{ref} = 140$ ℃

It is evident from Figure 4-21 that the master curves for the three samples are in good agreement. Also horizontal shift factors and vertical shift factors for the three samples are compared in Figure 4-22 and Figure 4-23. The results for the three samples are consistent. The discontinuity, observed in the vertical shift factors, is because of a minor increase in the unrelaxed moduli, right before the relaxation (Figure 4-15 and Figure 4-16).

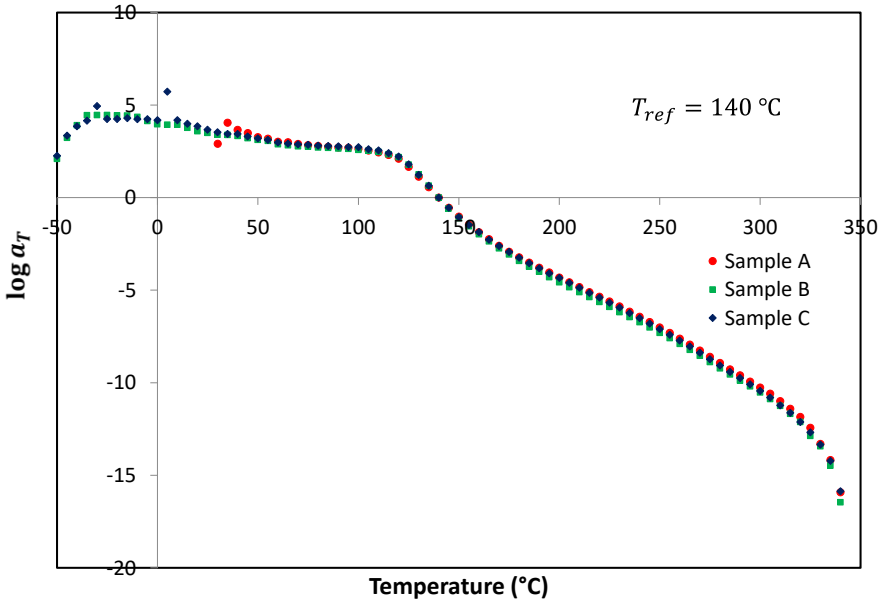

Figure 4-22 Horizontal shift factor of relaxation modulus, $E_2(t)$, for AS4/PEEK samples at T_{ref} = 140 ℃

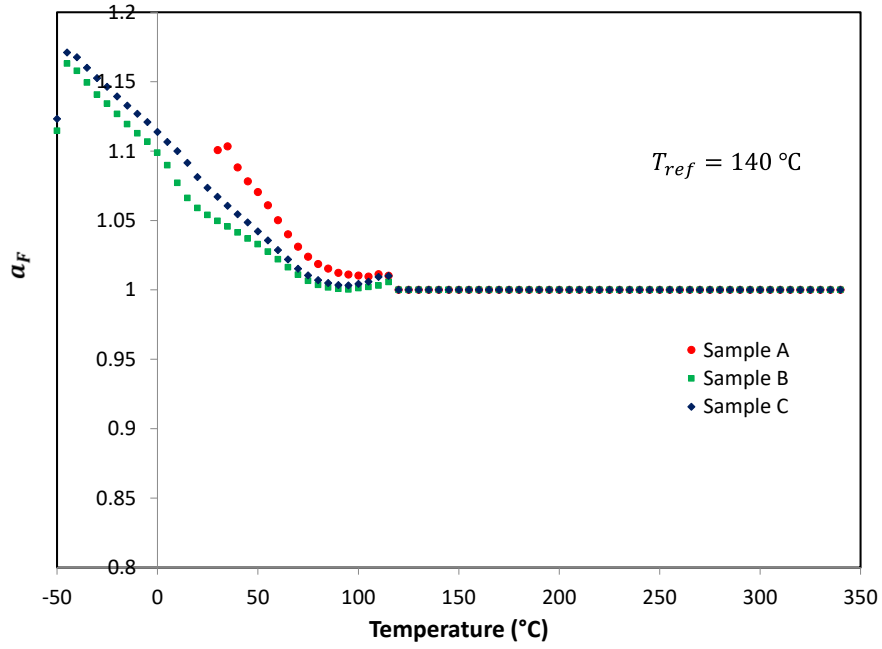

Figure 4-23 Vertical shift factor of relaxation modulus, $E_2(t)$, for AS4/PEEK samples at T_{ref} = 140 ℃

4.1.4.2 Master curves for neat PEEK

The isochronous curves at 6.98 second, $E(t = 6.98\ \mathrm{s})$, and the unrelaxed modulus for two neat PEEK samples are given in Figure 4-24 .

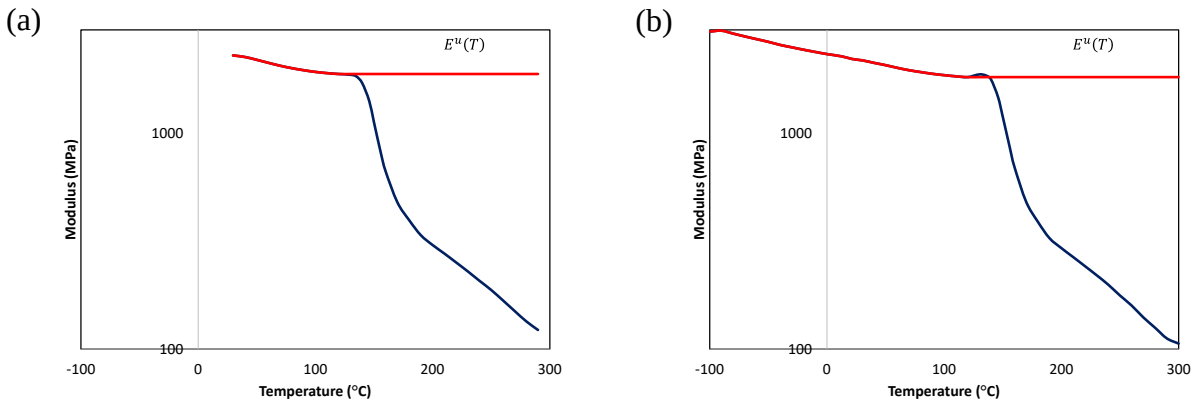

Figure 4-24 Isochronous moduli at 6.98 s and unrelaxed modulus, $E^u(T)$, for neat PEEK (a) Sample A (b) Sample B

Similar to the case of AS4/PEEK samples, the reference temperature is chosen to be 140 ℃. Employing the vertical shift factors as defined by Equation (4-1), the relaxation moduli are normalized using Equation (4-2). Next the normalized moduli are horizontally shifted in the logarithmic time space and the master curves are generated. The master curves for two samples are given in Figure 4-25. The horizontal and vertical shift factors are displayed in Figure 4-26. The results for two samples are consistent.

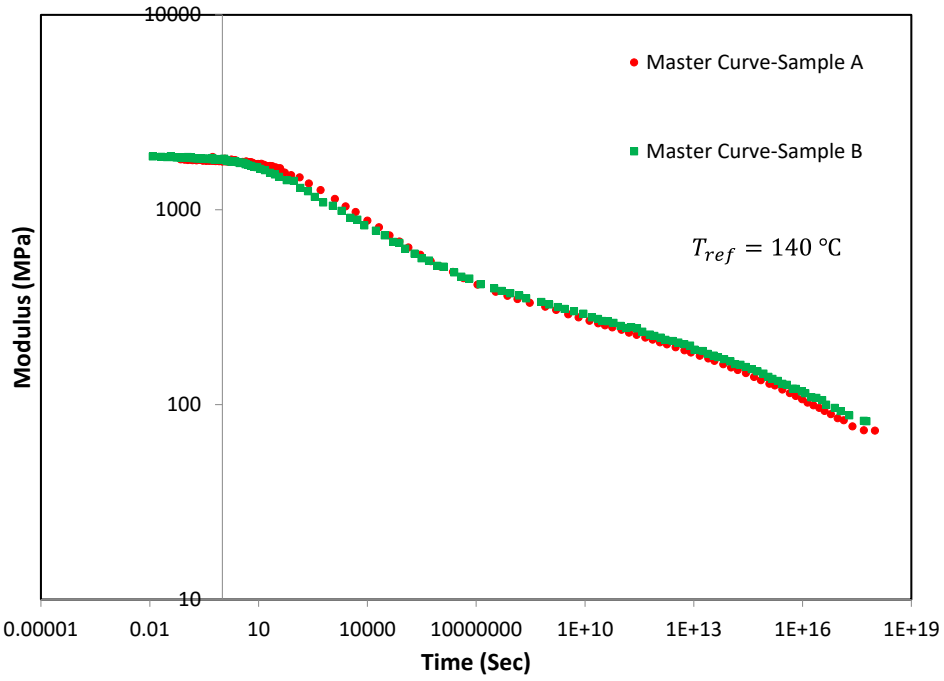

Figure 4-25 Master curves of relaxation modulus, $E(t)$, for neat PEEK samples at T_{ref} = 140 ℃

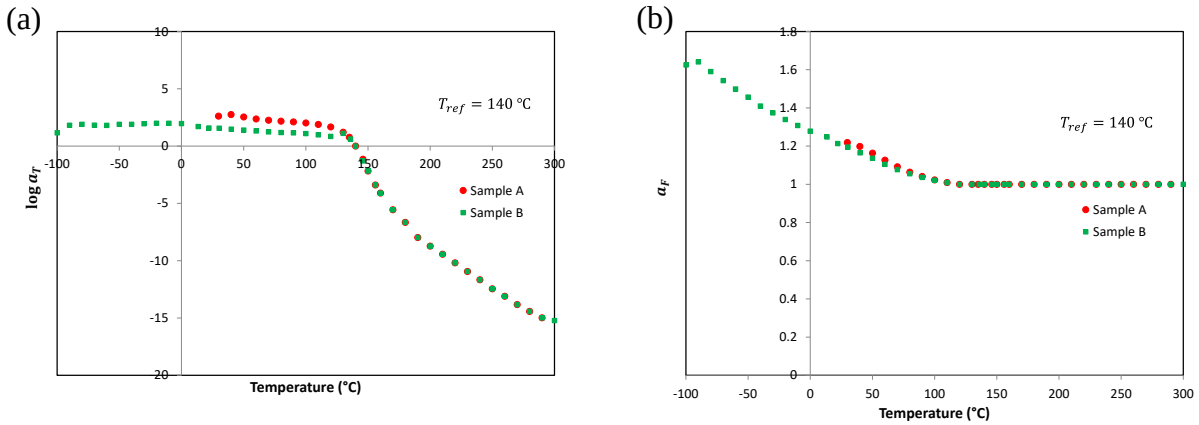

Figure 4-26 (a) Horizontal shift factor (b) Vertical shift factor of relaxation modulus, $E(t)$, for PEEK samples at T_{ref} = 140 ℃

4.1.4.3 Master curves for fully cured AS4/8552

Similar to the previous cases, the isochronous modulus curve, $E_2(t = 6.98\ \text{s})$, and the unrelaxed moduli, $E_2^u(T)$, for three AS4/8552 samples are given in Figure 4-27.

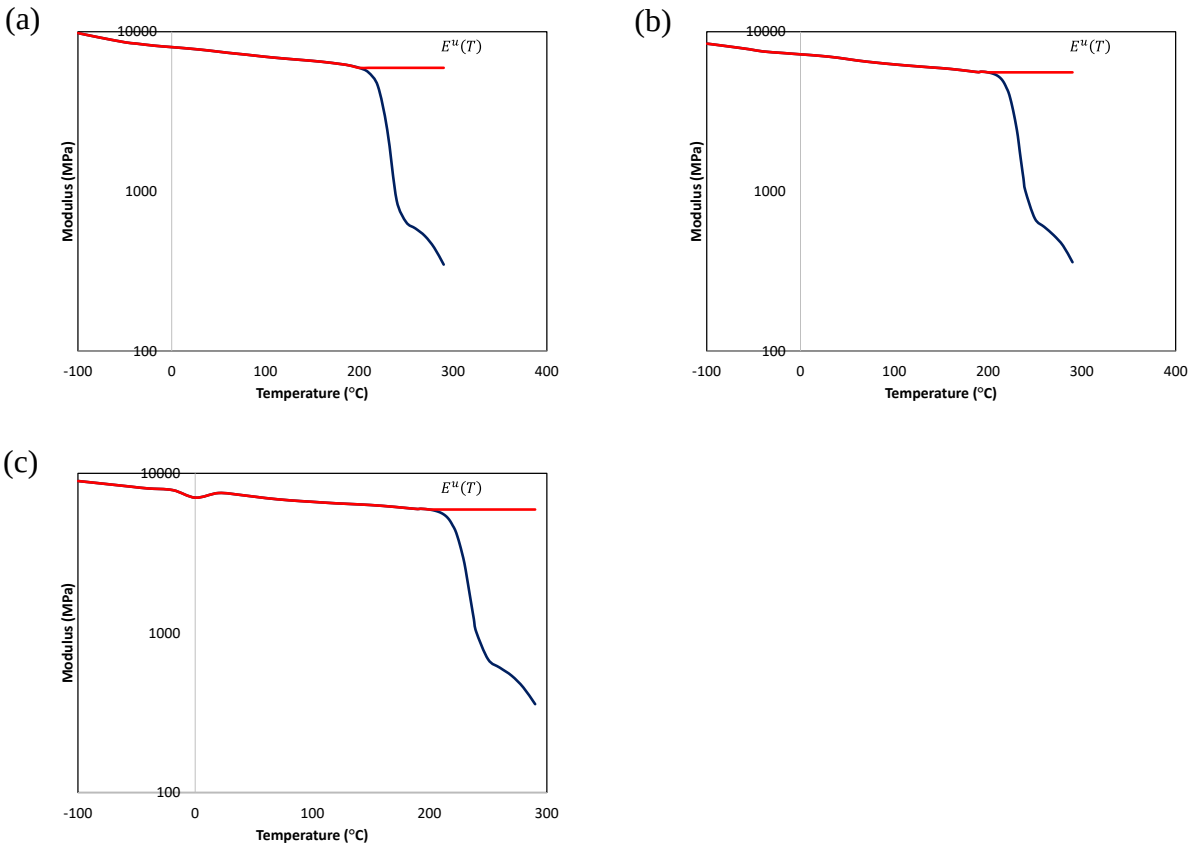

Figure 4-27 Isochronous moduli at 6.98 s and unrelaxed modulus, $E_2^u(T)$, for neat AS4/8552 (a) Sample A (b) Sample B (c) Sample C

Choosing the reference temperature as $T_{ref} = 200$ ℃, which is close to T_g, the moduli are normalized employing the Equations (4-1) and (4-2). Next the normalized moduli are shifted

horizontally in the logarithmic time space and the master curves are generated as presented in Figure 4-28.

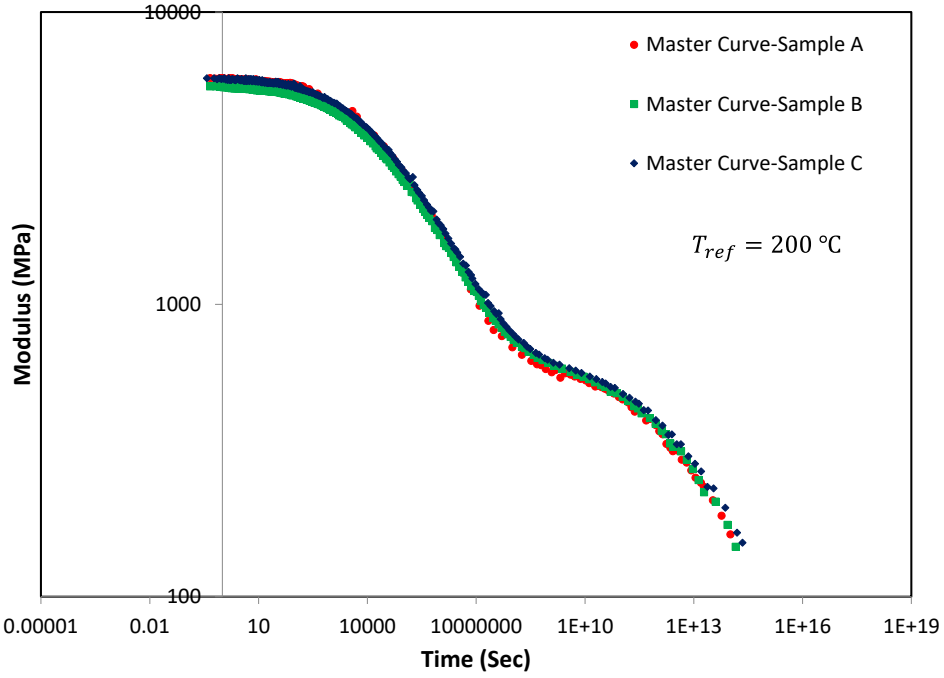

Figure 4-28 Master curves of relaxation modulus, $E_2(t)$, for AS4/8552 samples at $T_{ref} = 200$ ℃

The horizontal and vertical shift factors are given in Figure 4-29.

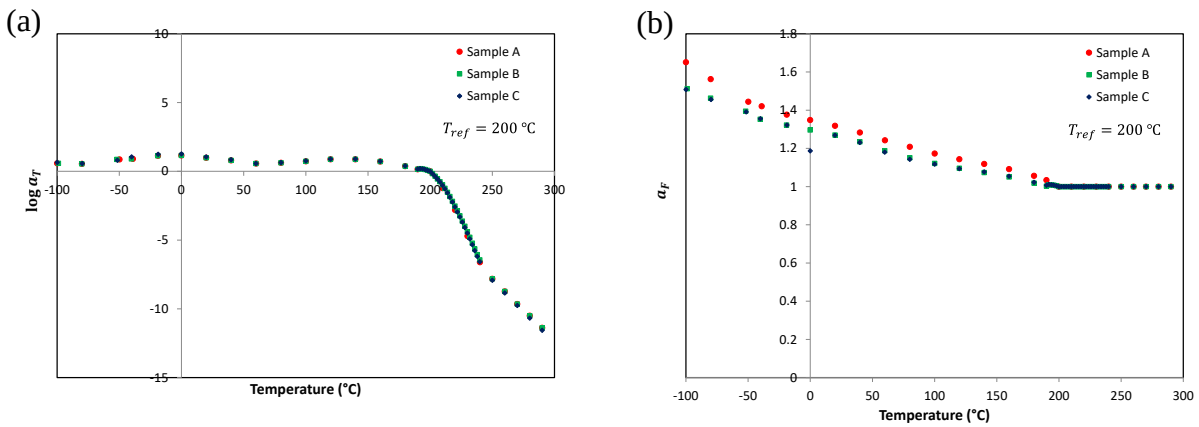

Figure 4-29 (a) Horizontal shift factor (b) Vertical shift factor of relaxation modulus, $E_2(t)$, for AS4/8552 samples at $T_{ref} = 200$ ℃

The results for the three samples are in good agreement.

4.1.4.4 Master curves for fully cured 8552 resin

The isochronous modulus curve, $E(t = 6.98\ \text{s})$, and the unrelaxed moduli, $E^u(T)$, for two fully cured 8552 resin samples are shown in Figure 4-30.

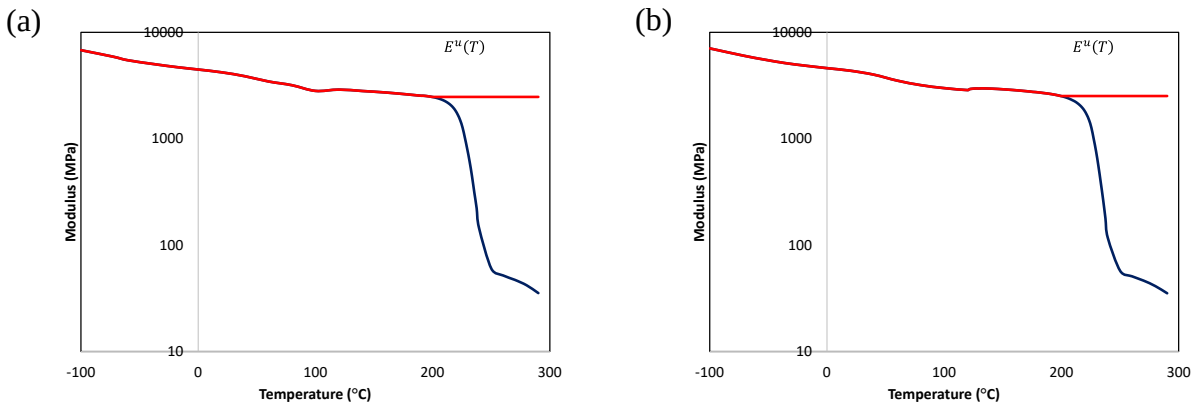

Figure 4-30 Isochronous moduli at 6.98 s and unrelaxed modulus, $E^u(T)$, for fully cured 8552 resin (a) Sample A (b) Sample B

Similar to the cases for AS4/8552, the reference temperature is chosen as $T_{ref} = 200$ ℃. The shift factors are calculated using Equation (4-1) and the moduli are normalized with the application of Equation (4-2). Shifting the normalized moduli in the logarithmic time space results in the master curves, as presented in Figure 4-31. Also the horizontal and vertical shift factors are given in Figure 4-32. All results for the two samples are consistent.

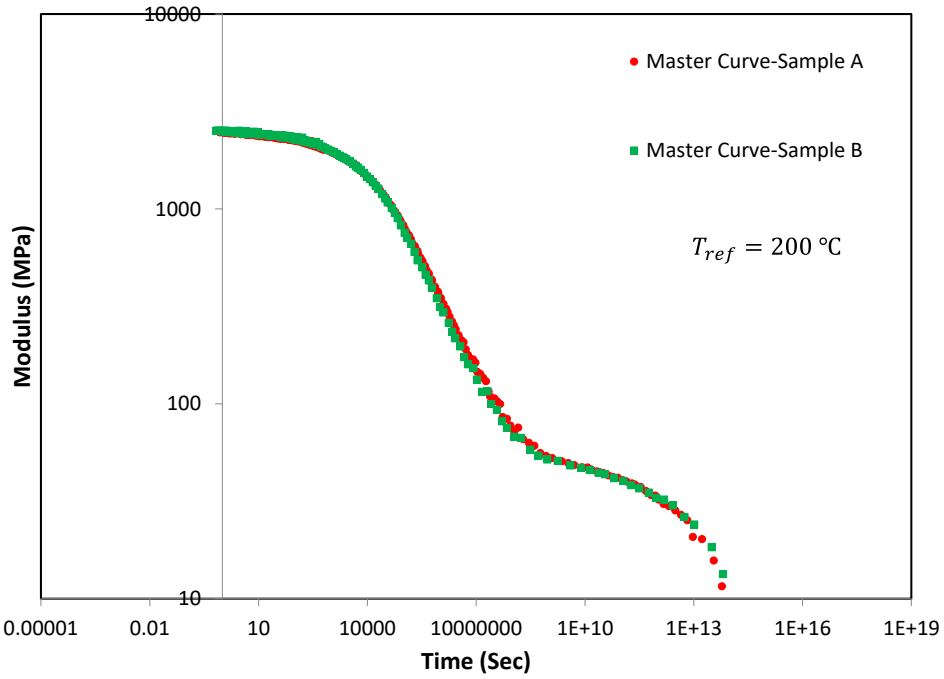

Figure 4-31 Master curves of relaxation modulus, $E(t)$, for fully cured 8552 resin samples at $T_{ref} = 200$ ℃

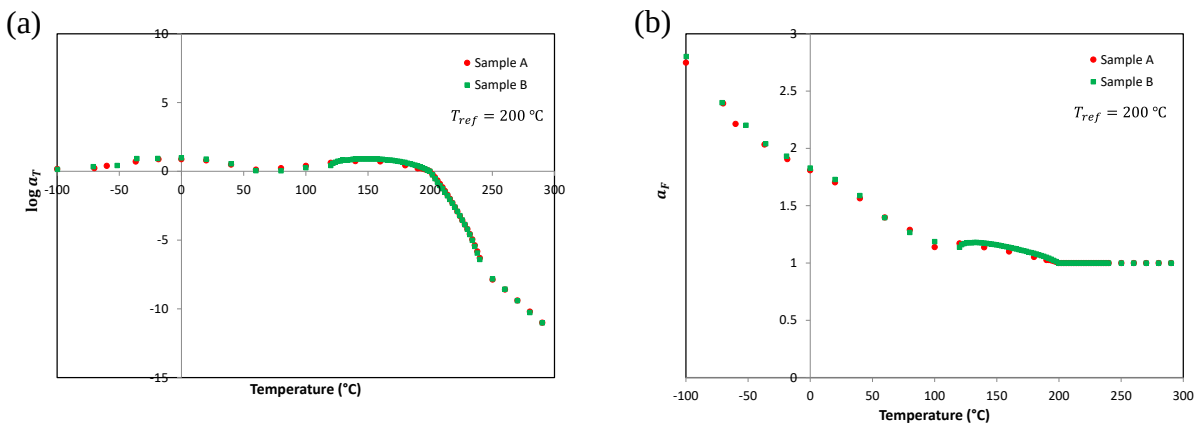

Figure 4-32 (a) Horizontal shift factor (b) Vertical shift factor of relaxation modulus, $E(t)$, for fully cured 8552 resin samples at $T_{ref} = 200$ ℃

4.1.5 Fitting Prony series

Subsequent to generating the master curves for relaxation modulus, the next step is expressing the modulus using a mathematical function, such as a Prony series:

$$E(t) = E_e + \sum_{i=1}^{N} E_i e^{-\frac{t}{\tau_i}} \qquad \textbf{(4-3)}$$

In order to fit Prony series to the experimental data, a regression algorithm may be used. If all parameters in Equation (4-3), i.e. E_e, E_i's and τ_i's are unknown (see [139]), a nonlinear regression algorithm should be employed (see [140]). An alternative approach is choosing the relaxations times, τ_i's, in advance and then using a linear regression algorithm for finding E_e and E_i's (see [141]-[144]). The relaxation times are usually chosen as uniformly spaced in the logarithmic time

space. In this section, the linear regression algorithm is adopted from the work of Zobeiry [69] and a Prony series of the form of Equation (4-3) is fitted to the master curves generated in section 4.1.4. The parameters E_e, E_i's and τ_i's for all cases are tabulated and the results are compared with the experimental data in the following sections.

4.1.5.1 Prony series for AS4/PEEK master curves

Fitted Prony series with $N = 36$ and $N = 10$ elements are compared with experimental master curve AS4/PEEK, sample A, in Figure 4-33.

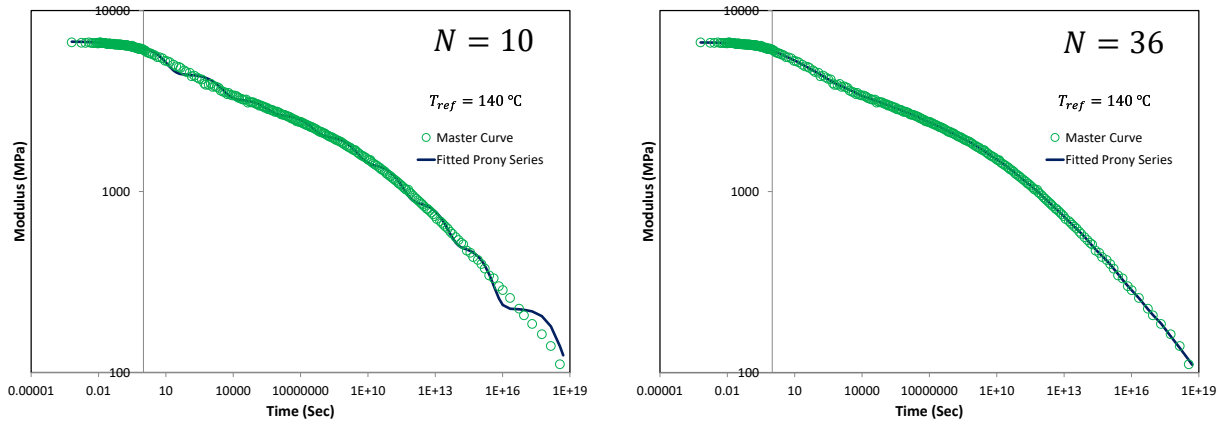

Figure 4-33 AS4/PEEK-Sample A-Master curves and fitted Prony series

Figure 4-33 shows that the Prony series with $N = 36$ terms results in a smooth curve which fits very well to the data. Considering that the computation effort is increased by increasing the number of Prony terms in a finite element code, it is advantageous to reduce the number of Prony terms. It is clear from Figure 4-33 that the Prony series with $N = 10$ does not create an as smooth curve,

however, the absolute values of the predicted moduli may be accurate enough for analysis. The results for samples B and C are presented in Figure 4-34 Figure 4-35.

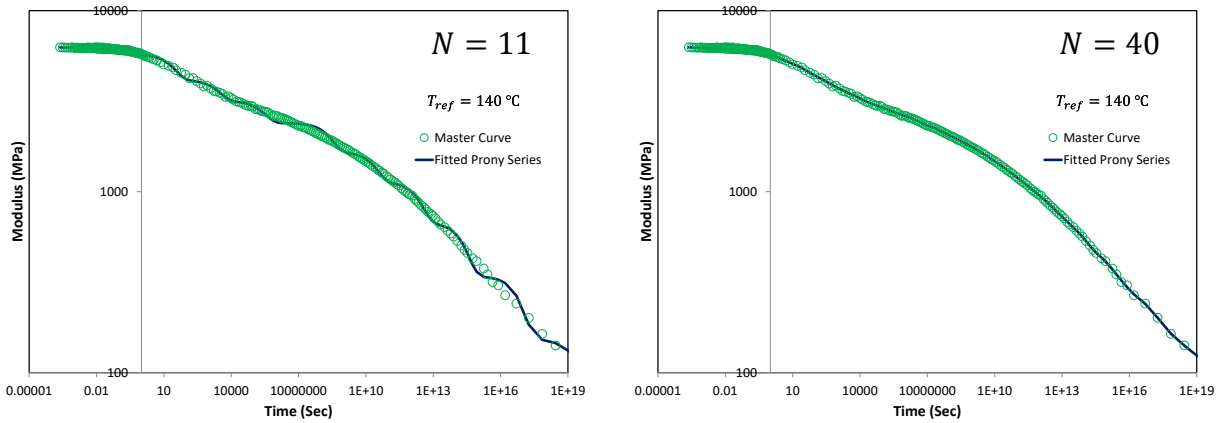

Figure 4-34 AS4/PEEK-Sample B-Master curves and fitted Prony series

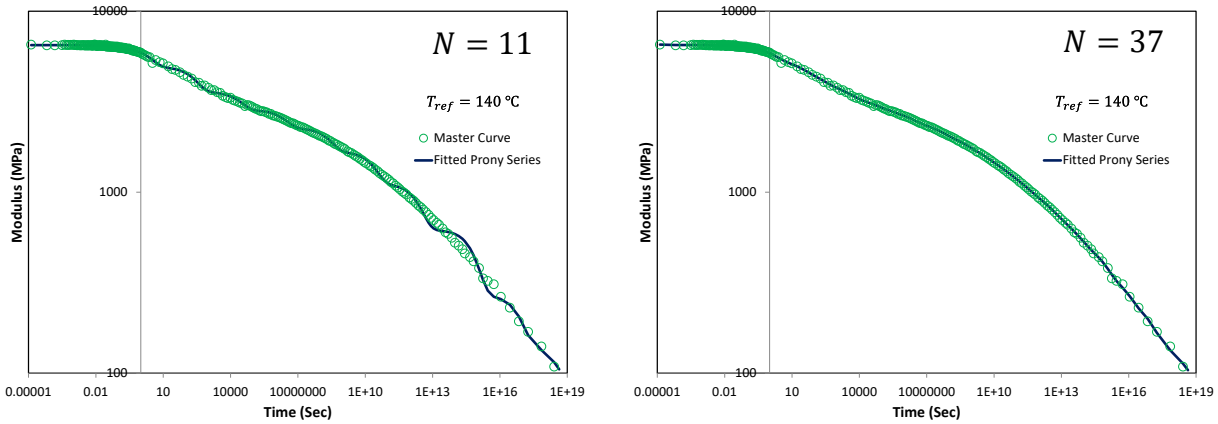

Figure 4-35 AS4/PEEK-Sample C-Master curves and fitted Prony series

The parameters E_e, E_i's and τ_i's for all fitted Prony series are given in Appendix A .

4.1.5.2 Prony series for neat PEEK master curves

Prony series are fitted to the experimental master curves for neat PEEK samples. The results are displayed in Figure 4-36 and Figure 4-37.

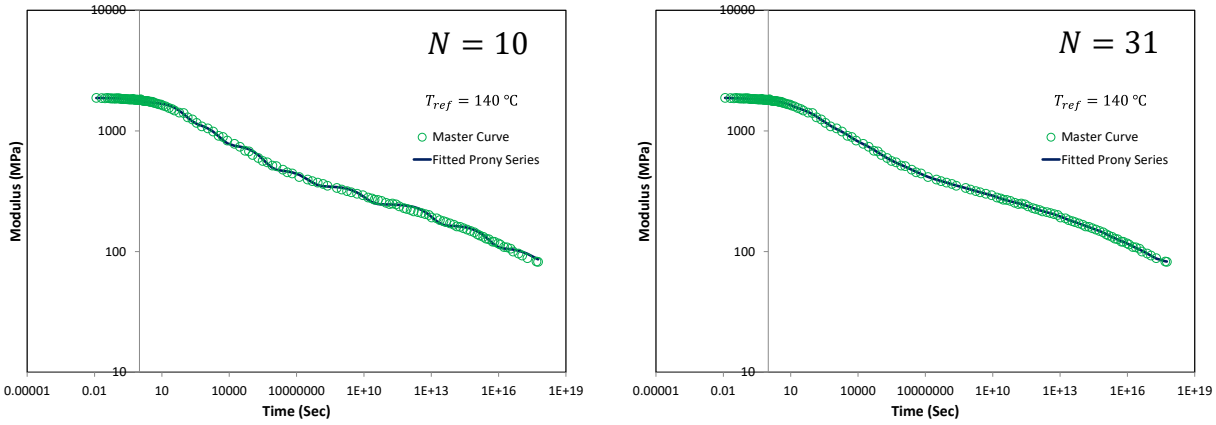

Figure 4-36 Neat PEEK-Sample A-Master curves and fitted Prony series

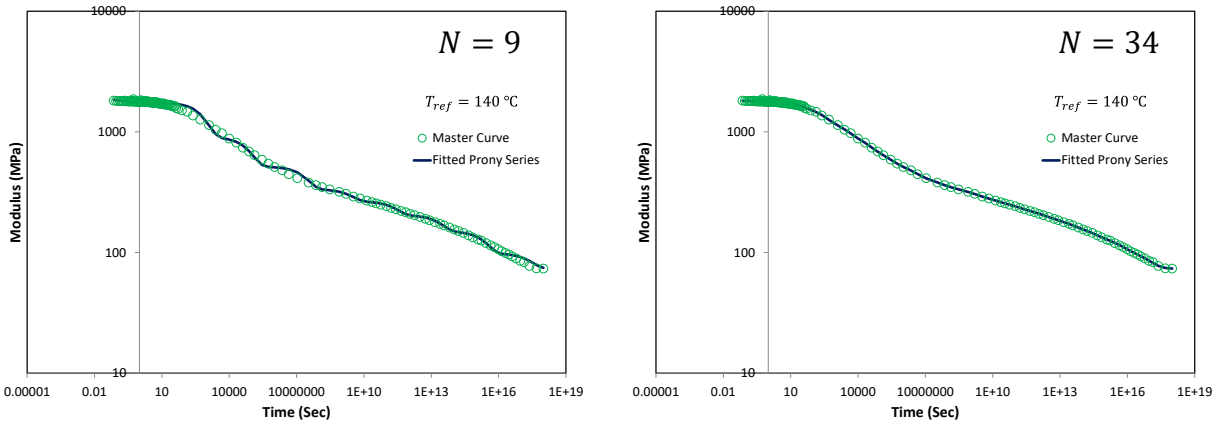

Figure 4-37 Neat PEEK-Sample B-Master curves and fitted Prony series

It is noticeable from Figure 4-36 and Figure 4-37 that increasing the number of Prony terms results in higher smoothness in fitted curves. The parameters E_e, E_i's and τ_i's for all fitted Prony series are given in Appendix A .

4.1.5.3 Prony series for fully cured AS4/8552 master curves

Fitted Prony series are plotted along with the experimental master curves for three fully cured AS4/8552 samples in Figure 4-38, Figure 4-39 and Figure 4-40. Similar to previous cases, smoother curves are obtained with higher number of Prony terms.

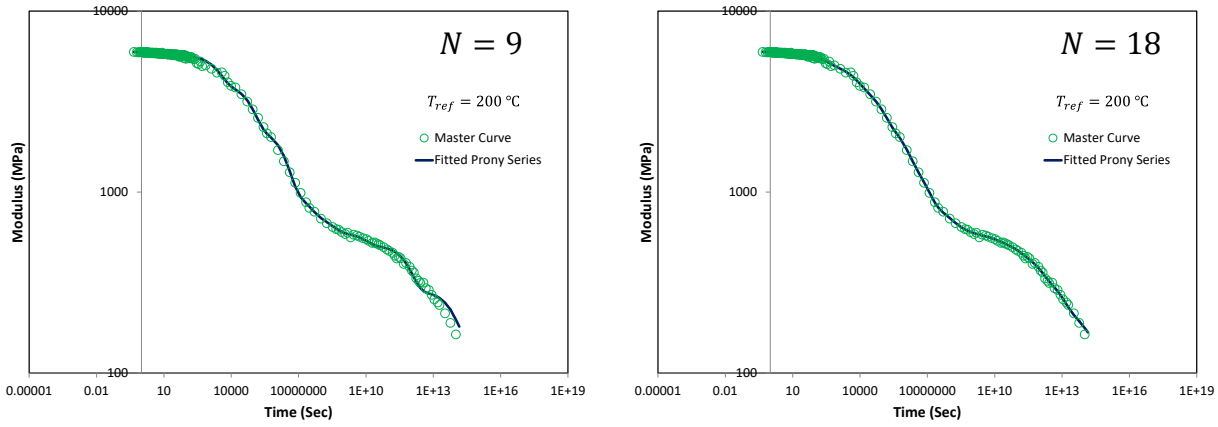

Figure 4-38 AS4/8552-Sample A-Master curves and fitted Prony series

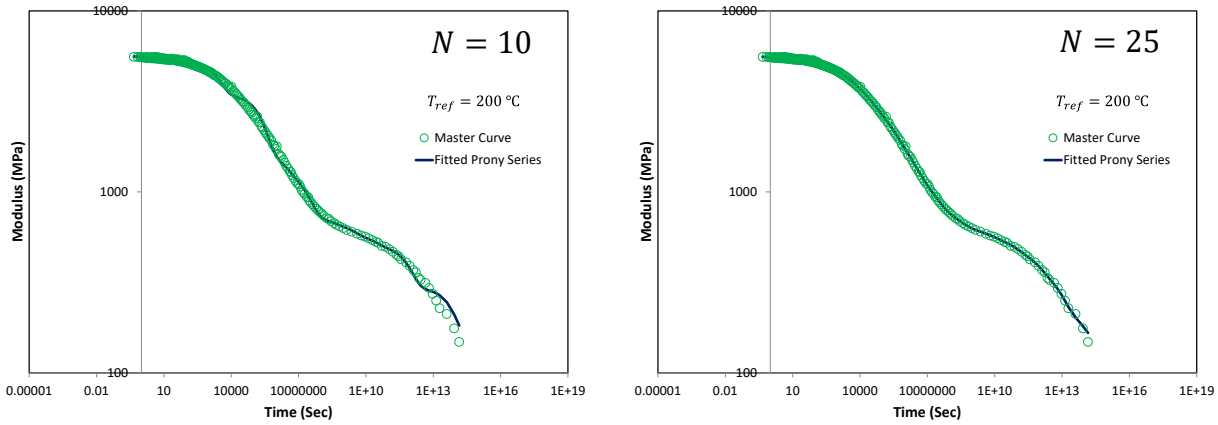

Figure 4-39 AS4/8552-Sample B-Master curves and fitted Prony series

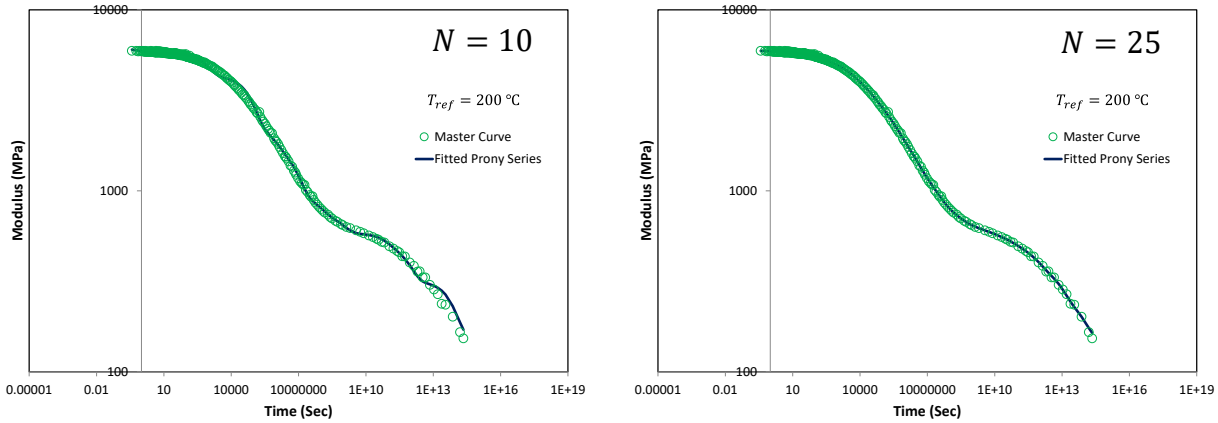

Figure 4-40 AS4/8552-Sample C-Master curves and fitted Prony series

The parameters E_e, E_i's and τ_i's for all fitted Prony series are given in Appendix A .

4.1.5.4 Prony series for fully cured 8552 resin master curves

Prony series are fitted to the master curves for fully cured 8552 resin samples. The results are presented in Figure 4-41 and Figure 4-42. The parameters E_e, E_i's and τ_i's for all fitted Prony series are given in Appendix A .

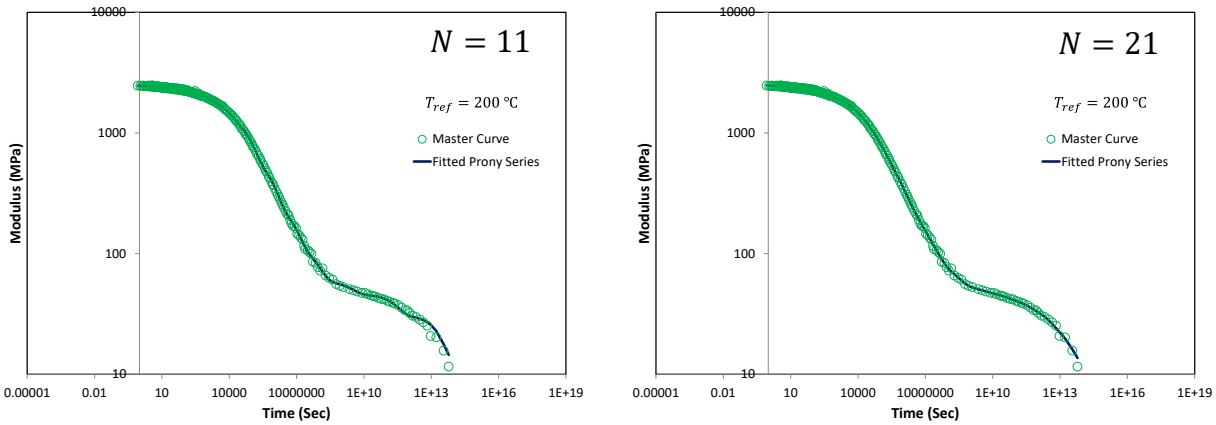

Figure 4-41 8552 resin-Sample A-Master curves and fitted Prony series

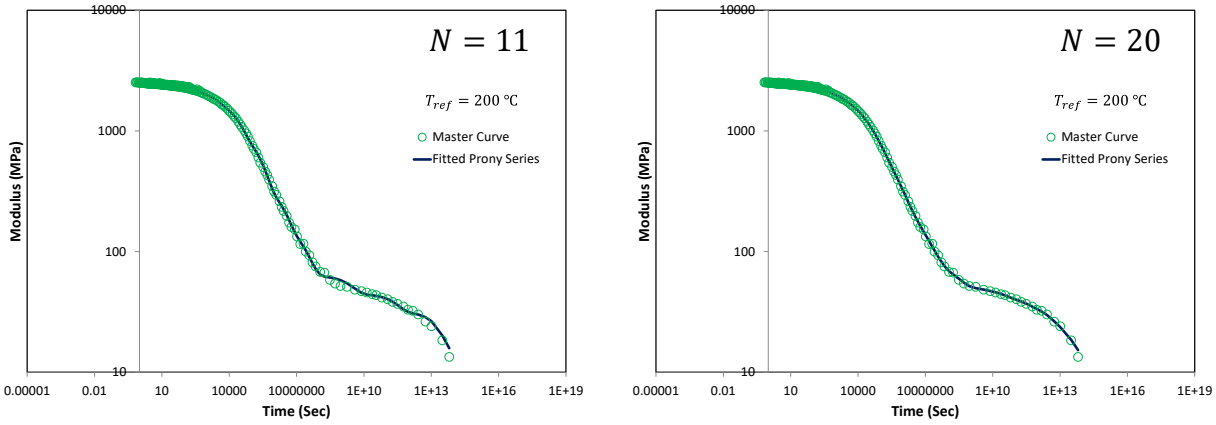

Figure 4-42 8552 resin-Sample B-Master curves and fitted Prony series

4.2 Thermo-elastic behaviour in the glassy regime

In section 4.1.4, it was shown that the unrelaxed moduli for all samples were temperature dependent. In this section, the nature of temperature dependence of unrelaxed moduli, $E^u(T)$, is studied. More specifically it is desired to investigate if the stress is proportional to strain (elastic behaviour) or the rate of stress is proportional to the rate of strain (hypo-elastic behaviour). The elastic behaviour in the uni-axial form is stated as

$$\sigma = E^u(T)\epsilon \qquad \textbf{(4-4)}$$

The uni-axial hypo-elastic constitutive model [145] is expressed as

$$\dot{\sigma} = E^u(T)\dot{\epsilon} \qquad \textbf{(4-5)}$$

Let us consider the curve for bond energy as a function of bond length for atomic materials such as metals, as shown schematically in Figure 4-43. Elastic deformation in metals is due to increasing the average separation of atoms. On the other hand, when the temperature is increased, due to the effects of thermal expansion, the average separation of atoms increases. Therefore, thermal expansion and change of elastic modulus as a result of change of temperature are two coupled phenomena.

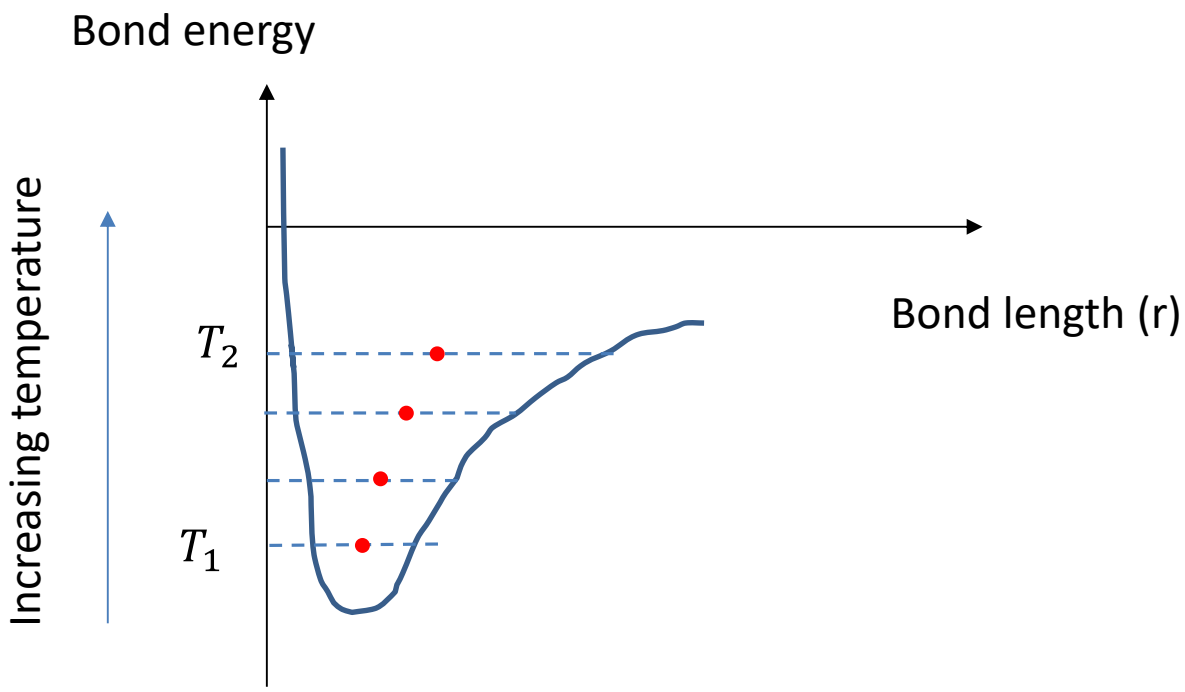

Figure 4-43 Bond energy as a function of bond length in an atomic structure

In a glassy polymer, the covalent bond between two carbon atoms is very stiff, such that both bond length and bond angle are fixed. Deformation of glassy polymers, subjected to an external load is due to rotation of chain segments around the carbon-carbon bond. The elastic behaviour in glassy polymers is resisted by intramolecular and intermolecular energy barriers. On the other hand, thermal expansion in polymers is due to increasing the average separation of molecular chains and is resisted by weak van der Waals bonds. Therefore, there is no significant coupling between the elastic moduli and thermal expansion of glassy polymers.

As explained above, a change of temperature results in two different effects in the material; thermal expansion/shrinkage and change of stiffness. Therefore, in order to inspect the nature of temperature dependence of the modulus, thermal expansion effects should be subtracted.

Let us consider a bar in a tensile test setup, as sketched in Figure 4-44. A load is applied to the

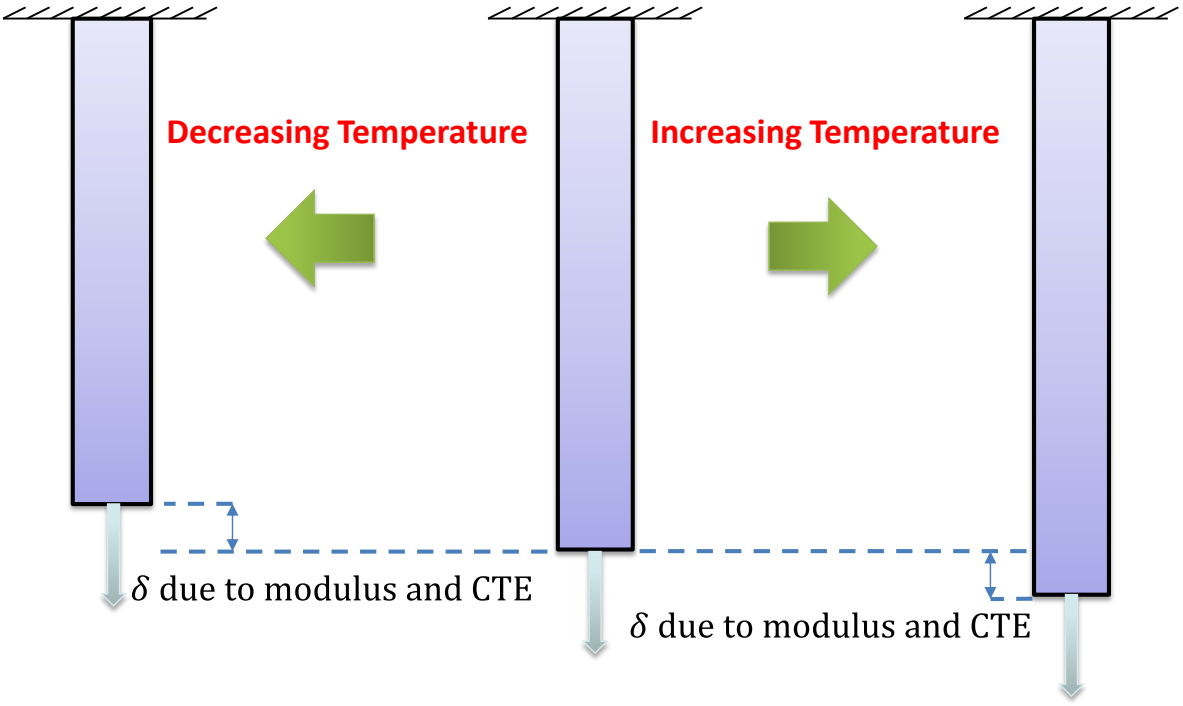

Figure 4-44 Bar under a constant load subjected to a change of temperature

bar and kept constant during the experiment. If the temperature is increased, due to thermal expansion effects (CTE effects), the length of the bar increases. At the same time, some softening occurs in the material which may contribute to more length increase. Therefore the resulting net length increase is due to contribution of two different causes. Similarly, if the temperature is

decreased, there is some contraction due to CTE effects. Similarly, stiffening of the material may cause some length reduction. The net length decrease is due to a combination two different effects.

In order to uncouple the thermal expansion effects, a 3-point bending setup in the DMA machine is employed.

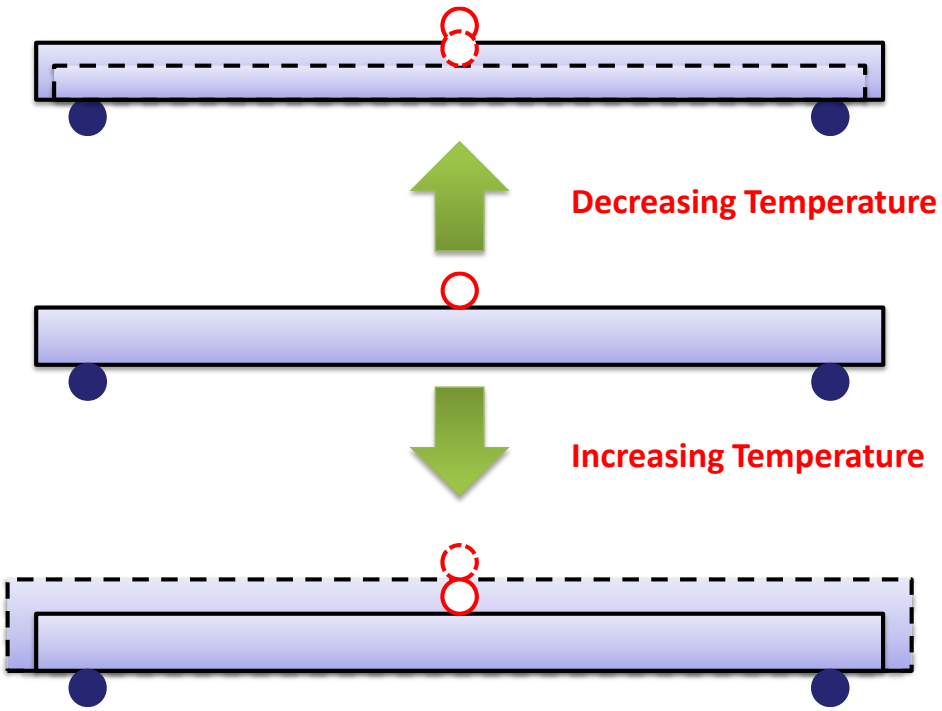

Figure 4-45 Beam specimen in 3-point bending setup, subjected to a change of temperature

If the temperature is changed without applying any load to the sample (in practice a small load, in the order of 0.001~0.01 N is applied to ensure the probe keeps contact with the sample during the experiment), the position of the probe changes due to thermal expansion effects, as shown in Figure 4-45. The DMA software reports this as some mid-point deflection in the beam sample. With this explanation, the sample is once tested under a constant load, with some arbitrary temperature

profile, and then the test is repeated with the same temperature profile with no load. Subtracting the beam mid-point deflection, measured during the two tests, the deflection due to change in the modulus is obtained. A further complementary constant frequency DMA test is performed on the sample, with the same temperature profile, for measuring the modulus as a function of temperature.

4.2.1 Thermo-elastic experiments on the steel sample

A steel sample was tested initially as a benchmark in order to validate the test method. Sample dimensions are given in Table 4-2.

Table 4-2 Steel sample dimensions

Material	Length (mm)	Width (mm)	Thickness (mm)
Steel	50.00	12.62	0.51

The sample temperature was equilibrated at 200 ℃. A constant force of 15 N was applied and the sample was cooled to −100 ℃ at the cooling rate of 2 ℃/min. The force was removed and the temperature was held constant for 30 min. Next the constant load of 15 N was applied once again and the sample was heated at the rate of 2 ℃/min to 200 ℃. The experiment was repeated with the same temperature profile and the force was kept constant at 0.01 N. The difference between the deflections, measured during the two experiments is the pure deflection due to the application

of the force, hereafter referred to as the 'mechanical deflection'. The total deflection, the deflection due to thermal expansion/shrinkage and the mechanical deflection for cooling and heating experiments are presented in Figure 4-46.

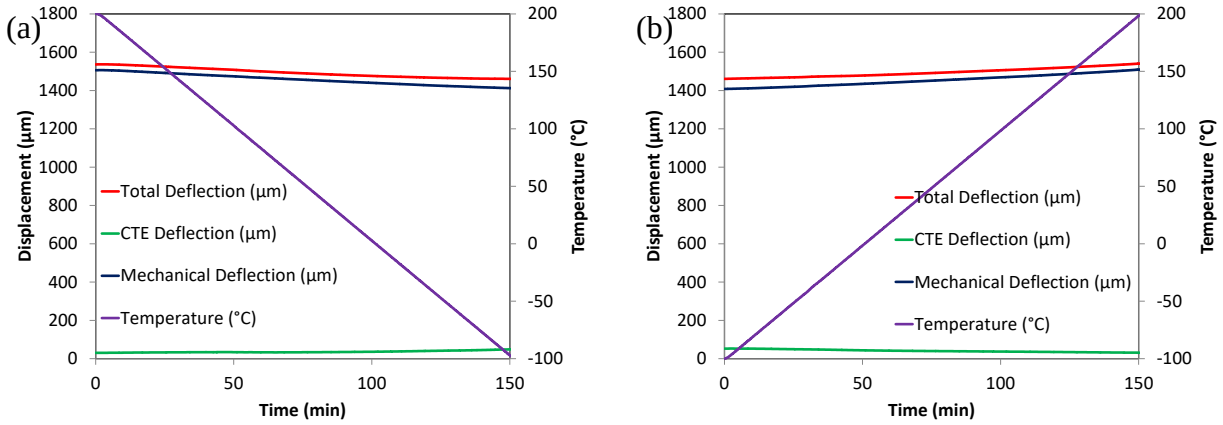

Figure 4-46 Total deflection, deflection due to thermal expansion/shrinkage, mechanical deflection and temperature profile for (a) cooling (b) heating experiments for steel

It is noticeable from Figure 4-46 that in the cooling and heating experiments, the deflection due to CTE is increasing and decreasing, respectively. This indicates that the thickness of the sample is decreasing during the cooling experiment and it is increasing during the heating experiment, as expected. The change in the modulus of the sample, during the cooling and heating, measured independently using a constant frequency DMA experiment is displayed in Figure 4-47.

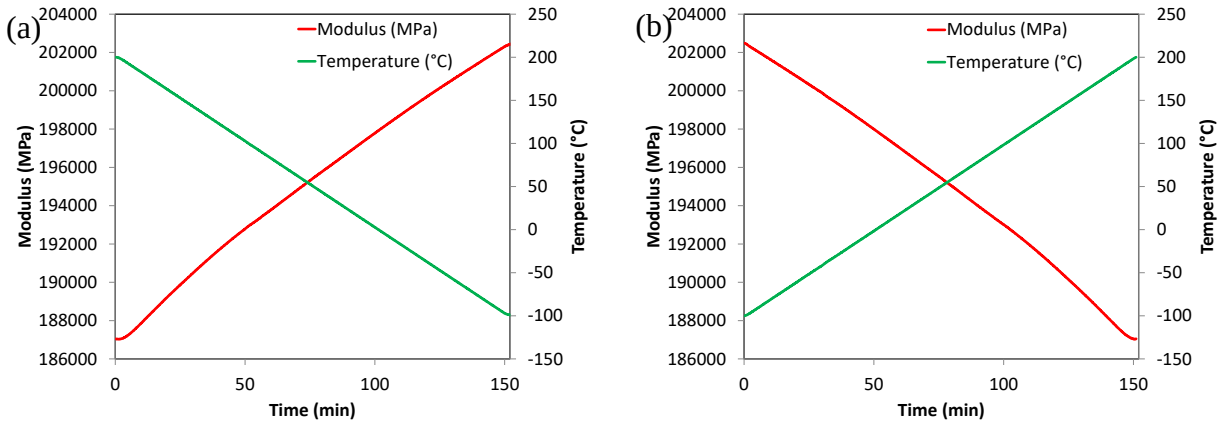

Figure 4-47 Modulus of steel sample in (a) cooling (b) heating

It is recognized from Figure 4-47 that the modulus of the steel sample varies between 202 GPa and 187 GPa, when the temperature changes between −100 ℃ and 200 ℃, in both cooling and heating experiments. According to Frost and Ashby [146], when the temperature is changed from 200 ℃ to −100 ℃, the elastic modulus of stainless steel changes from 190 GPa to 218 GPa (actual data is provided for shear modulus). Considering different experimental methods, these numbers are consistent.

Subtracting the deflection due to thermal expansion/shrinkage from the total deflection, the mechanical deflection is obtained and plotted along with the modulus for both cooling and heating tests in Figure 4-48.

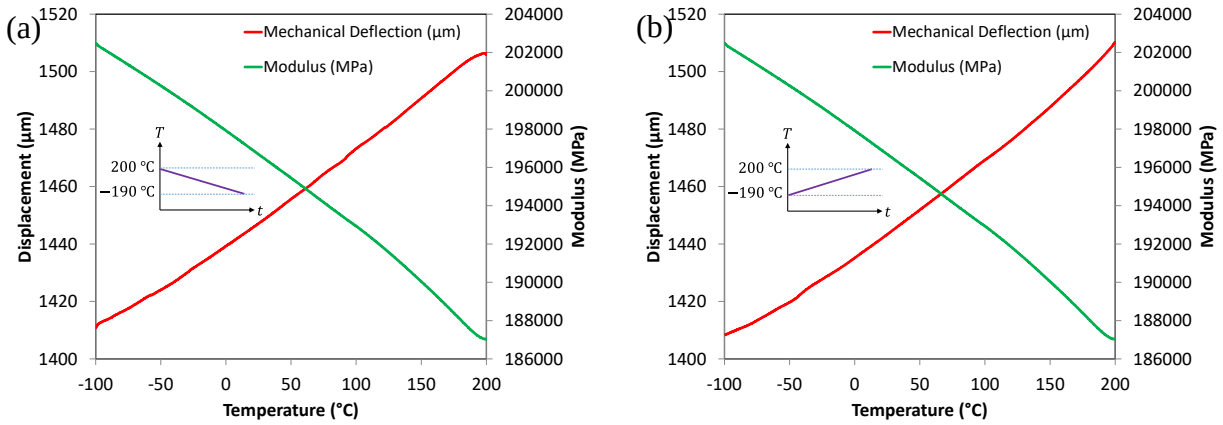

Figure 4-48 Mechanical deflection and modulus as a function of temperature for steel sample in (a) cooling (b) heating

Figure 4-48 shows that as the modulus is increased, the mechanical deflection is decreased. This is an important observation. Stiffening or softening of the steel sample, subjected to a constant load, contributes to the mechanical deflection of the sample.

The product of the normalized values of modulus and mechanical deflection, Modulus × Mechanical Deflection (normalized), during cooling and heating experiments are shown in Figure 4-49.

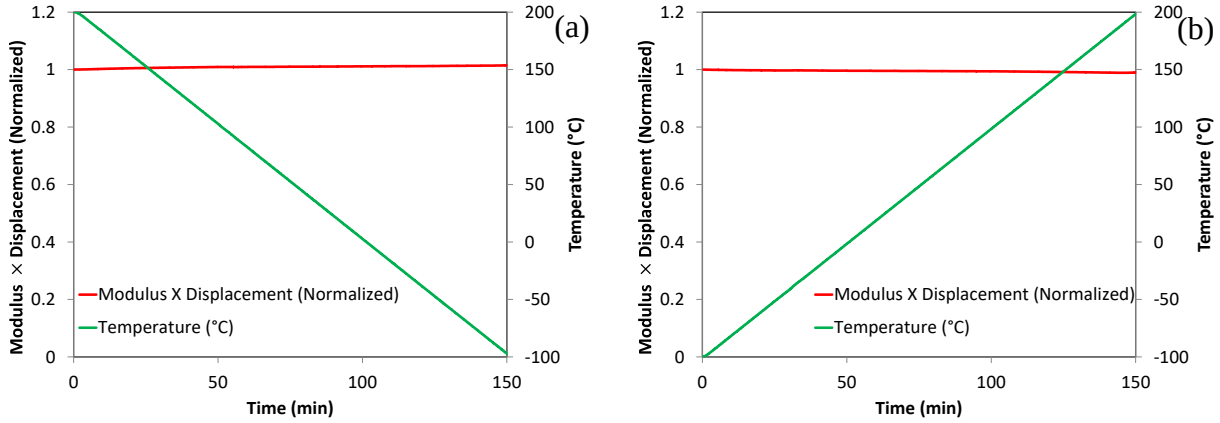

Figure 4-49 Modulus × Mechanical Deflection (normalized) for steel sample in (a) cooling (b) heating

It is concluded from Figure 4-49 that Modulus × Mechanical Deflection (normalized), stays constant in both cooling and heating experiments, during the test. From solid mechanics (e.g. see [147]), for a linear elastic Euler-Bernoulli beam, in a 3-point bending test, and with length L, width b, and depth h, under the load P, the mid-span deflection, δ, is calculated as

$$\delta = \frac{PL^3}{48EI} \qquad \textbf{(4-6)}$$

In Equation (4-6), I is the second moment of area and for a rectangular cross section is obtained as

$$I = \frac{bh^3}{12} \qquad \textbf{(4-7)}$$

Equation (4-6) may be rewritten as

$$E\delta = \frac{PL^3}{48I} \quad \textbf{(4-8)}$$

For a constant load experiment, the right hand side of Equation (4-8), is a constant, i.e.,

$$E\delta = \text{const.} \quad \textbf{(4-9)}$$

From Figure 4-49, it is seen that Equation (4-9) is valid, which implies that for the steel sample, during both cooling and heating experiments, the following equation is valid:

$$\delta(T) = \frac{PL^3}{48E(T)I} \quad \textbf{(4-10)}$$

From Equation (4-10), it is concluded that the material behaviour for a steel sample, during both cooling and heating experiments, is linear elastic and the constitutive relation is

$$\sigma = E(T)\epsilon \quad \textbf{(4-11)}$$

Now that the test method is validated, it is used in the next section for studying the behaviour of a polymer material in the glassy regime.

4.2.2 Thermo-elastic experiments on the fully cured 8552 resin sample

In this section, the procedure used for the steel sample in section 4.2.1 is repeated for a fully cured 8552 resin sample. The sample dimensions are given in Table 4-3.

Table 4-3 Fully cured 8552 resin sample

Material	Length (mm)	Width (mm)	Thickness (mm)
Fully cured 8552 resin	50.00	12.46	3.38

The results from the constant frequency DMA experiment, conducted on the sample in the temperature range between -100 ℃ to 100 ℃ are presented in Figure 4-50.

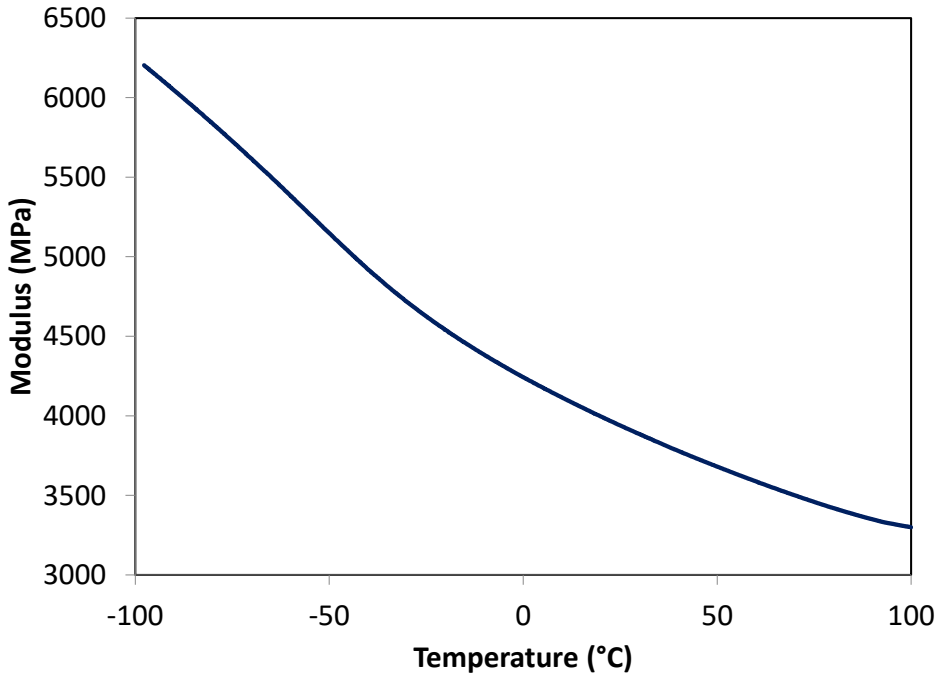

Figure 4-50 Storage modulus of fully cured 8552 resin

Because of the shape of the modulus curve, the constant load experiments were performed in two different temperature ranges; between -100 ℃ to -10 ℃, and between -10 ℃ to 100 ℃.

In each test, the sample temperature was equilibrated at the higher temperature (-10 ℃ or 100 ℃). A constant load of 10 N was applied and the sample was cooled at 2 ℃/min to the lower temperature (-100 ℃ or -10 ℃). The load was removed and the temperature was held constant for 30 min. Subsequently, the load of 10 N was reapplied and the sample was heated at 2 ℃/min to the higher temperature (-10 ℃ or 100 ℃). The experiments were repeated with a small load of 0.01 N and with the same temperature profile to capture the deflection of the sample due to thermal expansion/shrinkage. The total deflection and the deflection due to thermal

shrinkage/expansion during cooling and heating experiments, in two temperature ranges are given in Figure 4-51 and Figure 4-52.

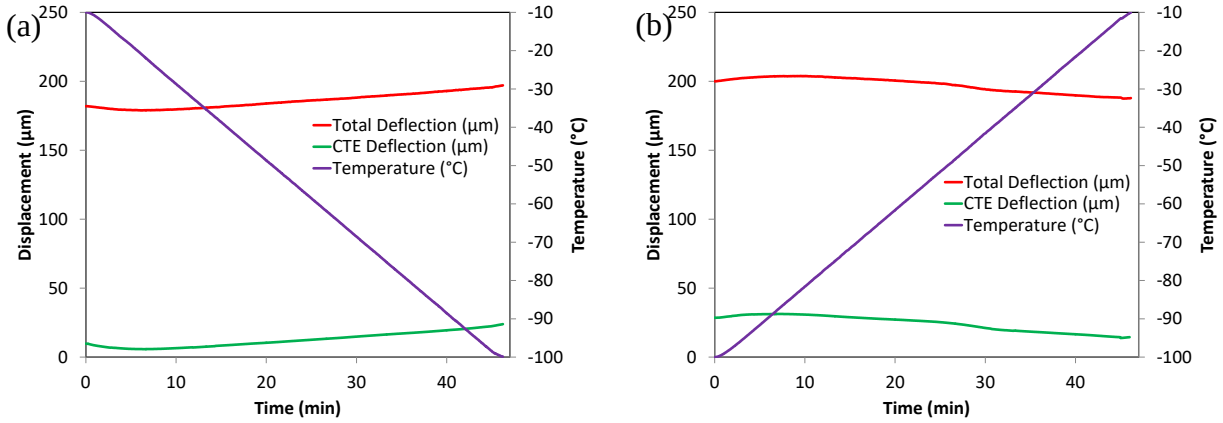

Figure 4-51 Total deflection and deflection due to thermal expansion/shrinkage and temperature profile for (a) cooling (b) heating experiments for fully cured 8552 resin between −100 ℃ and −10 ℃

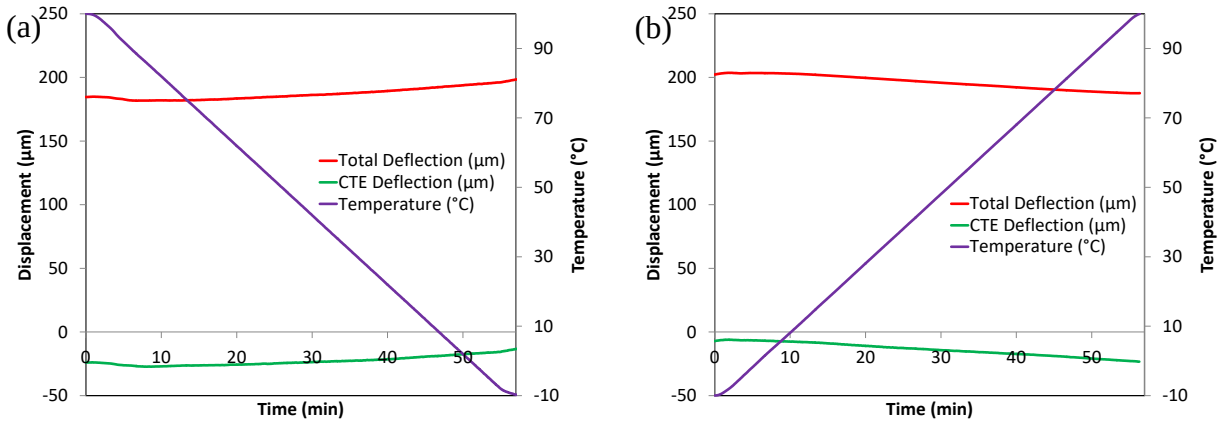

Figure 4-52 Total deflection and deflection due to thermal expansion/shrinkage and temperature profile for (a) cooling (b) heating experiments for fully cured 8552 resin between −10 ℃ and 100 ℃

From Figure 4-51 and Figure 4-52, it is recognized that for both temperature ranges, during cooling and heating, total deflection and deflection due to thermal expansion/shrinkage follow the same trend.

Subtracting the deflection due to thermal expansion/shrinkage from the total deflection, the deflection due to load (mechanical deflection) is obtained. The results are presented in Figure 4-53 and Figure 4-54.

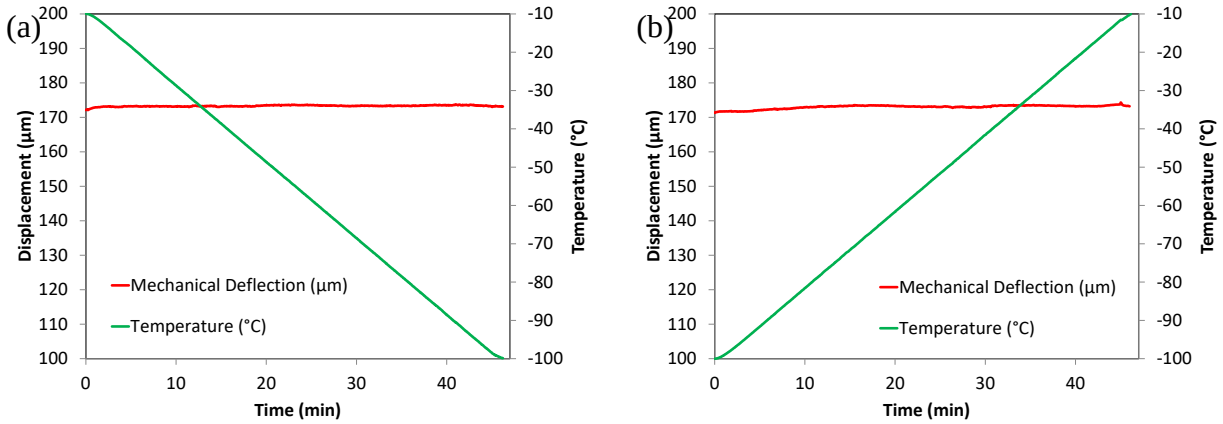

Figure 4-53 Mechanical deflection and temperature profile for (a) cooling (b) heating experiments for fully cured 8552 resin between −100 ℃ and −10 ℃

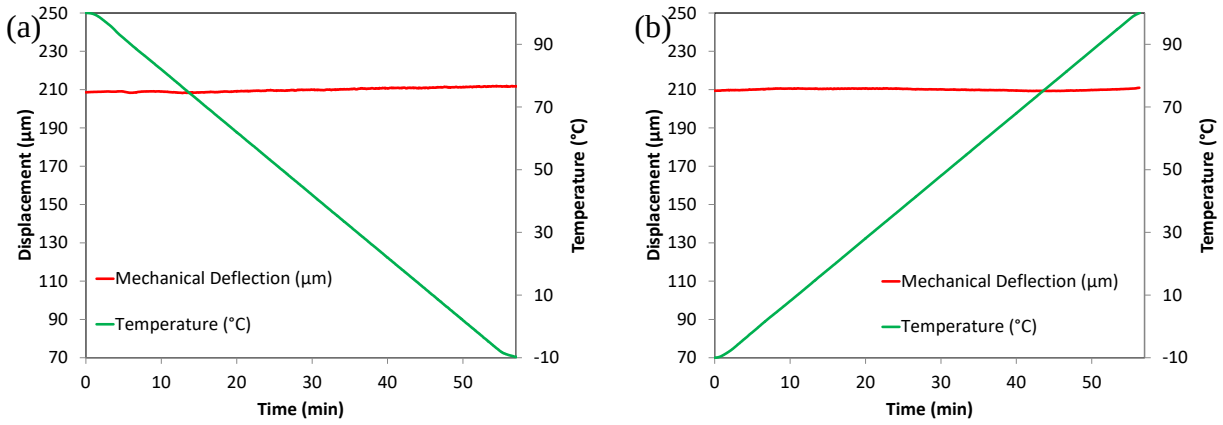

Figure 4-54 Mechanical deflection and temperature profile for (a) cooling (b) heating experiments for fully cured 8552 resin between −10 ℃ and 100 ℃

From the results in Figure 4-53 and Figure 4-54, it is concluded that for both temperature ranges and during cooling and heating, change of modulus does not cause any change in the deflection and the mechanical deflection is constant. To express this behaviour mathematically, uniaxial Hooke's law (Equation (4-11)) is rewritten in rate form as

$$\dot{\sigma} = \frac{d[E(T)\epsilon]}{dt} = E(T)\dot{\epsilon} + \dot{E}(T)\epsilon \qquad \textbf{(4-12)}$$

Since the change of modulus does not contribute to the deflection, the second term on the right hand side of Equation (4-12) is dismissed and therefore the constitutive relation is expressed as

$$\dot{\sigma} = E(T)\dot{\epsilon} \qquad \textbf{(4-13)}$$

Equation (4-13) suggests that the material behaviour of fully cured 8552 resin in the investigated temperature region is hypo-elastic [145]. The thermo-viscoelastic constitutive relations in the following section are modified to take into account this behaviour.

4.3 One-dimensional constitutive relations for thermo-rheologically complex materials

As explained in 2.3, Schapery introduced two different types of thermo-rheologically complex materials. He designated a composite material composed of thermo-rheologically simple materials

with different shift factors as TCM-1. Also he defined TCM-2 as a material whose uniaxial behaviour in terms of creep can be described by the following equation

$$\epsilon_x = D_I \sigma_x + \int_0^t \Delta D(\xi - \xi') \frac{d}{dt'} \left(\frac{\sigma_x(t')}{a_G} \right) dt' \qquad \textbf{(4-14)}$$

Equation (4-14) has been derived using irreversible thermodynamics [148]. In Eq.3, $D_I = D_I(T)$ is the initial value of creep compliance and it can be shown that a_G is a vertical shift factor for ΔD, $\xi = \xi(t) = \int_0^t d\tau / a_T$, $\xi' = \xi(t') = \int_0^{t'} d\tau / a_T$, ξ is called the "effective time" or "reduced time" and a_T is the temperature shift factor. According to Schapery [148], Equation (4-14) can be used for both composite and monolithic materials.

PEEK, which is a semi-crystalline thermoplastic polymer, and also 8552 resin which is a thermoset should be thermo-rheologically complex according to the discussions given by Schwarzl and Staverman [119].

From the test results we observe that the limiting values of the modulus (relaxed and unrelaxed modulus) are temperature dependent which is another manifestation of thermo-rheologically complex behaviour. The constitutive equation given in Equation (4-14) is an appropriate model for capturing the behaviour of such a material. This model can be converted to the differential form by approximating ΔD by a Prony series as

$$\Delta D(t) = \Delta D(0) + \sum_{i=1}^{N} D_i\left(1 - e^{-t/\tau_i}\right) = \sum_{i=1}^{N} D_i\left(1 - e^{-t/\tau_i}\right) \quad \textbf{(4-15)}$$

From definition of "reduced time", ξ', and using Leibniz rule for differentiation we have

$$\frac{d\xi'}{dt'} = \frac{d}{dt'}\left(\int_0^{t'} d\tau/a_T\right) = \frac{1}{a_T(t')} \quad \textbf{(4-16)}$$

Therefore,

$$\frac{d}{dt'} = \frac{1}{a_T(t')}\frac{d}{d\xi'} \quad \text{and} \quad dt' = a_T(t')d\xi' \quad \textbf{(4-17)}$$

Using Equation (4-17), Equation (4-14) is rewritten as

$$\epsilon_x = D_I\sigma_x + \int_0^{\xi} \Delta D(\xi - \xi')\frac{d}{d\xi'}\left(\frac{\sigma_x(\xi')}{a_G}\right)d\xi' \quad \textbf{(4-18)}$$

Carrying out the integration by parts

$$\epsilon_x = D_I\sigma_x - \int_0^{\xi} \frac{\partial \Delta D(\xi - \xi')}{\partial \xi'} \left(\frac{\sigma_x(\xi')}{a_G}\right) d\xi' + \Delta D(0)\frac{\sigma_x(\xi)}{a_G} - \Delta D(\xi)\frac{\sigma_x(0)}{a_G} \quad \textbf{(4-19)}$$

We assume the material is at rest at time zero and the initial compliance is D_I which means $\sigma_x(0) = 0$ and $\Delta D(0) = 0$. Therefore Equation (4-19) reduces to

$$\epsilon_x = D_I\sigma_x - \int_0^{\xi} \frac{\partial \Delta D(\xi - \xi')}{\partial \xi'} \left(\frac{\sigma_x(\xi')}{a_G}\right) d\xi' \quad \textbf{(4-20)}$$

Substituting from Equation (4-15) into Equation (4-20) yields

$$\epsilon_x = D_I\sigma_x + \sum_{i=1}^{N} \int_0^{\xi} \frac{D_i}{\tau_i} e^{-(\xi-\xi')/\tau_i} \frac{\sigma_x(\xi')}{a_G} d\xi' \quad \textbf{(4-21)}$$

Next we define the state variable $q_i(\xi)$ as [149]

$$q_i(\xi) = \int_0^{\xi} \frac{D_i}{\tau_i} e^{-(\xi-\xi')/\tau_i} \frac{\sigma_x(\xi')}{a_G} d\xi' \quad \textbf{(4-22)}$$

From Equation (4-22), Equation (4-21) is rewritten as

$$\epsilon_x = D_I \sigma_x + \sum_{i=1}^{N} q_i \qquad \textbf{(4-23)}$$

Also using Leibniz rule for differentiation and Equation (4-22)

$$\frac{dq_i(\xi)}{d\xi} = \int_0^{\xi} \frac{\partial}{\partial \xi}\left[\frac{D_i}{\tau_i} e^{-(\xi-\xi')/\tau_i} \frac{\sigma_x(\xi')}{a_G}\right] d\xi' + \frac{D_i}{\tau_i} e^{-(\xi-\xi)/\tau_i} \frac{\sigma_x(\xi)}{a_G}$$

$$= \frac{-1}{\tau_i} \int_0^{\xi} \frac{D_i}{\tau_i} e^{-(\xi-\xi')/\tau_i} \frac{\sigma_x(\xi')}{a_G} d\xi' + \frac{D_i}{\tau_i} \frac{\sigma_x(\xi)}{a_G} \qquad \textbf{(4-24)}$$

or

$$\frac{dq_i(\xi)}{d\xi} + \frac{q_i(\xi)}{\tau_i} = \frac{D_i}{\tau_i} \frac{\sigma_x(\xi)}{a_G}, \qquad i = 1,2,\dots,N \qquad \textbf{(4-25)}$$

Equations (4-23) and (4-25) are the governing equations of a generalized Kelvin-Voigt model, where q_i is the strain in the i^{th} Kelvin element, as shown in Figure 4-55.

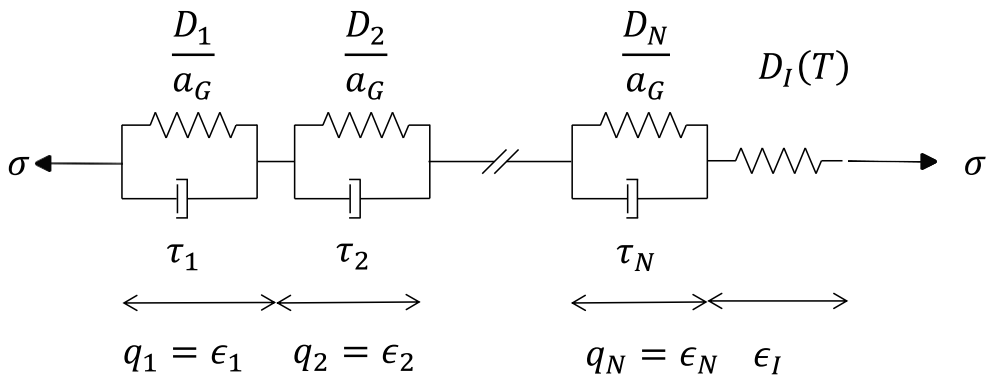

Figure 4-55 Generalized Kelvin-Voigt Model, mechanical analogue for Equations (4-23) and (4-25)

Equation (4-14) can be generalized and in a similar way converted to differential form for the cases of an isotropic material in 3D and also transversely isotropic material in 3D.

The resulting differential constitutive equations can be written in incremental form using a time integration scheme and then implemented in a UMAT. Since in Equation (4-23), strain is expressed as a function of stress, an iterative method such as Newton-Raphson is required for determining the increment of stress at the end of each time step (see [150]).

As mentioned previously, implementation of Kelvin type constitutive equations in a UMAT needs iteration. Maxwell type constitutive equations are therefore more desirable due to higher computational efficiency.

Based on nonlinear viscoelastic constitutive equations of Schapery [151] we may write the equivalent stress relaxation form of Equation (4-14) as

$$\sigma_x = E_e\epsilon_x + a_F \int_0^t \Delta E(t-t')\frac{d\epsilon_x}{dt'}dt' \qquad \textbf{(4-26)}$$

In Equation (4-26), $E_e = E_e(T)$ is the final (relaxed) value of relaxation modulus and it can be shown that a_F is a vertical shift factor for ΔE. Similar to the procedure used for deriving Equation (4-18), we may rewrite Equation (4-26) as

$$\sigma_x = E_e\epsilon_x + a_F \int_0^\xi \Delta E(\xi-\xi')\frac{d\epsilon_x}{d\xi'}d\xi' \qquad \textbf{(4-27)}$$

where $\xi = \xi(t) = \int_0^t d\tau/a_T$, $\xi' = \xi(t') = \int_0^{t'} d\tau/a_T$.

Next we approximate $E(\xi)$ by a Prony series

$$E(\xi) = E_e + \sum_{i=1}^{N} E_i e^{-\frac{\xi}{\tau_i}} \qquad \textbf{(4-28)}$$

From Equation (4-28) it is obvious that

$$\lim_{\xi\to\infty} E(\xi) = E_e \qquad \textbf{(4-29)}$$

and

$$\Delta E(\xi - \xi') = E(\xi - \xi') - E_e = \sum_{i=1}^{N} E_i e^{-\frac{\xi - \xi'}{\tau_i}} \qquad \textbf{(4-30)}$$

Substituting from Equation (4-30) into Equation (4-27) we have

$$\sigma_x = E_e \epsilon_x + \sum_{i=1}^{N} \left(a_F \int_0^{\xi} E_i e^{-\frac{\xi - \xi'}{\tau_i}} \frac{d\epsilon_x}{d\xi'} d\xi' \right) \qquad \textbf{(4-31)}$$

Now we define the state variables $q_i's$ [149] as

$$q_i(\xi) = a_F \int_0^{\xi} E_i e^{-\frac{\xi - \xi'}{\tau_i}} \frac{d\epsilon_x}{d\xi'} d\xi', \qquad i = 1,2 \dots, N \qquad \textbf{(4-32)}$$

Therefore from Equations (4-31) and (4-32) we have

$$\sigma_x = E_e \epsilon_x + \sum_{i=1}^{N} q_i \qquad \textbf{(4-33)}$$

Also, using Leibniz rule for differentiation from Equation (4-32) we obtain

$$\frac{dq_i(\xi)}{d\xi} = -\frac{a_F}{\tau_i}\int_0^{\xi} E_i e^{-\frac{\xi-\xi'}{\tau_i}}\frac{d\epsilon_x}{d\xi'}d\xi' + a_F E_i \frac{d\epsilon_x}{d\xi}$$
$$= -\frac{q_i(\xi)}{\tau_i} + a_F E_i \frac{d\epsilon_x}{d\xi}, \qquad i = 1,2\ldots,N \tag{4-34}$$

Therefore,

$$\frac{dq_i(\xi)}{d\xi} + \frac{q_i(\xi)}{\tau_i} = a_F E_i \frac{d\epsilon_x}{d\xi}, \qquad i = 1,2\ldots,N \tag{4-35}$$

From Equations (4-33) and (4-35) we conclude that q_i can be interpreted as stress of the i^{th} Maxwell element in a Maxwell chain as shown in Figure 4-56.

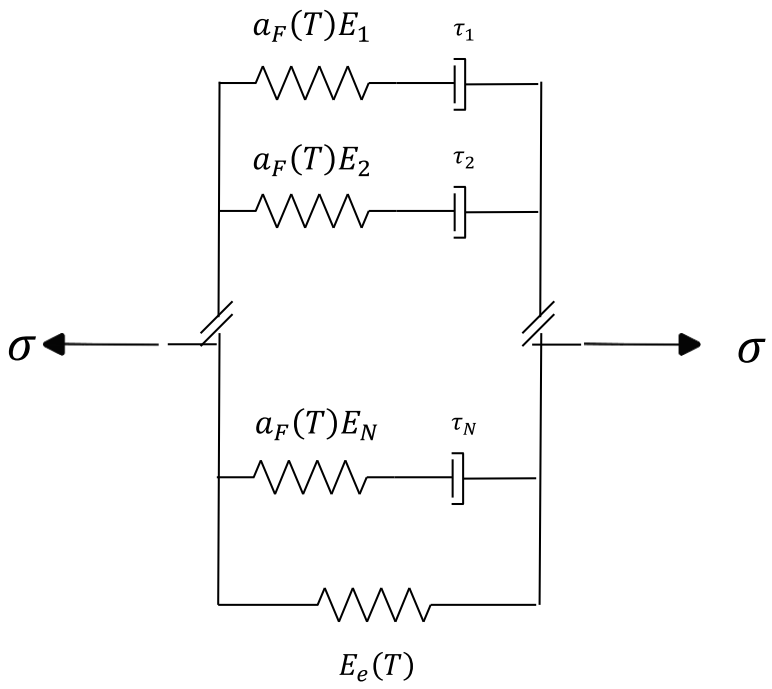

Figure 4-56 Maxwell Chain, mechanical analogue for Equations (4-33) and (4-35)

From the analogue model in Figure 4-56, the initial (unrelaxed) value of the modulus can be written as

$$E_I(T) = E_e(T) + a_F(T)\sum_{i=1}^{N} E_i \qquad \textbf{(4-36)}$$

According to our experiments for studying the thermo-elastic behaviour of a cured epoxy polymer in the glassy regime (see section 4.2), the material behaviour is hypo-elastic, i.e.,

$$\dot{\sigma}_x = E_I \dot{\epsilon}_x \qquad \textbf{(4-37)}$$

Substituting from Equation (4-36) into (4-37) results in

$$\dot{\sigma}_x = \left(E_e(T) + a_F(T) \sum_{i=1}^{N} E_i \right) \dot{\epsilon}_x = E_e(T)\dot{\epsilon}_x + \sum_{i=1}^{N} a_F(T) E_i \, \dot{\epsilon}_x = \dot{\sigma}_e + \sum_{i=1}^{N} \dot{\sigma}_i \qquad \textbf{(4-38)}$$

where

$$\dot{\sigma}_e = E_e(T)\dot{\epsilon}_x \qquad \text{and} \qquad \dot{\sigma}_i = a_F E_i(T)\dot{\epsilon}_x, \qquad i = 1,2 \ldots, N \qquad \textbf{(4-39)}$$

Equation (4-39) implies that each of the springs in the Maxwell chain in Figure 4-56 is instantaneously linear elastic (hypo-elastic).

So far it is assumed that all strains are mechanical strains (strains due to stresses). Now we will consider the effects of free strains as well.

4.3.1 Effect of free strains

Let us consider the one dimensional constitutive relation for an elastic material first.

$$\sigma = E(\epsilon - \alpha\Delta T) = E\epsilon - E\alpha\Delta T \quad \textbf{(4-40)}$$

We may rename $E\alpha$ as β and rewrite Equation (4-40) as

$$\sigma = E\epsilon - \beta\Delta T \quad \textbf{(4-41)}$$

In Equation (4-40), α which is the coefficient of thermal expansion (CTE) is thermal strain due to a unit change in temperature and in the absence of applied stresses. Similarly, in Equation (4-41), β is the magnitude of thermal stress due to a unit change in temperature in a completely constrained body.

Considering these thermal stresses, we may rewrite Equation (4-27) as

$$\sigma_x = E_e\epsilon_x + a_F \int_0^{\xi} \Delta E(\xi - \xi') \frac{d\epsilon_x}{d\xi'} d\xi' - \beta_e \Delta T - a_F \int_0^{\xi} \Delta\beta(\xi - \xi') \frac{d\left(\frac{\Delta T}{a_F}\right)}{d\xi'} d\xi' \quad \textbf{(4-42)}$$

In Equation (4-42), $\beta_e = \beta_e(T)$ is the final (relaxed) value of β and $\Delta\beta = \beta(\xi) - \beta_e$ is the time dependent (viscoelastic) part of β.

Next we approximate $\beta(\xi)$ by a Prony series

$$\beta(\xi) = \beta_e + \sum_{i=1}^{N} \beta_i e^{-\frac{\xi}{\tau_i}} \qquad \textbf{(4-43)}$$

Relaxation times are chosen arbitrarily and later on we will assume that they are the same for E and β. Substituting from Equations (4-28) and (4-43) into Equation (4-42) we have

$$\sigma_x = E_e \epsilon_x - \beta_e \Delta T + \sum_{i=1}^{N} \left(a_F \int_0^{\xi} \left(E_i e^{-\frac{\xi-\xi'}{\tau_i}} \frac{d\epsilon_x}{d\xi'} - \beta_i e^{-\frac{\xi-\xi'}{\tau_i}} \frac{d\left(\frac{\Delta T}{a_F}\right)}{d\xi'} \right) d\xi' \right) \qquad \textbf{(4-44)}$$

Now we define the state variables $q_i's$ as

$$q_i(\xi) = a_F \int_0^{\xi} \left(E_i e^{-\frac{\xi-\xi'}{\tau_i}} \frac{d\epsilon_x}{d\xi'} - \beta_i e^{-\frac{\xi-\xi'}{\tau_i}} \frac{d\left(\frac{\Delta T}{a_F}\right)}{d\xi'} \right) d\xi' , \qquad i = 1,2 \dots, N \qquad \textbf{(4-45)}$$

Using Leibniz rule of differentiation, the derivative of $q_i(\xi)$ with respect to ξ will be

$$\frac{dq_i(\xi)}{d\xi} = -\frac{a_F}{\tau_i} \int_0^{\xi} \left(E_i e^{-\frac{\xi-\xi'}{\tau_i}} \frac{d\epsilon_x}{d\xi'} - \beta_i e^{-\frac{\xi-\xi'}{\tau_i}} \frac{d\left(\frac{\Delta T}{a_F}\right)}{d\xi'} \right) d\xi' + a_F E_i \frac{d\epsilon_x}{d\xi} - \beta_i \frac{d\Delta T}{d\xi} \qquad \textbf{(4-46)}$$

$$= -\frac{q_i(\xi)}{\tau_i} + a_F E_i \frac{d\epsilon_x}{d\xi} - \beta_i \frac{d\Delta T}{d\xi}, \qquad i = 1,2 \dots, N$$

And therefore,

$$\frac{dq_i(\xi)}{d\xi} + \frac{q_i(\xi)}{\tau_i} = a_F E_i \frac{d\epsilon_x}{d\xi} - \beta_i \frac{d\Delta T}{d\xi}, \qquad i = 1,2 \dots, N \quad \textbf{(4-47)}$$

Also using Equation (4-45), we may rewrite Equation (4-44) as

$$\sigma_x = E_e \epsilon_x - \beta_e \Delta T + \sum_{i=1}^{N} q_i \quad \textbf{(4-48)}$$

Now if we consider stresses due to cure/crystallization shrinkage, Equation (4-40) is rewritten as

$$\sigma = E(\epsilon - \alpha \Delta T - \alpha^{cs} \Delta X) = E\epsilon - \beta \Delta T - \gamma \Delta X \quad \textbf{(4-49)}$$

In Equation (4-49), ΔX is change of degree of cure/crystallinity and α^{cs} is free strain due to a unit change in degree of cure/crystallinity and γ is stress due to a unit change in degree of cure/crystallinity in a completely constrained body.

Similarly if we take into account stresses due to cure/crystallization shrinkage, Equation (4-42) is rewritten as

$$\sigma_x = E_e\epsilon_x + a_F\int_0^{\xi}\Delta E(\xi-\xi')\frac{d\epsilon_x}{d\xi'}d\xi' - \beta_e\Delta T - a_F\int_0^{\xi}\Delta\beta(\xi-\xi')\frac{d\left(\frac{\Delta T}{a_F}\right)}{d\xi'}d\xi' \\ - \gamma_e\Delta X - a_F\int_0^{\xi}\Delta\gamma(\xi-\xi')\frac{d\left(\frac{\Delta X}{a_F}\right)}{d\xi'}d\xi' \quad \textbf{(4-50)}$$

In Equation (4-50), γ_e is the final (relaxed) value of γ and $\Delta\gamma = \gamma(\xi) - \gamma_e$ is the time dependent (viscoelastic) part of γ. Similar to the procedure we followed for thermal stresses we approximate $\gamma(\xi)$ by a Prony series

$$\gamma(\xi) = \gamma_e + \sum_{i=1}^{N}\gamma_i e^{-\frac{\xi}{\tau_i}} \quad \textbf{(4-51)}$$

Defining the state variables $q_i's$ as

$$q_i(\xi) = a_F \int_0^{\xi} \left(E_i e^{-\frac{\xi-\xi'}{\tau_i}} \frac{d\epsilon_x}{d\xi'} - \beta_i e^{-\frac{\xi-\xi'}{\tau_i}} \frac{d\left(\frac{\Delta T}{a_F}\right)}{d\xi'} - \gamma_i e^{-\frac{\xi-\xi'}{\tau_i}} \frac{d\left(\frac{\Delta X}{a_F}\right)}{d\xi'} \right) d\xi' , \qquad i = 1,2 \dots, N \quad \textbf{(4-52)}$$

Equation (4-50) reduces to

$$\frac{dq_i(\xi)}{d\xi} + \frac{q_i(\xi)}{\tau_i} = a_F E_i \frac{d\epsilon_x}{d\xi} - \beta_i \frac{d\Delta T}{d\xi} - \gamma_i \frac{d\Delta X}{d\xi}, \qquad i = 1,2 \dots, N \quad \textbf{(4-53)}$$

and

$$\sigma_x = E_e \epsilon_x - \beta_e \Delta T - \gamma_e \Delta X + \sum_{i=1}^{N} q_i \quad \textbf{(4-54)}$$

Equations (4-53) and (4-54) can be interpreted as constitutive equations for a Maxwell chain as shown in Figure 4-57, with $q_i's$ being stresses of each Maxwell element.

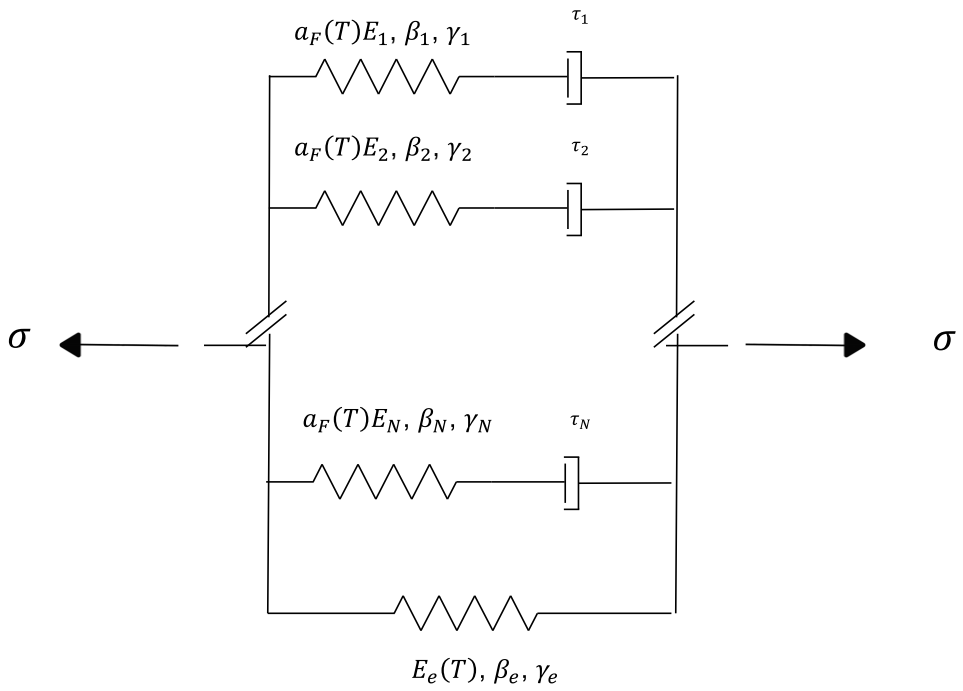

Figure 4-57 Maxwell Chain, mechanical analogue for Equations (4-53) and (4-54)

In Equation (4-53), β_i is equal to $E_i\alpha_i$ and γ_i is equal to $E_i\alpha_i^{cs}$ with $\frac{\alpha_i}{a_F}$ and $\frac{\alpha_i^{cs}}{a_F}$ being the coefficient of thermal expansion and the coefficient of cure/crystallization shrinkage for the $i'th$ Maxwell element, respectively.

As discussed in the previous section, experimental results show that the material behaviour in the glassy regime is instantaneously linear elastic (hypo-elastic) and therefore Equation (4-54) will be modified as

$$\dot{\sigma}_x = E_e \dot{\epsilon}_x - \beta_e \dot{\Delta T} - \gamma_e \dot{\Delta X} + \sum_{i=1}^{N} \dot{q}_i \qquad \textbf{(4-55)}$$

Thermo-viscoelastic constitutive equations, developed in this chapter are generalized for three dimensional isotropic, transversely isotropic and orthotropic cases. Time integration of the equations is also carried out to prepare them for implementation in a UMAT. Details and derivations are presented in Appendix B .

4.4 Verification of implementation

In this section, a simple example is analyzed using the implemented model. The results are compared with other available solutions for verification of implementation. This example is taken from ABAQUS Benchmark Guide, Version 6.14.

A rod of the dimensions shown in Figure 4-58, is fixed at one end and a constant axial load is applied suddenly to the other end. The magnitude of the load is 100 as shown in the figure.

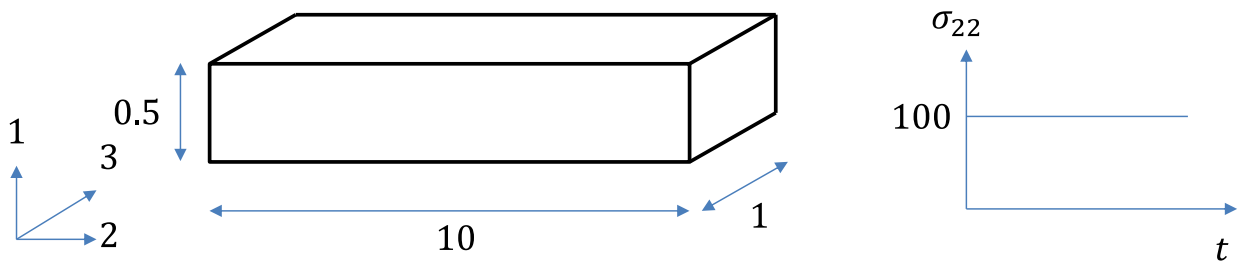

Figure 4-58 Rod subjected to constant axial load

The material properties, shear and bulk modulus, are as follows:

$$G = 333.7 + 3037.1e^{(-t/0.9899)}$$
$$K = 100000 \quad \textbf{(4-56)}$$

A closed form solution is provided in the ABAQUS Benchmark Guide as

$$\epsilon_{22} = 0.1\left(1 - 0.9e^{-t/10}\right) \quad \textbf{(4-57)}$$

This example was also solved by Zobeiry [69], using the differential form of viscoelasticity.

The analysis results for creep strain are compared with the closed form solution, ABAQUS viscoelastic solution and Zobeiry's solution in Figure 4-59.

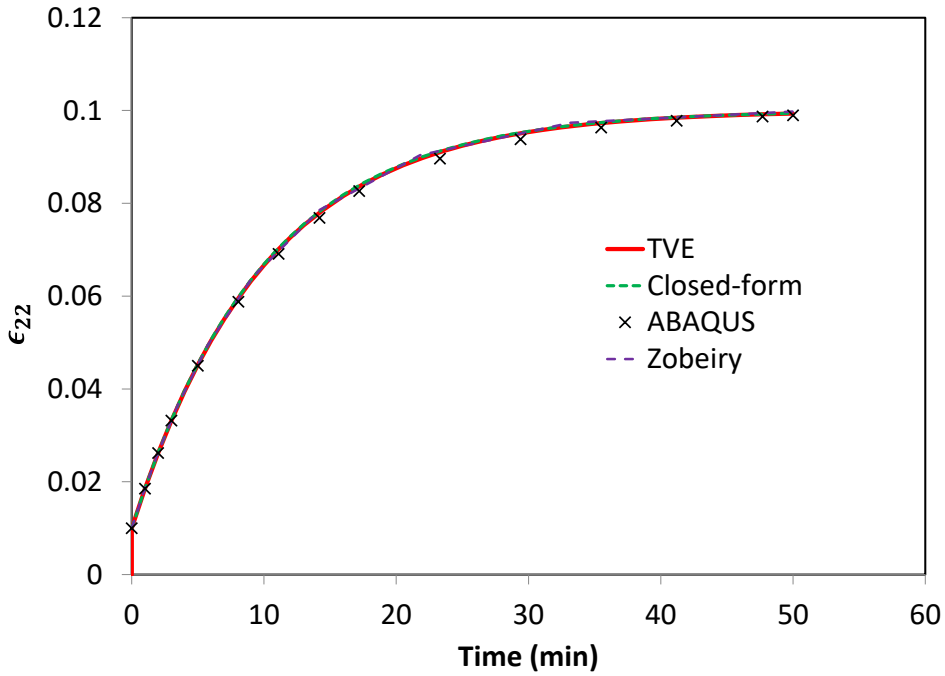

Figure 4-59 Rod subjected to constant axial load

It is seen from Figure 4-59 the analysis results from the TVE model is very close to the closed form solution and other analysis results.

4.5 Summary

In this chapter, thermo-viscoelastic behaviour of AS4/PEEK, neat PEEK, fully cured AS4/8552 and fully cured 8552 resin was characterized using stress relaxation tests. A vertical shift factor was defined and the master curves of relaxation moduli were generated. Prony series were fitted

to all master curves. Constant load experiments were performed and it was shown that the material behaviour of fully cured 8552 resin, in the glassy regime, is hypo-elastic.

Based on the integral equation of Schapery for creep of thermo-rheologically complex materials, a thermo-viscoelastic integral equation was proposed for stress relaxation. The integral equation was converted into a system of first order ordinary differential equations. The developed model was generalized for three dimensional isotropic, transversely isotropic and orthotropic cases. Finally a simple case study was analyzed and the implementation of the model was verified.

Chapter 5: Case Studies

In this chapter, two case studies are analyzed and capabilities of the crystallization/melt kinetics model and thermo-viscoelastic model for real industrial cases are investigated.

The first case study is a L-shape angle, manufactured at different tool temperatures in a hot press. The developed models are used for studying both crystallization history and distribution, and process distortions in the final product.

The second case study is investigation of crystallization history at a material point during the automatic fibre placement (AFP) process.

5.1 L-shape angles

L-shape angles with a corner angle designed at $90°$ were manufactured from AS4/PEEK by Fortin [128]. Parts were manufactured by thermoforming previously manufactured laminated flat panels in a hot press. The laminates consisted of 16 layers with a symmetric quasi-isotropic lay-up; $[0/+45/\text{-}45/90]_{2S}$, resulting in a consolidated thickness of $2.20\ \text{mm} \pm 0.05\ \text{mm}$. A thermocouple was embedded in the mid-thickness and in the center of laminate as shown in Figure 5-1.

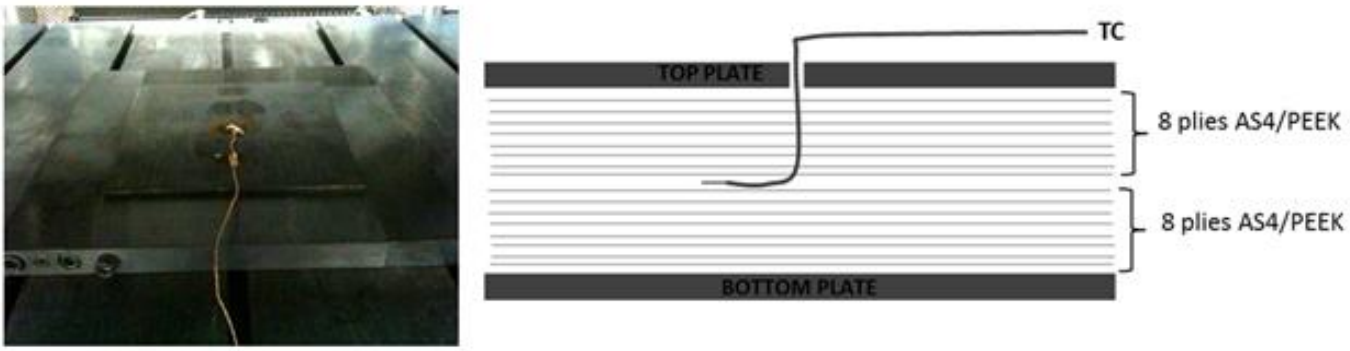

Figure 5-1 Picture and schematic of the thermocouple location (courtesy Fortin [128])

Flat panels were pre-heated to the processing temperature of 390 ℃ in a furnace next to the hot press. The part was transported as rapidly as possible to the forming tool, followed by closure of the press. During the process, the platen temperature was held constant at three temperatures: 290 ℃, 215 ℃, and 105 ℃. The part was cooled down within the tool for 5 min, while the consolidation pressure of 40 bar was applied. Finally the part was removed from the tool and was allowed to cool down to ambient temperature by natural convection. Male and female tools are shown in Figure 5-2.

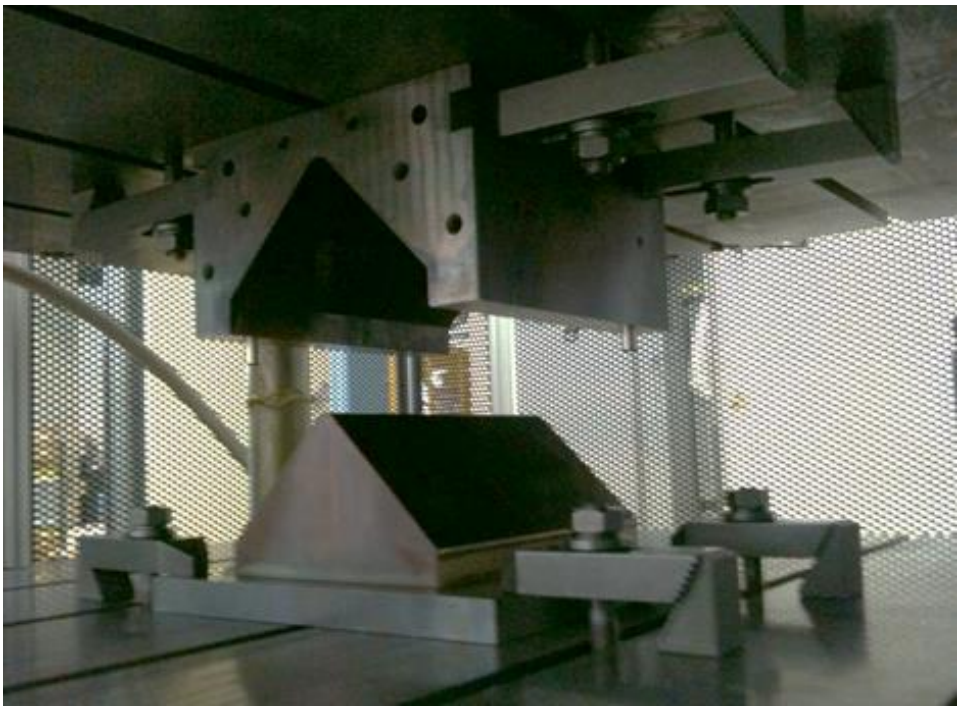

Figure 5-2 Male and female tool assembly (courtesy Fortin [128])

Spring-in angles and also failure loads for the manufactured samples were measured by Fortin [128]. In this chapter, initially the experimental methods and measured results are briefly explained. The processing is then simulated using the process modelling package, ABAQUS COMPRO CCA, with inputs being the experimental temperature and pressure profiles used during manufacturing of the parts. Analysis is performed using the crystallization kinetics model, developed in Chapter 3, CHILE constitutive model and the thermo-viscoelastic (TVE) constitutive model, developed in Chapter 4. Crystallinity in the part is correlated with the strength (measured failure load). Also spring-in angles predicted using CHILE and TVE models are compared with experimental measurements.

5.1.1 Spring-in angles

The L-shape angles, manufactured in the hot press, were scanned in a Nikon CMM for measuring the spring-in angle.

(a) 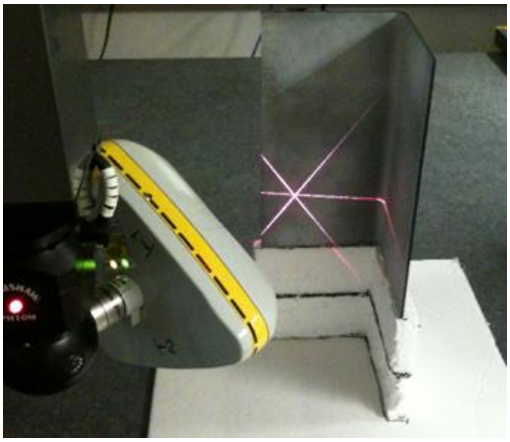

(b) 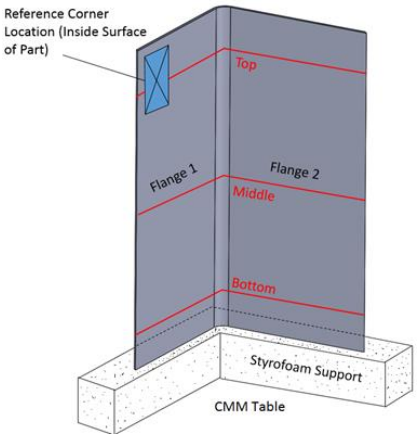

Figure 5-3 (a) Scanning the inside surface of the L-shape angle with the CMM laser head (b) Locations of cross-section lines for angle measurement (Courtesy Fortin [128])

Measurement was performed on the inside surface and the angles were measured at three locations; top, middle and bottom and within one inch from the corner region, as shown in Figure 5-3. The results of the measured spring-in angles are presented in Table 5-1. Spring-in for the three tool temperatures are visually compared in Figure 5-4.

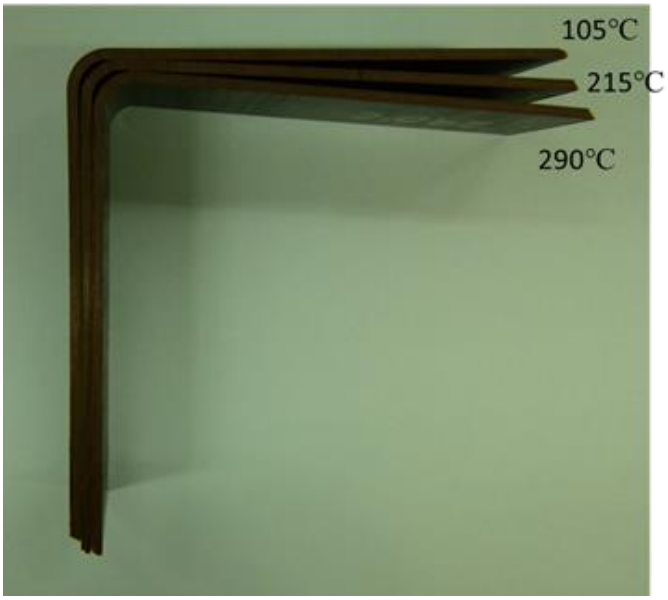

Figure 5-4 Spring-in of quasi-isotropic L-shape angles consolidated at 290 ℃, 215 ℃ and 105 ℃ (Courtesy Fortin [128])

Table 5-1 Measured spring-in for manufactured L-shape angles (courtesy Fortin [128])

Tool Temperature (° C)	Spring-in angle (°)	Average Spring-in angle (°)
290	3.29	3.28
	3.36	
	3.18	
215	2.21	2.14
	2.21	

Tool Temperature (° C)	Spring-in angle (°)	Average Spring-in angle (°)
	2.01	
105	0.44	0.58
	0.61	
	0.70	

5.1.2 Mechanical strength

The three specimens were cut according to ASTM D6145 [152] and were tested using a four-point bending clamp in an Instron® dual-column system by Fortin [128]. The sample and the test set up are shown in Figure 5-5. The failure load results for the samples are presented in Table 5-2.

Table 5-2 Measured failure load for manufactured L-shape angles (courtesy Fortin [128])

Tool Temperature (° C)	Failure Load (N)	Average Failure Load (N)
290	3516.9	3379.3
	2942.9	
	3678.1	
215	2655.7	2953.5
	2917.4	
	3287.4	
105	857.4	899.4
	921.9	
	919.0	

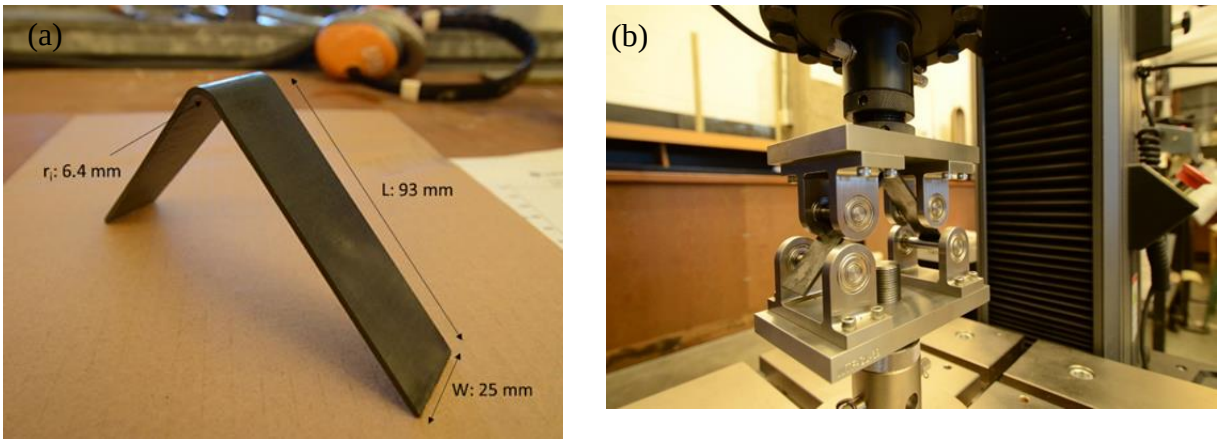

Figure 5-5 (a) L-shape specimen cut to dimensions (b) Specimen mounted on the test fixture (Courtesy Fortin [128])

5.2 Simulations

In this section, consolidation of the L-shape angles in the hot press is simulated using ABAQUS COMPRO CCA. The composite part, female tool and male tool are all meshed using 20-node solid elements and are shown in Figure 5-8.

The first step in the simulations is performing the heat transfer analysis. The crystallization kinetics model is used along with the energy equation for prediction of temperature distribution and degree of crystallinity distribution in the part during the process. The next step is stress and deformation analysis. The results from the heat transfer analysis are used and stress and deformation analysis is performed using CHILE or TVE constitutive models. The coefficients of thermal expansion in fibre direction (CTE_1), transverse direction (CTE_2), and thickness directions (CTE_3) for AS4/PEEK are taken from Fortin's M.A.Sc. thesis [128] and are presented in Figure 5-6. For specific heat and conductivity, the data provided by Lee and Springer [110] is used. Density data are used from the

work of Velisaris and Seferis [19]. Cure shrinkage and modulus data is taken from the work of Chapman *et al* [112].

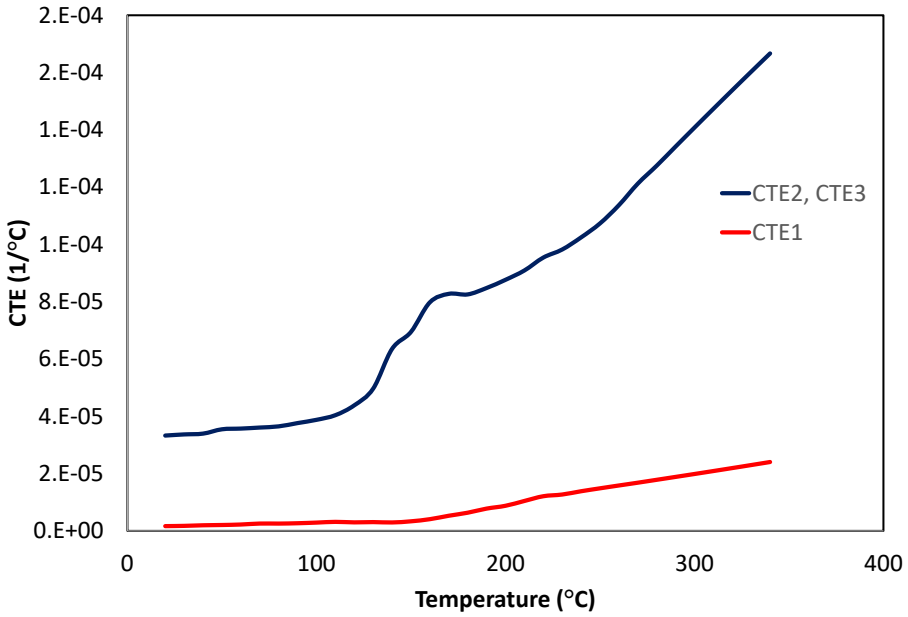

Figure 5-6 CTE values for AS4/PEEK (From Fortin [128])

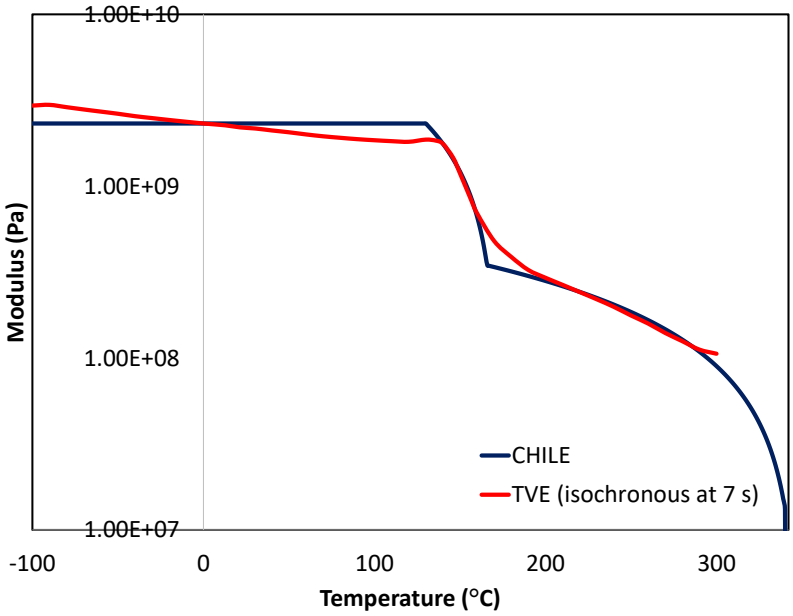

Figure 5-7 Modulus for neat PEEK, used in CHILE analysis, compared with TVE isochronous modulus at 7 s

The modulus model from reference [112] is used for stress analysis using the CHILE model. The constants in the model are modified such that the modulus is consistent with the unrelaxed modulus used for TVE analysis. For stress analysis using the TVE model, the material characterization data from the section 4.1.5.2 is used. The modulus for neat PEEK, used for CHILE analysis and TVE modulus are shown in Figure 5-7.

Both male and female tools are made of steel and their properties are available from the COMPRO CCA material library.

5.2.1 Heat transfer analysis

For thermal analysis, DC3D20 (20 noded diffusive heat transfer quadratic elements) are used. The actual temperature profile used for processing the parts is used here for simulations.

The part temperature is initially at $390\ ℃$. The male tool temperature is set at the tool target temperature ($290\ ℃$, $215\ ℃$ or $105\ ℃$). In the first step, the composite part comes into contact with the male tool. After 4 sec, in the second step, the female comes into contact with the part and both male and female tool stay in contact with the part for 300 sec. In the third step, both male and female tools become inactive (tool removal) and the part is cooled down by natural convection to the ambient temperature for 2400 sec. The heat transfer coefficient, HTC, is assumed as $10\ \mathrm{W/m^2K}$.

(a)

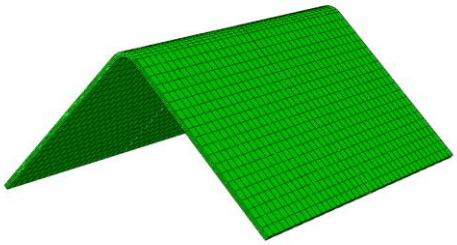

(b)

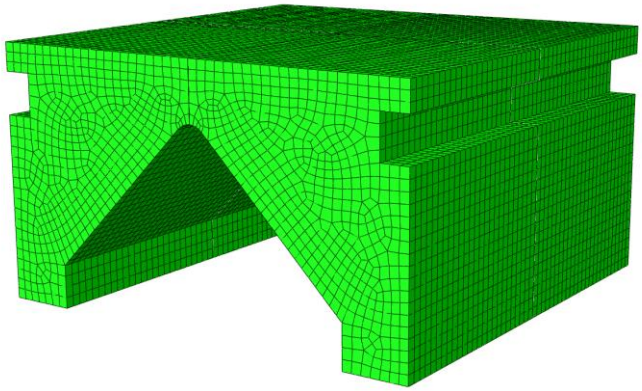

(c)

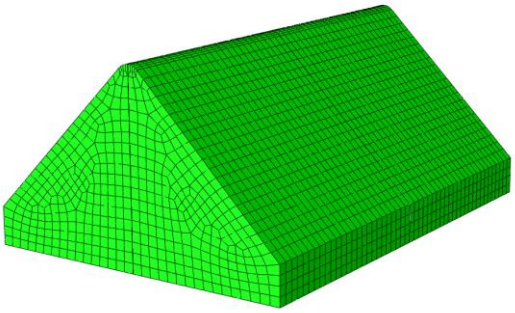

Figure 5-8 Meshes for (a) composite part (b) female tool (c) male tool

To validate the heat transfer analysis, the temperature measured by the thermocouple shown in Figure 5-1 was compared with the predicted values for the three cases. The results are given in Figure 5-9, Figure 5-10 and Figure 5-11.

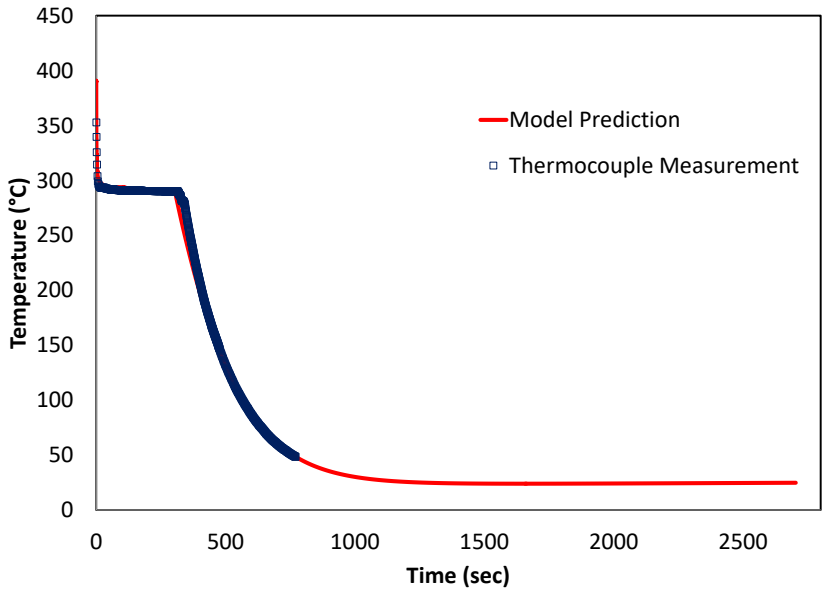

Figure 5-9 Temperature at the location of the thermocouple shown in Figure 5-1, predicted and measured values, tool temperature at 290 ℃

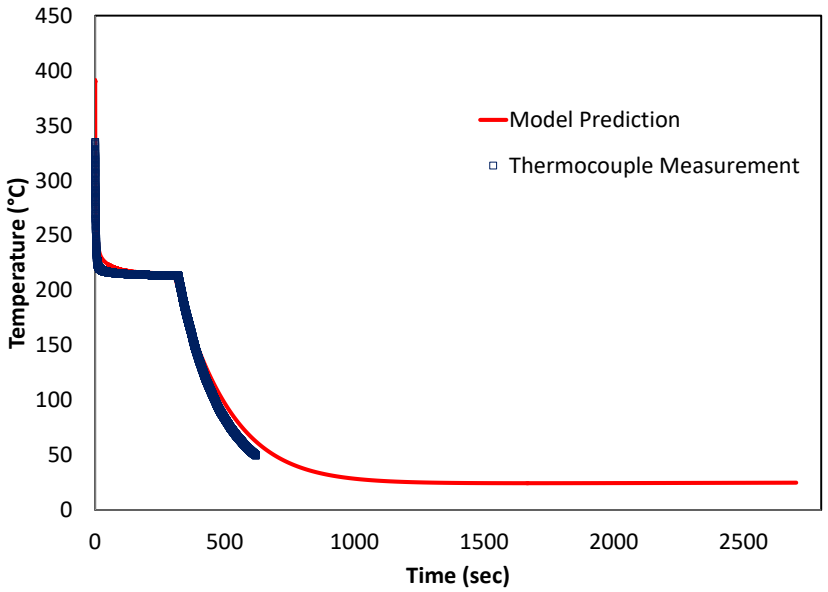

Figure 5-10 Temperature at the location of the thermocouple shown in Figure 5-1, predicted and measured values, tool temperature at 215 ℃

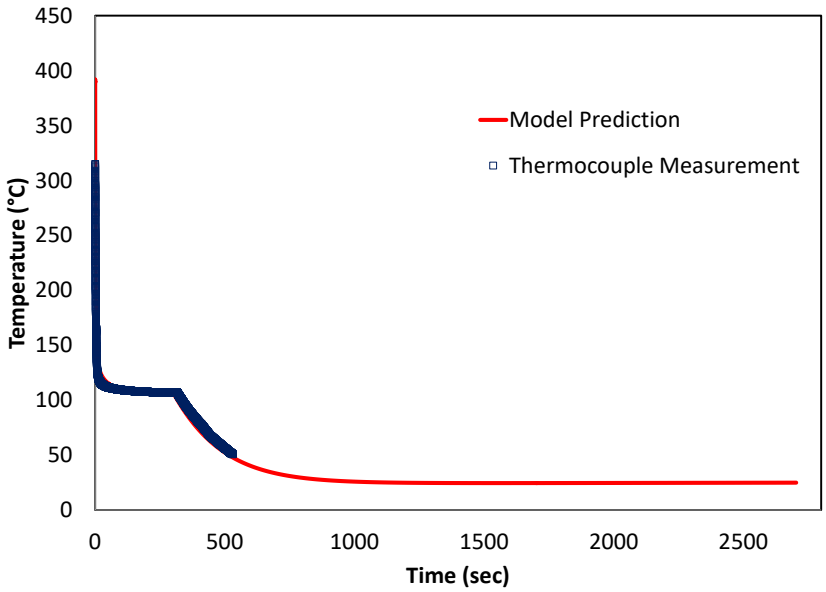

Figure 5-11 Temperature at the location of the thermocouple shown in Figure 5-1, predicted and measured values, tool temperature at 105 ℃

From the results in Figure 5-9, Figure 5-10 and Figure 5-11, it is seen that model predictions are in good agreement with thermocouple measurements.

Contour plots of the degree of crystallinity in the part at the end of the process for three tool temperatures are given in Figure 5-12.

(a)

(b)

(c)

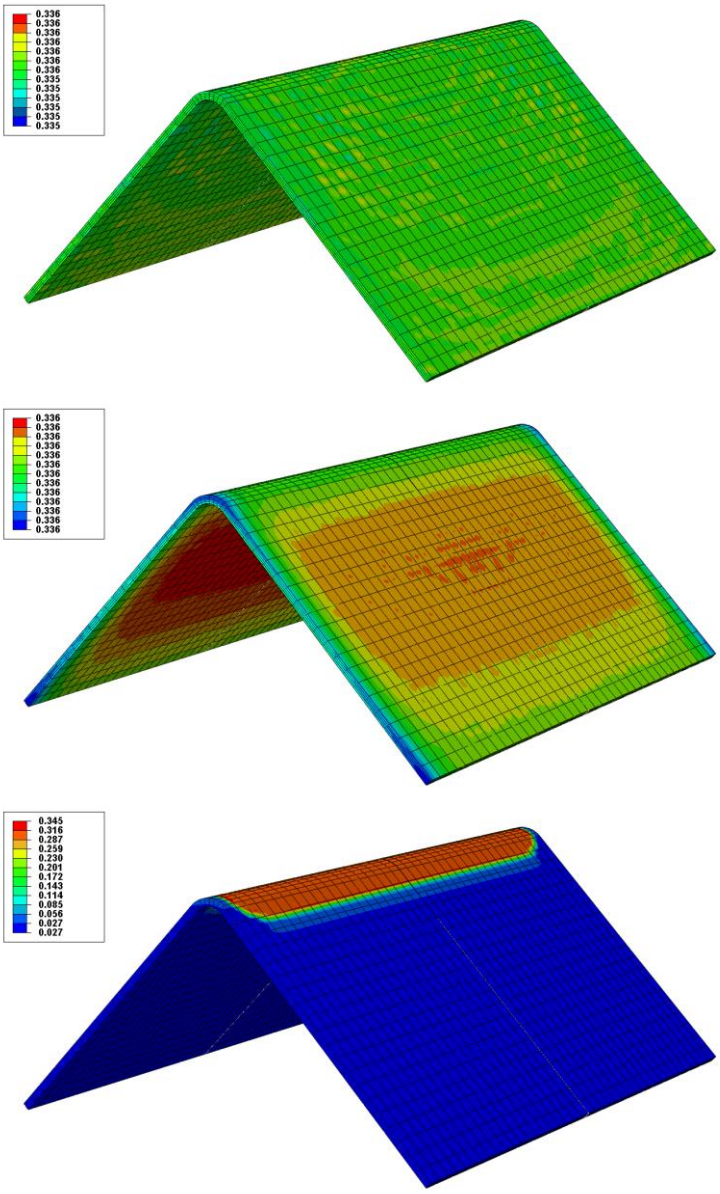

Figure 5-12 Crystallinity distribution in the composite part at the end of the process for tool temperature at (a) 290 ℃ (b) 215 ℃ (c) 105 ℃

Plots in Figure 5-12 show that for tool temperature at 290 ℃ and 215 ℃, crystallinity is uniform in the sample and the part is fully crystallized (relative). For the tool temperature at 105 ℃, the crystallinity is not uniform in the part. The material is fully amorphous in the flanges. Near the

corner, the crystallinity increases and the material is fully crystallized (relative) at a narrow region around the corner.

To have some insight into the temperature and crystallinity history and also crystallinity gradient through the thickness of the part, some points and paths are defined as described in Table 5-3 and shown in the wireframe sketch of a quarter of the part in Figure 5-13.

Table 5-3 List and location of defined points and paths in the part

Point or Line (path)	Location
Point C	At the corner, mid-plane, mid-thickness
Point F	At the corner, edge, mid-thickness
Point I	At the flange tip, edge, mid-thickness
Point L	At the flange tip, mid-plane, mid-thickness
Line AB	At the corner, mid-plane, through the thickness
Line DE	At the corner, edge, through the thickness
Line GH	At the flange tip, edge, through the thickness
Line JK	At the flange tip, mid-plane, through the thickness

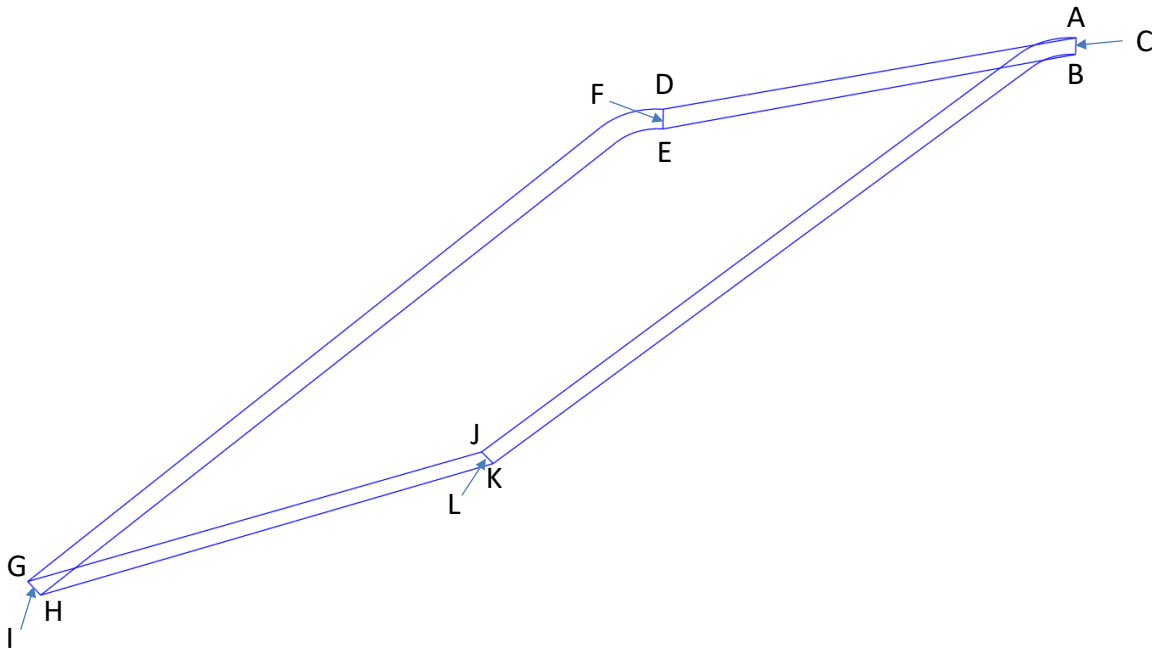

Figure 5-13 Wireframe sketch of a quarter of the part

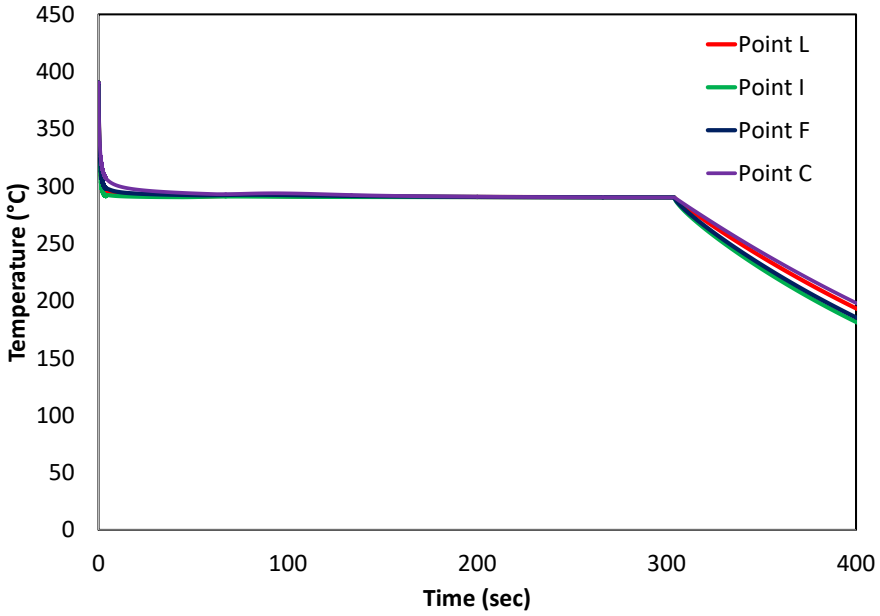

Figure 5-14 Temperature history for the four points at mid-thickness of the part, tool temperature at 290 ℃

Temperature and Crystallization history for the four points at the mid-thickness of the part, for tool temperature at 290 ℃ are given in Figure 5-14 and Figure 5-15, respectively.

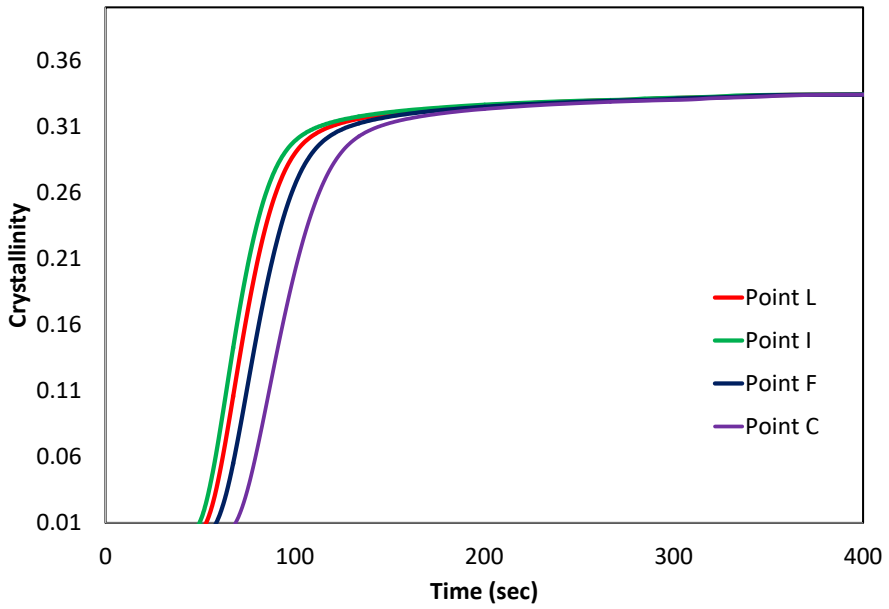

Figure 5-15 Crystallinity history for the four points at mid-thickness of the part, tool temperature at 290 ℃

Figure 5-14 and Figure 5-15 show that for the four points, crystallization is complete while the part is under the press. The material starts to crystallize at the flange tip and at the edge of the part (point I). Crystallization at the flange tip in the middle starts subsequently (Point L). Later, crystallization occurs in the corner of the part at the edges (point F). The point in the corner of the part at the middle is the last point for crystallization (Point C). The time difference for start of crystallization at these points results in time difference in modulus development in the material, which in turn results in the residual stresses in the part. Temperature and crystallization history of the four points in the material for the part manufactured with the tool temperature at 215 ℃ and 105 ℃ are given in Figure 5-16, Figure 5-17 Figure 5-18 and Figure 5-19.

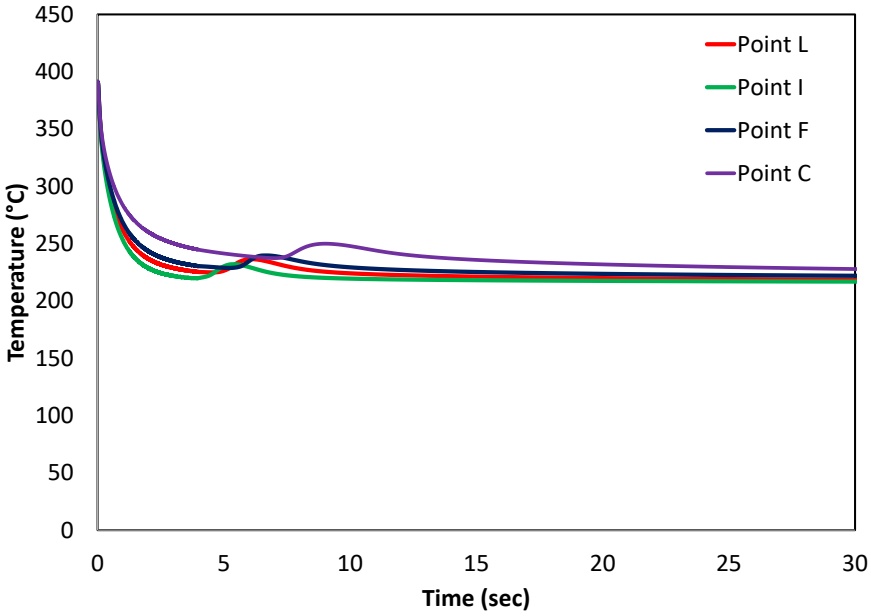

Figure 5-16 Temperature history for the four points at mid-thickness of the part, tool temperature at 215 ℃

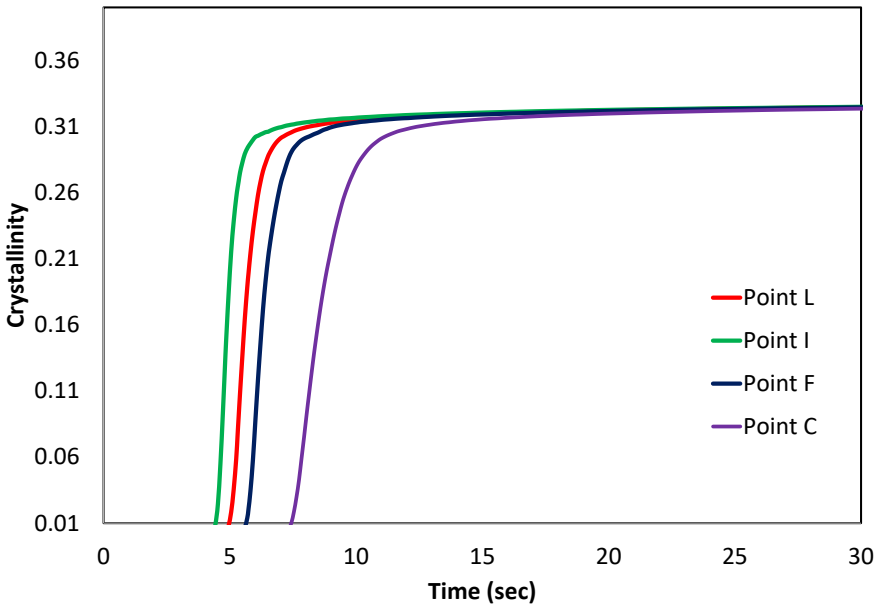

Figure 5-17 Crystallinity history for the four points at mid-thickness of the part, tool temperature at 215 ℃

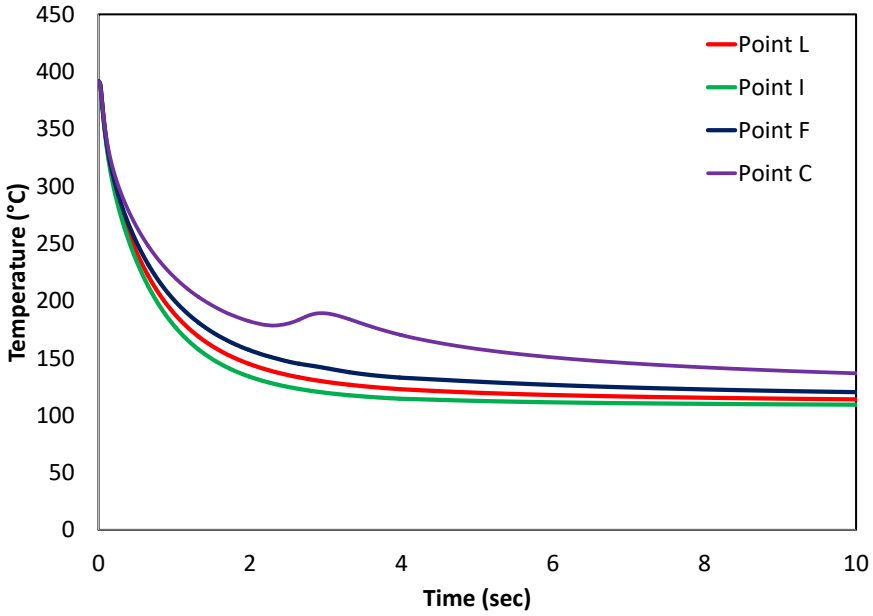

Figure 5-18 Temperature history for the four points at mid-thickness of the part, tool temperature at 105 ℃

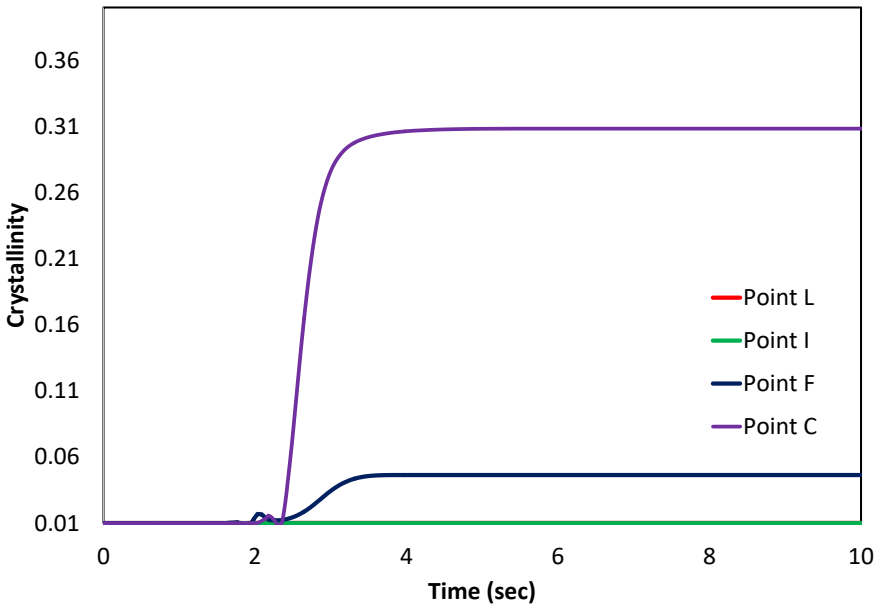

Figure 5-19 Crystallinity history for the four points at mid-thickness of the part, tool temperature at 105 ℃

Figure 5-17 shows that time priority of start of crystallization for the four points at the mid-thickness of the part is similar to the case of tool temperature at 290 ℃ . For both tool temperatures at 290 ℃ and 215 ℃, material at the four points is fully crystallized at the end of the process and there is no crystallinity gradient in the final part.

The temperature history curves in Figure 5-16 show that subsequent to the rapid cooling and at the beginning of isothermal hold, there is a sudden increase in the temperature. After that, the temperature is decreasing and is asymptotically approaching the isothermal hold. For explaining this sudden change of temperature, we consider the crystallization curves in Figure 5-17. Figure 5-16 and Figure 5-17 show that approximately at the same time as the sudden increase in the temperature, the corresponding crystallization curve is passing through its inflection point. This means the crystallization rate is maximum at the same time. Therefore the sudden temperature increase is happening when the corresponding heat flow curve is going through an exotherm. The latent heat of crystallization released by the material at this time causes a sudden increase in the temperature.

Figure 5-19 shows that at the points L and I (at the flange tip), the material is fully amorphous at the end of the process. There is a minor amount of crystallinity (approximately 0.05) at point F (in the corner of the part at the edge). At point C (in the corner at the middle) the crystallinity grows significantly, however, the material is not fully crystalline (relatively) at the end of the process.

Variation of crystallinity through the thickness of the part, manufactured with the tool temperature at 105 ℃ , at four different points are presented in Figure 5-20.

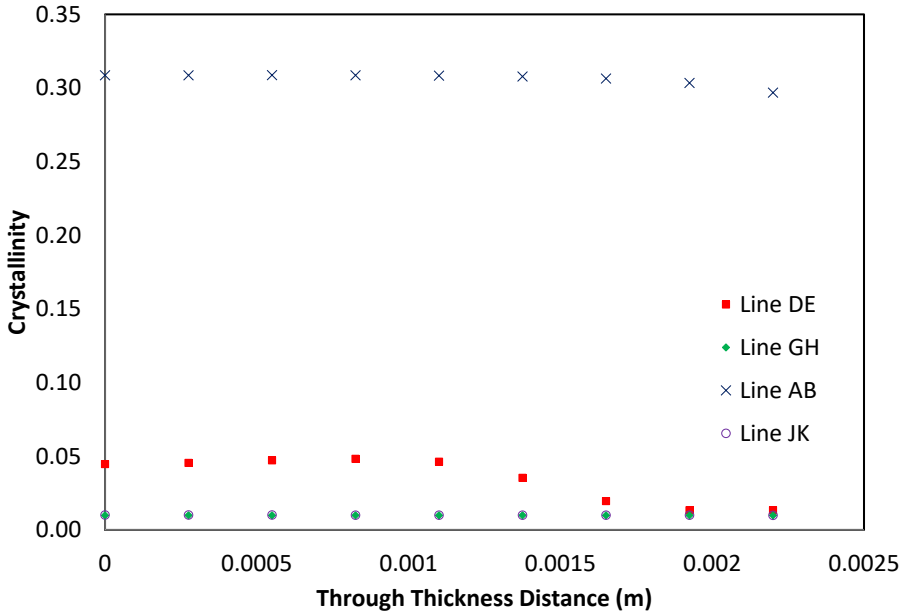

Figure 5-20 Variation of crystallinity through the thickness of the part, tool temperature at 105 ℃

In the corner at the middle, crystallinity is uniform through the thickness and a slight crystallinity gradient is observed in the corner at the edges (approximately 0.04)

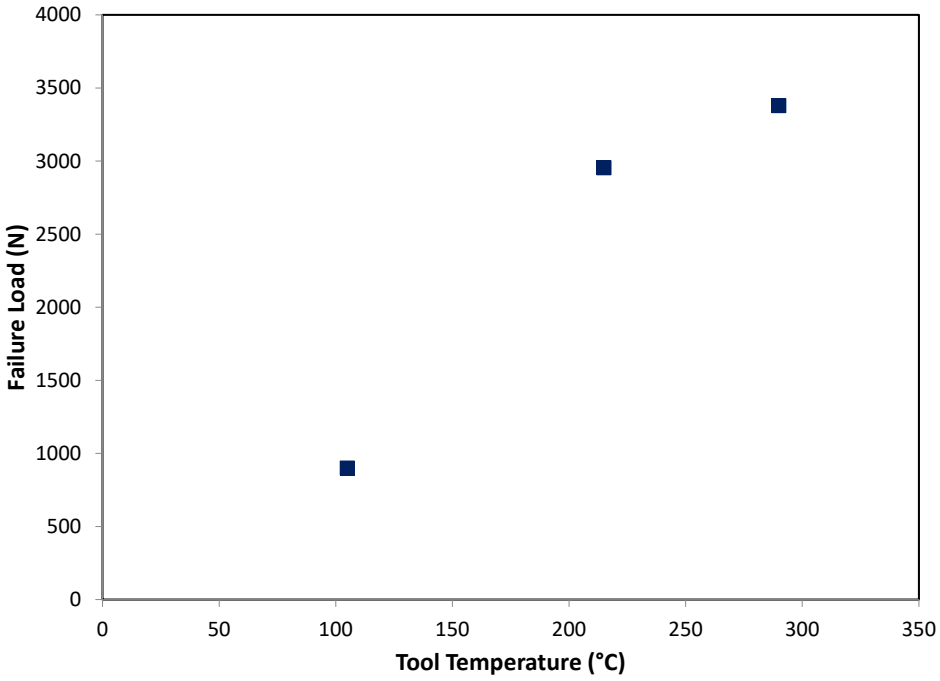

Figure 5-21 Average failure load for parts consolidated at different tool temperatures (from Fortin [128])

The average failure load results for the three samples from Table 5-2 are presented in Figure 5-21. Strength of the part can be affected by different factors. One important factor is the residual stresses. It is also shown in the literature [111] that crystallinity can affect the strength of thermoplastic composite parts.

Comparing the crystallinity history results from Figure 5-15, Figure 5-17, and Figure 5-19 and failure load results in Figure 5-21, it is observed that the part processed at 105 ℃ has the lowest final crystallinity and the lowest strength. The failure load for the part processed at 215 ℃ is lower than that for the part processed at 290 ℃, however, the final crystallinity is the same for these

parts. This can be due to more residual stresses in the part manufactured at 215 ℃. Furthermore, this can be partially due to spring-in angles in the two parts.

5.2.2 Stress and deformation analysis

Using the results from heat transfer analysis, stress and deformation analysis is conducted. C3D20 elements are used which are consistent with the 20-noded elements used in heat transfer analysis. Normal contact with no friction is enforced between the part and both female and male tools. The temperature profile is the same as was explained in section 5.2.1. In the second step, a uniform force, equivalent to a pressure of 40 bar is applied such that the part is under pressure between the male and female tool. The pressure is removed in the third step. The analysis is done using CHILE and TVE models. As it is always desired to have fully crystalline (relatively) final parts, TVE material characterization in section 4.1 was performed for the fully crystalline material. The modulus model used for CHILE analysis does not take into account the effect crystallinity. Therefore, based on the crystallization history from Figure 5-15, Figure 5-17 and Figure 5-19, only the two parts manufactured at 290 ℃ and 215 ℃ were analyzed.

5.2.2.1 Analysis using CHILE model

Using the heat transfer analysis results, CHILE constitutive model is used and stress and deformation analysis is performed for the three tool consolidation temperature cases. Three

dimensional contour plots of the displacement magnitude for the deformed composite part at the end of the processing, along with the un-deformed part are presented in Figure 5-22.

(a)

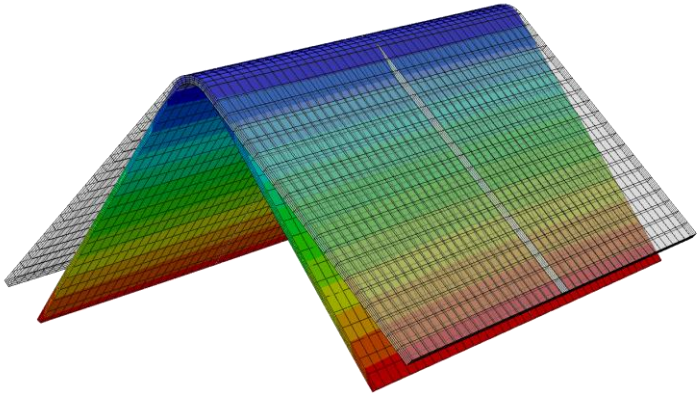

(b)

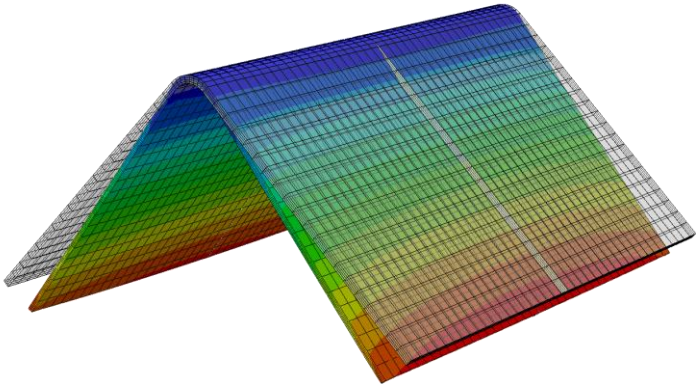

Figure 5-22 Displacement magnitude in the composite part at the end of the process for tool temperature at (a) 290 ℃ (b) 215 ℃, predicted using CHILE (scale factor = 5)

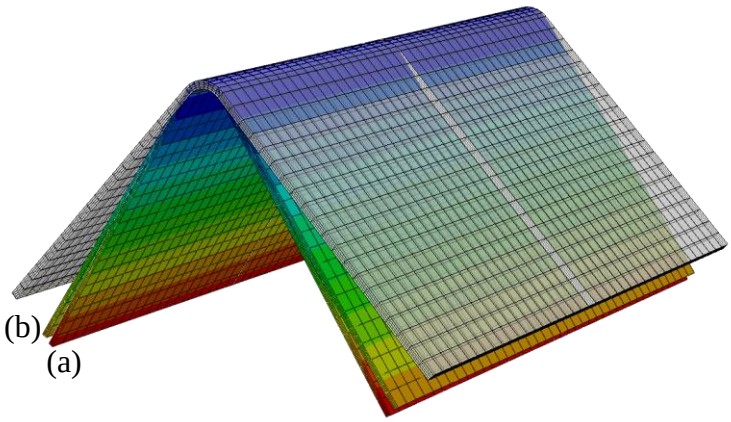

Figure 5-23 Displacement magnitude in the composite part at the end of the process for tool temperature at (a) 290 ℃ (b) 215 ℃, predicted using CHILE (scale factor = 5)

Three dimensional contours of the deformed parts for the two cases and the un-deformed part are displayed in Figure 5-23. Figure 5-23 shows that decreasing the tool temperature results in decreasing the spring in angle in the manufactured part.

(a)

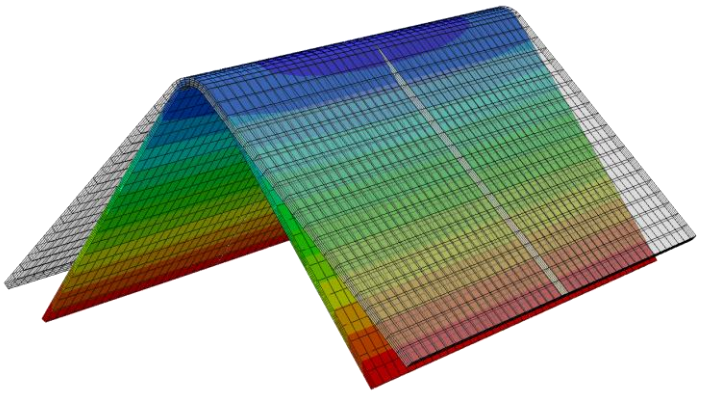

(b)

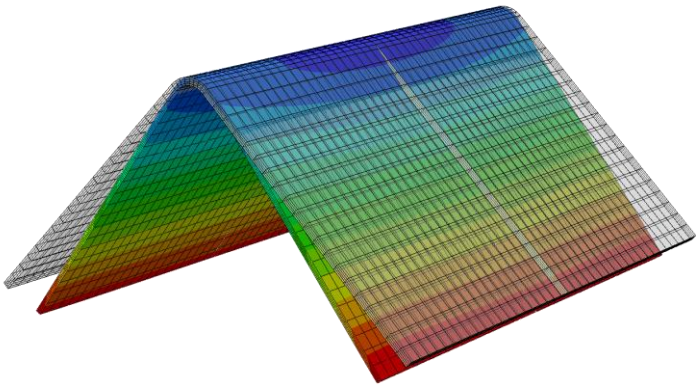

Figure 5-24 Displacement magnitude in the composite part at the end of the process for tool temperature at (a) 290 ℃ (b) 215 ℃, predicted using TVE (scale factor = 5)

5.2.2.2 Analysis using TVE model

Using the results from heat transfer analysis, stress and deformation analysis is performed using the TVE model, similar to the CHILE analysis cases. Two cases of tool temperature at 290 ℃ and 215 ℃ are analyzed.

Three dimensional contours of displacement magnitude and the un-deformed part are presented in Figure 5-24.

5.2.2.3 Spring-in angles

Similar to the experimental measurement of spring-in as explained in 5.1.1, analysis is performed on the inside surface and the angles are measured at three locations; top, middle and bottom and within one inch from the corner region (Figure 5-3). The spring-in angles, predicted based on CHILE analysis are presented in Table 5-4.

Table 5-4 Predicted spring-in for manufactured L-shape angles, CHILE analysis

Tool Temperature (° C)	Spring-in angle (°)	Average Spring-in angle (°)
290	3.68	3.75
	3.88	
	3.68	
215	3.07	3.09
	3.14	
	3.07	

The spring-in angles, predicted based on TVE analysis are given in Table 5-5.

Predicted spring-in angles based on CHILE and TVE are compared with experimental measurements in Figure 5-25. Predicted values using the Nelson-Cairns equation, Equation (2-13), are taken from work of Fortin [128] and added to the plot for comparison. The results are also shown in a bar chart in Figure 5-26.

Table 5-5 Predicted spring-in for manufactured L-shape angles, TVE analysis

Tool Temperature (° C)	**Spring-in angle (°)**	**Average Spring-in angle (°)**
290	3.12	3.19
	3.33	
	3.12	
215	2.46	2.51
	2.60	
	2.45	

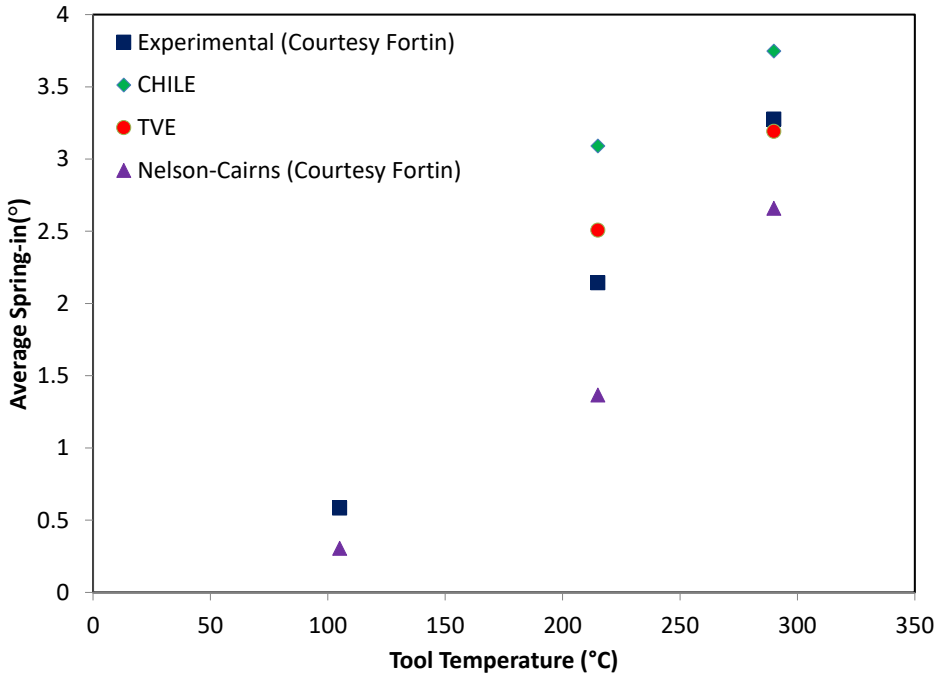

Figure 5-25 Average spring-in angle for L-shape angles, processed at different temperatures, model predictions and experimental measurements

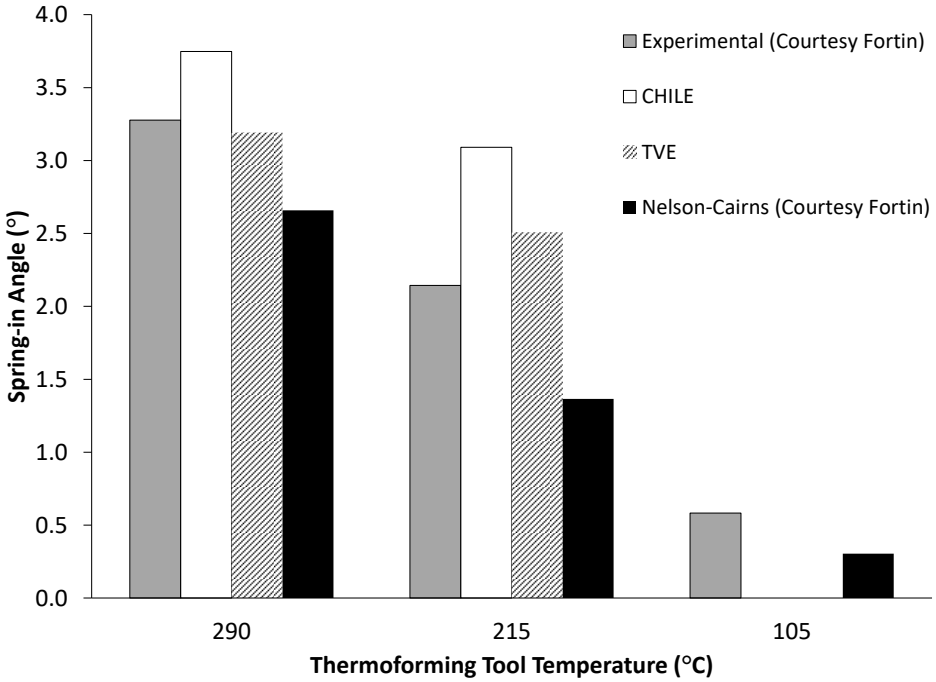

Figure 5-26 Average spring-in angle for L-shape angles, processed at different temperatures, model predictions and experimental measurements

The results from Nelson-Cairns equation under-predict the spring-in angle. The spring-in values predicted using CHILE are significantly higher than the experimental values. For tool temperature at 290 ℃ and 215 ℃, the over-prediction error is approximately 14.4 % and 44.2 %, respectively. TVE prediction for the case of tool temperature at 290 ℃ is very accurate. For the case of tool temperature at 215 ℃, TVE over-predicts the spring-in with an error of approximately 17 %.

In the CHILE analysis, the residual stresses develop in the material which result in significant values of spring-in after tool removal. In the TVE analysis however, the residual stresses develop and relax. At the tool removal step, most of the residual stresses are relaxed. This results in lower

values of spring-in angle, compared to CHILE analysis, which are closer to experimental results. One reason for over-prediction of distortions in TVE analysis is due to not taking into account the effect of crystallinity in the model. TVE material characterization in section 4.1 is performed for fully crystalline (relatively) material. For amorphous polymers, relaxation occurs at much smaller relaxation times and therefore the residual stresses relax earlier in the process. Therefore, modifying the models for taking into account the effect of crystallinity is suggested as part of the future work.

5.3 Automated Fibre Placement (AFP)

Automated fibre placement is an in-situ consolidation process for manufacturing of composite structures. The moving head of the AFP machine consists of a heat source and a roller for compaction. During the AFP process, as shown schematically in Figure 5-27, the heat is applied by the torch to create a molten zone between the incoming material tape and the composite substrate. Based on the temperature of the heating source and the tool, the adjacent layers of the material may undergo melting and recrystallization.

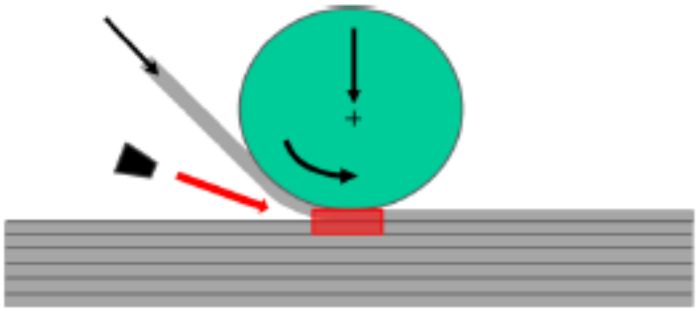

Figure 5-27 Schematic of AFP process (Courtesy Dr. Ali Yousefpour)

The temperature history for a material point in the first layer, during the AFP process for AS4/PEEK was measured using a thermocouple. The manufacturing process was conducted at National Research Council Canada, and the temperature data was provided for analysis.

In order to show how simulations, using the developed crystallization/melt kinetics models, are useful for understanding the effects of process parameters on crystallinity history and distribution, two different cases of tool temperature at 175 ℃ and 190 ℃ , and two cases of torch temperature at 800 ℃ and 900 ℃ were analyzed.

Figure 5-28 shows a wide view of the temperature and crystallinity history at a material data point. It is seen that during the first few passes, the material becomes highly crystalline, however, it is not fully crystallized. Full crystallization occurs later during the process, when the torch is sufficiently far from this point, such that there is no significant change in the temperature.

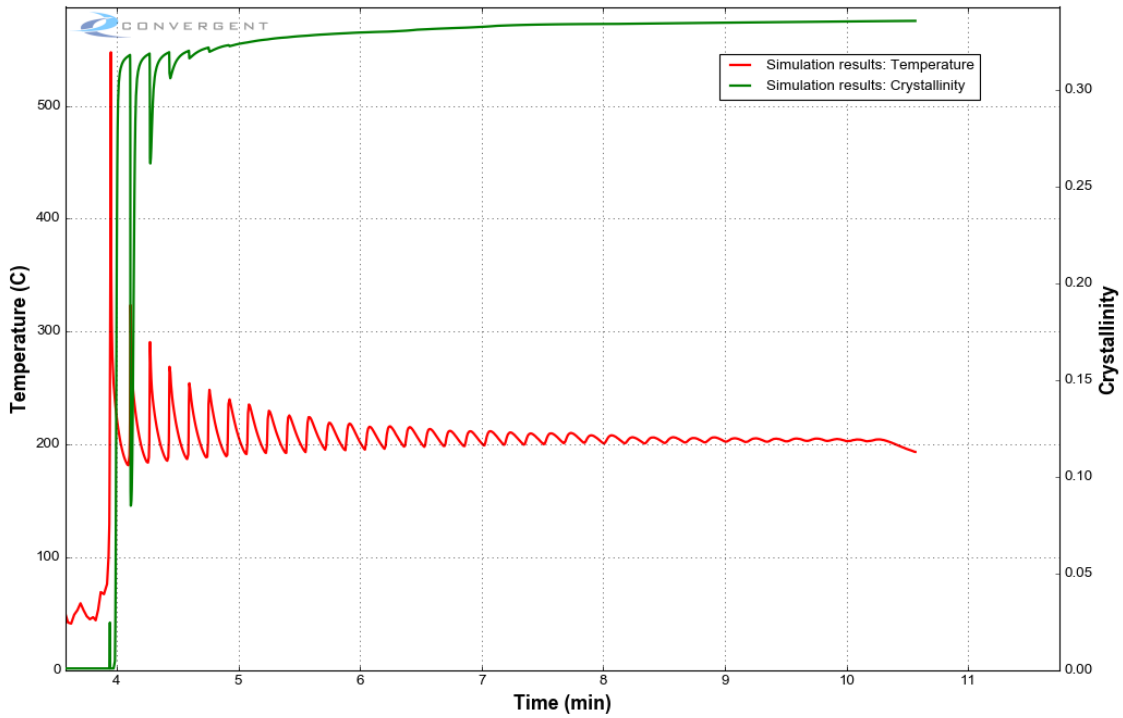

Figure 5-28 Temperature and crystallization history, tool temperature at 175 ℃, torch temperature at 800 ℃

To study the effect of tool temperature on crystallization history, the torch temperature is kept constant at 800 ℃. Analysis results for two tool temperatures are given in Figure 5-29 and Figure 5-30.

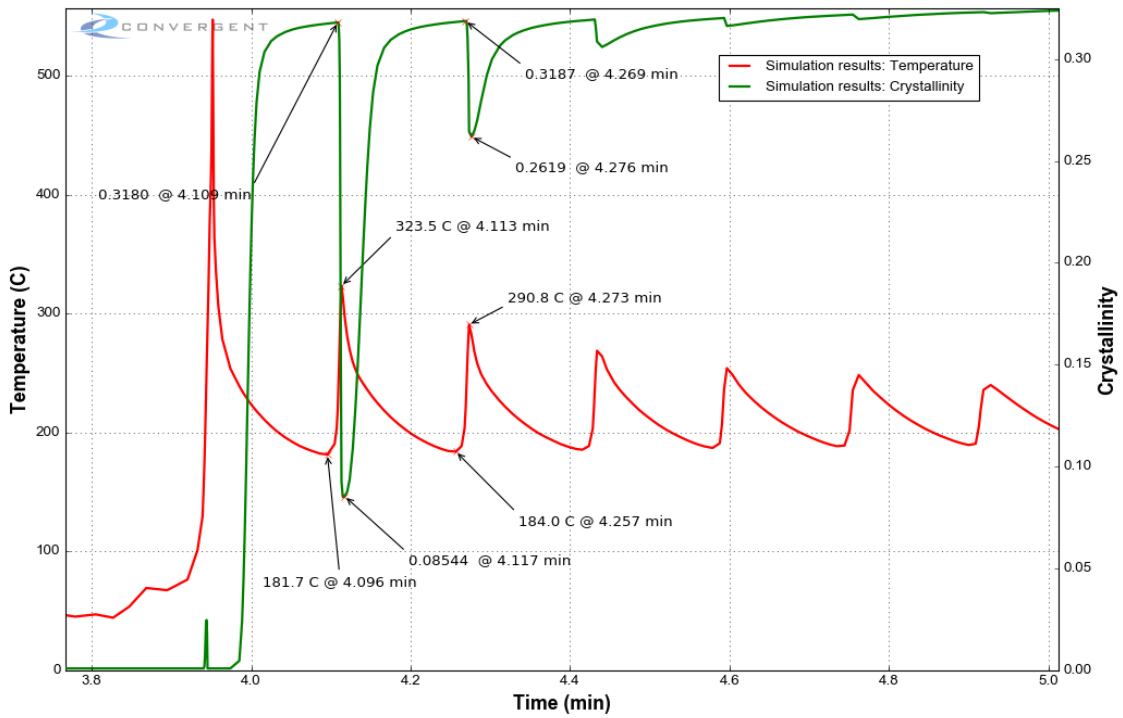

Figure 5-29 Temperature and crystallization history, tool temperature at 175 ℃, torch temperature at 800 ℃

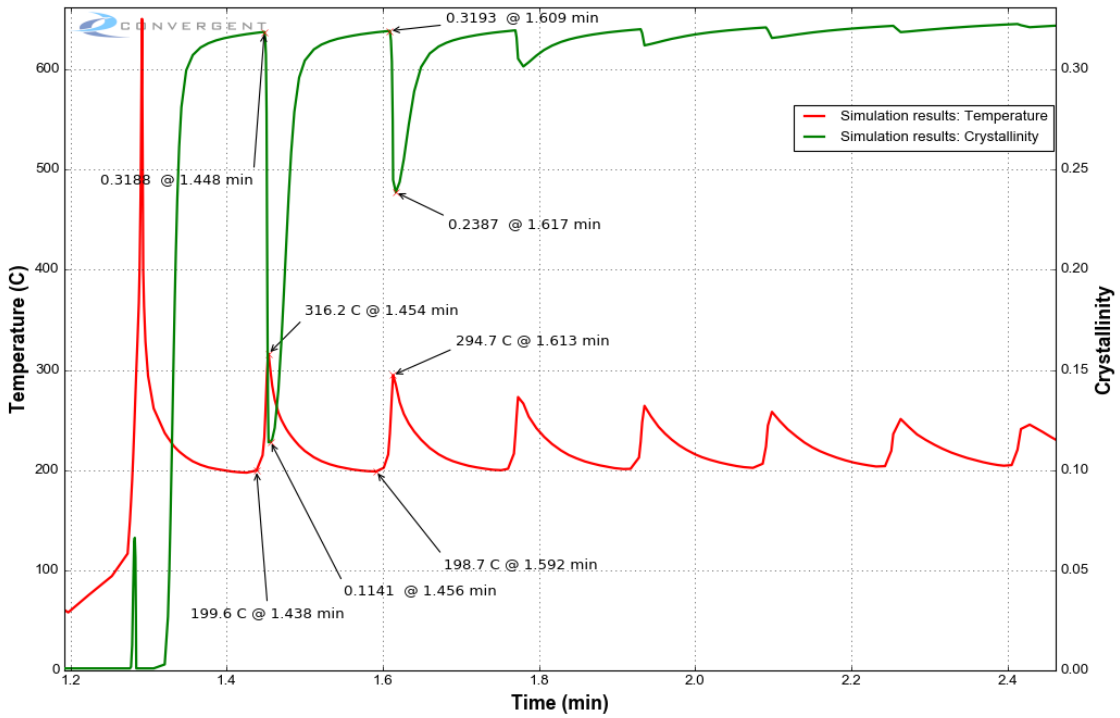

Figure 5-30 Temperature and crystallization history, tool temperature at 190 ℃, torch temperature at 800 ℃

Figure 5-29 shows that for tool temperature at 175 ℃ , after the second pass, the material loses a significant amount of crystallinity ($X = 0.08$). If the tool temperature is increased to 190 ℃, according to Figure 5-30, the degree of crystallinity after the second pass is $X = 0.11$. Therefore, higher tool temperatures result in lower melting of the material point during the subsequent passes.

Next, the torch temperature is kept constant at 900 ℃ and two tool temperatures are considered. The analysis results are shown in Figure 5-31 and Figure 5-32

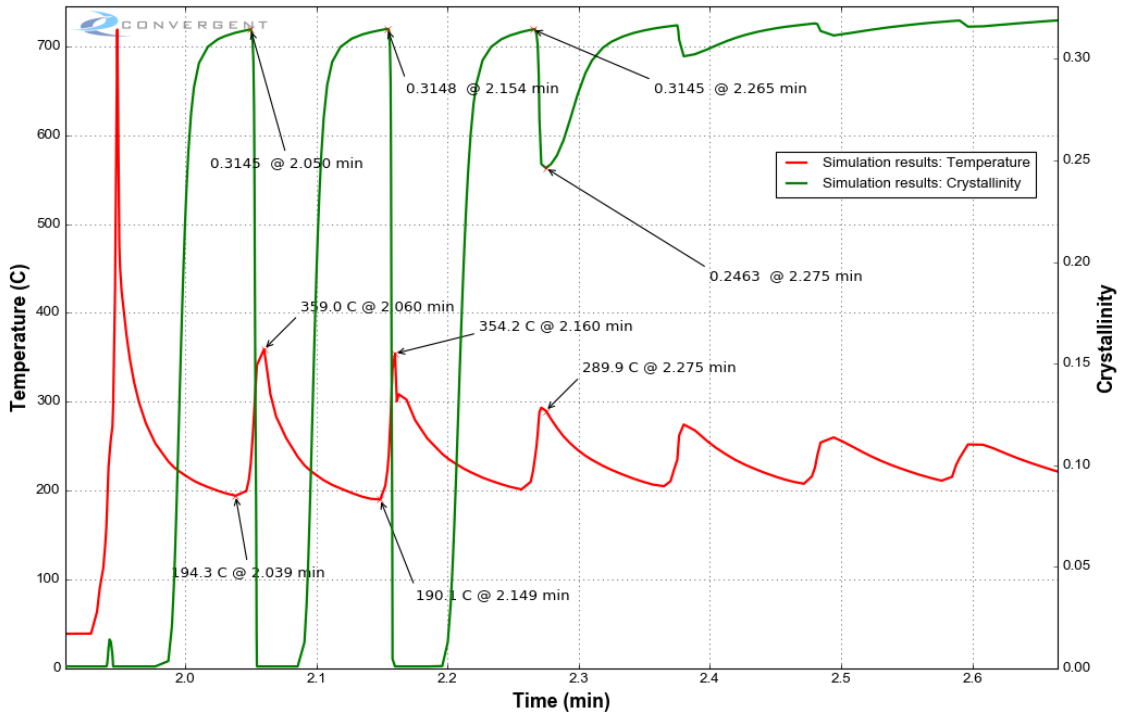

Figure 5-31 Temperature and crystallization history, tool temperature at 175 ℃, torch temperature at 900 ℃

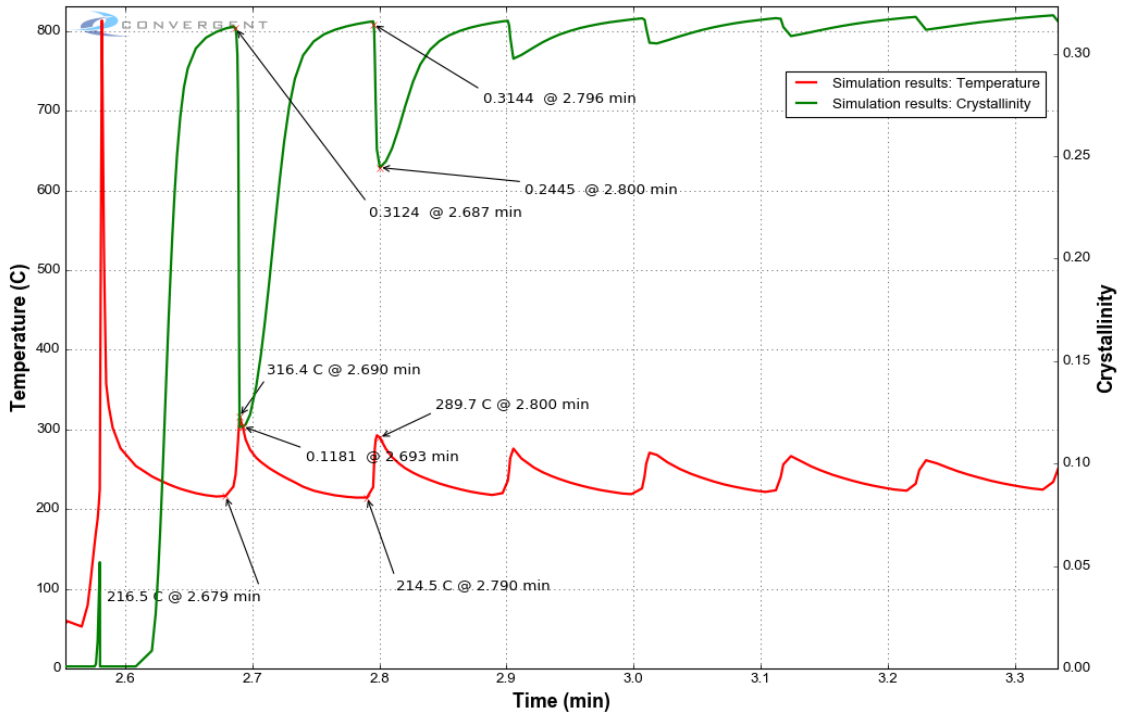

Figure 5-32 Temperature and crystallization history, tool temperature at 190 ℃, torch temperature at 900 ℃

From Figure 5-31 it is seen that for tool temperature at 175 ℃, after the second pass, the material is fully melted. An induction time is observed during the subsequent cool down, before the crystallization starts. The material is fully melted again after the third pass. By increasing the tool temperature to 190 ℃, from Figure 5-32 it is observed that the degree of crystallinity is decreased after the second pass, however, the material is not fully melted.

From these case studies, it is evident that the crystallization/melt kinetics model is a useful tool for designing AFP processes with the optimum crystallization history.

Stress and deformation analysis can also be performed similar to the L-shape case study. This is suggested as a task for future work.

Chapter 6: Conclusions and Future Work

6.1 Summary

In this work, the crystallization kinetics of AS4/PEEK was studied using isothermal and non-isothermal DSC experiments. Isoconversional data was extracted from the experimental results to study the temperature dependence of crystallization rate. Plots of crystallization rate as a function of temperature for different constant degrees of crystallinity indicated that the data points for isothermal and non-isothermal melt crystallization fall on the same curve. This implied that there was no significant difference between isothermal and non-isothermal crystallization mechanisms and a unified model should be used for the prediction of both. It was assumed that the crystallization kinetics of AS4/PEEK can be modelled using a separable differential form model (Equation (3-5)). Isoconversional plots showed that crystallization rate was increased by increasing the under-cooling. The data points, extracted from the cold crystallization experiments showed that cold crystallization rate increased as the temperature was increased above the glass transition temperature. Cold crystallization occurs as the molecular chains, frozen in place due to high cooling rates, recover their mobility as the temperature is increased. Following the same logic, when the temperature was decreased during the cool down, molecular chains lost their mobility gradually. Therefore, the crystallization rate decreased as the temperature approached the glass transition temperature. Based on these discussions, a model (Equation (3-8)) was proposed for temperature dependence of crystallization rate.

Experimental results showed that crystallization started subsequent to an induction time. Induction time was measured as the time where the degree of crystallinity reached a small but measurable value ($X = 0.001$). A simple empirical model (Equation (3-9)) was fitted to the induction time data for isothermal crystallization. For non-isothermal cases, the additivity rule (Equation (3-10)) along with the model for isothermal induction time (Equation (3-9)) were used for calculation of the induction time, (or the time when the degree of crystallinity reaches the value 0.001). Using the differential model (Equation (3-8)) with the induction time values, degree of crystallinity was calculated for all isothermal and non-isothermal cases. Model calculations were in good agreement with experimental results.

Melting kinetics of AS4/PEEK was also studied using DSC experiments. Experimental results showed that in comparison with crystallization, melting occurred over a wider temperature range. Moreover, unlike crystallization, melting ends approximately at the same temperature for all heating rates. Two separate peaks were observed in the heat flow curves of melting tests for all heating rates. Some annealing experiments, with different annealing times and temperatures, were performed to investigate the double peak behaviour of the material in melting. Experimental results showed that with increasing annealing time, at the same annealing temperature, the first peak shifted towards higher temperatures. However, the temperature for the second peak did not change. This indicated that the melting onset temperature increased with increasing annealing time. In other words, the crystals become more stable with increased annealing time. Similar results were observed for experiments with the same annealing time but different annealing temperatures, i.e. more stable crystals are formed at higher annealing temperatures. From these observations, it was concluded that crystals are continuously melting and recrystallizing during both heating and

isothermal (annealing) cases. The crystals after recrystallization are more stable in comparison with the original crystals.

Based on the discussions on continuous melting and recrystallization of the crystals during a heating cycle, it was concluded that at extremely high heating rates, there would not be sufficient time for the melted crystals to crystallize and therefore pure melting would occur as a result of the heating cycle. A plot of variation of crystallinity with respect to temperature (dX/dT) as a function of temperature (T), extracted from the pure melting results should be considered as a 'master melt curve'. This master melt curve, along with the crystallization model, can be used for prediction of continuous melting and recrystallization in a heating process. Since extremely high heating rates were not possible with the DSC machine, melting results from one of the heating experiments were used. Using the crystallization kinetics model, the recrystallization amount was calculated during each time step and was subtracted from the net melting results. The resulting melting curve was used as an estimation of the pure melting curve and the master curve data was extracted. Using this estimated master melt curve, along with the crystallization kinetics model, variations of crystallinity for all experiments were calculated. Predicted results were in good agreement with the experiments for all melting cases. For the annealing cases, predictions were in reasonable agreement with measurements.

To study the thermo-viscoelastic behaviour of AS4/PEEK, neat PEEK, fully cured AS4/8552 and fully cured 8552 resin, stress relaxation experiments were performed at different temperatures in a DMA machine. Experimental results showed that for all cases, the unrelaxed values of the moduli were temperature dependent. A vertical shift factor was defined using the values of the moduli and unrelaxed moduli at each temperature. The relaxation moduli were normalized using the vertical

shift factor. The normalized moduli were shifted horizontally in logarithmic time space. Prony series were fitted to all master curves. It was shown that how increasing the number of Prony terms affect the smoothness of the fit. To further investigate the nature of temperature dependence of the unrelaxed moduli, a fully cured 8552 sample was tested in the DMA by being subjected to a constant force and temperature change in cool down and heat up. The same temperature cycle was repeated without application of any load to measure the deflections due to thermal expansion/shrinkage. The change in modulus of the material with temperature was measured independently using a constant frequency test. Experimental results showed that the change in modulus due to temperature change did not contribute to the beam deflection. In other words, the material behaviour in the glassy regime is hypo-elastic.

Based on the thermo-viscoelastic integral equation of Schapery for creep of thermo-rheologically complex materials, a thermo-viscoelastic integral equation was proposed for stress relaxation. By defining suitable state variables, the integral equation was converted into a system of first order ordinary differential equations. The developed model was generalized for three dimensional isotropic, transversely isotropic and orthotropic cases. Using an integrating factor, the time integration of equations was carried out for implementation in a UMAT.

Two case studies were analyzed as model applications. In case study 1, L-shape angles, manufactured at two different tool temperatures were simulated. The temperature history at a point in the part was compared with experimental results. Model predictions for temperature are in good agreement with the measured values. Spring-in angles, predicted by the model, using both CHILE and TVE models were compared with average measured values and the values obtained using a simple closed-form equation (thermo-elastic). The TVE model very accurately predicted a spring-

in value for the higher tool temperature trials. At lower tool temperatures, TVE model overpredicted the spring-in angle with an error of approximately 17 %. The overprediction using the CHILE model had an error of approximately 45 %. In CHILE analysis, the residual stresses are developed in the part during the process. Since the CHILE model is not capable of relaxing these stresses, the residual stresses in the final part cause a significant amount of spring-in. However, in the TVE analysis, a significant amount of the residual stresses are relaxed during the analysis. In material characterization for the TVE analysis, it was assumed that the material is fully crystalline. Relaxation times for amorphous material are lower than those for crystalline material. Therefore the relaxation times during the analysis are higher than the real values which results in some unrelaxed residual stresses in the final part.

In case study 2, crystallization history of a material point during an AFP process was analyzed, using experimentally measured temperature history. Simulation results show how parameters such as tool temperature and torch temperature affect the crystallization history of the part. It is concluded that the developed models can be used as useful tools for designing optimal and efficient process parameters in the AFP process.

6.2 Conclusions

Based on the research performed in this thesis, conclusions are as follows:

- There is no significant difference between isothermal and non-isothermal crystallization mechanisms of AS4/PEEK and a unified model can be used for the prediction of both.

- Crystallization rate is controlled by two competing mechanisms. Crystallization rate is increased by increasing the under-cooling, and is decreased when approaching the glass transition temperature.
- In comparison with crystallization, melting of AS4/PEEK occurs over a wider temperature range. Moreover, unlike crystallization, melting ends approximately at the same temperature for all heating rates.
- Crystals continuously melt and recrystallize during both heating and isothermal (annealing) cases. The crystals after recrystallization are more stable in comparison with the original crystals.
- Stress relaxation experiments show that for AS4/PEEK, neat PEEK, fully cured AS4/8552 and fully cured 8552 resin, the unrelaxed values of the moduli are temperature dependent and the behaviour is thermo-rheologically complex.
- The material behaviour of fully cured 8552 resin, in the glassy regime, is hypo-elastic.
- In process simulation of L-shaped angles, using thermo-viscoelastic models, a significant amount of residual stresses relax out. Therefore, predicted spring-in values, compared to CHILE predictions, are smaller and closer to experimental measurements. Over estimation is due to the fact that the model does not account for incomplete (partial) crystallization.

6.3 Future Work

The following tasks are suggested as the future work for advancement of this study:

- Having the crystallization and melt kinetics model, more case studies will be analyzed for validation. A few examples include:
  - L-shape parts manufactured at other tool temperatures for studying the crystallization history
  - Thick L-shape parts for studying the through-thickness crystallization gradient
  - Parts processed while a cooling cycle is applied to the platens
  - Parts with complex geometry
  - Stress and deformation analysis in processes such as AFP where the material undergoes high heating and cooling rate temperature cycles.
- Thermo-viscoelastic characterization of both neat PEEK and AS4/PEEK with different degrees of crystallinity. The crystallization/melt kinetics model can be used for designing temperature cycles that result in different degrees of crystallinity in a flat panel. DMA sample will be cut from these panels for performing material characterization.
- Further developing the TVE model to include the effect of incomplete crystallinity.
- Studying the relationship between the viscoelastic behaviour of neat resins and their composites.
- Performing constant load experiments for a full range of polymer materials in their glassy regime and investigating the hypo-elastic behaviour.
- Studying the morphology of crystalline structures using other techniques such as polarized optical microscopy.

References

[1] A. C. Loos and G. S. Springer, "Curing of epoxy matrix composites," *J. Composite Mater.*, vol. 17, *(2)*, pp. 135-169, 1983, 1983.

[2] S. C. Mantell and G. S. Springer, "Manufacturing process models for thermoplastic composites," *J. Composite Mater.*, vol. 26, *(16)*, pp. 2348-2377, 1992.

[3] C. Bunn and R. Hill, "Fibres from Synthetic Polymers," *Elsevier, Amsterdam*, pp. 253, 1953.

[4] A. Keller, "A note on single crystals in polymers: evidence for a folded chain configuration," *Phil Mag*, vol. 2, *(21)*, pp. 1171-1175, 1957.

[5] R. Palmer and A. Cobbold, "The texture of melt crystallised polythene as revealed by selective oxidation," *Macromol Chem Physic*, vol. 74, *(1)*, pp. 174-189, 1964.

[6] M. Avrami, "Kinetics of phase change. I General theory," *J. Chem. Phys.*, vol. 7, *(12)*, pp. 1103-1112, 1939.

[7] M. Avrami, "Kinetics of phase change. II Transformation-time relations for random distribution of nuclei," *J. Chem. Phys.*, vol. 8, *(2)*, pp. 212-224, 1940.

[8] M. Avrami, "Kinetics of phase change. III Granulation, phase change, and microstructure," *J. Chem. Phys.*, vol. 9, *(2)*, pp. 177-184, 1941.

[9] U. Evans, "The laws of expanding circles and spheres in relation to the lateral growth of surface films and the grain-size of metals," *Transactions of the Faraday Society*, vol. 41, pp. 365-374, 1945.

[10] J. Go *et al*, "Modelling recovery and recrystallisation during annealing of AA 5754 aluminium alloy," *Mater Sci Tech Ser*, vol. 19, *(10)*, pp. 1361-1368, 2003.

[11] B. Raeisinia *et al*, "A model for predicting the yield stress of AA6111 after multistep heat treatments," *Metall Mater Trans A*, vol. 37, *(4)*, pp. 1183-1190, 2006.

[12] R. M. Patel and J. E. Spruiell, "Crystallization kinetics during polymer processing-Analysis of available approaches for process modeling," *Polym. Eng. Sci.*, vol. 31, *(10)*, pp. 730-738, 1991.

[13] T. Ozawa, "Kinetics of non-isothermal crystallization," *Polymer*, vol. 12, *(3)*, pp. 150-&, 1971.

[14] K. Nakamura *et al*, "Some aspects of nonisothermal crystallization of polymers. I. Relationship between crystallization temperature, crystallinity, and cooling conditions," *J Appl Polym Sci*, vol. 16, *(5)*, pp. 1077-1091, 1972.

[15] N. Billon, P. Barq and J. Haudin, "Modelling of the cooling of semi-crystalline polymers during their processing," *Int Polym Proc*, vol. 6, *(4)*, pp. 348-355, 1991.

[16] M. R. Kamal and E. Chu, "Isothermal and nonisothermal crystallization of polyethylene," *Polym. Eng. Sci.*, vol. 23, *(1)*, pp. 27-31, 1983.

[17] I. W. Dietz, "Sphärolithwachstum in polymeren," *Colloid Polym. Sci.,* vol. 259, *(4),* pp. 413-429, 1981.

[18] M. L. Di Lorenzo and C. Silvestre, "Non-isothermal crystallization of polymers," *Prog. Polym. Sci.,* vol. 24, *(6),* pp. 917-950, 1999.

[19] C. N. Velisaris and J. C. Seferis, "Crystallization kinetics of Polyetheretherketone (PEEK) matrices," *Polym. Eng. Sci.,* vol. 26, *(22),* pp. 1574-1581, 1986.

[20] E. Bessard, O. De Almeida and G. Bernhart, "Unified isothermal and non-isothermal modelling of neat PEEK crystallization," *J Therm Anal Calorim,* vol. 115, *(2),* pp. 1669-1678, 2014.

[21] P. Cebe, "Application of the parallel Avrami model to crystallization of Poly (etheretherketone)," *Polym. Eng. Sci.,* vol. 28, *(18),* pp. 1192-1197, 1988.

[22] J. J. Weeks, "Melting temperature and change of lamellar thickness with time for bulk polyethylene," *J.Res.Natl Bur.Stand.A,* vol. 67, pp. 441-451, 1963.

[23] M. Jaffe and B. Wunderlich, "Melting of polyoxymethylene," *Colloid Polym. Sci.,* vol. 216, *(1),* pp. 203-216, 1967.

[24] P. Cebe and S. Hong, "Crystallization behaviour of poly(ether-ether-ketone)," *Polymer,* vol. 27, *(8),* pp. 1183-1192, 1986.

[25] S. Z. Cheng, M. Cao and B. Wunderlich, "Glass transition and melting behavior of poly (oxy-1, 4-phenyleneoxy-1, 4-phenylenecarbonyl-1, 4-phenylene)(PEEK)," *Macromolecules,* vol. 19, *(7),* pp. 1868-1876, 1986.

[26] D. Blundell and B. Osborn, "The morphology of poly (aryl-ether-ether-ketone)," *Polymer,* vol. 24, *(8),* pp. 953-958, 1983.

[27] D. Blundell, "On the interpretation of multiple melting peaks in poly (ether ether ketone)," *Polymer,* vol. 28, *(13),* pp. 2248-2251, 1987.

[28] Y. Lee and R. S. Porter, "Double-melting behavior of poly(ether ether ketone)," *Macromolecules,* vol. 20, *(6),* pp. 1336-1341, 06/01, 1987.

[29] D. Ivanov, R. Legras and A. Jonas, "The crystallization of poly (aryl-ether-ether-ketone)(PEEK): reorganization processes during gradual reheating of cold-crystallized samples," *Polymer,* vol. 41, *(10),* pp. 3719-3727, 2000.

[30] A. Maffezzoli, J. Kenny and L. Nicolais, "Welding of PEEK/carbon fiber composite laminates." *Sampe J.,* vol. 25, *(1),* pp. 35-40, 1989.

[31] T. B. Jakobsen, R. C. Don and J. W. Gillespie, "Two-Dimensional thermal analysis of resistance welded thermoplastic composites," *Polym. Eng. Sci.,* vol. 29, *(23),* pp. 1722-1729, 1989.

[32] C. Ageorges *et al,* "Characteristics of resistance welding of lap-shear coupons. Part III. Crystallinity," *Compos. Part A-Appl. S.,* vol. 29, *(8),* pp. 921-932, 1998.

[33] C. R. Choe and K. H. Lee, "Nonisothermal crystallization kinetics of Poly (etheretherketone)(PEEK)," *Polym. Eng. Sci.,* vol. 29, *(12),* pp. 801-805, 1989.

[34] C. Nicodeau, "Continuous Welding Modeling of Thermoplastic Matrix Composites." , Arts et Métiers ParisTech, 2005.

[35] S. C. Mantell and G. S. Springer, "Filament winding process models," *Compos. Struct.,* vol. 27, *(1-2),* pp. 141-147, 1994.

[36] H. Sarrazin and G. S. Springer, "Thermochemical and mechanical aspects of composite tape laying," *J. Composite Mater.,* vol. 29, *(14),* pp. 1908-1943, 1995.

[37] F. O. Sonmez and H. T. Hahn, "Modeling of heat transfer and crystallization in thermoplastic composite tape placement process," *J. Thermoplast. Compos. Mater.,* vol. 10, *(3),* pp. 198-240, 1997.

[38] M. C. Tobin, "Theory of phase transition kinetics with growth site impingement. I. Homogeneous nucleation," *J Polym Sci Pol Phys,* vol. 12, *(2),* pp. 399-406, 1974.

[39] M. C. Tobin, "Theory of phase transition kinetics with growth site impingement. II. Heterogeneous nucleation," *J Polym Sci Pol Phys,* vol. 14, *(12),* pp. 2253-2257, 1976.

[40] M. C. Tobin, "Theory of phase transition kinetics with growth site impingement. III. Mixed heterogeneous–homogeneous nucleation and nonintegral exponents of the time," *J Polym Sci Pol Phys,* vol. 15, *(12),* pp. 2269-2270, 1977.

[41] J. J. Tierney and J. Gillespie Jr, "Crystallization kinetics behavior of PEEK based composites exposed to high heating and cooling rates," *Compos. Part A-Appl. S.,* vol. 35, *(5),* pp. 547-558, 2004.

[42] H. T. Hahn and N. J. Pagano, "Curing stresses in composite laminates," *J. Composite Mater.,* vol. 9, pp. 91-106, 1975.

[43] R. H. Nelson and D. S. Cairns, "Prediction of dimensional changes in composite laminates during cure," *Tomorrow's Materials: Today.,* vol. 34, pp. 2397-2410, 1989.

[44] M. Levitsky and B. W. Shaffer, "Thermal stresses in chemically hardening elastic media with application to molding process," *J Appl Mech-T Asme,* vol. 41, *(3),* pp. 647-651, 1974.

[45] B. W. Shaffer and M. Levitsky, "Thermoelastic constitutive equations for chemically hardening materials," *J Appl Mech-T Asme,* vol. 41, *(3),* pp. 652-657, 1974.

[46] M. Levitsky and B. W. Shaffer, "Residual thermal stresses in a solid sphere cast from a thermosetting material," *J Appl Mech-T Asme,* vol. 42, *(3),* pp. 651-655, 1975.

[47] T. A. Bogetti and J. W. Gillespie, "Process-induced stress and deformation in thick-section thermoset composite laminates," *J. Composite Mater.,* vol. 26, *(5),* pp. 626-660, 1992.

[48] J. Lange *et al,* "Residual stress buildup in thermoset films cured above their ultimate glass transition temperature," *Polymer,* vol. 36, *(16),* pp. 3135-3141, 1995.

[49] A. Johnston *et al,* "Process modelling of composite structures employing a virtual autoclave concept," *Sci Eng Compos Mater,* vol. 5, *(3-4),* pp. 235-252, 1996.

[50] A. Johnston, R. Vaziri and A. Poursartip, "A plane strain model for process-induced deformation of laminated composite structures," *J. Composite Mater.,* vol. 35, *(16),* pp. 1435-1469, 2001.

[51] G. Fernlund *et al*, "Finite element based prediction of process-induced deformation of autoclaved composite structures using 2D process analysis and 3D structural analysis," *Compos. Struct.*, vol. 62, *(2)*, pp. 223-234, 2003.

[52] V. Antonucci *et al*, "Cure-induced residual strain build-up in a thermoset resin," *Compos. Part A-Appl. S.*, vol. 37, *(4)*, pp. 592-601, 2006.

[53] Y. Weitsman, "Residual thermal stresses due to cool down of epoxy resin composites," *J Appl Mech-T Asme*, vol. 46, *(3)*, pp. 563-567, 1979.

[54] Y. Weitsman, "Optimal cool down in linear viscoelasticity," *J Appl Mech-T Asme*, vol. 47, *(1)*, pp. 35-39, 1980.

[55] B. D. Harper and Y. Weitsman, "On the effects of environmental conditioning on residual-stresses in composite laminates," *Int J Solids Struct*, vol. 21, *(8)*, pp. 907-926, 1985.

[56] Y. T. Yeow, D. H. Morris and H. F. Brinson, "Time-temperature behavior of a unidirectional graphite/epoxy composite," *ASTM Spec. Tech. Publ., (674)*, pp. 263-281, 1979.

[57] A. S. D. Wang, E. J. McQuillen and A. S. Ahmadi, "Analytical and experimental investigation of time-temperature creep of graphite epoxy composite laminates," *Mechanical Behavior of Materials*, pp. 407-426, 1974.

[58] D. J. Plazek and I. -. Choy, "Physical properties of bisphenol-A-based epoxy resins during and after curing. II. Creep behavior above and below the glass transition temperature," *J. Polym. Sci. Part B*, vol. 27, *(2)*, pp. 307-324, 1989.

[59] D. Adolf and J. E. Martin, "Time-cure superposition during cross-linking," *Macromolecules*, vol. 23, *(15)*, pp. 3700-3704, 1990.

[60] S. R. White and H. T. Hahn, "Process modeling of composite-materials - residual-stress development during cure .1. Model formulation," *J. Composite Mater.*, vol. 26, *(16)*, pp. 2402-2422, 1992.

[61] S. R. White and H. T. Hahn, "Process modeling of composite-materials - residual-stress development during cure .2. Experimental validation," *J. Composite Mater.*, vol. 26, *(16)*, pp. 2423-2453, 1992.

[62] Y. K. Kim and S. R. White, "Viscoelastic analysis of processing-induced residual stresses in thick composite laminates," *Mech Compos Mater St*, vol. 4, *(4)*, pp. 361-387, 1997.

[63] Y. K. Kim and S. R. White, "Cure-dependent viscoelastic residual stress analysis of filament-wound composite cylinders," *Mech Compos Mater St*, vol. 5, *(4)*, pp. 327-354, 1998.

[64] S. R. White and Y. K. Kim, "Process-induced residual stress analysis of AS4/3501-6 composite material," *Mech Compos Mater St*, vol. 5, *(2)*, pp. 153-186, 1998.

[65] Q. Zhu *et al*, "Dimensional accuracy of thermoset composites: Simulation of process-induced residual stresses," *J. Composite Mater.*, vol. 35, *(24)*, pp. 2171-2205, 2001.

[66] J. M. Svanberg and J. A. Holmberg, "Prediction of shape distortions Part I. FE-implementation of a path dependent constitutive model," *Compos. Part A-Appl. S.*, vol. 35, *(6)*, pp. 711-721, 2004.

[67] J. M. Svanberg and J. A. Holmberg, "Prediction of shape distortions. Part II. Experimental validation and analysis of boundary conditions," *Compos. Part A-Appl. S.,* vol. 35, *(6),* pp. 723-734, 2004.

[68] S. Clifford *et al*, "Thermoviscoelastic anisotropic analysis of process induced residual stresses and dimensional stability in real polymer matrix composite components," *Compos. Part A-Appl. S.,* vol. 37, *(4),* pp. 538-545, 2006.

[69] N. Zobeiry, R. Vaziri and A. Poursartip, "Differential implementation of the viscoelastic response of a curing thermoset matrix for composites processing," *J Eng Mater-T Asme,* vol. 128, *(1),* pp. 90-95, 2006.

[70] N. Zobeiry, R. Vaziri and A. Poursartip, "Computationally efficient pseudo-viscoelastic models for evaluation of residual stresses in thermoset polymer composites during cure," *Compos. Part A-Appl. S.,* vol. 41, *(2),* pp. 247-256, 2010.

[71] R. A. Schapery, "On characterization of nonlinear viscoelastic materials," *Polym. Eng. Sci.,* vol. 9, *(4),* pp. 295, 1969.

[72] Y. C. Lou and R. A. Schapery, "Viscoelastic characterization of a nonlinear fiber-reinforced plastic," *J. Composite Mater.,* vol. 5, pp. 208-&, 1971.

[73] D. Touati and G. Cederbaum, "On the prediction of stress relaxation from known creep of nonlinear materials," *J Eng Mater Technol Trans ASME,* vol. 119, *(2),* pp. 121-124, 1997.

[74] D. Touati and G. Cederbaum, "Postbuckling of non-linear viscoelastic imperfect laminated plates - Part II: structural analysis," *Compos. Struct.,* vol. 42, *(1),* pp. 43-51, 1998.

[75] D. Touati and G. Cederbaum, "Postbuckling of non-linear viscoelastic imperfect laminated plates - Part I: material considerations," *Compos. Struct.,* vol. 42, *(1),* pp. 33-41, 1998.

[76] R. M. Haj-Ali and A. H. Muliana, "Numerical finite element formulation of the Schapery non-linear viscoelastic material model," *Int J Numer Methods Eng,* vol. 59, *(1),* pp. 25-45, 2004.

[77] C. Huang *et al*, "Nonlinearly viscoelastic analysis of asphalt mixes subjected to shear loading," *Mechanics of Time-Dependent Materials,* vol. 11, *(2),* pp. 91-110, 2007.

[78] H. Markovitz, "Boltzmann and beginnings of linear viscoelasticity," *T Soc Rheol,* vol. 21, *(3),* pp. 381-398, 1977.

[79] B. D. Harper and Y. Weitsman, "Residual thermal stresses in an unsymmetrical cross-ply graphite/epoxy laminate," *Collection of Technical Papers - AIAA/ASME/ASCE/AHS/ASC Structures, Structural Dynamics and Materials Conference,* pp. 325-332, 1981.

[80] M. Klasztorny and A. P. Wilczynski, "Viscoelastic modelling of fibre-reinforced resin matrix composites," in *First International Conference on High Performance Structures and Composites,* 2002, pp. 231-242.

[81] R. L. Taylor, K. S. Pister and G. L. Goudreau, "Thermomechanical analysis of viscoelastic solids," *Int J Numer Methods Eng,* vol. 2, *(1),* pp. 45-59, 1970.

[82] K. Y. Lin and I. H. Hwang, "Thermo-viscoelastic analysis of composite materials," *J. Composite Mater.,* vol. 23, *(6),* pp. 554-569, 1989.

[83] J. Maxwell, "On the dynamical theory of gases," *Philos T Roy Soc A,* vol. 157, pp. 49, 1867.

[84] O. E. Meyer, "Theorie der elastischen nachwirkung," *Annalen Der Physik*, vol. 227, *(1)*, pp. 108, 1874.

[85] O. C. Zienkiewicz, M. Watson and I. P. King, "A numerical method of viscoelastic stress analysis," *Int. J. Mech. Sci.*, vol. 10, *(10)*, pp. 807, 1968.

[86] Z. P. Bazant, "Matrix differential equation and higher-order numerical methods for problems of non-linear creep, viscoelasticity and elasto-plasticity," *Int J Numer Methods Eng*, vol. 4, *(1)*, pp. 11-15, 1972.

[87] Z. Bazant and S. T. Wu, "Dirichlet series creep function for aging concrete," *J Eng Mech*, vol. 99, pp. 367-387, 1973.

[88] Z. P. Bazant and S. T. Wu, "Rate-type creep law of aging concrete based on Maxwell chain," *Mater. Struct.*, vol. 7, *(37)*, pp. 45-60, 1974.

[89] Z. P. Bazant and A. Asghari, "Computation of kelvin chain retardation spectra of aging concrete," *Cement Concrete Res*, vol. 4, *(5)*, pp. 797-806, 1974.

[90] Z. P. Bazant and S. T. Wu, "Thermoviscoelasticity of aging concrete," *J Eng Mech*, vol. 100, pp. 575-597, 1974.

[91] W. C. Carpenter, "Viscoelastic stress analysis," *Int J Numer Methods Eng*, vol. 4, *(3)*, pp. 357-366, 1972.

[92] B. Jurkiewiez, J. Destrebecq and A. Vergne, "Incremental analysis of time-dependent effects in composite structures," *Comput. Struct.*, vol. 73, *(1-5)*, pp. 425-435, 1999.

[93] B. Jurkiewiez, S. Buzon and J. G. Sieffert, "Incremental viscoelastic analysis of composite beams with partial interaction," *Comput. Struct.*, vol. 83, *(21-22)*, pp. 1780-1791, 2005.

[94] A. Idesman, R. Niekamp and E. Stein, "Continuous and discontinuous Galerkin methods with finite elements in space and time for parallel computing of viscoelastic deformation," *Comput. Methods Appl. Mech. Eng.*, vol. 190, *(8-10)*, pp. 1049-1063, 2000.

[95] A. Idesman, R. Niekamp and E. Stein, "Finite elements in space and time for generalized viscoelastic maxwell model," *Comput. Mech.*, vol. 27, *(1)*, pp. 49-60, 2001.

[96] A. D. Mesquita, H. B. Coda and W. S. Venturini, "Alternative time marching process for BEM and FEM viscoelastic analysis," *Int J Numer Methods Eng*, vol. 51, *(10)*, pp. 1157-1173, 2001.

[97] A. D. Mesquita and H. B. Coda, "An alternative time integration procedure for Boltzmann viscoelasticity: A BEM approach," *Comput. Struct.*, vol. 79, *(16)*, pp. 1487-1496, 2001.

[98] A. D. Mesquita and H. B. Coda, "Boundary integral equation method for general viscoelastic analysis," *Int J Solids Struct*, vol. 39, *(9)*, pp. 2643-2664, 2002.

[99] A. D. Mesquita and H. B. Coda, "Alternative Kelvin viscoelastic procedure for finite elements," *Appl. Math. Model.*, vol. 26, *(4)*, pp. 501-516, 2002.

[100] A. D. Mesquita and H. B. Coda, "A two-dimensional BEM/FEM coupling applied to viscoelastic analysis of composite domains," *Int J Numer Methods Eng*, vol. 57, *(2)*, pp. 251-270, 2003.

[101] A. D. Mesquita and H. B. Coda, "New methodology for the treatment of two dimensional viscoelastic coupling problems," *Comput. Methods Appl. Mech. Eng.*, vol. 192, *(16-18)*, pp. 1911-1927, 2003.

[102] A. D. Mesquita and H. B. Coda, "A simple Kelvin and Boltzmann viscoelastic analysis of three-dimensional solids by the boundary element method," *Eng. Anal. Boundary Elements*, vol. 27, *(9)*, pp. 885-895, 2003.

[103] A. D. Mesquita and H. B. Coda, "A boundary element methodology for viscoelastic analysis: Part I with cells," *Appl. Math. Model.*, vol. 31, *(6)*, pp. 1149-1170, 2007.

[104] A. D. Mesquita and H. B. Coda, "A boundary element methodology for viscoelastic analysis: Part II without cells," *Appl. Math. Model.*, vol. 31, *(6)*, pp. 1171-1185, 2007.

[105] D. Kokan and K. Gramoll, "Development of a viscoelastic filament-winding process model," in *37th Structure, Structural Dynamics and Materials Conference*, 1996, pp. 1524.

[106] Z. Xia and F. Ellyin, "Time-dependent behaviour and viscoelastic constitutive modelling of an epoxy polymer," *Polym Polym Compos*, vol. 6, *(2)*, pp. 75-83, 1998.

[107] H. W. Wiersma, L. J. B. Peeters and R. Akkerman, "Prediction of springforward in continuous-fibre/polymer L-shaped parts," *Compos. Part A-Appl. S.*, vol. 29, *(11)*, pp. 1333-1342, 1998.

[108] Y. Chen, Z. Xia and F. Ellyin, "Evolution of residual stresses induced during curing processing using a viscoelastic micromechanical model," *J. Composite Mater.*, vol. 35, *(6)*, pp. 522-542, 2001.

[109] F. Ellyin and Z. Xia, "Nonlinear viscoelastic constitutive model for thermoset polymers," *J Eng Mater-T Asme*, vol. 128, *(4)*, pp. 579-585, 2006.

[110] W. I. Lee and G. S. Springer, "Model of the manufacturing process of thermoplastic matrix composites," *J. Composite Mater.*, vol. 21, *(11)*, pp. 1017-1055, 1987.

[111] M. F. Talbott, G. S. Springer and L. A. Berglund, "Effects of crystallinity on the mechanical properties of peek polymer and graphite fiber reinforced PEEK," *J. Composite Mater.*, vol. 21, *(11)*, pp. 1056-1081, 1987.

[112] T. J. Chapman *et al*, "Prediction of process induced residual stresses in thermoplastic composites," *J. Composite Mater.*, vol. 24, *(6)*, pp. 616-643, 1990.

[113] A. A. Ogale and R. L. Mccullough, "Influence of microstructure on elastic and viscoelastic properties of Polyether ether ketone," *Composites Sci. Technol.*, vol. 30, *(3)*, pp. 185-201, 1987.

[114] M. C. Li *et al*, "Plane-strain finite element model for process-induced residual stresses in a graphite/PEEK composite," *J. Composite Mater.*, vol. 31, *(3)*, pp. 212-243, 1997.

[115] A. Trende, B. T. Astrom and G. Nilsson, "Modelling of residual stresses in compression moulded glass-mat reinforced thermoplastics," *Compos. Part A-Appl. S.*, vol. 31, *(11)*, pp. 1241-1254, 2000.

[116] P. Sunderland, W. J. Yu and J. A. Manson, "A thermoviscoelastic analysis of process-induced internal stresses in thermoplastic matrix composites," *Polym Composite*, vol. 22, *(5)*, pp. 579-592, 2001.

[117] B. S. Kim *et al*, "Numerical analysis of the dimensional stability of thermoplastic composites using a thermoviscoelastic approach," *J. Composite Mater.*, vol. 36, *(20)*, pp. 2389-2403, 2002.

[118] F. O. Sonmez, H. T. Hahn and M. Akbulut, "Analysis of process-induced residual stresses in tape placement," *J. Thermoplast. Compos. Mater.*, vol. 15, *(6)*, pp. 525-544, 2002.

[119] F. Schwarzl and A. J. Staverman, "Time-temperature dependence of linear viscoelastic behavior," *J. Appl. Phys.*, vol. 23, *(8)*, pp. 838-843, 1952.

[120] L. W. Morland and E. H. Lee, "Stress analysis for linear viscoelastic materials with temperature variation," *T Soc Rheol*, vol. 4, pp. 233-263, 1960.

[121] R. A. Schapery, "Viscoelastic behavior and analysis of composite materials," in *Mechanics of Composite Materials, Vol. 2*, Academic ed., G. P. Sendeckj, Ed. New York: 1974, pp. 85.

[122] N. Zobeiry, "Viscoelastic Constitutive Models for Evaluation of Residual Stresses in Thermoset Composites during Cure." , The University of British Columbia, 2006.

[123] B. D. Harper and Y. Weitsman, "Characterization method for a class of thermorheologically complex materials," *J. Rheol.*, vol. 29, *(1)*, pp. 49-66, 1985.

[124] Z. Hashin, E. A. Humphreys and J. Goering, "Analysis of thermoviscoelastic behavior of unidirectional fiber composites," *Composites Sci. Technol.*, vol. 29, *(2)*, pp. 103-131, 1987.

[125] Y. Sadkin and J. Aboudi, "Viscoelastic behavior of thermorheologically complex resin matrix composites," *Composites Sci. Technol.*, vol. 36, *(4)*, pp. 351-365, 1989.

[126] S. Vyazovkin and C. A. Wight, "Model-free and model-fitting approaches to kinetic analysis of isothermal and nonisothermal data," *Thermochim Acta*, vol. 340–341, pp. 53-68, 12/14, 1999.

[127] "Cetex® TC1200 product data sheet," 2017.

[128] G. Y. Fortin, "Process-Induced Shape Distortions in Aerospace Thermoplastic Composites." , University of British Columbia, 2016.

[129] G. Höhne, W. Hemminger and H. Flammersheim, *Differential Scanning Calorimetry*. Springer Verlag, 2003.

[130] D. A. Cerqueira, G. Rodrigues Filho and R. M. Assunção, "A new value for the heat of fusion of a perfect crystal of cellulose acetate," *Polym Bull*, vol. 56, *(4)*, pp. 475-484, 2006.

[131] A. Maffezzoli, J. M. Kenny and L. Nicolais, "A macrokinetic approach to crystallization modeling of semicrystalline thermoplastic matrices for advanced composites," *J. Mater. Sci.*, vol. 28, *(18)*, pp. 4994-5001, 1993.

[132] J. W. Christian, *The Theory of Transformations in Metals and Alloys, Pt. 1-2*. Great Britain: Pergamon : Elsevier Science Pub, 2002.

[133] Y. K. Godovsky and G. L. Slonimsky, "Kinetics of polymer crystallization from the melt (calorimetric approach)," *J Polym Sci Pol Phys*, vol. 12, *(6)*, pp. 1053-1080, 1974.

[134] D. Dykeman, "Minimizing Uncertainty in Cure Modeling for Composites Manufacturing." , 2008.

[135] "Victrex® PEEK 150P product data sheet," 2014.

[136] "CRIAQ COMP412 Project, Personal Communication, 2013," .

[137] H. F. Brinson and L. C. Brinson, *Polymer Engineering Science and Viscoelasticity: An Introduction.* Springer, 2015.

[138] A. S. Wineman and K. R. Rajagopal, *Mechanical Response of Polymers: An Introduction.* Cambridge University Press, 2000.

[139] M. Baumgaertel and H. H. Winter, "Determination of discrete relaxation and retardation time spectra from dynamic mechanical data," *Rheol Acta,* vol. 28, *(6),* pp. 511-519, 1989.

[140] D. M. Bates and D. G. Watts, "Nonlinear regression: Iterative estimation and linear approximations," in *Nonlinear Regression Analysis and its Applications* Wiley Online Library, 1988, pp. 32-66.

[141] Y. Yi, S. Park and S. Youn, "Asymptotic homogenization of viscoelastic composites with periodic microstructures," *Int J Solids Struct,* vol. 35, *(17),* pp. 2039-2055, 1998.

[142] S. L. Simon, G. B. Mckenna and O. Sindt, "Modeling the evolution of the dynamic mechanical properties of a commercial epoxy during cure after gelation," *J Appl Polym Sci,* vol. 76, *(4),* pp. 495-508, 2000.

[143] G. A. Arzoumanidis and K. M. Liechti, "Linear viscoelastic property measurement and its significance for some nonlinear viscoelasticity models," *Mechanics Time-Dependent Materials,* vol. 7, *(3-4),* pp. 209-250, 2003.

[144] I. Emri and N. W. Tschoegl, "Determination of mechanical spectra from experimental responses," *Int J Solids Struct,* vol. 32, *(6–7),* pp. 817-826, 0, 1995.

[145] N. S. Ottosen and M. Ristinmaa, *The Mechanics of Constitutive Modeling.* Elsevier, 2005.

[146] H. J. Frost and M. F. Ashby, *Deformation Mechanism Maps: The Plasticity and Creep of Metals and Ceramics.* Pergamon press, 1982.

[147] B. J. Goodno and J. M. Gere, *Mechanics of Materials.* Cengage Learning, 2016.

[148] R. A. Schapery, *Further Development of a Thermodynamic Constitutive Theory: Stress Formulation,* Lafayette, Indiana: Purdue Research Foundation, 1969.

[149] S. P. C. Marques and G. J. Creus, *Computational Viscoelasticity.* New York: Springer, 2012.

[150] T. Crochon *et al*, "On finite-element implementation strategies of Schapery-type constitutive theories," *Mechanics of Time-Dependent Materials,* vol. 14, *(4),* pp. 359-387, 2010.

[151] R. A. Schapery, "A theory of non-linear thermoviscoelasticity based on irreversible thermodynamics," in *Proc. 5Th U. S. National Congress of Applied Mechanics, ASME,* 1966, pp. 511-530.

[152] "Standard test method for measuring the curved beam strength of a fiber-reinforced polymer-matrix composite (ASTM D6415)," 2006.

[153] J. Sorvari and J. Hämäläinen, "Time integration in linear viscoelasticity—a comparative study," *Mechanics of Time-Dependent Materials,* vol. 14, *(3),* pp. 307-328, 2010.

Appendices

Appendix A Prony series constants

Prony series constants for all samples are given in this appendix.

A.1 Prony series constants for AS4/PEEK samples

The parameters E_e, E_i's and τ_i's for three AS4/PEEK samples are given in Table A-1, Table A-2 and Table A-3.

Table A-1 Prony series parameters E_e, E_i's and τ_i's for AS4/PEEK-Sample A

$N = 36$		$N = 10$	
E_e(MPa)	98.50	E_e(MPa)	98.50
E_i(MPa)	τ_i(s)	E_i(MPa)	τ_i(s)
142.98	3.16E-02	359.10	3.16E-02
549.74	1.00E+00	1921.20	1.00E+01
297.91	3.16E+00	1209.08	3.16E+03
354.05	1.00E+01	588.21	3.16E+05
441.54	3.16E+01	624.68	3.16E+07
283.57	1.00E+02	608.20	3.16E+09
616.88	3.16E+02	545.60	3.16E+11
475.06	3.16E+03	380.99	3.16E+13
92.26	1.00E+04	273.87	3.16E+15
236.28	3.16E+04	127.22	3.16E+18
71.53	1.00E+05		
273.51	3.16E+05		
23.35	1.00E+06		
306.94	3.16E+06		

$N = 36$		$N = 10$	
E_e(MPa)	98.50	E_e(MPa)	98.50
E_i(MPa)	τ_i(s)	E_i(MPa)	τ_i(s)
19.47	1.00E+07		
256.60	3.16E+07		
102.37	1.00E+08		
155.65	3.16E+08		
144.66	1.00E+09		
185.25	3.16E+09		
113.78	1.00E+10		
170.15	3.16E+10		
153.04	1.00E+11		
101.60	3.16E+11		
170.12	1.00E+12		
84.53	3.16E+12		
139.55	1.00E+13		
48.20	3.16E+13		
141.10	1.00E+14		
36.73	3.16E+14		
76.41	1.00E+15		
79.62	3.16E+15		
21.67	1.00E+16		
76.32	3.16E+16		
64.23	3.16E+17		
58.57	3.16E+18		

Table A-2 Prony series parameters E_e, E_i's and τ_i's for AS4/PEEK-Sample B

$N = 40$		$N = 11$	
E_e(MPa)	120.00	E_e(MPa)	120.00
E_i(MPa)	τ_i(s)	E_i(MPa)	τ_i(s)
317.24	1.00E-04	47.73	1.00E-03
13.24	1.00E-03	489.68	3.16E-01
94.12	3.16E-02	1596.18	3.16E+01
64.43	3.16E-01	966.22	3.16E+03
285.03	1.00E+00	779.28	3.16E+05
483.08	3.16E+00	740.69	3.16E+08
72.77	1.00E+01	525.50	3.16E+10
614.14	3.16E+01	458.01	3.16E+12
187.95	1.00E+02	332.70	3.16E+14
456.76	3.16E+02	186.35	1.00E+17
274.66	1.00E+03	34.23	1.00E+19
161.18	3.16E+03		
359.72	1.00E+04		
105.84	3.16E+04		
164.99	1.00E+05		
213.97	3.16E+05		
310.43	3.16E+06		
239.99	3.16E+07		
84.94	1.00E+08		
183.29	3.16E+08		
109.95	1.00E+09		
160.67	3.16E+09		
146.40	1.00E+10		
127.46	3.16E+10		
159.70	1.00E+11		
107.60	3.16E+11		
127.70	1.00E+12		

$N = 40$		$N = 11$	
E_e(MPa)	120.00	E_e(MPa)	120.00
E_i(MPa)	τ_i(s)	E_i(MPa)	τ_i(s)
106.82	3.16E+12		
140.68	1.00E+13		
25.96	3.16E+13		
174.73	1.00E+14		
18.08	3.16E+14		
78.55	1.00E+15		
70.61	3.16E+15		
60.26	1.00E+16		
54.00	1.00E+17		
44.60	3.16E+17		
6.09	1.00E+18		
36.64	3.16E+18		
7.53	1.00E+19		

Table A-3 Prony series parameters E_e, E_i's and τ_i's for AS4/PEEK-Sample C

$N = 37$		$N = 11$	
E_e(MPa)	91.90	E_e(MPa)	91.90
E_i(MPa)	τ_i(s)	E_i(MPa)	τ_i(s)
124.83	1.00E-05	226.85	1.00E-01
42.44	1.00E-02	1346.49	3.16E+00
118.06	1.00E-01	1332.56	3.16E+02
480.61	1.00E+00	743.23	3.16E+04
574.15	3.16E+00	580.23	3.16E+06
61.08	1.00E+01	588.94	3.16E+08
534.87	3.16E+01	563.61	3.16E+10
250.00	1.00E+02	493.15	3.16E+12

$N = 37$		$N = 11$	
E_e(MPa)	91.90	E_e(MPa)	91.90
E_i(MPa)	τ_i(s)	E_i(MPa)	τ_i(s)
524.10	3.16E+02	350.65	1.00E+15
56.16	1.00E+03	125.08	1.00E+17
425.23	3.16E+03	52.67	3.16E+18
182.93	1.00E+04		
153.17	3.16E+04		
190.87	1.00E+05		
123.98	3.16E+05		
119.78	1.00E+06		
251.97	3.16E+06		
28.47	1.00E+07		
232.26	3.16E+07		
84.34	1.00E+08		
184.30	3.16E+08		
130.08	1.00E+09		
151.49	3.16E+09		
151.44	1.00E+10		
139.76	3.16E+10		
130.39	1.00E+11		
154.10	3.16E+11		
89.15	1.00E+12		
139.19	3.16E+12		
93.89	1.00E+13		
82.79	3.16E+13		
129.29	1.00E+14		
154.71	1.00E+15		
99.18	1.00E+16		
69.49	1.00E+17		
32.67	3.16E+17		

$N = 37$		$N = 11$	
E_e(MPa)	91.90	E_e(MPa)	91.90
E_i(MPa)	τ_i(s)	E_i(MPa)	τ_i(s)
47.93	3.16E+18		

A.2 Prony series constants for neat PEEK samples

The parameters E_e, E_i's and τ_i's for two neat PEEK samples are given in Table A-4 and Table A-5.

Table A-4 Prony series parameters E_e, E_i's and τ_i's for neat PEEK-Sample A

$N = 31$		$N = 10$	
E_e(MPa)	82.20	E_e(MPa)	82.20
E_i(MPa)	τ_i(s)	E_i(MPa)	τ_i(s)
16.66	1.00E-02	5.34	1.00E-02
28.16	1.00E-01	141.91	1.00E+00
30.91	1.00E+00	561.67	1.00E+02
243.63	1.00E+01	405.67	3.16E+03
192.34	1.00E+02	290.43	3.16E+05
276.69	3.16E+02	127.95	3.16E+07
231.35	3.16E+03	101.92	1.00E+10
40.22	1.00E+04	82.15	1.00E+13
97.15	3.16E+04	57.52	3.16E+15
120.67	1.00E+05	25.08	3.16E+17
53.11	3.16E+05		
47.04	1.00E+06		
54.10	3.16E+06		
51.33	1.00E+07		
8.99	3.16E+07		

$N = 31$		$N = 10$	
E_e(MPa)	82.20	E_e(MPa)	82.20
E_i(MPa)	τ_i(s)	E_i(MPa)	τ_i(s)
40.18	1.00E+08		
5.95	3.16E+08		
37.89	1.00E+09		
31.65	1.00E+10		
21.86	3.16E+10		
26.97	3.16E+11		
19.06	1.00E+12		
28.72	1.00E+13		
6.13	3.16E+13		
21.28	1.00E+14		
26.84	1.00E+15		
4.29	3.16E+15		
18.17	1.00E+16		
2.05	3.16E+16		
24.94	1.00E+17		
3.26	3.16E+17		

Table A-5 Prony series parameters E_e, E_i's and τ_i's for neat PEEK-Sample B

$N = 34$		$N = 9$	
E_e(MPa)	73.60	E_e(MPa)	73.60
E_i(MPa)	τ_i(s)	E_i(MPa)	τ_i(s)
48.27	3.16E-02	131.50	3.16E-01
7.24	3.16E-01	837.62	1.00E+03
27.80	3.16E+00	385.49	1.00E+05
172.64	3.16E+01	179.37	3.16E+07
361.60	3.16E+02	69.10	3.16E+09

$N = 34$		$N = 9$	
E_e(MPa)	73.60	E_e(MPa)	73.60
E_i(MPa)	τ_i(s)	E_i(MPa)	τ_i(s)
25.47	1.00E+03	61.84	3.16E+11
248.28	3.16E+03	53.87	3.16E+13
51.33	1.00E+04	51.56	3.16E+15
193.22	3.16E+04	24.58	3.16E+17
37.54	1.00E+05		
144.27	3.16E+05		
101.16	3.16E+06		
20.08	1.00E+07		
39.46	3.16E+07		
30.83	1.00E+08		
7.89	3.16E+08		
27.14	1.00E+09		
20.00	3.16E+09		
21.51	1.00E+10		
10.17	3.16E+10		
21.31	1.00E+11		
13.33	3.16E+11		
12.15	1.00E+12		
20.79	3.16E+12		
5.81	1.00E+13		
21.08	3.16E+13		
6.32	1.00E+14		
20.12	3.16E+14		
7.03	1.00E+15		
12.71	3.16E+15		
17.77	1.00E+16		
1.20	3.16E+16		
23.38	1.00E+17		

$N = 34$		$N = 9$	
E_e(MPa)	73.60	E_e(MPa)	73.60
E_i(MPa)	τ_i(s)	E_i(MPa)	τ_i(s)
3.71	3.16E+17		

A.3 Prony series constants for fully cured AS4/8552 samples

The parameters E_e, E_i's and τ_i's for three AS4/8552 samples are given in Table A-6, Table A-7 and Table A-8.

Table A-6 Prony series parameters E_e, E_i's and τ_i's for AS4/8552-Sample A

$N = 18$		$N = 9$	
E_e(MPa)	**149.00**	E_e(MPa)	**149.00**
E_i(MPa)	τ_i(s)	E_i(MPa)	τ_i(s)
106.86	1.00E+00	280.02	1.00E+01
76.88	1.00E+01	1755.16	3.16E+03
750.55	3.16E+02	1716.83	1.00E+05
392.19	3.16E+03	1208.94	3.16E+06
931.34	1.00E+04	251.93	3.16E+07
1313.50	1.00E+05	149.40	3.16E+08
830.04	1.00E+06	92.12	1.00E+10
184.59	3.16E+06	224.42	1.00E+12
551.07	1.00E+07	134.19	1.00E+14
32.60	3.16E+07		
141.65	1.00E+08		
62.09	3.16E+08		
36.67	1.00E+09		
47.47	1.00E+10		

$N = 18$		$N = 9$	
E_e(MPa)	**149.00**	E_e(MPa)	**149.00**
E_i(MPa)	τ_i(s)	E_i(MPa)	τ_i(s)
78.43	1.00E+11		
119.96	1.00E+12		
113.78	1.00E+13		
78.69	1.00E+14		

Table A-7 Prony series parameters E_e, E_i's and τ_i's for AS4/8552-Sample B

$N = 25$		$N = 10$	
E_e(MPa)	148.00	E_e(MPa)	148.00
E_i(MPa)	τ_i(s)	E_i(MPa)	τ_i(s)
45.28	3.16E-01	345.36	1.00E+01
67.50	1.00E+00	1841.24	3.16E+03
100.43	1.00E+01	1803.13	3.16E+05
150.79	1.00E+02	359.08	3.16E+06
346.38	3.16E+02	538.65	3.16E+07
191.42	1.00E+03	59.99	3.16E+08
504.07	3.16E+03	91.40	3.16E+09
489.94	1.00E+04	72.79	3.16E+10
633.77	3.16E+04	207.96	1.00E+12
431.25	1.00E+05	146.30	1.00E+14
584.29	3.16E+05		
382.55	1.00E+06		
440.35	3.16E+06		
197.43	1.00E+07		
257.77	3.16E+07		
55.82	1.00E+08		
112.76	3.16E+08		

$N = 25$		$N = 10$	
E_e(MPa)	148.00	E_e(MPa)	148.00
E_i(MPa)	τ_i(s)	E_i(MPa)	τ_i(s)
25.83	1.00E+09		
21.38	3.16E+09		
52.64	1.00E+10		
2.94	3.16E+10		
83.26	1.00E+11		
106.41	1.00E+12		
133.01	1.00E+13		
77.58	1.00E+14		

Table A-8 Prony series parameters E_e, E_i's and τ_i's for AS4/8552-Sample C

$N = 25$		$N = 10$	
E_e(MPa)	153.00	E_e(MPa)	153.00
E_i(MPa)	τ_i(s)	E_i(MPa)	τ_i(s)
62.58	1.00E+00	373.30	1.00E+00
89.81	1.00E+01	1490.72	1.00E+03
205.08	1.00E+02	1998.54	1.00E+05
314.96	3.16E+02	563.71	1.00E+06
202.42	1.00E+03	778.66	1.00E+07
555.32	3.16E+03	195.01	1.00E+08
480.29	1.00E+04	163.03	1.00E+09
673.81	3.16E+04	86.21	1.00E+11
466.31	1.00E+05	182.28	1.00E+12
649.67	3.16E+05	162.41	1.00E+14
394.86	1.00E+06		
475.80	3.16E+06		
233.34	1.00E+07		

$N = 25$		$N = 10$	
E_e(MPa)	153.00	E_e(MPa)	153.00
E_i(MPa)	τ_i(s)	E_i(MPa)	τ_i(s)
269.20	3.16E+07		
109.57	1.00E+08		
98.46	3.16E+08		
40.73	1.00E+09		
24.97	3.16E+09		
33.64	1.00E+10		
31.02	3.16E+10		
48.43	1.00E+11		
25.83	3.16E+11		
100.14	1.00E+12		
118.39	1.00E+13		
101.55	1.00E+14		

A.4 Prony series constants for fully cured 8552 neat resin samples

The parameters E_e, E_i's and τ_i's for two 8552 neat resin samples are given in Table A-9 and Table A-10.

Table A-9 Prony series parameters E_e, E_i's and τ_i's for 8552 resin-Sample A

$N = 21$		$N = 11$	
E_e(MPa)	11.60	E_e(MPa)	11.60
E_i(MPa)	τ_i(s)	E_i(MPa)	τ_i(s)
47.14	3.16E-01	93.98	1.00E+01
113.08	1.00E+01	142.23	1.00E+02
51.69	1.00E+02	317.52	1.00E+03
192.33	3.16E+02	597.25	1.00E+04

$N = 21$		$N = 11$	
E_e(MPa)	11.60	E_e(MPa)	11.60
E_i(MPa)	τ_i(s)	E_i(MPa)	τ_i(s)
103.40	1.00E+03	718.93	1.00E+05
209.16	3.16E+03	352.82	1.00E+06
313.33	1.00E+04	134.76	1.00E+07
367.55	3.16E+04	54.10	1.00E+08
375.22	1.00E+05	12.91	3.16E+09
243.36	3.16E+05	15.23	3.16E+11
195.77	1.00E+06	19.08	3.16E+13
109.95	3.16E+06		
50.53	1.00E+07		
66.31	3.16E+07		
5.37	1.00E+08		
24.44	3.16E+08		
5.45	3.16E+09		
5.46	3.16E+10		
7.14	3.16E+11		
10.44	3.16E+12		
13.80	3.16E+13		

Table A-10 Prony series parameters E_e, E_i's and τ_i's for 8552 resin-Sample B

$N = 20$		$N = 11$	
E_e(MPa)	13.40	E_e(MPa)	13.40
E_i(MPa)	τ_i(s)	E_i(MPa)	τ_i(s)
73.64	1.00E+00	64.05	1.00E+00
82.41	1.00E+01	94.48	1.00E+01
57.04	1.00E+02	284.84	3.16E+02
139.89	3.16E+02	438.43	3.16E+03

$N = 20$		$N = 11$	
E_e(MPa)	13.40	E_e(MPa)	13.40
E_i(MPa)	τ_i(s)	E_i(MPa)	τ_i(s)
218.23	1.00E+03	786.29	3.16E+04
174.72	3.16E+03	559.56	3.16E+05
320.53	1.00E+04	182.38	3.16E+06
386.48	3.16E+04	89.78	3.16E+07
431.06	1.00E+05	18.24	3.16E+09
210.90	3.16E+05	12.84	3.16E+11
205.63	1.00E+06	18.09	3.16E+13
84.45	3.16E+06		
51.27	1.00E+07		
57.47	3.16E+07		
23.05	3.16E+08		
2.76	3.16E+09		
6.58	3.16E+10		
6.24	3.16E+11		
8.54	3.16E+12		
13.75	3.16E+13		

Appendix B Three dimensional constitutive relations for thermo-rheologically complex materials

In this appendix, thermo-viscoelastic constitutive equations, developed in section 4.3 are generalized for three dimensional cases. Time integration of equations are carried out for implementation in a UMAT.

B.1 Isotropic case

Recall the constitutive relations for an elastic isotropic material (Hooke's law)

$$\sigma_{11} = \left(K + \frac{4}{3}G\right)\epsilon_{11} + \left(K - \frac{2}{3}G\right)(\epsilon_{22} + \epsilon_{33}) - 3K\alpha\Delta T - 3K\alpha^{cs}\Delta X$$

$$\sigma_{22} = \left(K + \frac{4}{3}G\right)\epsilon_{22} + \left(K - \frac{2}{3}G\right)(\epsilon_{33} + \epsilon_{11}) - 3K\alpha\Delta T - 3K\alpha^{cs}\Delta X$$

$$\sigma_{33} = \left(K + \frac{4}{3}G\right)\epsilon_{33} + \left(K - \frac{2}{3}G\right)(\epsilon_{11} + \epsilon_{22}) - 3K\alpha\Delta T - 3K\alpha^{cs}\Delta X \qquad \textbf{(B-1)}$$

$$\sigma_{23} = G\gamma_{23}$$

$$\sigma_{13} = G\gamma_{13}$$

$$\sigma_{12} = G\gamma_{12}$$

In Equation (B-1), K is the bulk modulus, G is the shear modulus, α is the coefficient of thermal expansion (linear) and α^{cs} is the coefficient of cure/crystallization (linear) shrinkage. Let's rename $3K\alpha$ as β_K and $3K\alpha^{cs}$ as γ_K and rewrite Equation (B-1) as

$$\sigma_{11} = \left(K + \frac{4}{3}G\right)\epsilon_{11} + \left(K - \frac{2}{3}G\right)(\epsilon_{22} + \epsilon_{33}) - \beta_K\Delta T - \gamma_K\Delta X$$

$$\sigma_{22} = \left(K + \frac{4}{3}G\right)\epsilon_{22} + \left(K - \frac{2}{3}G\right)(\epsilon_{33} + \epsilon_{11}) - \beta_K\Delta T - \gamma_K\Delta X \qquad \textbf{(B-2)}$$

$$\sigma_{33} = \left(K + \frac{4}{3}G\right)\epsilon_{33} + \left(K - \frac{2}{3}G\right)(\epsilon_{11} + \epsilon_{22}) - \beta_K \Delta T - \gamma_K \Delta X$$

$$\sigma_{23} = G\gamma_{23}$$

$$\sigma_{13} = G\gamma_{13}$$

$$\sigma_{12} = G\gamma_{12}$$

Considering Equation (B-2), we generalize Equation (4-50) for the three-dimensional isotropic case as

$$\begin{aligned}\sigma_{11} = {} & \left(K_e + \frac{4}{3}G_e\right)\epsilon_{11} + \left(K_e - \frac{2}{3}G_e\right)(\epsilon_{22} + \epsilon_{33}) - \beta_{K_e}\Delta T - \gamma_{K_e}\Delta X \\ & + a_F \int_0^{\xi} \left(\Delta K(\xi - \xi') + \frac{4}{3}\Delta G(\xi - \xi')\right)\frac{d\epsilon_{11}}{d\xi'}d\xi' \\ & + a_F \int_0^{\xi} \left(\Delta K(\xi - \xi') - \frac{2}{3}\Delta G(\xi - \xi')\right)\frac{d(\epsilon_{22} + \epsilon_{33})}{d\xi'}d\xi' \\ & - a_F \int_0^{\xi} \Delta\beta_K(\xi - \xi')\frac{d\left(\frac{\Delta T}{a_F}\right)}{d\xi'}d\xi' \\ & - a_F \int_0^{\xi} \Delta\gamma_K(\xi - \xi')\frac{d\left(\frac{\Delta X}{a_F}\right)}{d\xi'}d\xi'\end{aligned} \qquad \textbf{(B-3)}$$

Similarly

$$\sigma_{22} = \left(K_e + \frac{4}{3}G_e\right)\epsilon_{22} + \left(K_e - \frac{2}{3}G_e\right)(\epsilon_{33} + \epsilon_{11}) - \beta_{K_e}\Delta T - \gamma_{K_e}\Delta X$$

$$+ a_F \int_0^{\xi} \left(\Delta K(\xi - \xi') + \frac{4}{3}\Delta G(\xi - \xi')\right)\frac{d\epsilon_{22}}{d\xi'}d\xi'$$

$$+ a_F \int_0^{\xi} \left(\Delta K(\xi - \xi') - \frac{2}{3}\Delta G(\xi - \xi')\right)\frac{d(\epsilon_{33} + \epsilon_{11})}{d\xi'}d\xi' \qquad \textbf{(B-4)}$$

$$- a_F \int_0^{\xi} \Delta\beta_K(\xi - \xi')\frac{d\left(\frac{\Delta T}{a_F}\right)}{d\xi'}d\xi'$$

$$- a_F \int_0^{\xi} \Delta\gamma_K(\xi - \xi')\frac{d\left(\frac{\Delta X}{a_F}\right)}{d\xi'}d\xi'$$

$$\sigma_{33} = \left(K_e + \frac{4}{3}G_e\right)\epsilon_{33} + \left(K_e - \frac{2}{3}G_e\right)(\epsilon_{11} + \epsilon_{22}) - \beta_{K_e}\Delta T - \gamma_{K_e}\Delta X$$

$$+ a_F \int_0^{\xi} \left(\Delta K(\xi - \xi') + \frac{4}{3}\Delta G(\xi - \xi')\right)\frac{d\epsilon_{33}}{d\xi'}d\xi'$$

$$+ a_F \int_0^{\xi} \left(\Delta K(\xi - \xi') - \frac{2}{3}\Delta G(\xi - \xi')\right)\frac{d(\epsilon_{11} + \epsilon_{22})}{d\xi'}d\xi' \qquad \textbf{(B-5)}$$

$$- a_F \int_0^{\xi} \Delta\beta_K(\xi - \xi')\frac{d\left(\frac{\Delta T}{a_F}\right)}{d\xi'}d\xi'$$

$$- a_F \int_0^{\xi} \Delta\gamma_K(\xi - \xi')\frac{d\left(\frac{\Delta X}{a_F}\right)}{d\xi'}d\xi'$$

$$\sigma_{23} = G_e\gamma_{23} + a_F \int_0^{\xi} \Delta G(\xi - \xi')\frac{d\gamma_{23}}{d\xi'}d\xi' \qquad \textbf{(B-6)}$$

$$\sigma_{13} = G_e\gamma_{13} + a_F \int_0^{\xi} \Delta G(\xi - \xi') \frac{d\gamma_{13}}{d\xi'} d\xi' \qquad \textbf{(B-7)}$$

$$\sigma_{12} = G_e\gamma_{12} + a_F \int_0^{\xi} \Delta G(\xi - \xi') \frac{d\gamma_{12}}{d\xi'} d\xi' \qquad \textbf{(B-8)}$$

Next we approximate $K(\xi)$, $G(\xi)$, $\beta_K(\xi)$ and $\gamma_K(\xi)$ by Prony series as

$$\begin{aligned} K(\xi) &= K_e + \sum_{i=1}^{N_K} K_i e^{-\frac{\xi}{\tau_{Ki}}}, \\ G(\xi) &= G_e + \sum_{j=1}^{N_G} K_j e^{-\frac{\xi}{\tau_{Gj}}}, \\ \beta_K(\xi) &= \beta_{K_e} + \sum_{i=1}^{N_K} \beta_{K_i} e^{-\frac{\xi}{\tau_{Ki}}} \\ \gamma_K(\xi) &= \gamma_{K_e} + \sum_{i=1}^{N_K} \gamma_{K_i} e^{-\frac{\xi}{\tau_{Ki}}} \end{aligned} \qquad \textbf{(B-9)}$$

Substituting from Equation (B-9) into Equations (B-3) to (B-8) yields

$$\sigma_{11} = K_e(\epsilon_{11} + \epsilon_{22} + \epsilon_{33}) - \beta_{K_e}\Delta T + \frac{2}{3}G_e(2\epsilon_{11} - \epsilon_{22} - \epsilon_{33})$$

$$+ \sum_{i=1}^{N_K}\left(a_F \int_0^{\xi}\left(K_i e^{-\frac{\xi-\xi'}{\tau_{Ki}}} \frac{d(\epsilon_{11} + \epsilon_{22} + \epsilon_{33})}{d\xi'} \right.\right.$$

$$\left.\left. - \beta_{K_i} e^{-\frac{\xi-\xi'}{\tau_{Ki}}} \frac{d\left(\frac{\Delta T}{a_F}\right)}{d\xi'} - \gamma_{K_i} e^{-\frac{\xi-\xi'}{\tau_{Ki}}} \frac{d\left(\frac{\Delta X}{a_F}\right)}{d\xi'} \right) d\xi' \right) \qquad \textbf{(B-10)}$$

$$+ \frac{2}{3}\sum_{j=1}^{N_G}\left(a_F \int_0^{\xi}\left(G_j e^{-\frac{\xi-\xi'}{\tau_{Gj}}} \frac{d(2\epsilon_{11} - \epsilon_{22} - \epsilon_{33})}{d\xi'} \right) d\xi' \right)$$

$$\sigma_{22} = K_e(\epsilon_{11} + \epsilon_{22} + \epsilon_{33}) - \beta_{K_e}\Delta T + \frac{2}{3}G_e(2\epsilon_{22} - \epsilon_{33} - \epsilon_{11})$$

$$+ \sum_{i=1}^{N_K}\left(a_F \int_0^{\xi}\left(K_i e^{-\frac{\xi-\xi'}{\tau_{Ki}}} \frac{d(\epsilon_{11} + \epsilon_{22} + \epsilon_{33})}{d\xi'} \right.\right.$$

$$\left.\left. - \beta_{K_i} e^{-\frac{\xi-\xi'}{\tau_{Ki}}} \frac{d\left(\frac{\Delta T}{a_F}\right)}{d\xi'} - \gamma_{K_i} e^{-\frac{\xi-\xi'}{\tau_{Ki}}} \frac{d\left(\frac{\Delta X}{a_F}\right)}{d\xi'} \right) d\xi' \right) \qquad \textbf{(B-11)}$$

$$+ \frac{2}{3}\sum_{j=1}^{N_G}\left(a_F \int_0^{\xi}\left(G_j e^{-\frac{\xi-\xi'}{\tau_{Gj}}} \frac{d(2\epsilon_{22} - \epsilon_{33} - \epsilon_{11})}{d\xi'} \right) d\xi' \right)$$

$$\sigma_{33} = K_e(\epsilon_{11} + \epsilon_{22} + \epsilon_{33}) - \beta_{K_e}\Delta T + \frac{2}{3}G_e(2\epsilon_{33} - \epsilon_{11} - \epsilon_{22})$$

$$+ \sum_{i=1}^{N_K}\left(a_F \int_0^{\xi}\left(K_i e^{-\frac{\xi-\xi'}{\tau_{Ki}}} \frac{d(\epsilon_{11} + \epsilon_{22} + \epsilon_{33})}{d\xi'} \right.\right.$$

$$\left.\left. - \beta_{K_i} e^{-\frac{\xi-\xi'}{\tau_{Ki}}} \frac{d\left(\frac{\Delta T}{a_F}\right)}{d\xi'} - \gamma_{K_i} e^{-\frac{\xi-\xi'}{\tau_{Ki}}} \frac{d\left(\frac{\Delta X}{a_F}\right)}{d\xi'} \right) d\xi' \right) \quad \textbf{(B-12)}$$

$$+ \frac{2}{3}\sum_{j=1}^{N_G}\left(a_F \int_0^{\xi}\left(G_j e^{-\frac{\xi-\xi'}{\tau_{Gj}}} \frac{d(2\epsilon_{33} - \epsilon_{11} - \epsilon_{22})}{d\xi'} \right) d\xi' \right)$$

$$\sigma_{23} = G_e\gamma_{23} + \sum_{j=1}^{N_G}\left(a_F \int_0^{\xi}\left(G_j e^{-\frac{\xi-\xi'}{\tau_{Gj}}} \frac{d\gamma_{23}}{d\xi'} \right) d\xi' \right) \quad \textbf{(B-13)}$$

$$\sigma_{13} = G_e\gamma_{13} + \sum_{j=1}^{N_G}\left(a_F \int_0^{\xi}\left(G_j e^{-\frac{\xi-\xi'}{\tau_{Gj}}} \frac{d\gamma_{13}}{d\xi'} \right) d\xi' \right) \quad \textbf{(B-14)}$$

$$\sigma_{12} = G_e\gamma_{12} + \sum_{j=1}^{N_G}\left(a_F \int_0^{\xi}\left(G_j e^{-\frac{\xi-\xi'}{\tau_{Gj}}} \frac{d\gamma_{12}}{d\xi'} \right) d\xi' \right) \quad \textbf{(B-15)}$$

Now we define the following state variables

$$q_{Ki}(\xi) = a_F \int_0^{\xi}\left(K_i e^{-\frac{\xi-\xi'}{\tau_{Ki}}} \frac{d(\epsilon_{11} + \epsilon_{22} + \epsilon_{33})}{d\xi'} - \beta_{K_i} e^{-\frac{\xi-\xi'}{\tau_{Ki}}} \frac{d\left(\frac{\Delta T}{a_F}\right)}{d\xi'} \right.$$

$$\left. - \gamma_{K_i} e^{-\frac{\xi-\xi'}{\tau_{Ki}}} \frac{d\left(\frac{\Delta X}{a_F}\right)}{d\xi'} \right) d\xi' , \qquad i = 1,2 \dots, N_K \quad \textbf{(B-16)}$$

$$q_{Gj}^{11}(\xi) = \frac{2}{3} a_F \int_0^{\xi} \left(G_j e^{-\frac{\xi-\xi'}{\tau_{Gj}}} \frac{d(2\epsilon_{11} - \epsilon_{22} - \epsilon_{33})}{d\xi'} \right) d\xi' , \qquad j = 1,2 \dots, N_G \quad \textbf{(B-17)}$$

$$q_{Gj}^{22}(\xi) = \frac{2}{3} a_F \int_0^{\xi} \left(G_j e^{-\frac{\xi-\xi'}{\tau_{Gj}}} \frac{d(2\epsilon_{22} - \epsilon_{33} - \epsilon_{11})}{d\xi'} \right) d\xi' , \qquad j = 1,2 \dots, N_G \quad \textbf{(B-18)}$$

$$q_{Gj}^{23}(\xi) = a_F \int_0^{\xi} \left(G_j e^{-\frac{\xi-\xi'}{\tau_{Gj}}} \frac{d\gamma_{23}}{d\xi'} \right) d\xi' , \qquad j = 1,2 \dots, N_G \quad \textbf{(B-19)}$$

$$q_{Gj}^{13}(\xi) = a_F \int_0^{\xi} \left(G_j e^{-\frac{\xi-\xi'}{\tau_{Gj}}} \frac{d\gamma_{13}}{d\xi'} \right) d\xi' , \qquad j = 1,2 \dots, N_G \quad \textbf{(B-20)}$$

$$q_{Gj}^{12}(\xi) = a_F \int_0^{\xi} \left(G_j e^{-\frac{\xi-\xi'}{\tau_{Gj}}} \frac{d\gamma_{12}}{d\xi'} \right) d\xi' , \qquad j = 1,2 \dots, N_G \quad \textbf{(B-21)}$$

Using Leibniz rule of differentiation, we take the derivative of each of the state variables in Equations (B-16) to (B-21) and obtain

$$\frac{dq_{Ki}(\xi)}{d\xi} + \frac{q_{Ki}(\xi)}{\tau_{Ki}} = a_F K_i \left(\frac{d\epsilon_{11}}{d\xi} + \frac{d\epsilon_{22}}{d\xi} + \frac{d\epsilon_{33}}{d\xi} \right) - \beta_{K_i} \frac{d\Delta T}{d\xi} - \gamma_{K_i} \frac{d\Delta X}{d\xi}, \qquad \textbf{(B-22)}$$

$$i = 1,2 \dots, N_K$$

$$\frac{dq_{Gj}^{11}(\xi)}{d\xi} + \frac{q_{Gj}^{11}(\xi)}{\tau_{Gj}} = \frac{2}{3} a_F G_j \left(2\frac{d\epsilon_{11}}{d\xi} - \frac{d\epsilon_{22}}{d\xi} - \frac{d\epsilon_{33}}{d\xi} \right), \qquad i = 1,2 \dots, N_G \quad \textbf{(B-23)}$$

$$\frac{dq_{Gj}^{22}(\xi)}{d\xi} + \frac{q_{Gj}^{22}(\xi)}{\tau_{Gj}} = \frac{2}{3} a_F G_j \left(2\frac{d\epsilon_{22}}{d\xi} - \frac{d\epsilon_{33}}{d\xi} - \frac{d\epsilon_{11}}{d\xi} \right), \qquad i = 1,2 \dots, N_G \quad \textbf{(B-24)}$$

$$\frac{dq_{Gj}^{23}(\xi)}{d\xi} + \frac{q_{Gj}^{23}(\xi)}{\tau_{Gj}} = a_F G_j \frac{d\gamma_{23}}{d\xi}, \qquad i = 1,2 \dots, N_G \quad \textbf{(B-25)}$$

$$\frac{dq_{Gj}^{13}(\xi)}{d\xi} + \frac{q_{Gj}^{13}(\xi)}{\tau_{Gj}} = a_F G_j \frac{d\gamma_{13}}{d\xi}, \qquad i = 1,2 \dots, N_G \quad \textbf{(B-26)}$$

$$\frac{dq_{Gj}^{12}(\xi)}{d\xi} + \frac{q_{Gj}^{12}(\xi)}{\tau_{Gj}} = a_F G_j \frac{d\gamma_{12}}{d\xi}, \qquad i = 1,2 \dots, N_G \quad \textbf{(B-27)}$$

Also substituting from Equations (B-16) to (B-21) into Equations (B-10) to (B-15) we conclude

$$\sigma_{11} = K_e(\epsilon_{11} + \epsilon_{22} + \epsilon_{33}) - \beta_{K_e}\Delta T - \gamma_{K_e}\Delta X + \frac{2}{3}G_e(2\epsilon_{11} - \epsilon_{22} - \epsilon_{33}) + \sum_{i=1}^{N_K} q_{Ki} + \sum_{j=1}^{N_G} q_{Gj}^{11} \quad \textbf{(B-28)}$$

$$\sigma_{22} = K_e(\epsilon_{11} + \epsilon_{22} + \epsilon_{33}) - \beta_{K_e}\Delta T - \gamma_{K_e}\Delta X + \frac{2}{3}G_e(2\epsilon_{22} - \epsilon_{33} - \epsilon_{11}) + \sum_{i=1}^{N_K} q_{Ki} + \sum_{j=1}^{N_G} q_{Gj}^{22} \quad \textbf{(B-29)}$$

$$\sigma_{33} = K_e(\epsilon_{11} + \epsilon_{22} + \epsilon_{33}) - \beta_{K_e}\Delta T - \gamma_{K_e}\Delta X + \frac{2}{3}G_e(2\epsilon_{33} - \epsilon_{11} - \epsilon_{22}) + \sum_{i=1}^{N_K} q_{Ki} - \sum_{j=1}^{N_G}\left(q_{Gj}^{11} + q_{Gj}^{22}\right) \quad \textbf{(B-30)}$$

$$\sigma_{23} = G_e\gamma_{23} + \sum_{j=1}^{N_G} q_{Gj}^{23} \quad \textbf{(B-31)}$$

$$\sigma_{13} = G_e\gamma_{13} + \sum_{j=1}^{N_G} q_{Gj}^{13} \quad \textbf{(B-32)}$$

$$\sigma_{12} = G_e\gamma_{12} + \sum_{j=1}^{N_G} q_{Gj}^{12} \quad \textbf{(B-33)}$$

Finally, based on our discussions about hypo-elastic behaviour of the material in the glassy regime, Equations (B-28) to (B-33) are modified as

$$\dot{\sigma}_{11} = K_e(\dot{\epsilon}_{11} + \dot{\epsilon}_{22} + \dot{\epsilon}_{33}) - \beta_{K_e}\dot{\Delta T} - \gamma_{K_e}\dot{\Delta X} + \frac{2}{3}G_e(2\dot{\epsilon}_{11} - \dot{\epsilon}_{22} - \dot{\epsilon}_{33}) + \sum_{i=1}^{N_K}\dot{q}_{Ki} + \sum_{j=1}^{N_G}\dot{q}_{Gj}^{11} \quad \textbf{(B-34)}$$

$$\dot{\sigma}_{22} = K_e(\dot{\epsilon}_{11} + \dot{\epsilon}_{22} + \dot{\epsilon}_{33}) - \beta_{K_e}\dot{\Delta T} - \gamma_{K_e}\dot{\Delta X} + \frac{2}{3}G_e(2\dot{\epsilon}_{22} - \dot{\epsilon}_{33} - \dot{\epsilon}_{11}) + \sum_{i=1}^{N_K}\dot{q}_{Ki} + \sum_{j=1}^{N_G}\dot{q}_{Gj}^{22} \quad \textbf{(B-35)}$$

$$\dot{\sigma}_{33} = K_e(\dot{\epsilon}_{11} + \dot{\epsilon}_{22} + \dot{\epsilon}_{33}) - \beta_{K_e}\dot{\Delta T} - \gamma_{K_e}\dot{\Delta X} + \frac{2}{3}G_e(2\dot{\epsilon}_{33} - \dot{\epsilon}_{11} - \dot{\epsilon}_{22}) + \sum_{i=1}^{N_K}\dot{q}_{Ki} - \sum_{j=1}^{N_G}\left(\dot{q}_{Gj}^{11} + \dot{q}_{Gj}^{22}\right) \quad \textbf{(B-36)}$$

$$\dot{\sigma}_{23} = G_e\dot{\gamma}_{23} + \sum_{j=1}^{N_G}\dot{q}_{Gj}^{23} \quad \textbf{(B-37)}$$

$$\dot{\sigma}_{13} = G_e\dot{\gamma}_{13} + \sum_{j=1}^{N_G}\dot{q}_{Gj}^{13} \quad \textbf{(B-38)}$$

$$\dot{\sigma}_{12} = G_e\dot{\gamma}_{12} + \sum_{j=1}^{N_G}\dot{q}_{Gj}^{12} \quad \textbf{(B-39)}$$

Next step is solving (time integrating) Equations (B-22) to (B-27) and Equations (B-34) to (B-39) in order to prepare them for implementation in UMAT.

We start with one of the state variables, say q_{Gj}^{23}. We may use a numerical time integration scheme such as Euler forward, Euler backward, Crank-Nicolson, etc. and discretize Equation (B-25) and find the value of the state variable at each time step in terms of the values in previous time steps. Alternatively, we can assume some simplified variations of strain during a time step and create semi-analytical solutions [81], [153].

Let's use the following convention for any general variable P

$$\begin{aligned} P(t = t^{n-1}) &= P^{n-1} \\ P(t = t^{n}) &= P^{n} \\ \Delta P^n &= P^n - P^{n-1} \\ \Delta \xi^n &= \xi^n - \xi^{n-1} \\ \Delta t^n &= t^n - t^{n-1} \end{aligned} \qquad \textbf{(B-40)}$$

Multiplying both sides of Equation (B-25) by the integrating factor $e^{\frac{\xi}{\tau_{Gj}}}$ yields

$$e^{\frac{\xi}{\tau_{Gj}}}\left(\frac{dq_{Gj}^{23}(\xi)}{d\xi} + \frac{q_{Gj}^{23}(\xi)}{\tau_{Gj}}\right) = \frac{d\left(e^{\frac{\xi}{\tau_{Gj}}} q_{Gj}^{23}(\xi)\right)}{d\xi} = a_F G_j e^{\frac{\xi}{\tau_{Gj}}} \frac{d\gamma_{23}}{d\xi}, \quad i = 1,2 \dots, N_G \qquad \textbf{(B-41)}$$

Now we integrate from ξ^{n-1} to ξ^n

$$\int_{\xi^{n-1}}^{\xi^n} \frac{d\left(e^{\frac{\xi'}{\tau_{Gj}}} q_{Gj}^{23}(\xi')\right)}{d\xi'} d\xi' = \int_{\xi^{n-1}}^{\xi^n} a_F G_j e^{\frac{\xi'}{\tau_{Gj}}} \frac{d\gamma_{23}}{d\xi'} d\xi', \qquad j = 1,2 \dots, N_G \qquad \textbf{(B-42)}$$

That is

$$e^{\frac{\xi^{n-1}+\Delta\xi^n}{\tau_{Gj}}} q_{Gj}^{23}(\xi^n) - e^{\frac{\xi^{n-1}}{\tau_{Gj}}} q_{Gj}^{23}(\xi^{n-1}) = \int_{\xi^{n-1}}^{\xi^n} a_F G_j e^{\frac{\xi'}{\tau_{Gj}}} \frac{d\gamma_{23}}{d\xi'} d\xi' , \qquad \textbf{(B-43)}$$

$$j = 1,2 \dots, N_G$$

Now we assume γ_{23} varies linearly with ξ in the interval $[\xi^{n-1}, \xi^n]$, i.e., $\frac{d\gamma_{23}}{d\xi}$ is constant and we replace it with $\frac{\Delta\gamma_{23}{}^n}{\Delta\xi^n}$. Therefore Equation (B-43) reduces to

$$q_{Gj}^{23}(\xi^n) = e^{-\frac{\Delta\xi^n}{\tau_{Gj}}} q_{Gj}^{23}(\xi^{n-1}) + a_F G_j \Delta\gamma_{23}{}^n \left(\frac{1 - e^{-\frac{\Delta\xi^n}{\tau_{Gj}}}}{\frac{\Delta\xi^n}{\tau_{Gj}}} \right), \qquad j = 1,2 \dots, N_G \quad \textbf{(B-44)}$$

Following the same procedure for all other state variables in Equations (B-16) to (B-21) results in

$$\begin{aligned} q_{Ki}(\xi^n) = {} & e^{-\frac{\Delta\xi^n}{\tau_{Ki}}} q_{Ki}(\xi^{n-1}) \\ & + \left(a_F K_i (\Delta\epsilon_{11}{}^n + \Delta\epsilon_{22}{}^n + \Delta\epsilon_{33}{}^n) - \beta_{K_i} \Delta T^n \right. \\ & \left. - \gamma_{K_i} \Delta X^n \right) \left(\frac{1 - e^{-\frac{\Delta\xi^n}{\tau_{Ki}}}}{\frac{\Delta\xi^n}{\tau_{Ki}}} \right), \qquad i = 1,2 \dots, N_K \end{aligned} \qquad \textbf{(B-45)}$$

$$q_{Gj}^{11}(\xi^n) = e^{-\frac{\Delta\xi^n}{\tau_{Gj}}} q_{Gj}^{11}(\xi^{n-1}) + \frac{2}{3} a_F G_j (2\Delta\epsilon_{11}{}^n - \Delta\epsilon_{22}{}^n - \Delta\epsilon_{33}{}^n) \left(\frac{1 - e^{-\frac{\Delta\xi^n}{\tau_{Gj}}}}{\frac{\Delta\xi^n}{\tau_{Gj}}} \right), \quad j = 1,2 \ldots, N_G \qquad \textbf{(B-46)}$$

$$q_{Gj}^{22}(\xi^n) = e^{-\frac{\Delta\xi^n}{\tau_{Gj}}} q_{Gj}^{22}(\xi^{n-1}) + \frac{2}{3} a_F G_j (2\Delta\epsilon_{22}{}^n - \Delta\epsilon_{33}{}^n - \Delta\epsilon_{11}{}^n) \left(\frac{1 - e^{-\frac{\Delta\xi^n}{\tau_{Gj}}}}{\frac{\Delta\xi^n}{\tau_{Gj}}} \right), \quad j = 1,2 \ldots, N_G \qquad \textbf{(B-47)}$$

$$q_{Gj}^{13}(\xi^n) = e^{-\frac{\Delta\xi^n}{\tau_{Gj}}} q_{Gj}^{13}(\xi^{n-1}) + a_F G_j \Delta\gamma_{13}{}^n \left(\frac{1 - e^{-\frac{\Delta\xi^n}{\tau_{Gj}}}}{\frac{\Delta\xi^n}{\tau_{Gj}}} \right), \qquad j = 1,2 \ldots, N_G \qquad \textbf{(B-48)}$$

$$q_{Gj}^{12}(\xi^n) = e^{-\frac{\Delta\xi^n}{\tau_{Gj}}} q_{Gj}^{12}(\xi^{n-1}) + a_F G_j \Delta\gamma_{12}{}^n \left(\frac{1 - e^{-\frac{\Delta\xi^n}{\tau_{Gj}}}}{\frac{\Delta\xi^n}{\tau_{Gj}}} \right), \qquad j = 1,2 \ldots, N_G \qquad \textbf{(B-49)}$$

In Equations (B-44) to (B-49) we replace τ_{Gj} and τ_{Ki} by $a_T\tau_{Ki}$ and $a_T\tau_{Gj}$ (a_T is the horizontal shift factor) and rewrite the equations for real time as

$$q_{Ki}(t^n) = e^{-\frac{\Delta t^n}{a_T \tau_{Ki}}} q_{Ki}(t^{n-1})$$

$$+ \left(a_F K_i ({\Delta\epsilon_{11}}^n + {\Delta\epsilon_{22}}^n + {\Delta\epsilon_{33}}^n) - \beta_{K_i} \Delta T^n \right.$$

$$\left. - \gamma_{K_i} \Delta X^n \right) \left(\frac{1 - e^{-\frac{\Delta t^n}{a_T \tau_{Ki}}}}{\frac{\Delta t^n}{a_T \tau_{Ki}}} \right), \qquad i = 1,2 \dots, N_K \quad \textbf{(B-50)}$$

$$q_{Gj}^{11}(t^n) = e^{-\frac{\Delta t^n}{a_T \tau_{Gj}}} q_{Gj}^{11}(t^{n-1})$$

$$+ \frac{2}{3} a_F G_j (2{\Delta\epsilon_{11}}^n - {\Delta\epsilon_{22}}^n - {\Delta\epsilon_{33}}^n) \left(\frac{1 - e^{-\frac{\Delta t^n}{a_T \tau_{Gj}}}}{\frac{\Delta t^n}{a_T \tau_{Gj}}} \right), \quad \textbf{(B-51)}$$

$$j = 1,2 \dots, N_G$$

$$q_{Gj}^{22}(t^n) = e^{-\frac{\Delta t^n}{a_T \tau_{Gj}}} q_{Gj}^{22}(t^{n-1})$$

$$+ \frac{2}{3} a_F G_j (2{\Delta\epsilon_{22}}^n - {\Delta\epsilon_{33}}^n - {\Delta\epsilon_{11}}^n) \left(\frac{1 - e^{-\frac{\Delta t^n}{a_T \tau_{Gj}}}}{\frac{\Delta t^n}{a_T \tau_{Gj}}} \right), \quad \textbf{(B-52)}$$

$$j = 1,2 \dots, N_G$$

$$q_{Gj}^{23}(t^n) = e^{-\frac{\Delta t^n}{a_T \tau_{Gi}}} q_{Gj}^{23}(t^{n-1}) + a_F G_j {\Delta\gamma_{23}}^n \left(\frac{1 - e^{-\frac{\Delta t^n}{a_T \tau_{Gi}}}}{\frac{\Delta t^n}{a_T \tau_{Gi}}} \right), \qquad j = 1,2 \dots, N_G \quad \textbf{(B-53)}$$

$$q_{Gj}^{13}(t^n) = e^{-\frac{\Delta t^n}{a_T \tau_{Gj}}} q_{Gj}^{13}(t^{n-1}) + a_F G_j {\Delta\gamma_{13}}^n \left(\frac{1 - e^{-\frac{\Delta t^n}{a_T \tau_{Gj}}}}{\frac{\Delta t^n}{a_T \tau_{Gj}}} \right), \qquad j = 1,2 \dots, N_G \quad \textbf{(B-54)}$$

$$q_{Gj}^{12}(t^n) = e^{-\frac{\Delta t^n}{a_T \tau_{Gj}}} q_{Gj}^{12}(t^{n-1}) + a_F G_j {\Delta\gamma_{12}}^n \left(\frac{1 - e^{-\frac{\Delta t^n}{a_T \tau_{Gj}}}}{\frac{\Delta t^n}{a_T \tau_{Gj}}} \right), \qquad j = 1,2 \dots, N_G \quad \textbf{(B-55)}$$

Using Equations (B-50) to (B-65), we can calculate the value of each state variable at each time step in terms of its value at the previous time step and other parameters.

Now we use Equations (B-34) to (B-39) for evaluation of stresses. Let's start with Equation (B-34) and integrate both sides from t^{n-1} to t^n

$$\int_{t^{n-1}}^{t^n} \frac{d\sigma_{11}}{dt'}\,dt' = \int_{t^{n-1}}^{t^n} \left[K_e \left(\frac{d\epsilon_{11}}{dt'} + \frac{d\epsilon_{22}}{dt'} + \frac{d\epsilon_{33}}{dt'} \right) - \beta_{K_e} \frac{d\Delta T}{dt'} - \gamma_{K_e} \frac{d\Delta X}{dt'} + \frac{2}{3} G_e \left(2\frac{d\epsilon_{11}}{dt'} - \frac{d\epsilon_{22}}{dt'} - \frac{d\epsilon_{33}}{dt'} \right) + \sum_{i=1}^{N_K} \frac{dq_{Ki}}{dt'} + \sum_{j=1}^{N_G} \frac{dq_{Gj}^{11}}{dt'} \right] dt' \quad \textbf{(B-56)}$$

Now we assume $\frac{d\epsilon_{11}}{dt}, \frac{d\epsilon_{22}}{dt}, \frac{d\epsilon_{33}}{dt}, \frac{d\Delta T}{dt}$ and $\frac{d\Delta X}{dt}$ are constant in the interval $[t^{n-1}, t^n]$ and replace them with $\frac{\Delta\epsilon_{11}{}^n}{\Delta t^n}, \frac{\Delta\epsilon_{22}{}^n}{\Delta t^n}, \frac{\Delta\epsilon_{33}{}^n}{\Delta t^n}, \frac{\Delta T^n}{\Delta t^n}$ and $\frac{\Delta X^n}{\Delta t^n}$, respectively. Therefore we rewrite Equation (B-56) as

$$\sigma_{11}{}^n - \sigma_{11}{}^{n-1} = \left(\frac{\Delta\epsilon_{11}{}^n}{\Delta t^n} + \frac{\Delta\epsilon_{22}{}^n}{\Delta t^n} + \frac{\Delta\epsilon_{33}{}^n}{\Delta t^n} \right) \int_{t^{n-1}}^{t^n} K_e\,dt' - \frac{\Delta T^n}{\Delta t^n} \int_{t^{n-1}}^{t^n} \beta_{K_e}\,dt' - \frac{\Delta X^n}{\Delta t^n} \int_{t^{n-1}}^{t^n} \gamma_{K_e}\,dt' + \frac{2}{3} \left(2\frac{\Delta\epsilon_{11}{}^n}{\Delta t^n} - \frac{\Delta\epsilon_{22}{}^n}{\Delta t^n} - \frac{\Delta\epsilon_{33}{}^n}{\Delta t^n} \right) \int_{t^{n-1}}^{t^n} G_e\,dt' + \sum_{i=1}^{N_K} (q_{Ki}{}^n - q_{Ki}{}^{n-1}) + \sum_{j=1}^{N_G} \left(q_{Gj}^{11\,n} - q_{Gj}^{11\,n-1} \right) \quad \textbf{(B-57)}$$

Approximating the integrals in Equation (B-57) using Simpson's rule we will have

$$
\begin{aligned}
{\sigma_{11}}^{n} = {\sigma_{11}}^{n-1} &+ \left[\frac{1}{2}\left({K_e}^{n} + {K_e}^{n-1}\right) + \frac{2}{3}\left({G_e}^{n} + {G_e}^{n-1}\right)\right]{\Delta\epsilon_{11}}^{n} \\
&+ \left[\frac{1}{2}\left({K_e}^{n} + {K_e}^{n-1}\right) - \frac{1}{3}\left({G_e}^{n} + {G_e}^{n-1}\right)\right]\left({\Delta\epsilon_{22}}^{n} + {\Delta\epsilon_{33}}^{n}\right) \\
&- \Delta T^{n}\left(\frac{{\beta_{K_e}}^{n} + {\beta_{K_e}}^{n-1}}{2}\right) - \Delta \mathrm{X}^{n}\left(\frac{{\gamma_{K_e}}^{n} + {\gamma_{K_e}}^{n-1}}{2}\right) \\
&+ \sum_{i=1}^{N_K}\left({q_{Ki}}^{n} - {q_{Ki}}^{n-1}\right) + \sum_{j=1}^{N_G}\left(q_{Gj}^{11\,n} - q_{Gj}^{11\,n-1}\right)
\end{aligned}
\qquad \textbf{(B-58)}
$$

Similarly for all other stress components we will have

$$
\begin{aligned}
{\sigma_{22}}^{n} = {\sigma_{22}}^{n-1} &+ \left[\frac{1}{2}\left({K_e}^{n} + {K_e}^{n-1}\right) + \frac{2}{3}\left({G_e}^{n} + {G_e}^{n-1}\right)\right]{\Delta\epsilon_{22}}^{n} \\
&+ \left[\frac{1}{2}\left({K_e}^{n} + {K_e}^{n-1}\right) - \frac{1}{3}\left({G_e}^{n} + {G_e}^{n-1}\right)\right]\left({\Delta\epsilon_{33}}^{n} + {\Delta\epsilon_{11}}^{n}\right) \\
&- \Delta T^{n}\left(\frac{{\beta_{K_e}}^{n} + {\beta_{K_e}}^{n-1}}{2}\right) - \Delta \mathrm{X}^{n}\left(\frac{{\gamma_{K_e}}^{n} + {\gamma_{K_e}}^{n-1}}{2}\right) \\
&+ \sum_{i=1}^{N_K}\left({q_{Ki}}^{n} - {q_{Ki}}^{n-1}\right) + \sum_{j=1}^{N_G}\left(q_{Gj}^{22\,n} - q_{Gj}^{22\,n-1}\right)
\end{aligned}
\qquad \textbf{(B-59)}
$$

$$
\begin{aligned}
{\sigma_{33}}^{n} = {\sigma_{33}}^{n-1} &+ \left[\frac{1}{2}\left({K_e}^{n} + {K_e}^{n-1}\right) + \frac{2}{3}\left({G_e}^{n} + {G_e}^{n-1}\right)\right]{\Delta\epsilon_{33}}^{n} \\
&+ \left[\frac{1}{2}\left({K_e}^{n} + {K_e}^{n-1}\right) - \frac{1}{3}\left({G_e}^{n} + {G_e}^{n-1}\right)\right]\left({\Delta\epsilon_{11}}^{n} + {\Delta\epsilon_{22}}^{n}\right) \\
&- \Delta T^{n}\left(\frac{{\beta_{K_e}}^{n} + {\beta_{K_e}}^{n-1}}{2}\right) - \Delta \mathrm{X}^{n}\left(\frac{{\gamma_{K_e}}^{n} + {\gamma_{K_e}}^{n-1}}{2}\right) \\
&+ \sum_{i=1}^{N_K}\left({q_{Ki}}^{n} - {q_{Ki}}^{n-1}\right) - \sum_{j=1}^{N_G}\left(q_{Gj}^{11\,n} - q_{Gj}^{11\,n-1}\right) \\
&- \sum_{j=1}^{N_G}\left(q_{Gj}^{22\,n} - q_{Gj}^{22\,n-1}\right)
\end{aligned}
\qquad \textbf{(B-60)}
$$

$$
{\sigma_{23}}^{n} = {\sigma_{23}}^{n-1} + \left(\frac{{G_e}^{n} + {G_e}^{n-1}}{2}\right){\Delta\gamma_{23}}^{n} + \sum_{j=1}^{N_G}\left(q_{Gj}^{23\,n} - q_{Gj}^{23\,n-1}\right) \qquad \textbf{(B-61)}
$$

$$
{\sigma_{13}}^{n} = {\sigma_{13}}^{n-1} + \left(\frac{{G_e}^{n} + {G_e}^{n-1}}{2}\right){\Delta\gamma_{13}}^{n} + \sum_{j=1}^{N_G}\left(q_{Gj}^{13\,n} - q_{Gj}^{13\,n-1}\right) \qquad \textbf{(B-62)}
$$

$$
{\sigma_{12}}^{n} = {\sigma_{12}}^{n-1} + \left(\frac{{G_e}^{n} + {G_e}^{n-1}}{2}\right){\Delta\gamma_{12}}^{n} + \sum_{j=1}^{N_G}\left(q_{Gj}^{12\,n} - q_{Gj}^{12\,n-1}\right) \qquad \textbf{(B-63)}
$$

Using Equations (B-58) to (B-63), we may evaluate the value of each stress component at each time step in terms of its value at the previous time step, state variables and other parameters. In turn, the values of state variables will be obtained using Equations (B-50) to (B-55).

B.2 Transversely-isotropic case

Let's assume plane 2-3 is the plane of isotropy for a transversely isotropic material. We may write Hooke's law for the linear elastic transversely isotropic material as

$$\sigma_{11} = C_{11}(\epsilon_{11} - \alpha_1\Delta T - \alpha_1^{cs}\Delta X) + C_{12}(\epsilon_{22} - \alpha_2\Delta T - \alpha_2^{cs}\Delta X)$$
$$+ C_{12}(\epsilon_{33} - \alpha_2\Delta T - \alpha_2^{cs}\Delta X)$$
$$= C_{11}\epsilon_{11} + C_{12}(\epsilon_{22} + \epsilon_{33}) - (C_{11}\alpha_1 + 2C_{12}\alpha_2)\Delta T$$
$$- (C_{11}\alpha_1^{cs} + 2C_{12}\alpha_2^{cs})\Delta X$$
$$\sigma_{22} = C_{12}(\epsilon_{11} - \alpha_1\Delta T - \alpha_1^{cs}\Delta X) + C_{22}(\epsilon_{22} - \alpha_2\Delta T - \alpha_2^{cs}\Delta X)$$
$$+ C_{23}(\epsilon_{33} - \alpha_2\Delta T - \alpha_2^{cs}\Delta X)$$
$$= C_{12}\epsilon_{11} + C_{22}\epsilon_{22} + C_{23}\epsilon_{33} - (C_{12}\alpha_1 + (C_{22} + C_{23})\alpha_2)\Delta T$$
$$- (C_{12}\alpha_1^{cs} + (C_{22} + C_{23})\alpha_2^{cs})\Delta X \qquad \textbf{(B-64)}$$
$$\sigma_{33} = C_{12}(\epsilon_{11} - \alpha_1\Delta T - \alpha_1^{cs}\Delta X) + C_{23}(\epsilon_{22} - \alpha_2\Delta T - \alpha_2^{cs}\Delta X)$$
$$+ C_{22}(\epsilon_{33} - \alpha_2\Delta T - \alpha_2^{cs}\Delta X)$$
$$= C_{12}\epsilon_{11} + C_{23}\epsilon_{22} + C_{22}\epsilon_{33} - (C_{12}\alpha_1 + (C_{22} + C_{23})\alpha_2)\Delta T$$
$$- (C_{12}\alpha_1^{cs} + (C_{22} + C_{23})\alpha_2^{cs})\Delta X$$
$$\sigma_{23} = \frac{1}{2}(C_{22} - C_{23})\gamma_{23}$$
$$\sigma_{13} = C_{66}\gamma_{13}$$
$$\sigma_{12} = C_{66}\gamma_{12}$$

Defining

$$\beta_1 = C_{11}\alpha_1 + 2C_{12}\alpha_2, \qquad \beta_2 = C_{12}\alpha_1 + (C_{22} + C_{23})\alpha_2$$
$$\gamma_1 = C_{11}\alpha_1^{cs} + 2C_{12}\alpha_2^{cs}, \qquad \gamma_2 = C_{12}\alpha_1^{cs} + (C_{22} + C_{23})\alpha_2^{cs} \qquad \textbf{(B-65)}$$

We will rewrite Equation (B-64) as

$$\sigma_{11} = C_{11}\epsilon_{11} + C_{12}(\epsilon_{22} + \epsilon_{33}) - \beta_1 \Delta T - \gamma_1 \Delta X$$

$$\sigma_{22} = C_{12}\epsilon_{11} + C_{22}\epsilon_{22} + C_{23}\epsilon_{33} - \beta_2 \Delta T - \gamma_2 \Delta X$$

$$\sigma_{33} = C_{12}\epsilon_{11} + C_{23}\epsilon_{22} + C_{22}\epsilon_{33} - \beta_2 \Delta T - \gamma_2 \Delta X$$

$$\sigma_{23} = \frac{1}{2}(C_{22} - C_{23})\gamma_{23} \qquad \textbf{(B-66)}$$

$$\sigma_{13} = C_{66}\gamma_{13}$$

$$\sigma_{12} = C_{66}\gamma_{12}$$

From Equations (B-66) and Equation (4-42), we may write the thermo-viscoelastic (TVE) constitutive relations for a transversely isotropic material as

$$\sigma_{11} = C_{11_e}\epsilon_{11} + C_{12_e}(\epsilon_{22} + \epsilon_{33}) - \beta_{1_e}\Delta T + a_F \int_0^{\xi} \Delta C_{11}(\xi - \xi') \frac{d\epsilon_{11}}{d\xi'} d\xi'$$

$$+ a_F \int_0^{\xi} \Delta C_{12}(\xi - \xi') \frac{d(\epsilon_{22} + \epsilon_{33})}{d\xi'} d\xi' \qquad \textbf{(B-67)}$$

$$- a_F \int_0^{\xi} \Delta \beta_1(\xi - \xi') \frac{d\left(\frac{\Delta T}{a_F}\right)}{d\xi'} d\xi'$$

$$\sigma_{22} = C_{12_e}\epsilon_{11} + C_{22_e}\epsilon_{22} + C_{23_e}\epsilon_{33} - \beta_{2_e}\Delta T + a_F \int_0^{\xi} \Delta C_{12}(\xi - \xi') \frac{d\epsilon_{11}}{d\xi'} d\xi'$$

$$+ a_F \int_0^{\xi} \Delta C_{22}(\xi - \xi') \frac{d\epsilon_{22}}{d\xi'} d\xi' + a_F \int_0^{\xi} \Delta C_{23}(\xi - \xi') \frac{d\epsilon_{33}}{d\xi'} d\xi' \qquad \textbf{(B-68)}$$

$$- a_F \int_0^{\xi} \Delta \beta_2(\xi - \xi') \frac{d\left(\frac{\Delta T}{a_F}\right)}{d\xi'} d\xi'$$

$$\sigma_{33} = C_{12_e}\epsilon_{11} + C_{23_e}\epsilon_{22} + C_{22_e}\epsilon_{33} - \beta_{2_e}\Delta T + a_F \int_0^{\xi} \Delta C_{12}(\xi - \xi') \frac{d\epsilon_{11}}{d\xi'} d\xi'$$

$$+ a_F \int_0^{\xi} \Delta C_{23}(\xi - \xi') \frac{d\epsilon_{22}}{d\xi'} d\xi' + a_F \int_0^{\xi} \Delta C_{22}(\xi - \xi') \frac{d\epsilon_{33}}{d\xi'} d\xi' \quad \textbf{(B-69)}$$

$$- a_F \int_0^{\xi} \Delta\beta_2(\xi - \xi') \frac{d\left(\frac{\Delta T}{a_F}\right)}{d\xi'} d\xi'$$

$$\sigma_{23} = \frac{1}{2}\left(C_{22_e} - C_{23_e}\right)\gamma_{23} + a_F \int_0^{\xi} \frac{1}{2}\left(\Delta C_{22}(\xi - \xi') - \Delta C_{23}(\xi - \xi')\right) \frac{d\gamma_{23}}{d\xi'} d\xi' \quad \textbf{(B-70)}$$

$$\sigma_{13} = C_{66_e}\gamma_{13} + a_F \int_0^{\xi} \Delta C_{66}(\xi - \xi') \frac{d\gamma_{13}}{d\xi'} d\xi' \quad \textbf{(B-71)}$$

$$\sigma_{12} = C_{66_e}\gamma_{12} + a_F \int_0^{\xi} \Delta C_{66}(\xi - \xi') \frac{d\gamma_{12}}{d\xi'} d\xi' \quad \textbf{(B-72)}$$

Approximating $C_{ij}'s$, $\beta_1, \beta_2, \gamma_1$ and γ_2 by Prony series we will have

$$C_{ij}(\xi) = C_{ij_e} + \sum_{k=1}^{N_{C_{ij}}} C_{ij_k} e^{-\frac{\xi}{\tau_{C_{ijk}}}},$$

$$\beta_1(\xi) = \beta_{1_e} + \sum_{k=1}^{N_{\beta_1}} \beta_{1_k} e^{-\frac{\xi}{\tau_{\beta_1 k}}}, \qquad \beta_2(\xi) = \beta_{2_e} + \sum_{k=1}^{N_{\beta_2}} \beta_{2_k} e^{-\frac{\xi}{\tau_{\beta_2 k}}}, \quad \textbf{(B-73)}$$

$$\gamma_1(\xi) = \gamma_{1_e} + \sum_{k=1}^{N_{\gamma_1}} \gamma_{1_k} e^{-\frac{\xi}{\tau_{\gamma_1 k}}}, \qquad \gamma_2(\xi) = \gamma_{2_e} + \sum_{k=1}^{N_{\gamma_2}} \gamma_{2_k} e^{-\frac{\xi}{\tau_{\gamma_2 k}}}$$

Substituting from Equations (B-73) into Equations (B-67) to (B-72) gives us

$$\sigma_{11} = C_{11_e}\epsilon_{11} + C_{12_e}(\epsilon_{22} + \epsilon_{33}) - \beta_{1_e}\Delta T - \gamma_{1_e}\Delta X$$
$$+ \sum_{i=1}^{N_{C_{11}}} \left(a_F \int_0^{\xi} C_{11_i} e^{-\frac{\xi}{\tau_{C_{11}i}}} \frac{d\epsilon_{11}}{d\xi'} d\xi' \right)$$
$$+ \sum_{i=1}^{N_{C_{12}}} \left(a_F \int_0^{\xi} C_{12_i} e^{-\frac{\xi}{\tau_{C_{12}i}}} \frac{d(\epsilon_{22} + \epsilon_{33})}{d\xi'} d\xi' \right) \quad \textbf{(B-74)}$$
$$- \sum_{i=1}^{N_{\beta_1}} \left(a_F \int_0^{\xi} \beta_{1_i} e^{-\frac{\xi}{\tau_{\beta_1}i}} \frac{d\left(\frac{\Delta T}{a_F}\right)}{d\xi'} d\xi' \right)$$
$$- \sum_{i=1}^{N_{\gamma_1}} \left(a_F \int_0^{\xi} \gamma_{1_i} e^{-\frac{\xi}{\tau_{\gamma_1}i}} \frac{d\left(\frac{\Delta X}{a_F}\right)}{d\xi'} d\xi' \right)$$

$$\sigma_{22} = C_{12_e}\epsilon_{11} + C_{22_e}\epsilon_{22} + C_{23_e}\epsilon_{33} - \beta_{2_e}\Delta T - \gamma_{2_e}\Delta X$$

$$+ \sum_{i=1}^{N_{C_{12}}} \left(a_F \int_0^{\xi} C_{12_i} e^{-\frac{\xi}{\tau_{C_{12}i}}} \frac{d\epsilon_{11}}{d\xi'} d\xi' \right)$$

$$+ \sum_{i=1}^{N_{C_{22}}} \left(a_F \int_0^{\xi} C_{22_i} e^{-\frac{\xi}{\tau_{C_{22}i}}} \frac{d\epsilon_{22}}{d\xi'} d\xi' \right)$$

$$+ \sum_{i=1}^{N_{C_{23}}} \left(a_F \int_0^{\xi} C_{23_i} e^{-\frac{\xi}{\tau_{C_{23}i}}} \frac{d\epsilon_{33}}{d\xi'} d\xi' \right) \qquad \textbf{(B-75)}$$

$$- \sum_{i=1}^{N_{\beta_2}} \left(a_F \int_0^{\xi} \beta_{2_i} e^{-\frac{\xi}{\tau_{\beta_2}i}} \frac{d\left(\frac{\Delta T}{a_F}\right)}{d\xi'} d\xi' \right)$$

$$- \sum_{i=1}^{N_{\gamma_2}} \left(a_F \int_0^{\xi} \gamma_{2_i} e^{-\frac{\xi}{\tau_{\gamma_2}i}} \frac{d\left(\frac{\Delta X}{a_F}\right)}{d\xi'} d\xi' \right)$$

$$\sigma_{33} = C_{12_e}\epsilon_{11} + C_{23_e}\epsilon_{22} + C_{22_e}\epsilon_{33} - \beta_{2_e}\Delta T$$
$$+ \sum_{i=1}^{N_{C_{12}}} \left(a_F \int_0^{\xi} C_{12_i} e^{-\frac{\xi}{\tau_{C_{12}i}}} \frac{d\epsilon_{11}}{d\xi'} d\xi' \right)$$
$$+ \sum_{i=1}^{N_{C_{23}}} \left(a_F \int_0^{\xi} C_{23_i} e^{-\frac{\xi}{\tau_{C_{23}i}}} \frac{d\epsilon_{22}}{d\xi'} d\xi' \right)$$
$$+ \sum_{i=1}^{N_{C_{22}}} \left(a_F \int_0^{\xi} C_{22_i} e^{-\frac{\xi}{\tau_{C_{22}i}}} \frac{d\epsilon_{33}}{d\xi'} d\xi' \right) \quad \textbf{(B-76)}$$
$$- \sum_{i=1}^{N_{\beta_2}} \left(a_F \int_0^{\xi} \beta_{2_i} e^{-\frac{\xi}{\tau_{\beta_2}i}} \frac{d\left(\frac{\Delta T}{a_F}\right)}{d\xi'} d\xi' \right)$$
$$- \sum_{i=1}^{N_{\gamma_2}} \left(a_F \int_0^{\xi} \gamma_{2_i} e^{-\frac{\xi}{\tau_{\gamma_2}i}} \frac{d\left(\frac{\Delta X}{a_F}\right)}{d\xi'} d\xi' \right)$$

$$\sigma_{23} = \frac{1}{2}\left(C_{22_e} - C_{23_e}\right)\gamma_{23} + \frac{1}{2}\sum_{i=1}^{N_{C_{22}}} \left(a_F \int_0^{\xi} C_{22_i} e^{-\frac{\xi}{\tau_{C_{22}i}}} \frac{d\gamma_{23}}{d\xi'} d\xi' \right) \quad \textbf{(B-77)}$$
$$- \frac{1}{2}\sum_{i=1}^{N_{C_{23}}} \left(a_F \int_0^{\xi} C_{23_i} e^{-\frac{\xi}{\tau_{C_{23}i}}} \frac{d\gamma_{23}}{d\xi'} d\xi' \right)$$

$$\sigma_{13} = C_{66_e}\gamma_{13} + \sum_{i=1}^{N_{C_{66}}} \left(a_F \int_0^{\xi} C_{66_i} e^{-\frac{\xi}{\tau_{C_{66}i}}} \frac{d\gamma_{13}}{d\xi'} d\xi' \right) \quad \textbf{(B-78)}$$

$$\sigma_{12} = C_{66_e}\gamma_{12} + \sum_{i=1}^{N_{C_{66}}} \left(a_F \int_0^{\xi} C_{66_i} e^{-\frac{\xi}{\tau_{C_{66}i}}} \frac{d\gamma_{12}}{d\xi'} d\xi' \right) \quad \textbf{(B-79)}$$

Defining the state variables

$$q_{C_{11}i}^{11}(\xi) = a_F \int_0^{\xi} \left(C_{11_i} e^{-\frac{\xi-\xi'}{\tau_{C_{11}i}}} \frac{d\epsilon_{11}}{d\xi'} \right) d\xi', \qquad i = 1,2 \dots, N_{C_{11}} \quad \textbf{(B-80)}$$

$$q_{C_{12}i}^{22}(\xi) = a_F \int_0^{\xi} \left(C_{12_i} e^{-\frac{\xi-\xi'}{\tau_{C_{12}i}}} \frac{d\epsilon_{22}}{d\xi'} \right) d\xi', \qquad i = 1,2 \dots, N_{C_{12}} \quad \textbf{(B-81)}$$

$$q_{C_{12}i}^{22}(\xi) = a_F \int_0^{\xi} \left(C_{12_i} e^{-\frac{\xi-\xi'}{\tau_{C_{12}i}}} \frac{d\epsilon_{22}}{d\xi'} \right) d\xi', \qquad i = 1,2 \dots, N_{C_{12}} \quad \textbf{(B-82)}$$

$$q_{C_{12}i}^{33}(\xi) = a_F \int_0^{\xi} \left(C_{12_i} e^{-\frac{\xi-\xi'}{\tau_{C_{12}i}}} \frac{d\epsilon_{33}}{d\xi'} \right) d\xi', \qquad i = 1,2 \dots, N_{C_{12}} \quad \textbf{(B-83)}$$

$$q_{C_{12}i}^{11}(\xi) = a_F \int_0^{\xi} \left(C_{12_i} e^{-\frac{\xi-\xi'}{\tau_{C_{12}i}}} \frac{d\epsilon_{11}}{d\xi'} \right) d\xi', \qquad i = 1,2 \dots, N_{C_{12}} \quad \textbf{(B-84)}$$

$$q_{C_{22}i}^{22}(\xi) = a_F \int_0^{\xi} \left(C_{22_i} e^{-\frac{\xi-\xi'}{\tau_{C_{22}i}}} \frac{d\epsilon_{22}}{d\xi'} \right) d\xi', \qquad i = 1,2 \dots, N_{C_{22}} \quad \textbf{(B-85)}$$

$$q_{C_{23}i}^{33}(\xi) = a_F \int_0^{\xi} \left(C_{23_i} e^{-\frac{\xi-\xi'}{\tau_{C_{23}i}}} \frac{d\epsilon_{33}}{d\xi'} \right) d\xi', \qquad i = 1,2 \dots, N_{C_{23}} \quad \textbf{(B-86)}$$

$$q_{C_{23}i}^{22}(\xi) = a_F \int_0^{\xi} \left(C_{23_i} e^{-\frac{\xi-\xi'}{\tau_{C_{23}i}}} \frac{d\epsilon_{22}}{d\xi'} \right) d\xi', \qquad i = 1,2 \dots, N_{C_{23}} \quad \textbf{(B-87)}$$

$$q_{C_{22}i}^{33}(\xi) = a_F \int_0^{\xi} \left(C_{22_i} e^{-\frac{\xi-\xi'}{\tau_{C_{22}i}}} \frac{d\epsilon_{33}}{d\xi'} \right) d\xi', \qquad i = 1,2 \dots, N_{C_{22}} \quad \textbf{(B-88)}$$

$$q_{C_{22}i}^{23}(\xi) = a_F \int_0^{\xi} \left(C_{22_i} e^{-\frac{\xi-\xi'}{\tau_{C_{22}i}}} \frac{d\gamma_{23}}{d\xi'} \right) d\xi', \qquad i = 1,2 \dots, N_{C_{22}} \quad \textbf{(B-89)}$$

$$q_{C_{23}i}^{23}(\xi) = a_F \int_0^{\xi} \left(C_{23_i} e^{-\frac{\xi-\xi'}{\tau_{C_{23}i}}} \frac{d\gamma_{23}}{d\xi'} \right) d\xi', \qquad i = 1,2 \dots, N_{C_{23}} \quad \textbf{(B-90)}$$

$$q_{C_{66}i}^{13}(\xi) = a_F \int_0^{\xi} \left(C_{66_i} e^{-\frac{\xi-\xi'}{\tau_{C_{66}i}}} \frac{d\gamma_{13}}{d\xi'} \right) d\xi', \qquad i = 1,2 \dots, N_{C_{66}} \quad \textbf{(B-91)}$$

$$q_{C_{66}i}^{12}(\xi) = a_F \int_0^{\xi} \left(C_{66_i} e^{-\frac{\xi-\xi'}{\tau_{C_{66}i}}} \frac{d\gamma_{12}}{d\xi'} \right) d\xi', \qquad i = 1,2 \dots, N_{C_{66}} \quad \textbf{(B-92)}$$

$$q_{\beta_{1_i}}(\xi) = a_F \int_0^{\xi} \beta_{1_i} e^{-\frac{\xi}{\tau_{\beta_1 i}}} \frac{d\left(\frac{\Delta T}{a_F}\right)}{d\xi'} d\xi', \qquad i = 1,2 \dots, N_{\beta_1} \quad \textbf{(B-93)}$$

$$q_{\beta_{2_i}}(\xi) = a_F \int_0^{\xi} \beta_{2_i} e^{-\frac{\xi}{\tau_{\beta_2 i}}} \frac{d\left(\frac{\Delta T}{a_F}\right)}{d\xi'} d\xi', \qquad i = 1,2 \dots, N_{\beta_2} \quad \textbf{(B-94)}$$

$$q_{\gamma_{1_i}}(\xi) = a_F \int_0^{\xi} \gamma_{1_i} e^{-\frac{\xi}{\tau_{\gamma_1 i}}} \frac{d\left(\frac{\Delta X}{a_F}\right)}{d\xi'} d\xi', \qquad i = 1,2 \dots, N_{\gamma_1} \quad \textbf{(B-95)}$$

$$q_{\gamma_{2_i}}(\xi) = a_F \int_0^{\xi} \gamma_{2_i} e^{-\frac{\xi}{\tau_{\gamma_2 i}}} \frac{d\left(\frac{\Delta X}{a_F}\right)}{d\xi'} d\xi', \qquad i = 1,2 \dots, N_{\gamma_2} \quad \textbf{(B-96)}$$

Using Leibniz rule of differentiation, we take the derivative of each of the state variables in Equations (B-80) to (B-96) and conclude

$$\frac{dq_{C_{11}i}^{11}(\xi)}{d\xi} + \frac{q_{C_{11}i}^{11}(\xi)}{\tau_{C_{11}i}} = a_F C_{11_i} \frac{d\epsilon_{11}}{d\xi}, \qquad i = 1,2 \dots, N_{C_{11}} \quad \textbf{(B-97)}$$

$$\frac{dq_{C_{12}i}^{22}(\xi)}{d\xi} + \frac{q_{C_{12}i}^{22}(\xi)}{\tau_{C_{12}i}} = a_F C_{12_i} \frac{d\epsilon_{22}}{d\xi}, \qquad i = 1,2 \dots, N_{C_{12}} \quad \textbf{(B-98)}$$

$$\frac{dq_{C_{12}i}^{33}(\xi)}{d\xi}+\frac{q_{C_{12}i}^{33}(\xi)}{\tau_{C_{12}i}}=a_F C_{12_i}\frac{d\epsilon_{33}}{d\xi},\qquad i=1,2\ldots,N_{C_{12}}\quad \textbf{(B-99)}$$

$$\frac{dq_{C_{12}i}^{11}(\xi)}{d\xi}+\frac{q_{C_{12}i}^{11}(\xi)}{\tau_{C_{12}i}}=a_F C_{12_i}\frac{d\epsilon_{11}}{d\xi},\qquad i=1,2\ldots,N_{C_{12}}\quad \textbf{(B-100)}$$

$$\frac{dq_{C_{22}i}^{22}(\xi)}{d\xi}+\frac{q_{C_{22}i}^{22}(\xi)}{\tau_{C_{22}i}}=a_F C_{22_i}\frac{d\epsilon_{22}}{d\xi},\qquad i=1,2\ldots,N_{C_{22}}\quad \textbf{(B-101)}$$

$$\frac{dq_{C_{23}i}^{33}(\xi)}{d\xi}+\frac{q_{C_{23}i}^{33}(\xi)}{\tau_{C_{23}i}}=a_F C_{23_i}\frac{d\epsilon_{33}}{d\xi},\qquad i=1,2\ldots,N_{C_{23}}\quad \textbf{(B-102)}$$

$$\frac{dq_{C_{23}i}^{22}(\xi)}{d\xi}+\frac{q_{C_{23}i}^{22}(\xi)}{\tau_{C_{23}i}}=a_F C_{23_i}\frac{d\epsilon_{22}}{d\xi},\qquad i=1,2\ldots,N_{C_{23}}\quad \textbf{(B-103)}$$

$$\frac{dq_{C_{22}i}^{33}(\xi)}{d\xi}+\frac{q_{C_{22}i}^{33}(\xi)}{\tau_{C_{22}i}}=a_F C_{22_i}\frac{d\epsilon_{33}}{d\xi},\qquad i=1,2\ldots,N_{C_{22}}\quad \textbf{(B-104)}$$

$$\frac{dq_{C_{22}i}^{23}(\xi)}{d\xi}+\frac{q_{C_{22}i}^{23}(\xi)}{\tau_{C_{22}i}}=a_F C_{22_i}\frac{d\gamma_{23}}{d\xi},\qquad i=1,2\ldots,N_{C_{22}}\quad \textbf{(B-105)}$$

$$\frac{dq_{C_{23}i}^{23}(\xi)}{d\xi}+\frac{q_{C_{23}i}^{23}(\xi)}{\tau_{C_{23}i}}=a_F C_{23_i}\frac{d\gamma_{23}}{d\xi},\qquad i=1,2\ldots,N_{C_{23}}\quad \textbf{(B-106)}$$

$$\frac{dq_{C_{66}i}^{13}(\xi)}{d\xi}+\frac{q_{C_{66}i}^{13}(\xi)}{\tau_{C_{66}i}}=a_F C_{66_i}\frac{d\gamma_{13}}{d\xi},\qquad i=1,2\ldots,N_{C_{66}}\quad \textbf{(B-107)}$$

$$\frac{dq_{C_{66}i}^{12}(\xi)}{d\xi}+\frac{q_{C_{66}i}^{12}(\xi)}{\tau_{C_{66}i}}=a_F C_{66_i}\frac{d\gamma_{12}}{d\xi},\qquad i=1,2\ldots,N_{C_{66}}\quad \textbf{(B-108)}$$

$$\frac{dq_{\beta_{1_i}}(\xi)}{d\xi}+\frac{q_{\beta_{1_i}}(\xi)}{\tau_{\beta_1 i}}=\beta_{1_i}\frac{dT}{d\xi},\qquad i=1,2\ldots,N_{\beta_1}\quad \textbf{(B-109)}$$

$$\frac{dq_{\beta_{2_i}}(\xi)}{d\xi}+\frac{q_{\beta_{2_i}}(\xi)}{\tau_{\beta_2 i}}=\beta_{2_i}\frac{dT}{d\xi},\qquad i=1,2\ldots,N_{\beta_2}\quad \textbf{(B-110)}$$

$$\frac{dq_{\gamma_{1_i}}(\xi)}{d\xi}+\frac{q_{\gamma_{1_i}}(\xi)}{\tau_{\gamma_1 i}}=\gamma_{1_i}\frac{dX}{d\xi},\qquad i=1,2\ldots,N_{\gamma_1}\quad \textbf{(B-111)}$$

$$\frac{dq_{\gamma_{2_i}}(\xi)}{d\xi} + \frac{q_{\gamma_{2_i}}(\xi)}{\tau_{\gamma_2 i}} = \gamma_{2_i}\frac{dX}{d\xi}, \qquad i = 1,2 \dots, N_{\gamma_2} \quad \textbf{(B-112)}$$

Also using Equations (B-80) to (B-96) we rewrite Equations (B-74) to (B-79) as

$$\sigma_{11} = C_{11_e}\epsilon_{11} + C_{12_e}(\epsilon_{22} + \epsilon_{33}) - \beta_{1_e}\Delta T - \gamma_{1_e}\Delta X + \sum_{i=1}^{N_{C_{11}}} q_{C_{11}i}^{11} + \sum_{i=1}^{N_{C_{12}}} \left(q_{C_{12}i}^{22} + q_{C_{12}i}^{33}\right) - \sum_{i=1}^{N_{\beta_1}} q_{\beta_{1_i}} - \sum_{i=1}^{N_{\gamma_1}} q_{\gamma_{1_i}} \quad \textbf{(B-113)}$$

$$\sigma_{22} = C_{12_e}\epsilon_{11} + C_{22_e}\epsilon_{22} + C_{23_e}\epsilon_{33} - \beta_{2_e}\Delta T - \gamma_{2_e}\Delta X + \sum_{i=1}^{N_{C_{12}}} q_{C_{12}i}^{11} + \sum_{i=1}^{N_{C_{22}}} q_{C_{22}i}^{22} + \sum_{i=1}^{N_{C_{23}}} q_{C_{23}i}^{33} - \sum_{i=1}^{N_{\beta_2}} q_{\beta_{2_i}} - \sum_{i=1}^{N_{\gamma_2}} q_{\gamma_{2_i}} \quad \textbf{(B-114)}$$

$$\sigma_{33} = C_{12_e}\epsilon_{11} + C_{23_e}\epsilon_{22} + C_{22_e}\epsilon_{33} - \beta_{2_e}\Delta T - \gamma_{2_e}\Delta X + \sum_{i=1}^{N_{C_{12}}} q_{C_{12}i}^{11} + \sum_{i=1}^{N_{C_{23}}} q_{C_{23}i}^{22} + \sum_{i=1}^{N_{C_{22}}} q_{C_{22}i}^{33} - \sum_{i=1}^{N_{\beta_2}} q_{\beta_{2_i}} - \sum_{i=1}^{N_{\gamma_2}} q_{\gamma_{2_i}} \quad \textbf{(B-115)}$$

$$\sigma_{23} = \frac{1}{2}\left(C_{22_e} - C_{23_e}\right)\gamma_{23} + \frac{1}{2}\sum_{i=1}^{N_{C_{22}}} q_{C_{22}i}^{23} - \frac{1}{2}\sum_{i=1}^{N_{C_{23}}} q_{C_{23}i}^{23} \quad \textbf{(B-116)}$$

$$\sigma_{13} = C_{66_e}\gamma_{13} + \sum_{i=1}^{N_{C_{66}}} q_{C_{66}i}^{13} \quad \textbf{(B-117)}$$

$$\sigma_{12} = C_{66_e}\gamma_{12} + \sum_{i=1}^{N_{C_{66}}} q_{C_{66}i}^{12} \quad \textbf{(B-118)}$$

Finally, based on our discussions about hypo-elastic behaviour of the material in the glassy regime, Equations (B-113) to (B-118) are modified as

$$\dot{\sigma}_{11} = C_{11_e}\dot{\epsilon}_{11} + C_{12_e}(\dot{\epsilon}_{22} + \dot{\epsilon}_{33}) - \beta_{1_e}\dot{\Delta T} - \gamma_{1_e}\dot{\Delta X} + \sum_{i=1}^{N_{C_{11}}} \dot{q}_{C_{11}i}^{11} + \sum_{i=1}^{N_{C_{12}}} \left(\dot{q}_{C_{12}i}^{22} + \dot{q}_{C_{12}i}^{33}\right) - \sum_{i=1}^{N_{\beta_1}} \dot{q}_{\beta_{1_i}} - \sum_{i=1}^{N_{\gamma_1}} \dot{q}_{\gamma_{1_i}} \quad \textbf{(B-119)}$$

$$\dot{\sigma}_{22} = C_{12_e}\dot{\epsilon}_{11} + C_{22_e}\dot{\epsilon}_{22} + C_{23_e}\dot{\epsilon}_{33} - \beta_{2_e}\dot{\Delta T} - \gamma_{2_e}\dot{\Delta X} + \sum_{i=1}^{N_{C_{12}}} \dot{q}_{C_{12}i}^{11} + \sum_{i=1}^{N_{C_{22}}} \dot{q}_{C_{22}i}^{22} + \sum_{i=1}^{N_{C_{23}}} \dot{q}_{C_{23}i}^{33} - \sum_{i=1}^{N_{\beta_2}} \dot{q}_{\beta_{2_i}} - \sum_{i=1}^{N_{\gamma_2}} \dot{q}_{\gamma_{2_i}} \quad \textbf{(B-120)}$$

$$\dot{\sigma}_{33} = C_{12_e}\dot{\epsilon}_{11} + C_{23_e}\dot{\epsilon}_{22} + C_{22_e}\dot{\epsilon}_{33} - \beta_{2_e}\dot{\Delta T} - \gamma_{2_e}\dot{\Delta X} + \sum_{i=1}^{N_{C_{12}}} \dot{q}_{C_{12}i}^{11} + \sum_{i=1}^{N_{C_{23}}} \dot{q}_{C_{23}i}^{22} + \sum_{i=1}^{N_{C_{22}}} \dot{q}_{C_{22}i}^{33} - \sum_{i=1}^{N_{\beta_2}} \dot{q}_{\beta_{2_i}} - \sum_{i=1}^{N_{\gamma_2}} \dot{q}_{\gamma_{2_i}} \quad \textbf{(B-121)}$$

$$\dot{\sigma}_{23} = \frac{1}{2}\left(C_{22_e} - C_{23_e}\right)\dot{\gamma}_{23} + \frac{1}{2}\sum_{i=1}^{N_{C_{22}}} \dot{q}_{C_{22}i}^{23} - \frac{1}{2}\sum_{i=1}^{N_{C_{23}}} \dot{q}_{C_{23}i}^{23} \quad \textbf{(B-122)}$$

$$\dot{\sigma}_{13} = C_{66_e}\dot{\gamma}_{13} + \sum_{i=1}^{N_{C_{66}}} \dot{q}_{C_{66}i}^{13} \quad \textbf{(B-123)}$$

$$\dot{\sigma}_{12} = C_{66_e}\dot{\gamma}_{12} + \sum_{i=1}^{N_{C_{66}}} \dot{q}_{C_{66}i}^{12} \quad \textbf{(B-124)}$$

Next similar to the isotropic case, we carry out the time integration of equations to prepare them for implementation in UMAT.

Multiplying both sides of Equation (B-97) by the integrating factor $e^{\frac{\xi}{\tau_{C_{11}i}}}$ yields

$$e^{\frac{\xi}{\tau_{C_{11}i}}}\left(\frac{dq_{C_{11}i}^{11}(\xi)}{d\xi}+\frac{q_{C_{11}i}^{11}(\xi)}{\tau_{C_{11}i}}\right)=\frac{d\left(e^{\frac{\xi}{\tau_{C_{11}i}}}q_{C_{11}i}^{11}(\xi)\right)}{d\xi}=a_F C_{11_i}e^{\frac{\xi}{\tau_{C_{11}i}}}\frac{d\epsilon_{11}}{d\xi}, \qquad \textbf{(B-125)}$$

$$i=1,2\ldots,N_{C_{11}}$$

Now we integrate from ξ^{n-1} to ξ^n to obtain

$$e^{\frac{\xi^{n-1}+\Delta\xi^n}{\tau_{C_{11}i}}}q_{C_{11}i}^{11}(\xi^n)-e^{\frac{\xi^{n-1}}{\tau_{C_{11}i}}}q_{C_{11}i}^{11}(\xi^{n-1})=\int_{\xi^{n-1}}^{\xi^n}a_F C_{11_i}e^{\frac{\xi'}{\tau_{C_{11}i}}}\frac{d\epsilon_{11}}{d\xi'}d\xi', \qquad \textbf{(B-126)}$$

$$i=1,2\ldots,N_{C_{11}}$$

Now we assume ϵ_{11} varies linearly with ξ in the interval $[\xi^{n-1},\xi^n]$, i.e., $\frac{d\epsilon_{11}}{d\xi}$ is constant and we replace it with $\frac{\Delta\epsilon_{11}{}^n}{\Delta\xi^n}$. Therefore we simplify Equation (B-126) as

$$q_{C_{11}i}^{11}(\xi^n)=e^{-\frac{\Delta\xi^n}{\tau_{C_{11}i}}}q_{C_{11}i}^{11}(\xi^{n-1})+a_F C_{11_i}\Delta\epsilon_{11}{}^n\left(\frac{1-e^{-\frac{\Delta\xi^n}{\tau_{C_{11}i}}}}{\frac{\Delta\xi^n}{\tau_{C_{11}i}}}\right), \qquad \textbf{(B-127)}$$

$$i=1,2\ldots,N_{C_{11}}$$

Following the same procedure for all other state variables and replacing $\tau_{C_{kl}i}$ and $\tau_{\beta_k i}$ by $a_T\tau_{C_{kl}i}$ and $a_T\tau_{\beta_k i}$ we obtain

$$q_{C_{11}i}^{11}(t^n) = e^{-\frac{\Delta t^n}{a_T \tau_{C_{11}i}}} q_{C_{11}i}^{11}(t^{n-1}) + a_F C_{11_i} \Delta \epsilon_{11}{}^n \left(\frac{1 - e^{-\frac{\Delta t^n}{a_T \tau_{C_{11}i}}}}{\frac{\Delta t^n}{a_T \tau_{C_{11}i}}} \right), \quad \textbf{(B-128)}$$

$$i = 1,2 \ldots, N_{C_{11}}$$

$$q_{C_{12}i}^{22}(t^n) = e^{-\frac{\Delta t^n}{a_T \tau_{C_{12}i}}} q_{C_{12}i}^{22}(t^{n-1}) + a_F C_{12_i} \Delta \epsilon_{22}{}^n \left(\frac{1 - e^{-\frac{\Delta t^n}{a_T \tau_{C_{12}i}}}}{\frac{\Delta t^n}{a_T \tau_{C_{12}i}}} \right), \quad \textbf{(B-129)}$$

$$i = 1,2 \ldots, N_{C_{12}}$$

$$q_{C_{12}i}^{33}(t^n) = e^{-\frac{\Delta t^n}{a_T \tau_{C_{12}i}}} q_{C_{12}i}^{33}(t^{n-1}) + a_F C_{12_i} \Delta \epsilon_{33}{}^n \left(\frac{1 - e^{-\frac{\Delta t^n}{a_T \tau_{C_{12}i}}}}{\frac{\Delta t^n}{a_T \tau_{C_{12}i}}} \right), \quad \textbf{(B-130)}$$

$$i = 1,2 \ldots, N_{C_{12}}$$

$$q_{C_{12}i}^{11}(t^n) = e^{-\frac{\Delta t^n}{a_T \tau_{C_{12}i}}} q_{C_{12}i}^{11}(t^{n-1}) + a_F C_{12_i} \Delta \epsilon_{11}{}^n \left(\frac{1 - e^{-\frac{\Delta t^n}{a_T \tau_{C_{12}i}}}}{\frac{\Delta t^n}{a_T \tau_{C_{12}i}}} \right), \quad \textbf{(B-131)}$$

$$i = 1,2 \ldots, N_{C_{12}}$$

$$q_{C_{22}i}^{22}(t^n) = e^{-\frac{\Delta t^n}{a_T \tau_{C_{22}i}}} q_{C_{22}i}^{22}(t^{n-1}) + a_F C_{22_i} \Delta \epsilon_{22}{}^n \left(\frac{1 - e^{-\frac{\Delta t^n}{a_T \tau_{C_{22}i}}}}{\frac{\Delta t^n}{a_T \tau_{C_{22}i}}} \right), \quad \textbf{(B-132)}$$

$$i = 1,2 \ldots, N_{C_{22}}$$

$$q_{C_{23}i}^{33}(t^n) = e^{-\frac{\Delta t^n}{a_T \tau_{C_{23}i}}} q_{C_{23}i}^{33}(t^{n-1}) + a_F C_{23_i} \Delta \epsilon_{33}{}^n \left(\frac{1 - e^{-\frac{\Delta t^n}{a_T \tau_{C_{23}i}}}}{\frac{\Delta t^n}{a_T \tau_{C_{23}i}}} \right), \quad \textbf{(B-133)}$$

$$i = 1,2 \ldots, N_{C_{23}}$$

$$q_{C_{23}i}^{22}(t^n) = e^{-\frac{\Delta t^n}{a_T \tau_{C_{23}i}}} q_{C_{23}i}^{22}(t^{n-1}) + a_F C_{23_i} \Delta \epsilon_{22}{}^n \left(\frac{1 - e^{-\frac{\Delta t^n}{a_T \tau_{C_{23}i}}}}{\frac{\Delta t^n}{a_T \tau_{C_{23}i}}} \right), \quad \textbf{(B-134)}$$

$$i = 1,2 \ldots, N_{C_{23}}$$

$$q_{C_{22}i}^{33}(t^n) = e^{-\frac{\Delta t^n}{a_T \tau_{C_{22}i}}} q_{C_{22}i}^{33}(t^{n-1}) + a_F C_{22_i} \Delta \epsilon_{33}{}^n \left(\frac{1 - e^{-\frac{\Delta t^n}{a_T \tau_{C_{22}i}}}}{\frac{\Delta t^n}{a_T \tau_{C_{22}i}}} \right), \quad \textbf{(B-135)}$$

$$i = 1,2 \ldots, N_{C_{22}}$$

$$q_{C_{22}i}^{23}(t^n) = e^{-\frac{\Delta t^n}{a_T \tau_{C_{22}i}}} q_{C_{22}i}^{23}(t^{n-1}) + a_F C_{22_i} \Delta \gamma_{23}{}^n \left(\frac{1 - e^{-\frac{\Delta t^n}{a_T \tau_{C_{22}i}}}}{\frac{\Delta t^n}{a_T \tau_{C_{22}i}}} \right), \quad \textbf{(B-136)}$$

$$i = 1,2 \ldots, N_{C_{22}}$$

$$q_{C_{23}i}^{23}(t^n) = e^{-\frac{\Delta t^n}{a_T \tau_{C_{23}i}}} q_{C_{23}i}^{23}(t^{n-1}) + a_F C_{23_i} \Delta \gamma_{23}{}^n \left(\frac{1 - e^{-\frac{\Delta t^n}{a_T \tau_{C_{23}i}}}}{\frac{\Delta t^n}{a_T \tau_{C_{23}i}}} \right), \quad \textbf{(B-137)}$$

$$i = 1,2 \ldots, N_{C_{23}}$$

$$q_{C_{66}i}^{13}(t^n) = e^{-\frac{\Delta t^n}{a_T \tau_{C_{66}i}}} q_{C_{66}i}^{13}(t^{n-1}) + a_F C_{66_i} \Delta \gamma_{13}{}^n \left(\frac{1 - e^{-\frac{\Delta t^n}{a_T \tau_{C_{66}i}}}}{\frac{\Delta t^n}{a_T \tau_{C_{66}i}}} \right), \quad \textbf{(B-138)}$$

$$i = 1,2 \ldots, N_{C_{66}}$$

$$q_{C_{66}i}^{12}(t^n) = e^{-\frac{\Delta t^n}{a_T \tau_{C_{66}i}}} q_{C_{66}i}^{12}(t^{n-1}) + a_F C_{66_i} \Delta \gamma_{12}{}^n \left(\frac{1 - e^{-\frac{\Delta t^n}{a_T \tau_{C_{66}i}}}}{\frac{\Delta t^n}{a_T \tau_{C_{66}i}}} \right), \quad \textbf{(B-139)}$$

$$i = 1,2 \ldots, N_{C_{66}}$$

$$q_{\beta_{1_i}}(t^n) = e^{-\frac{\Delta t^n}{a_T \tau_{\beta_1 i}}} q_{\beta_{1_i}}(t^{n-1}) + \beta_{1_i} \Delta T^n \left(\frac{1 - e^{-\frac{\Delta t^n}{a_T \tau_{\beta_1 i}}}}{\frac{\Delta t^n}{a_T \tau_{\beta_1 i}}} \right), i = 1,2 \dots, N_{\beta_1} \quad \textbf{(B-140)}$$

$$q_{\beta_{2_i}}(t^n) = e^{-\frac{\Delta t^n}{a_T \tau_{\beta_2 i}}} q_{\beta_{2_i}}(t^{n-1}) + \beta_{2_i} \Delta T^n \left(\frac{1 - e^{-\frac{\Delta t^n}{a_T \tau_{\beta_2 i}}}}{\frac{\Delta t^n}{a_T \tau_{\beta_2 i}}} \right), i = 1,2 \dots, N_{\beta_2} \quad \textbf{(B-141)}$$

$$q_{\gamma_{1_i}}(t^n) = e^{-\frac{\Delta t^n}{a_T \tau_{\gamma_1 i}}} q_{\gamma_{1_i}}(t^{n-1}) + \gamma_{1_i} \Delta T^n \left(\frac{1 - e^{-\frac{\Delta t^n}{a_T \tau_{\gamma_1 i}}}}{\frac{\Delta t^n}{a_T \tau_{\gamma_1 i}}} \right), i = 1,2 \dots, N_{\gamma_1} \quad \textbf{(B-142)}$$

$$q_{\gamma_{2_i}}(t^n) = e^{-\frac{\Delta t^n}{a_T \tau_{\gamma_2 i}}} q_{\gamma_{2_i}}(t^{n-1}) + \gamma_{2_i} \Delta T^n \left(\frac{1 - e^{-\frac{\Delta t^n}{a_T \tau_{\gamma_2 i}}}}{\frac{\Delta t^n}{a_T \tau_{\gamma_2 i}}} \right), i = 1,2 \dots, N_{\gamma_2} \quad \textbf{(B-143)}$$

Next we integrate both sides of Equation (B-119) from t^{n-1} to t^n

$$\begin{aligned} \int_{t^{n-1}}^{t^n} \frac{d\sigma_{11}}{dt'} dt' = \int_{t^{n-1}}^{t^n} \Bigg[& C_{11_e} \frac{d\epsilon_{11}}{dt'} + C_{12_e} \left(\frac{d\epsilon_{22}}{dt'} + \frac{d\epsilon_{33}}{dt'} \right) - \beta_{1_e} \frac{d\Delta T}{dt'} - \gamma_{1_e} \frac{d\Delta X}{dt'} \\ & + \sum_{i=1}^{N_{C_{11}}} \frac{dq_{C_{11}i}^{11}}{dt'} + \sum_{i=1}^{N_{C_{12}}} \left(\frac{dq_{C_{12}i}^{22}}{dt'} + \frac{dq_{C_{12}i}^{33}}{dt'} \right) - \sum_{i=1}^{N_{\beta_1}} \frac{dq_{\beta_{1_i}}}{dt'} \\ & - \sum_{i=1}^{N_{\gamma_1}} \frac{dq_{\gamma_{1_i}}}{dt'} \Bigg] dt' \end{aligned} \quad \textbf{(B-144)}$$

Now we assume $\frac{d\epsilon_{11}}{dt}, \frac{d\epsilon_{22}}{dt}, \frac{d\epsilon_{33}}{dt}, \frac{d\Delta T}{dt}$ and $\frac{d\Delta X}{dt}$ are constant in the interval $[t^{n-1}, t^n]$ and replace them with $\frac{\Delta \epsilon_{11}{}^n}{\Delta t^n}, \frac{\Delta \epsilon_{22}{}^n}{\Delta t^n}, \frac{\Delta \epsilon_{33}{}^n}{\Delta t^n}, \frac{\Delta T^n}{\Delta t^n}$ and $\frac{\Delta X^n}{\Delta t^n}$, respectively. Also we approximate the integrals using Simpson's rule and rewrite Equation (B-144) as

$$
\begin{aligned}
{\sigma_{11}}^n = {\sigma_{11}}^{n-1} &+ {\Delta\epsilon_{11}}^n \left(\frac{{C_{11_e}}^n + {C_{11_e}}^{n-1}}{2}\right) \\
&+ \left({\Delta\epsilon_{22}}^n + {\Delta\epsilon_{33}}^n\right)\left(\frac{{C_{12_e}}^n + {C_{12_e}}^{n-1}}{2}\right) \\
&- \Delta T^n \left(\frac{{\beta_{1_e}}^n + {\beta_{1_e}}^{n-1}}{2}\right) - \Delta X^n \left(\frac{{\gamma_{1_e}}^n + {\gamma_{1_e}}^{n-1}}{2}\right) \\
&+ \sum_{i=1}^{N_{C_{11}}} \left({q_{C_{11}i}^{11}}^n - {q_{C_{11}i}^{11}}^{n-1}\right) \\
&+ \sum_{i=1}^{N_{C_{12}}} \left({q_{C_{12}i}^{22}}^n - {q_{C_{12}i}^{22}}^{n-1} + {q_{C_{12}i}^{33}}^n - {q_{C_{12}i}^{33}}^{n-1}\right) \\
&- \sum_{i=1}^{N_{\beta_1}} \left({q_{\beta_{1_i}}}^n - {q_{\beta_{1_i}}}^{n-1}\right) - \sum_{i=1}^{N_{\gamma_1}} \left({q_{\gamma_{1_i}}}^n - {q_{\gamma_{1_i}}}^{n-1}\right)
\end{aligned}
\qquad \textbf{(B-145)}
$$

Similarly for all other stress components we have

$$
\begin{aligned}
{\sigma_{22}}^n = {\sigma_{22}}^{n-1} &+ {\Delta\epsilon_{11}}^n \left(\frac{{C_{12_e}}^n + {C_{12_e}}^{n-1}}{2}\right) + {\Delta\epsilon_{22}}^n \left(\frac{{C_{22_e}}^n + {C_{22_e}}^{n-1}}{2}\right) \\
&+ {\Delta\epsilon_{33}}^n \left(\frac{{C_{23_e}}^n + {C_{23_e}}^{n-1}}{2}\right) - \Delta T^n \left(\frac{{\beta_{2_e}}^n + {\beta_{2_e}}^{n-1}}{2}\right) \\
&- \Delta X^n \left(\frac{{\gamma_{2_e}}^n + {\gamma_{2_e}}^{n-1}}{2}\right) + \sum_{i=1}^{N_{C_{12}}} \left({q_{C_{12}i}^{11}}^n - {q_{C_{12}i}^{11}}^{n-1}\right) \\
&+ \sum_{i=1}^{N_{C_{22}}} \left({q_{C_{22}i}^{22}}^n - {q_{C_{22}i}^{22}}^{n-1}\right) + \sum_{i=1}^{N_{C_{23}}} \left({q_{C_{23}i}^{33}}^n - {q_{C_{23}i}^{33}}^{n-1}\right) \\
&- \sum_{i=1}^{N_{\beta_2}} \left({q_{\beta_{2_i}}}^n - {q_{\beta_{2_i}}}^{n-1}\right) - \sum_{i=1}^{N_{\gamma_2}} \left({q_{\gamma_{2_i}}}^n - {q_{\gamma_{2_i}}}^{n-1}\right)
\end{aligned}
\qquad \textbf{(B-146)}
$$

$$\sigma_{33}{}^{n} = \sigma_{33}{}^{n-1} + \Delta\epsilon_{11}{}^{n}\left(\frac{C_{12_e}{}^{n} + C_{12_e}{}^{n-1}}{2}\right) + \Delta\epsilon_{22}{}^{n}\left(\frac{C_{23_e}{}^{n} + C_{23_e}{}^{n-1}}{2}\right)$$
$$+ \Delta\epsilon_{33}{}^{n}\left(\frac{C_{22_e}{}^{n} + C_{22_e}{}^{n-1}}{2}\right) - \Delta T^{n}\left(\frac{\beta_{2_e}{}^{n} + \beta_{2_e}{}^{n-1}}{2}\right)$$
$$- \Delta X^{n}\left(\frac{\gamma_{2_e}{}^{n} + \gamma_{2_e}{}^{n-1}}{2}\right) + \sum_{i=1}^{N_{C_{12}}}\left(q_{C_{12}i}^{11}{}^{n} - q_{C_{12}i}^{11}{}^{n-1}\right) \quad \textbf{(B-147)}$$
$$+ \sum_{i=1}^{N_{C_{23}}}\left(q_{C_{23}i}^{22}{}^{n} - q_{C_{23}i}^{22}{}^{n-1}\right) + \sum_{i=1}^{N_{C_{22}}}\left(q_{C_{22}i}^{33}{}^{n} - q_{C_{22}i}^{33}{}^{n-1}\right)$$
$$- \sum_{i=1}^{N_{\beta_2}}\left(q_{\beta_{2_i}}{}^{n} - q_{\beta_{2_i}}{}^{n-1}\right) - \sum_{i=1}^{N_{\gamma_2}}\left(q_{\gamma_{2_i}}{}^{n} - q_{\gamma_{2_i}}{}^{n-1}\right)$$

$$\sigma_{23}{}^{n} = \sigma_{23}{}^{n-1} + \Delta\gamma_{23}{}^{n}\left(\frac{C_{22_e}{}^{n} + C_{22_e}{}^{n-1} - C_{23_e}{}^{n} - C_{23_e}{}^{n-1}}{4}\right)$$
$$+ \frac{1}{2}\sum_{i=1}^{N_{C_{22}}}\left(q_{C_{22}i}^{23}{}^{n} - q_{C_{22}i}^{23}{}^{n-1}\right) - \frac{1}{2}\sum_{i=1}^{N_{C_{23}}}\left(q_{C_{23}i}^{23}{}^{n} - q_{C_{23}i}^{23}{}^{n-1}\right) \quad \textbf{(B-148)}$$

$$\sigma_{13}{}^{n} = \sigma_{13}{}^{n-1} + \Delta\gamma_{13}{}^{n}\left(\frac{C_{66_e}{}^{n} + C_{66_e}{}^{n-1}}{2}\right) + \sum_{i=1}^{N_{C_{66}}}\left(q_{C_{66}i}^{13}{}^{n} - q_{C_{66}i}^{13}{}^{n-1}\right) \quad \textbf{(B-149)}$$

$$\sigma_{12}{}^{n} = \sigma_{12}{}^{n-1} + \Delta\gamma_{12}{}^{n}\left(\frac{C_{66_e}{}^{n} + C_{66_e}{}^{n-1}}{2}\right) + \sum_{i=1}^{N_{C_{66}}}\left(q_{C_{66}i}^{12}{}^{n} - q_{C_{66}i}^{12}{}^{n-1}\right) \quad \textbf{(B-150)}$$

B.3 Orthotropic case

We may write Hooke's law for a linear elastic orthotropic material as

$$\sigma_{11} = C_{11}(\epsilon_{11} - \alpha_1\Delta T - \alpha_1^{cs}\Delta X) + C_{12}(\epsilon_{22} - \alpha_2\Delta T - \alpha_2^{cs}\Delta X)$$
$$+ C_{13}(\epsilon_{33} - \alpha_3\Delta T - \alpha_3^{cs}\Delta X)$$
$$= C_{11}\epsilon_{11} + C_{12}\epsilon_{22} + C_{13}\epsilon_{33} - (C_{11}\alpha_1 + C_{12}\alpha_2 + C_{13}\alpha_3)\Delta T$$
$$- (C_{11}\alpha_1^{cs} + C_{12}\alpha_2^{cs} + C_{13}\alpha_3^{cs})\Delta X$$
$$\sigma_{22} = C_{12}(\epsilon_{11} - \alpha_1\Delta T - \alpha_1^{cs}\Delta X) + C_{22}(\epsilon_{22} - \alpha_2\Delta T - \alpha_2^{cs}\Delta X)$$
$$+ C_{23}(\epsilon_{33} - \alpha_3\Delta T - \alpha_3^{cs}\Delta X)$$
$$= C_{12}\epsilon_{11} + C_{22}\epsilon_{22} + C_{23}\epsilon_{33} - (C_{12}\alpha_1 + C_{22}\alpha_2 + C_{23}\alpha_3)\Delta T$$
$$- (C_{12}\alpha_1^{cs} + C_{22}\alpha_2^{cs} + C_{23}\alpha_3^{cs})\Delta X \qquad \textbf{(B-151)}$$
$$\sigma_{33} = C_{13}(\epsilon_{11} - \alpha_1\Delta T - \alpha_1^{cs}\Delta X) + C_{23}(\epsilon_{22} - \alpha_2\Delta T - \alpha_2^{cs}\Delta X)$$
$$+ C_{33}(\epsilon_{33} - \alpha_3\Delta T - \alpha_3^{cs}\Delta X)$$
$$= C_{13}\epsilon_{11} + C_{23}\epsilon_{22} + C_{33}\epsilon_{33} - (C_{13}\alpha_1 + C_{23}\alpha_2 + C_{33}\alpha_3)\Delta T$$
$$- (C_{13}\alpha_1^{cs} + C_{23}\alpha_2^{cs} + C_{33}\alpha_3^{cs})\Delta X$$
$$\sigma_{23} = C_{44}\gamma_{23}$$
$$\sigma_{13} = C_{55}\gamma_{13}$$
$$\sigma_{12} = C_{66}\gamma_{12}$$

Defining

$$\beta_1 = C_{11}\alpha_1 + C_{12}\alpha_2 + C_{13}\alpha_3, \qquad \gamma_1 = C_{11}\alpha_1^{cs} + C_{12}\alpha_2^{cs} + C_{13}\alpha_3^{cs}$$
$$\beta_2 = C_{12}\alpha_1 + C_{22}\alpha_2 + C_{23}\alpha_3, \qquad \gamma_2 = C_{12}\alpha_1^{cs} + C_{22}\alpha_2^{cs} + C_{23}\alpha_3^{cs} \qquad \textbf{(B-152)}$$
$$\beta_3 = C_{13}\alpha_1 + C_{23}\alpha_2 + C_{33}\alpha_3, \qquad \gamma_3 = C_{13}\alpha_1^{cs} + C_{23}\alpha_2^{cs} + C_{33}\alpha_3^{cs}$$

We rewrite Equation (B-151) as

$$\sigma_{11} = C_{11}\epsilon_{11} + C_{12}\epsilon_{22} + C_{13}\epsilon_{33} - \beta_1\Delta T - \gamma_1\Delta X$$

$$\sigma_{22} = C_{12}\epsilon_{11} + C_{22}\epsilon_{22} + C_{23}\epsilon_{33} - \beta_2\Delta T - \gamma_2\Delta X$$

$$\sigma_{33} = C_{13}\epsilon_{11} + C_{23}\epsilon_{22} + C_{33}\epsilon_{33} - \beta_3\Delta T - \gamma_3\Delta X \qquad \textbf{(B-153)}$$

$$\sigma_{23} = C_{44}\gamma_{23}$$

$$\sigma_{13} = C_{55}\gamma_{13}$$

$$\sigma_{12} = C_{66}\gamma_{12}$$

Considering Equation (B-153), we may generalize Equation (4-50) as the thermo-viscoelastic (TVE) constitutive relations for an orthotropic material as

$$\begin{aligned}\sigma_{11} = {} & C_{11_e}\epsilon_{11} + C_{12_e}\epsilon_{22} + C_{13_e}\epsilon_{33} - \beta_{1_e}\Delta T - \gamma_{1_e}\Delta X \\ & + a_F\int_0^{\xi} \Delta C_{11}(\xi-\xi')\frac{d\epsilon_{11}}{d\xi'}d\xi' + a_F\int_0^{\xi} \Delta C_{12}(\xi-\xi')\frac{d\epsilon_{22}}{d\xi'}d\xi' \\ & + a_F\int_0^{\xi} \Delta C_{13}(\xi-\xi')\frac{d\epsilon_{33}}{d\xi'}d\xi' - a_F\int_0^{\xi} \Delta\beta_1(\xi-\xi')\frac{d\left(\frac{\Delta T}{a_F}\right)}{d\xi'}d\xi' \\ & - a_F\int_0^{\xi} \Delta\gamma_1(\xi-\xi')\frac{d\left(\frac{\Delta X}{a_F}\right)}{d\xi'}d\xi'\end{aligned} \qquad \textbf{(B-154)}$$

$$\sigma_{22} = C_{12_e}\epsilon_{11} + C_{22_e}\epsilon_{22} + C_{23_e}\epsilon_{33} - \beta_{2_e}\Delta T - \gamma_{2_e}\Delta X$$

$$+ a_F \int_0^{\xi} \Delta C_{12}(\xi - \xi') \frac{d\epsilon_{11}}{d\xi'} d\xi' + a_F \int_0^{\xi} \Delta C_{22}(\xi - \xi') \frac{d\epsilon_{22}}{d\xi'} d\xi'$$

$$+ a_F \int_0^{\xi} \Delta C_{23}(\xi - \xi') \frac{d\epsilon_{33}}{d\xi'} d\xi' - a_F \int_0^{\xi} \Delta \beta_2(\xi - \xi') \frac{d\left(\frac{\Delta T}{a_F}\right)}{d\xi'} d\xi' \quad \textbf{(B-155)}$$

$$- a_F \int_0^{\xi} \Delta \gamma_2(\xi - \xi') \frac{d\left(\frac{\Delta X}{a_F}\right)}{d\xi'} d\xi'$$

$$\sigma_{33} = C_{13_e}\epsilon_{11} + C_{23_e}\epsilon_{22} + C_{33_e}\epsilon_{33} - \beta_{3_e}\Delta T - \gamma_{3_e}\Delta X$$

$$+ a_F \int_0^{\xi} \Delta C_{13}(\xi - \xi') \frac{d\epsilon_{11}}{d\xi'} d\xi' + a_F \int_0^{\xi} \Delta C_{23}(\xi - \xi') \frac{d\epsilon_{22}}{d\xi'} d\xi'$$

$$+ a_F \int_0^{\xi} \Delta C_{33}(\xi - \xi') \frac{d\epsilon_{33}}{d\xi'} d\xi' - a_F \int_0^{\xi} \Delta \beta_3(\xi - \xi') \frac{d\left(\frac{\Delta T}{a_F}\right)}{d\xi'} d\xi' \quad \textbf{(B-156)}$$

$$- a_F \int_0^{\xi} \Delta \gamma_3(\xi - \xi') \frac{d\left(\frac{\Delta X}{a_F}\right)}{d\xi'} d\xi'$$

$$\sigma_{23} = C_{44_e}\gamma_{23} + a_F \int_0^{\xi} \Delta C_{44}(\xi - \xi') \frac{d\gamma_{23}}{d\xi'} d\xi' \quad \textbf{(B-157)}$$

$$\sigma_{13} = C_{55_e}\gamma_{13} + a_F \int_0^{\xi} \Delta C_{55}(\xi - \xi') \frac{d\gamma_{13}}{d\xi'} d\xi' \quad \textbf{(B-158)}$$

$$\sigma_{12} = C_{66_e}\gamma_{12} + a_F \int_0^{\xi} \Delta C_{66}(\xi - \xi') \frac{d\gamma_{12}}{d\xi'} d\xi' \quad \textbf{(B-159)}$$

Next we approximate $C_{ij}'s, \beta_i's$ and $\gamma_i's$ by Prony series

$$C_{ij}(\xi) = C_{ij_e} + \sum_{k=1}^{N_{C_{ij}}} C_{ij_k} e^{-\frac{\xi}{\tau_{C_{ijk}}}},$$

$$\beta_i(\xi) = \beta_{i_e} + \sum_{k=1}^{N_{\beta_i}} \beta_{i_k} e^{-\frac{\xi}{\tau_{\beta_i k}}}, \qquad \textbf{(B-160)}$$

$$\gamma_i(\xi) = \gamma_{i_e} + \sum_{k=1}^{N_{\gamma_i}} \gamma_{i_k} e^{-\frac{\xi}{\tau_{\gamma_i k}}}$$

Substituting from Equation (B-160) into Equations (B-154) to (B-159) results in

$$\begin{aligned}
\sigma_{11} = {} & C_{11_e}\epsilon_{11} + C_{12_e}\epsilon_{22} + C_{13_e}\epsilon_{33} - \beta_{1_e}\Delta T - \gamma_{1_e}\Delta X \\
& + \sum_{i=1}^{N_{C_{11}}} \left(a_F \int_0^{\xi} C_{11_i} e^{-\frac{\xi}{\tau_{C_{11}i}}} \frac{d\epsilon_{11}}{d\xi'} d\xi' \right) \\
& + \sum_{i=1}^{N_{C_{12}}} \left(a_F \int_0^{\xi} C_{12_i} e^{-\frac{\xi}{\tau_{C_{12}i}}} \frac{d\epsilon_{22}}{d\xi'} d\xi' \right) \\
& + \sum_{i=1}^{N_{C_{13}}} \left(a_F \int_0^{\xi} C_{13_i} e^{-\frac{\xi}{\tau_{C_{13}i}}} \frac{d\epsilon_{33}}{d\xi'} d\xi' \right) \qquad \textbf{(B-161)} \\
& - \sum_{i=1}^{N_{\beta_1}} \left(a_F \int_0^{\xi} \beta_{1_i} e^{-\frac{\xi}{\tau_{\beta_1}i}} \frac{d\left(\frac{\Delta T}{a_F}\right)}{d\xi'} d\xi' \right) \\
& - \sum_{i=1}^{N_{\gamma_1}} \left(a_F \int_0^{\xi} \gamma_{1_i} e^{-\frac{\xi}{\tau_{\gamma_1}i}} \frac{d\left(\frac{\Delta X}{a_F}\right)}{d\xi'} d\xi' \right)
\end{aligned}$$

$$\sigma_{22} = C_{12_e}\epsilon_{11} + C_{22_e}\epsilon_{22} + C_{23_e}\epsilon_{33} - \beta_{2_e}\Delta T - \gamma_{2_e}\Delta X$$

$$+ \sum_{i=1}^{N_{C_{12}}} \left(a_F \int_0^{\xi} C_{12_i} e^{-\frac{\xi}{\tau_{C_{12}i}}} \frac{d\epsilon_{11}}{d\xi'} d\xi' \right)$$

$$+ \sum_{i=1}^{N_{C_{22}}} \left(a_F \int_0^{\xi} C_{22_i} e^{-\frac{\xi}{\tau_{C_{22}i}}} \frac{d\epsilon_{22}}{d\xi'} d\xi' \right)$$

$$+ \sum_{i=1}^{N_{C_{23}}} \left(a_F \int_0^{\xi} C_{23_i} e^{-\frac{\xi}{\tau_{C_{23}i}}} \frac{d\epsilon_{33}}{d\xi'} d\xi' \right) \qquad \textbf{(B-162)}$$

$$- \sum_{i=1}^{N_{\beta_2}} \left(a_F \int_0^{\xi} \beta_{2_i} e^{-\frac{\xi}{\tau_{\beta_2}i}} \frac{d\left(\frac{\Delta T}{a_F}\right)}{d\xi'} d\xi' \right)$$

$$- \sum_{i=1}^{N_{\gamma_2}} \left(a_F \int_0^{\xi} \gamma_{2_i} e^{-\frac{\xi}{\tau_{\gamma_2}i}} \frac{d\left(\frac{\Delta X}{a_F}\right)}{d\xi'} d\xi' \right)$$

$$\sigma_{33} = C_{13_e}\epsilon_{11} + C_{23_e}\epsilon_{22} + C_{33_e}\epsilon_{33} - \beta_{3_e}\Delta T - \gamma_{3_e}\Delta X$$
$$+ \sum_{i=1}^{N_{C_{13}}} \left(a_F \int_0^{\xi} C_{13_i} e^{-\frac{\xi}{\tau_{C_{13}i}}} \frac{d\epsilon_{11}}{d\xi'} d\xi' \right)$$
$$+ \sum_{i=1}^{N_{C_{23}}} \left(a_F \int_0^{\xi} C_{23_i} e^{-\frac{\xi}{\tau_{C_{23}i}}} \frac{d\epsilon_{22}}{d\xi'} d\xi' \right)$$
$$+ \sum_{i=1}^{N_{C_{33}}} \left(a_F \int_0^{\xi} C_{33_i} e^{-\frac{\xi}{\tau_{C_{33}i}}} \frac{d\epsilon_{33}}{d\xi'} d\xi' \right) \quad \textbf{(B-163)}$$
$$- \sum_{i=1}^{N_{\beta_3}} \left(a_F \int_0^{\xi} \beta_{3_i} e^{-\frac{\xi}{\tau_{\beta_3}i}} \frac{d\left(\frac{\Delta T}{a_F}\right)}{d\xi'} d\xi' \right)$$
$$- \sum_{i=1}^{N_{\gamma_3}} \left(a_F \int_0^{\xi} \gamma_{3_i} e^{-\frac{\xi}{\tau_{\gamma_3}i}} \frac{d\left(\frac{\Delta X}{a_F}\right)}{d\xi'} d\xi' \right)$$

$$\sigma_{23} = C_{44_e}\gamma_{23} + \sum_{i=1}^{N_{C_{44}}} \left(a_F \int_0^{\xi} C_{44_i} e^{-\frac{\xi}{\tau_{C_{44}i}}} \frac{d\gamma_{23}}{d\xi'} d\xi' \right) \quad \textbf{(B-164)}$$

$$\sigma_{13} = C_{55_e}\gamma_{13} + \sum_{i=1}^{N_{C_{55}}} \left(a_F \int_0^{\xi} C_{55_i} e^{-\frac{\xi}{\tau_{C_{55}i}}} \frac{d\gamma_{13}}{d\xi'} d\xi' \right) \quad \textbf{(B-165)}$$

$$\sigma_{12} = C_{66_e}\gamma_{12} + \sum_{i=1}^{N_{C_{66}}} \left(a_F \int_0^{\xi} C_{66_i} e^{-\frac{\xi}{\tau_{C_{66}i}}} \frac{d\gamma_{12}}{d\xi'} d\xi' \right) \quad \textbf{(B-166)}$$

Now we define the state variables as follows

$$q_{C_{11}i}^{11}(\xi) = a_F \int_0^{\xi} \left(C_{11_i} e^{-\frac{\xi-\xi'}{\tau_{C_{11}i}}} \frac{d\epsilon_{11}}{d\xi'} \right) d\xi', \qquad i = 1,2 \dots, N_{C_{11}} \quad \textbf{(B-167)}$$

$$q_{C_{12}i}^{22}(\xi) = a_F \int_0^{\xi} \left(C_{12_i} e^{-\frac{\xi-\xi'}{\tau_{C_{12}i}}} \frac{d\epsilon_{22}}{d\xi'} \right) d\xi', \qquad i = 1,2 \dots, N_{C_{12}} \quad \textbf{(B-168)}$$

$$q_{C_{13}i}^{33}(\xi) = a_F \int_0^{\xi} \left(C_{13_i} e^{-\frac{\xi-\xi'}{\tau_{C_{13}i}}} \frac{d\epsilon_{33}}{d\xi'} \right) d\xi', \qquad i = 1,2 \dots, N_{C_{13}} \quad \textbf{(B-169)}$$

$$q_{C_{12}i}^{11}(\xi) = a_F \int_0^{\xi} \left(C_{12_i} e^{-\frac{\xi-\xi'}{\tau_{C_{12}i}}} \frac{d\epsilon_{11}}{d\xi'} \right) d\xi', \qquad i = 1,2 \dots, N_{C_{12}} \quad \textbf{(B-170)}$$

$$q_{C_{22}i}^{22}(\xi) = a_F \int_0^{\xi} \left(C_{22_i} e^{-\frac{\xi-\xi'}{\tau_{C_{22}i}}} \frac{d\epsilon_{22}}{d\xi'} \right) d\xi', \qquad i = 1,2 \dots, N_{C_{22}} \quad \textbf{(B-171)}$$

$$q_{C_{23}i}^{33}(\xi) = a_F \int_0^{\xi} \left(C_{23_i} e^{-\frac{\xi-\xi'}{\tau_{C_{23}i}}} \frac{d\epsilon_{33}}{d\xi'} \right) d\xi', \qquad i = 1,2 \dots, N_{C_{23}} \quad \textbf{(B-172)}$$

$$q_{C_{13}i}^{11}(\xi) = a_F \int_0^{\xi} \left(C_{13_i} e^{-\frac{\xi-\xi'}{\tau_{C_{13}i}}} \frac{d\epsilon_{11}}{d\xi'} \right) d\xi', \qquad i = 1,2 \dots, N_{C_{13}} \quad \textbf{(B-173)}$$

$$q_{C_{23}i}^{22}(\xi) = a_F \int_0^{\xi} \left(C_{23_i} e^{-\frac{\xi-\xi'}{\tau_{C_{23}i}}} \frac{d\epsilon_{22}}{d\xi'} \right) d\xi', \qquad i = 1,2 \dots, N_{C_{23}} \quad \textbf{(B-174)}$$

$$q_{C_{33}i}^{33}(\xi) = a_F \int_0^{\xi} \left(C_{33_i} e^{-\frac{\xi-\xi'}{\tau_{C_{33}i}}} \frac{d\epsilon_{33}}{d\xi'} \right) d\xi', \qquad i = 1,2 \dots, N_{C_{33}} \quad \textbf{(B-175)}$$

$$q_{C_{44}i}^{23}(\xi) = a_F \int_0^{\xi} \left(C_{44_i} e^{-\frac{\xi-\xi'}{\tau_{C_{44}i}}} \frac{d\gamma_{23}}{d\xi'} \right) d\xi', \qquad i = 1,2 \dots, N_{C_{44}} \quad \textbf{(B-176)}$$

$$q_{C_{55}i}^{13}(\xi) = a_F \int_0^{\xi} \left(C_{55_i} e^{-\frac{\xi-\xi'}{\tau_{C_{55}i}}} \frac{d\gamma_{13}}{d\xi'} \right) d\xi', \qquad i = 1,2 \dots, N_{C_{55}} \quad \textbf{(B-177)}$$

$$q_{C_{66}i}^{12}(\xi) = a_F \int_0^{\xi} \left(C_{66_i} e^{-\frac{\xi-\xi'}{\tau_{C_{66}i}}} \frac{d\gamma_{12}}{d\xi'} \right) d\xi', \qquad i = 1,2 \dots, N_{C_{66}} \quad \textbf{(B-178)}$$

$$q_{\beta_{1_i}}(\xi) = a_F \int_0^{\xi} \beta_{1_i} e^{-\frac{\xi}{\tau_{\beta_1 i}}} \frac{d\left(\frac{\Delta T}{a_F}\right)}{d\xi'} d\xi', \qquad i = 1,2 \dots, N_{\beta_1} \quad \textbf{(B-179)}$$

$$q_{\beta_{2_i}}(\xi) = a_F \int_0^{\xi} \beta_{2_i} e^{-\frac{\xi}{\tau_{\beta_2 i}}} \frac{d\left(\frac{\Delta T}{a_F}\right)}{d\xi'} d\xi', \qquad i = 1,2 \dots, N_{\beta_2} \quad \textbf{(B-180)}$$

$$q_{\beta_{3_i}}(\xi) = a_F \int_0^{\xi} \beta_{3_i} e^{-\frac{\xi}{\tau_{\beta_3 i}}} \frac{d\left(\frac{\Delta T}{a_F}\right)}{d\xi'} d\xi', \qquad i = 1,2 \dots, N_{\beta_3} \quad \textbf{(B-181)}$$

$$q_{\gamma_{1_i}}(\xi) = a_F \int_0^{\xi} \gamma_{1_i} e^{-\frac{\xi}{\tau_{\gamma_1 i}}} \frac{d\left(\frac{\Delta T}{a_F}\right)}{d\xi'} d\xi', \qquad i = 1,2 \dots, N_{\gamma_1} \quad \textbf{(B-182)}$$

$$q_{\gamma_{2_i}}(\xi) = a_F \int_0^{\xi} \gamma_{2_i} e^{-\frac{\xi}{\tau_{\gamma_2 i}}} \frac{d\left(\frac{\Delta T}{a_F}\right)}{d\xi'} d\xi', \qquad i = 1,2 \dots, N_{\gamma_2} \quad \textbf{(B-183)}$$

$$q_{\gamma_{3_i}}(\xi) = a_F \int_0^{\xi} \gamma_{3_i} e^{-\frac{\xi}{\tau_{\gamma_3 i}}} \frac{d\left(\frac{\Delta T}{a_F}\right)}{d\xi'} d\xi', \qquad i = 1,2 \dots, N_{\gamma_3} \quad \textbf{(B-184)}$$

Calculating the derivative of each state variable in Equations (B-167) to (B-184) using Leibniz rule of differentiation we conclude

$$\frac{dq_{C_{11}i}^{11}(\xi)}{d\xi} + \frac{q_{C_{11}i}^{11}(\xi)}{\tau_{C_{11}i}} = a_F C_{11_i} \frac{d\epsilon_{11}}{d\xi}, \qquad i = 1,2 \dots, N_{C_{11}} \quad \textbf{(B-185)}$$

$$\frac{dq_{C_{12}i}^{22}(\xi)}{d\xi}+\frac{q_{C_{12}i}^{22}(\xi)}{\tau_{C_{12}i}}=a_F C_{12_i}\frac{d\epsilon_{22}}{d\xi},\qquad i=1,2\ldots,N_{C_{12}}\quad \textbf{(B-186)}$$

$$\frac{dq_{C_{13}i}^{33}(\xi)}{d\xi}+\frac{q_{C_{13}i}^{33}(\xi)}{\tau_{C_{13}i}}=a_F C_{13_i}\frac{d\epsilon_{33}}{d\xi},\qquad i=1,2\ldots,N_{C_{13}}\quad \textbf{(B-187)}$$

$$\frac{dq_{C_{12}i}^{11}(\xi)}{d\xi}+\frac{q_{C_{12}i}^{11}(\xi)}{\tau_{C_{12}i}}=a_F C_{12_i}\frac{d\epsilon_{11}}{d\xi},\qquad i=1,2\ldots,N_{C_{12}}\quad \textbf{(B-188)}$$

$$\frac{dq_{C_{22}i}^{22}(\xi)}{d\xi}+\frac{q_{C_{22}i}^{22}(\xi)}{\tau_{C_{22}i}}=a_F C_{22_i}\frac{d\epsilon_{22}}{d\xi},\qquad i=1,2\ldots,N_{C_{22}}\quad \textbf{(B-189)}$$

$$\frac{dq_{C_{23}i}^{33}(\xi)}{d\xi}+\frac{q_{C_{23}i}^{33}(\xi)}{\tau_{C_{23}i}}=a_F C_{23_i}\frac{d\epsilon_{33}}{d\xi},\qquad i=1,2\ldots,N_{C_{23}}\quad \textbf{(B-190)}$$

$$\frac{dq_{C_{13}i}^{11}(\xi)}{d\xi}+\frac{q_{C_{13}i}^{11}(\xi)}{\tau_{C_{13}i}}=a_F C_{13_i}\frac{d\epsilon_{11}}{d\xi},\qquad i=1,2\ldots,N_{C_{13}}\quad \textbf{(B-191)}$$

$$\frac{dq_{C_{23}i}^{22}(\xi)}{d\xi}+\frac{q_{C_{23}i}^{22}(\xi)}{\tau_{C_{23}i}}=a_F C_{23_i}\frac{d\epsilon_{22}}{d\xi},\qquad i=1,2\ldots,N_{C_{23}}\quad \textbf{(B-192)}$$

$$\frac{dq_{C_{33}i}^{33}(\xi)}{d\xi}+\frac{q_{C_{33}i}^{33}(\xi)}{\tau_{C_{33}i}}=a_F C_{33_i}\frac{d\epsilon_{33}}{d\xi},\qquad i=1,2\ldots,N_{C_{33}}\quad \textbf{(B-193)}$$

$$\frac{dq_{C_{44}i}^{23}(\xi)}{d\xi}+\frac{q_{C_{44}i}^{23}(\xi)}{\tau_{C_{44}i}}=a_F C_{44_i}\frac{d\gamma_{23}}{d\xi},\qquad i=1,2\ldots,N_{C_{44}}\quad \textbf{(B-194)}$$

$$\frac{dq_{C_{55}i}^{13}(\xi)}{d\xi}+\frac{q_{C_{55}i}^{13}(\xi)}{\tau_{C_{55}i}}=a_F C_{55_i}\frac{d\gamma_{13}}{d\xi},\qquad i=1,2\ldots,N_{C_{55}}\quad \textbf{(B-195)}$$

$$\frac{dq_{C_{66}i}^{12}(\xi)}{d\xi}+\frac{q_{C_{66}i}^{12}(\xi)}{\tau_{C_{66}i}}=a_F C_{66_i}\frac{d\gamma_{12}}{d\xi},\qquad i=1,2\ldots,N_{C_{66}}\quad \textbf{(B-196)}$$

$$\frac{dq_{\beta_{1_i}}(\xi)}{d\xi}+\frac{q_{\beta_{1_i}}(\xi)}{\tau_{\beta_1 i}}=\beta_{1_i}\frac{dT}{d\xi},\qquad i=1,2\ldots,N_{\beta_1}\quad \textbf{(B-197)}$$

$$\frac{dq_{\beta_{2_i}}(\xi)}{d\xi}+\frac{q_{\beta_{2_i}}(\xi)}{\tau_{\beta_2 i}}=\beta_{2_i}\frac{dT}{d\xi},\qquad i=1,2\ldots,N_{\beta_2}\quad \textbf{(B-198)}$$

$$\frac{dq_{\beta_{3_i}}(\xi)}{d\xi} + \frac{q_{\beta_{3_i}}(\xi)}{\tau_{\beta_3 i}} = \beta_{3_i}\frac{dT}{d\xi}, \qquad i = 1,2\ldots, N_{\beta_2} \quad \textbf{(B-199)}$$

$$\frac{dq_{\gamma_{1_i}}(\xi)}{d\xi} + \frac{q_{\gamma_{1_i}}(\xi)}{\tau_{\gamma_1 i}} = \gamma_{1_i}\frac{dX}{d\xi}, \qquad i = 1,2\ldots, N_{\gamma_1} \quad \textbf{(B-200)}$$

$$\frac{dq_{\gamma_{2_i}}(\xi)}{d\xi} + \frac{q_{\gamma_{2_i}}(\xi)}{\tau_{\gamma_2 i}} = \gamma_{2_i}\frac{dX}{d\xi}, \qquad i = 1,2\ldots, N_{\gamma_2} \quad \textbf{(B-201)}$$

$$\frac{dq_{\gamma_{3_i}}(\xi)}{d\xi} + \frac{q_{\gamma_{3_i}}(\xi)}{\tau_{\gamma_3 i}} = \gamma_{3_i}\frac{dX}{d\xi}, \qquad i = 1,2\ldots, N_{\gamma_3} \quad \textbf{(B-202)}$$

Using Equations (B-167) to (B-184) we rewrite Equations (B-161) to (B-166) as

$$\sigma_{11} = C_{11_e}\epsilon_{11} + C_{12_e}\epsilon_{22} + C_{13_e}\epsilon_{33} - \beta_{1_e}\Delta T - \gamma_{1_e}\Delta X + \sum_{i=1}^{N_{C_{11}}} q_{C_{11}i}^{11} + \sum_{i=1}^{N_{C_{12}}} q_{C_{12}i}^{22} + \sum_{i=1}^{N_{C_{13}}} q_{C_{13}i}^{33} - \sum_{i=1}^{N_{\beta_1}} q_{\beta_{1_i}} - \sum_{i=1}^{N_{\gamma_1}} q_{\gamma_{1_i}} \quad \textbf{(B-203)}$$

$$\sigma_{22} = C_{12_e}\epsilon_{11} + C_{22_e}\epsilon_{22} + C_{23_e}\epsilon_{33} - \beta_{2_e}\Delta T - \gamma_{2_e}\Delta X + \sum_{i=1}^{N_{C_{12}}} q_{C_{12}i}^{11} + \sum_{i=1}^{N_{C_{22}}} q_{C_{22}i}^{22} + \sum_{i=1}^{N_{C_{23}}} q_{C_{23}i}^{33} - \sum_{i=1}^{N_{\beta_2}} q_{\beta_{2_i}} - \sum_{i=1}^{N_{\gamma_2}} q_{\gamma_{2_i}} \quad \textbf{(B-204)}$$

$$\sigma_{33} = C_{13_e}\epsilon_{11} + C_{23_e}\epsilon_{22} + C_{33_e}\epsilon_{33} - \beta_{3_e}\Delta T - \gamma_{3_e}\Delta X + \sum_{i=1}^{N_{C_{13}}} q_{C_{13}i}^{11} + \sum_{i=1}^{N_{C_{23}}} q_{C_{23}i}^{22} + \sum_{i=1}^{N_{C_{33}}} q_{C_{33}i}^{33} - \sum_{i=1}^{N_{\beta_3}} q_{\beta_{3_i}} - \sum_{i=1}^{N_{\gamma_3}} q_{\gamma_{3_i}} \quad \textbf{(B-205)}$$

$$\sigma_{23} = C_{44_e}\gamma_{23} + \sum_{i=1}^{N_{C_{44}}} q_{C_{44}i}^{23} \qquad \textbf{(B-206)}$$

$$\sigma_{13} = C_{55_e}\gamma_{13} + \sum_{i=1}^{N_{C_{55}}} q_{C_{55}i}^{13} \qquad \textbf{(B-207)}$$

$$\sigma_{12} = C_{66_e}\gamma_{12} + \sum_{i=1}^{N_{C_{66}}} q_{C_{66}i}^{12} \qquad \textbf{(B-208)}$$

Finally, based on our discussions about hypo-elastic behaviour of the material in the glassy regime, Equations (B-203) to (B-208) are modified as

$$\dot{\sigma}_{11} = C_{11_e}\dot{\epsilon}_{11} + C_{12_e}\dot{\epsilon}_{22} + C_{13_e}\dot{\epsilon}_{33} - \beta_{1_e}\Delta\dot{T} - \gamma_{1_e}\Delta\dot{X} + \sum_{i=1}^{N_{C_{11}}} \dot{q}_{C_{11}i}^{11} + \sum_{i=1}^{N_{C_{12}}} \dot{q}_{C_{12}i}^{22} + \sum_{i=1}^{N_{C_{13}}} \dot{q}_{C_{13}i}^{33} - \sum_{i=1}^{N_{\beta_1}} \dot{q}_{\beta_{1}i} - \sum_{i=1}^{N_{\gamma_1}} \dot{q}_{\gamma_{1}i} \qquad \textbf{(B-209)}$$

$$\dot{\sigma}_{22} = C_{12_e}\dot{\epsilon}_{11} + C_{22_e}\dot{\epsilon}_{22} + C_{23_e}\dot{\epsilon}_{33} - \beta_{2_e}\Delta\dot{T} - \gamma_{2_e}\Delta\dot{X} + \sum_{i=1}^{N_{C_{12}}} \dot{q}_{C_{12}i}^{11} + \sum_{i=1}^{N_{C_{22}}} \dot{q}_{C_{22}i}^{22} + \sum_{i=1}^{N_{C_{23}}} \dot{q}_{C_{23}i}^{33} - \sum_{i=1}^{N_{\beta_2}} \dot{q}_{\beta_{2}i} - \sum_{i=1}^{N_{\gamma_2}} \dot{q}_{\gamma_{2}i} \qquad \textbf{(B-210)}$$

$$\dot{\sigma}_{33} = C_{13_e}\dot{\epsilon}_{11} + C_{23_e}\dot{\epsilon}_{22} + C_{33_e}\dot{\epsilon}_{33} - \beta_{3_e}\Delta\dot{T} - \gamma_{3_e}\Delta\dot{X} + \sum_{i=1}^{N_{C_{13}}} \dot{q}_{C_{13}i}^{11} + \sum_{i=1}^{N_{C_{23}}} \dot{q}_{C_{23}i}^{22} + \sum_{i=1}^{N_{C_{33}}} \dot{q}_{C_{33}i}^{33} - \sum_{i=1}^{N_{\beta_3}} \dot{q}_{\beta_{3}i} - \sum_{i=1}^{N_{\gamma_3}} \dot{q}_{\gamma_{3}i} \qquad \textbf{(B-211)}$$

$$\dot{\sigma}_{23} = C_{44_e}\dot{\gamma}_{23} + \sum_{i=1}^{N_{C_{44}}} \dot{q}_{C_{44}i}^{23} \qquad \textbf{(B-212)}$$

$$\dot{\sigma}_{13} = C_{55_e}\dot{\gamma}_{13} + \sum_{i=1}^{N_{C_{55}}} \dot{q}_{C_{55}i}^{13} \qquad \textbf{(B-213)}$$

$$\dot{\sigma}_{12} = C_{66_e}\dot{\gamma}_{12} + \sum_{i=1}^{N_{C_{66}}} \dot{q}_{C_{66}i}^{12} \qquad \textbf{(B-214)}$$

Next similar to the isotropic and transversely isotropic cases, we carry out the time integration of equations to prepare them for implementation in a UMAT.

Following a procedure similar to what we did for derivation of Equation (B-127), for state variables in Equations (B-167) to (B-184), and replacing $\tau_{C_{kl}i}, \tau_{\beta_k i}$ and $\tau_{\gamma_k i}$ by $a_T\tau_{C_{kl}i}, a_T\tau_{\beta_k i}$ and $a_T\tau_{\gamma_k i}$, respectively, we have

$$q_{C_{11}i}^{11}(t^n) = e^{-\frac{\Delta t^n}{a_T\tau_{C_{11}i}}} q_{C_{11}i}^{11}(t^{n-1}) + a_F C_{11_i} \Delta\epsilon_{11}{}^n \left(\frac{1 - e^{-\frac{\Delta t^n}{a_T\tau_{C_{11}i}}}}{\frac{\Delta t^n}{a_T\tau_{C_{11}i}}} \right), \qquad \textbf{(B-215)}$$

$$i = 1,2 \ldots, N_{C_{11}}$$

$$q_{C_{12}i}^{22}(t^n) = e^{-\frac{\Delta t^n}{a_T\tau_{C_{12}i}}} q_{C_{12}i}^{22}(t^{n-1}) + a_F C_{12_i} \Delta\epsilon_{22}{}^n \left(\frac{1 - e^{-\frac{\Delta t^n}{a_T\tau_{C_{12}i}}}}{\frac{\Delta t^n}{a_T\tau_{C_{12}i}}} \right), \qquad \textbf{(B-216)}$$

$$i = 1,2 \ldots, N_{C_{12}}$$

$$q_{C_{13}i}^{33}(t^n) = e^{-\frac{\Delta t^n}{a_T \tau_{C_{13}i}}} q_{C_{13}i}^{33}(t^{n-1}) + a_F C_{13_i} \Delta\epsilon_{33}{}^n \left(\frac{1 - e^{-\frac{\Delta t^n}{a_T \tau_{C_{13}i}}}}{\frac{\Delta t^n}{a_T \tau_{C_{13}i}}} \right), \quad \textbf{(B-217)}$$

$$i = 1,2 \ldots, N_{C_{13}}$$

$$q_{C_{12}i}^{11}(t^n) = e^{-\frac{\Delta t^n}{a_T \tau_{C_{12}i}}} q_{C_{12}i}^{11}(t^{n-1}) + a_F C_{12_i} \Delta\epsilon_{11}{}^n \left(\frac{1 - e^{-\frac{\Delta t^n}{a_T \tau_{C_{12}i}}}}{\frac{\Delta t^n}{a_T \tau_{C_{12}i}}} \right), \quad \textbf{(B-218)}$$

$$i = 1,2 \ldots, N_{C_{12}}$$

$$q_{C_{22}i}^{22}(t^n) = e^{-\frac{\Delta t^n}{a_T \tau_{C_{22}i}}} q_{C_{22}i}^{22}(t^{n-1}) + a_F C_{22_i} \Delta\epsilon_{22}{}^n \left(\frac{1 - e^{-\frac{\Delta t^n}{a_T \tau_{C_{22}i}}}}{\frac{\Delta t^n}{a_T \tau_{C_{22}i}}} \right), \quad \textbf{(B-219)}$$

$$i = 1,2 \ldots, N_{C_{22}}$$

$$q_{C_{23}i}^{33}(t^n) = e^{-\frac{\Delta t^n}{a_T \tau_{C_{23}i}}} q_{C_{23}i}^{33}(t^{n-1}) + a_F C_{23_i} \Delta\epsilon_{33}{}^n \left(\frac{1 - e^{-\frac{\Delta t^n}{a_T \tau_{C_{23}i}}}}{\frac{\Delta t^n}{a_T \tau_{C_{23}i}}} \right), \quad \textbf{(B-220)}$$

$$i = 1,2 \ldots, N_{C_{23}}$$

$$q_{C_{13}i}^{11}(t^n) = e^{-\frac{\Delta t^n}{a_T \tau_{C_{13}i}}} q_{C_{13}i}^{11}(t^{n-1}) + a_F C_{13_i} \Delta\epsilon_{11}{}^n \left(\frac{1 - e^{-\frac{\Delta t^n}{a_T \tau_{C_{13}i}}}}{\frac{\Delta t^n}{a_T \tau_{C_{13}i}}} \right), \quad \textbf{(B-221)}$$

$$i = 1,2 \ldots, N_{C_{13}}$$

$$q_{C_{23}i}^{22}(t^n) = e^{-\frac{\Delta t^n}{a_T \tau_{C_{23}i}}} q_{C_{23}i}^{22}(t^{n-1}) + a_F C_{23_i} \Delta\epsilon_{22}{}^n \left(\frac{1 - e^{-\frac{\Delta t^n}{a_T \tau_{C_{23}i}}}}{\frac{\Delta t^n}{a_T \tau_{C_{23}i}}} \right), \quad \textbf{(B-222)}$$

$$i = 1,2 \ldots, N_{C_{23}}$$

$$q_{C_{33}i}^{33}(t^n) = e^{-\frac{\Delta t^n}{a_T \tau_{C_{33}i}}} q_{C_{33}i}^{33}(t^{n-1}) + a_F C_{33_i} \Delta \epsilon_{33}{}^n \left(\frac{1 - e^{-\frac{\Delta t^n}{a_T \tau_{C_{33}i}}}}{\frac{\Delta t^n}{a_T \tau_{C_{33}i}}} \right), \quad \textbf{(B-223)}$$

$$i = 1,2 \dots, N_{C_{33}}$$

$$q_{C_{44}i}^{23}(t^n) = e^{-\frac{\Delta t^n}{a_T \tau_{C_{44}i}}} q_{C_{44}i}^{23}(t^{n-1}) + a_F C_{44_i} \Delta \gamma_{23}{}^n \left(\frac{1 - e^{-\frac{\Delta t^n}{a_T \tau_{C_{44}i}}}}{\frac{\Delta t^n}{a_T \tau_{C_{44}i}}} \right), \quad \textbf{(B-224)}$$

$$i = 1,2 \dots, N_{C_{44}}$$

$$q_{C_{55}i}^{13}(t^n) = e^{-\frac{\Delta t^n}{a_T \tau_{C_{55}i}}} q_{C_{55}i}^{13}(t^{n-1}) + a_F C_{55_i} \Delta \gamma_{13}{}^n \left(\frac{1 - e^{-\frac{\Delta t^n}{a_T \tau_{C_{55}i}}}}{\frac{\Delta t^n}{a_T \tau_{C_{55}i}}} \right), \quad \textbf{(B-225)}$$

$$i = 1,2 \dots, N_{C_{55}}$$

$$q_{C_{66}i}^{12}(t^n) = e^{-\frac{\Delta t^n}{a_T \tau_{C_{66}i}}} q_{C_{66}i}^{12}(t^{n-1}) + a_F C_{66_i} \Delta \gamma_{12}{}^n \left(\frac{1 - e^{-\frac{\Delta t^n}{a_T \tau_{C_{66}i}}}}{\frac{\Delta t^n}{a_T \tau_{C_{66}i}}} \right), \quad \textbf{(B-226)}$$

$$i = 1,2 \dots, N_{C_{66}}$$

$$q_{\beta_{1_i}}(t^n) = e^{-\frac{\Delta t^n}{a_T \tau_{\beta_1 i}}} q_{\beta_{1_i}}(t^{n-1}) + \beta_{1_i} \Delta T^n \left(\frac{1 - e^{-\frac{\Delta t^n}{a_T \tau_{\beta_1 i}}}}{\frac{\Delta t^n}{a_T \tau_{\beta_1 i}}} \right), i = 1,2 \dots, N_{\beta_1} \quad \textbf{(B-227)}$$

$$q_{\beta_{2_i}}(t^n) = e^{-\frac{\Delta t^n}{a_T \tau_{\beta_2 i}}} q_{\beta_{2_i}}(t^{n-1}) + \beta_{2_i} \Delta T^n \left(\frac{1 - e^{-\frac{\Delta t^n}{a_T \tau_{\beta_2 i}}}}{\frac{\Delta t^n}{a_T \tau_{\beta_2 i}}} \right), i = 1,2 \dots, N_{\beta_2} \quad \textbf{(B-228)}$$

$$q_{\beta_{3_i}}(t^n) = e^{-\frac{\Delta t^n}{a_T \tau_{\beta_3 i}}} q_{\beta_{3_i}}(t^{n-1}) + \beta_{3_i} \Delta T^n \left(\frac{1 - e^{-\frac{\Delta t^n}{a_T \tau_{\beta_3 i}}}}{\frac{\Delta t^n}{a_T \tau_{\beta_3 i}}} \right), i = 1,2 \dots, N_{\beta_3} \quad \textbf{(B-229)}$$

$$q_{\gamma_{1_i}}(t^n) = e^{-\frac{\Delta t^n}{a_T \tau_{\gamma_1 i}}} q_{\gamma_{1_i}}(t^{n-1}) + \gamma_{1_i} \Delta T^n \left(\frac{1 - e^{-\frac{\Delta t^n}{a_T \tau_{\gamma_1 i}}}}{\frac{\Delta t^n}{a_T \tau_{\gamma_1 i}}} \right), i = 1,2 \dots, N_{\gamma_1} \qquad \textbf{(B-230)}$$

$$q_{\gamma_{2_i}}(t^n) = e^{-\frac{\Delta t^n}{a_T \tau_{\gamma_2 i}}} q_{\gamma_{2_i}}(t^{n-1}) + \gamma_{2_i} \Delta T^n \left(\frac{1 - e^{-\frac{\Delta t^n}{a_T \tau_{\gamma_2 i}}}}{\frac{\Delta t^n}{a_T \tau_{\gamma_2 i}}} \right), i = 1,2 \dots, N_{\gamma_2} \qquad \textbf{(B-231)}$$

$$q_{\gamma_{3_i}}(t^n) = e^{-\frac{\Delta t^n}{a_T \tau_{\gamma_3 i}}} q_{\gamma_{3_i}}(t^{n-1}) + \gamma_{3_i} \Delta T^n \left(\frac{1 - e^{-\frac{\Delta t^n}{a_T \tau_{\gamma_3 i}}}}{\frac{\Delta t^n}{a_T \tau_{\gamma_3 i}}} \right), i = 1,2 \dots, N_{\gamma_3} \qquad \textbf{(B-232)}$$

Next we integrate both sides of Equation (B-209) from t^{n-1} to t^n

$$\begin{aligned} \int_{t^{n-1}}^{t^n} \frac{d\sigma_{11}}{dt'} dt' = \int_{t^{n-1}}^{t^n} \Bigg[& C_{11_e} \frac{d\epsilon_{11}}{dt'} + C_{12_e} \frac{d\epsilon_{22}}{dt'} + C_{13_e} \frac{d\epsilon_{33}}{dt'} - \beta_{1_e} \frac{d\Delta T}{dt'} \\ & - \gamma_{1_e} \frac{d\Delta X}{dt'} + \sum_{i=1}^{N_{C_{11}}} \frac{dq_{C_{11}i}^{11}}{dt'} + \sum_{i=1}^{N_{C_{12}}} \frac{dq_{C_{12}i}^{22}}{dt'} + \sum_{i=1}^{N_{C_{13}}} \frac{dq_{C_{13}i}^{33}}{dt'} \\ & - \sum_{i=1}^{N_{\beta_1}} \frac{dq_{\beta_{1_i}}}{dt'} - \sum_{i=1}^{N_{\gamma_1}} \frac{dq_{\gamma_{1_i}}}{dt'} \Bigg] dt' \end{aligned} \qquad \textbf{(B-233)}$$

Now we assume $\frac{d\epsilon_{11}}{dt}, \frac{d\epsilon_{22}}{dt}, \frac{d\epsilon_{33}}{dt}, \frac{d\Delta T}{dt}$ and $\frac{d\Delta X}{dt}$ are constant in the interval $[t^{n-1}, t^n]$ and replace them with $\frac{\Delta \epsilon_{11}{}^n}{\Delta t^n}, \frac{\Delta \epsilon_{22}{}^n}{\Delta t^n}, \frac{\Delta \epsilon_{33}{}^n}{\Delta t^n}, \frac{\Delta T^n}{\Delta t^n}$ and $\frac{\Delta X^n}{\Delta t^n}$, respectively. Also we approximate the integrals using Simpson's rule. Equation (B-233) is rewritten as

$$\sigma_{11}{}^{n} = \sigma_{11}{}^{n-1} + \Delta\epsilon_{11}{}^{n}\left(\frac{C_{11_e}{}^{n} + C_{11_e}{}^{n-1}}{2}\right) + \Delta\epsilon_{22}{}^{n}\left(\frac{C_{12_e}{}^{n} + C_{12_e}{}^{n-1}}{2}\right)$$
$$+ \Delta\epsilon_{33}{}^{n}\left(\frac{C_{13_e}{}^{n} + C_{13_e}{}^{n-1}}{2}\right) - \Delta T^{n}\left(\frac{\beta_{1_e}{}^{n} + \beta_{1_e}{}^{n-1}}{2}\right)$$
$$- \Delta X^{n}\left(\frac{\gamma_{1_e}{}^{n} + \gamma_{1_e}{}^{n-1}}{2}\right) + \sum_{i=1}^{N_{C_{11}}}\left(q_{C_{11}i}^{11}{}^{n} - q_{C_{11}i}^{11}{}^{n-1}\right) \qquad \textbf{(B-234)}$$
$$+ \sum_{i=1}^{N_{C_{12}}}\left(q_{C_{12}i}^{22}{}^{n} - q_{C_{12}i}^{22}{}^{n-1}\right) + \sum_{i=1}^{N_{C_{13}}}\left(q_{C_{13}i}^{33}{}^{n} - q_{C_{13}i}^{33}{}^{n-1}\right)$$
$$- \sum_{i=1}^{N_{\beta_1}}\left(q_{\beta_{1_i}}{}^{n} - q_{\beta_{1_i}}{}^{n-1}\right) - \sum_{i=1}^{N_{\gamma_1}}\left(q_{\gamma_{1_i}}{}^{n} - q_{\gamma_{1_i}}{}^{n-1}\right)$$

Similarly for all other stress components we will have

$$\sigma_{22}{}^{n} = \sigma_{22}{}^{n-1} + \Delta\epsilon_{11}{}^{n}\left(\frac{C_{12_e}{}^{n} + C_{12_e}{}^{n-1}}{2}\right) + \Delta\epsilon_{22}{}^{n}\left(\frac{C_{22_e}{}^{n} + C_{22_e}{}^{n-1}}{2}\right)$$
$$+ \Delta\epsilon_{33}{}^{n}\left(\frac{C_{23_e}{}^{n} + C_{23_e}{}^{n-1}}{2}\right) - \Delta T^{n}\left(\frac{\beta_{2_e}{}^{n} + \beta_{2_e}{}^{n-1}}{2}\right)$$
$$- \Delta X^{n}\left(\frac{\gamma_{2_e}{}^{n} + \gamma_{2_e}{}^{n-1}}{2}\right) + \sum_{i=1}^{N_{C_{12}}}\left(q_{C_{12}i}^{11}{}^{n} - q_{C_{12}i}^{11}{}^{n-1}\right) \qquad \textbf{(B-235)}$$
$$+ \sum_{i=1}^{N_{C_{22}}}\left(q_{C_{22}i}^{22}{}^{n} - q_{C_{22}i}^{22}{}^{n-1}\right) + \sum_{i=1}^{N_{C_{23}}}\left(q_{C_{23}i}^{33}{}^{n} - q_{C_{23}i}^{33}{}^{n-1}\right)$$
$$- \sum_{i=1}^{N_{\beta_2}}\left(q_{\beta_{2_i}}{}^{n} - q_{\beta_{2_i}}{}^{n-1}\right) - \sum_{i=1}^{N_{\gamma_2}}\left(q_{\gamma_{2_i}}{}^{n} - q_{\gamma_{2_i}}{}^{n-1}\right)$$

$$\sigma_{33}{}^{n} = \sigma_{33}{}^{n-1} + \Delta\epsilon_{11}{}^{n}\left(\frac{C_{13_e}{}^{n} + C_{13_e}{}^{n-1}}{2}\right) + \Delta\epsilon_{22}{}^{n}\left(\frac{C_{23_e}{}^{n} + C_{23_e}{}^{n-1}}{2}\right)$$
$$+ \Delta\epsilon_{33}{}^{n}\left(\frac{C_{33_e}{}^{n} + C_{33_e}{}^{n-1}}{2}\right) - \Delta T^{n}\left(\frac{\beta_{3_e}{}^{n} + \beta_{3_e}{}^{n-1}}{2}\right)$$
$$- \Delta X^{n}\left(\frac{\gamma_{3_e}{}^{n} + \gamma_{3_e}{}^{n-1}}{2}\right) + \sum_{i=1}^{N_{C_{13}}}\left(q_{C_{13}i}^{11}{}^{n} - q_{C_{13}i}^{11}{}^{n-1}\right) \quad \textbf{(B-236)}$$
$$+ \sum_{i=1}^{N_{C_{23}}}\left(q_{C_{23}i}^{22}{}^{n} - q_{C_{23}i}^{22}{}^{n-1}\right) + \sum_{i=1}^{N_{C_{33}}}\left(q_{C_{33}i}^{33}{}^{n} - q_{C_{33}i}^{33}{}^{n-1}\right)$$
$$- \sum_{i=1}^{N_{\beta_3}}\left(q_{\beta_{3_i}}{}^{n} - q_{\beta_{3_i}}{}^{n-1}\right) - \sum_{i=1}^{N_{\gamma_3}}\left(q_{\gamma_{3_i}}{}^{n} - q_{\gamma_{3_i}}{}^{n-1}\right)$$

$$\sigma_{23}{}^{n} = \sigma_{23}{}^{n-1} + \Delta\gamma_{23}{}^{n}\left(\frac{C_{44_e}{}^{n} + C_{44_e}{}^{n-1}}{2}\right) + \sum_{i=1}^{N_{C_{44}}}\left(q_{C_{44}i}^{23}{}^{n} - q_{C_{44}i}^{23}{}^{n-1}\right) \quad \textbf{(B-237)}$$

$$\sigma_{13}{}^{n} = \sigma_{13}{}^{n-1} + \Delta\gamma_{13}{}^{n}\left(\frac{C_{55_e}{}^{n} + C_{55_e}{}^{n-1}}{2}\right) + \sum_{i=1}^{N_{C_{55}}}\left(q_{C_{55}i}^{13}{}^{n} - q_{C_{55}i}^{13}{}^{n-1}\right) \quad \textbf{(B-238)}$$

$$\sigma_{12}{}^{n} = \sigma_{12}{}^{n-1} + \Delta\gamma_{12}{}^{n}\left(\frac{C_{66_e}{}^{n} + C_{66_e}{}^{n-1}}{2}\right) + \sum_{i=1}^{N_{C_{66}}}\left(q_{C_{66}i}^{12}{}^{n} - q_{C_{66}i}^{12}{}^{n-1}\right) \quad \textbf{(B-239)}$$

Using Equations (B-215) to (B-232) and Equations (B-234) to (B-239), we can find stress components at each time step in terms of their peers at previous time step and other parameters. Now we consider Equations (B-215) to (B-232) for some extreme cases of relaxation times. From Equation (B-215) we have

$$\lim_{a_T\tau_{C_{11}i}\to 0} q_{C_{11}i}^{11}(t^n) = 0 \qquad ,i = 1,2\ldots,N_{C_{11}} \quad \textbf{(B-240)}$$

Similarly, for all other state variables, for very short relaxation times we may write

$$\lim_{a_T\tau_{C_{kl}i}\to 0} q^{ms}_{C_{kl}i}(t^n) = 0 \qquad ,i = 1,2\dots,N_{C_{kl}} \quad \textbf{(B-241)}$$

Equation (B-241) implies that when relaxation times are very short, the stresses in Maxwell elements relax very fast.

On the other hand, for very long relaxation times, i.e. when $a_T\tau_{C_{11}i} \to \infty$, $\frac{1-e^{-\frac{\Delta t^n}{a_T\tau_{C_{11}i}}}}{\frac{\Delta t^n}{a_T\tau_{C_{11}i}}}$ is indeterminate. Using L'Hospital's rule we have

$$\lim_{a_T\tau_{C_{11}i}\to\infty} \frac{1-e^{-\frac{\Delta t^n}{a_T\tau_{C_{11}i}}}}{\frac{\Delta t^n}{a_T\tau_{C_{11}i}}} = \lim_{x\to 0}\frac{1-e^{-x}}{x} = \lim_{x\to 0}\frac{e^{-x}}{1} = 1 \quad \textbf{(B-242)}$$

and therefore,

$$\lim_{a_T\tau_{C_{11}i}\to\infty} q^{11}_{C_{11}i}(t^n) = q^{11}_{C_{11}i}(t^{n-1}) + a_F C_{11_i}\Delta\epsilon_{11}{}^n, \qquad i = 1,2\dots,N_{C_{11}} \quad \textbf{(B-243)}$$

Similarly for all other state variables

$$\lim_{a_T\tau_{C_{kl}i}\to\infty} q^{ms}_{C_{kl}i}(t^n) = q^{ms}_{C_{kl}i}(t^{n-1}) + a_F C_{kl_i}\Delta\epsilon_{ms}{}^n, \qquad i = 1,2\dots,N_{C_{kl}} \quad \textbf{(B-244)}$$

As an alternative way of fixing the indeterminacy for large relaxation times, we consider $\frac{1-e^{-x}}{x}$ and expand a Taylor series around $x = 0$

$$\frac{1-e^{-x}}{x} = 1 - \frac{1}{2}x + \frac{1}{6}x^2 + O(x^3) \qquad \textbf{(B-245)}$$

From the plots in Figure B-1we observe that for $x < 0.2$, the Taylor expansion in Equation (B-245) is accurate.

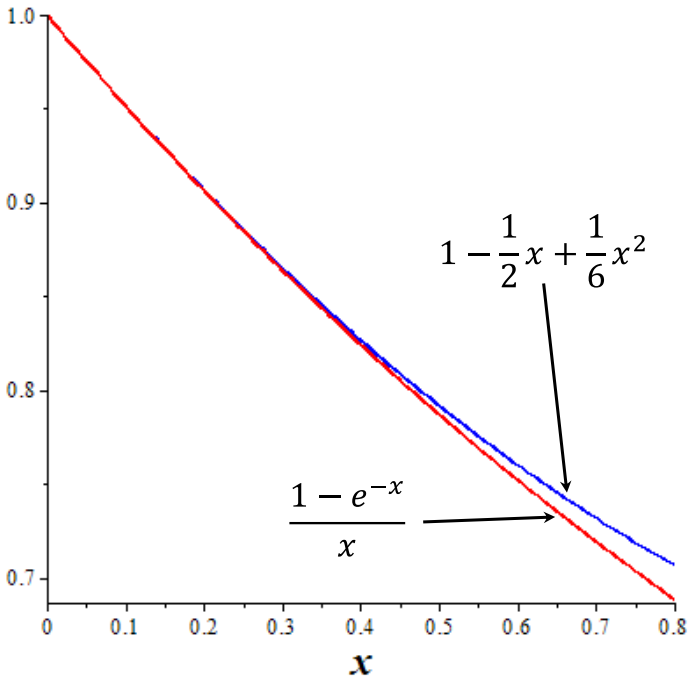

Figure B-1 $\frac{1-e^{-x}}{x}$ compared with its Taylor expansion

Therefore, we rewrite Equations (B-215) to (B-232) as

$$q_{C_{11}i}^{11}(t^n)$$

$$= e^{-\frac{\Delta t^n}{a_T \tau_{C_{11}i}}} q_{C_{11}i}^{11}(t^{n-1})$$

$$+ a_F C_{11_i} \Delta\epsilon_{11}{}^n \begin{cases} \left(\dfrac{1 - e^{-\frac{\Delta t^n}{a_T \tau_{C_{11}i}}}}{\dfrac{\Delta t^n}{a_T \tau_{C_{11}i}}} \right) & \dfrac{\Delta t^n}{a_T \tau_{C_{11}i}} \geq 0.2 \\ \left(1 - \dfrac{1}{2} \dfrac{\Delta t^n}{a_T \tau_{C_{11}i}} + \dfrac{1}{6} \left(\dfrac{\Delta t^n}{a_T \tau_{C_{11}i}} \right)^2 \right) & \dfrac{\Delta t^n}{a_T \tau_{C_{11}i}} \leq 0.2 \end{cases}, \quad \textbf{(B-246)}$$

$$i = 1,2 \ldots, N_{C_{11}}$$

$$q_{C_{12}i}^{22}(t^n)$$

$$= e^{-\frac{\Delta t^n}{a_T \tau_{C_{12}i}}} q_{C_{12}i}^{22}(t^{n-1})$$

$$+ a_F C_{12_i} \Delta\epsilon_{22}{}^n \begin{cases} \left(\dfrac{1 - e^{-\frac{\Delta t^n}{a_T \tau_{C_{12}i}}}}{\dfrac{\Delta t^n}{a_T \tau_{C_{12}i}}} \right) & \dfrac{\Delta t^n}{a_T \tau_{C_{12}i}} \geq 0.2 \\ \left(1 - \dfrac{1}{2} \dfrac{\Delta t^n}{a_T \tau_{C_{12}i}} + \dfrac{1}{6} \left(\dfrac{\Delta t^n}{a_T \tau_{C_{12}i}} \right)^2 \right) & \dfrac{\Delta t^n}{a_T \tau_{C_{12}i}} \leq 0.2 \end{cases}, \quad \textbf{(B-247)}$$

$$i = 1,2 \ldots, N_{C_{12}}$$

$$q_{C_{13}i}^{33}(t^n)$$

$$= e^{-\frac{\Delta t^n}{a_T \tau_{C_{13}i}}} q_{C_{13}i}^{33}(t^{n-1})$$

$$+ a_F C_{13_i} \Delta \epsilon_{33}{}^n \begin{cases} \left(\dfrac{1 - e^{-\frac{\Delta t^n}{a_T \tau_{C_{13}i}}}}{\dfrac{\Delta t^n}{a_T \tau_{C_{13}i}}} \right) & \dfrac{\Delta t^n}{a_T \tau_{C_{13}i}} \geq 0.2 \\ \left(1 - \dfrac{1}{2} \dfrac{\Delta t^n}{a_T \tau_{C_{13}i}} + \dfrac{1}{6} \left(\dfrac{\Delta t^n}{a_T \tau_{C_{13}i}} \right)^2 \right) & \dfrac{\Delta t^n}{a_T \tau_{C_{13}i}} \leq 0.2 \end{cases}, \quad \textbf{(B-248)}$$

$$i = 1,2 \ldots, N_{C_{13}}$$

$$q_{C_{12}i}^{11}(t^n)$$

$$= e^{-\frac{\Delta t^n}{a_T \tau_{C_{12}i}}} q_{C_{12}i}^{11}(t^{n-1})$$

$$+ a_F C_{12_i} \Delta \epsilon_{11}{}^n \begin{cases} \left(\dfrac{1 - e^{-\frac{\Delta t^n}{a_T \tau_{C_{12}i}}}}{\dfrac{\Delta t^n}{a_T \tau_{C_{12}i}}} \right) & \dfrac{\Delta t^n}{a_T \tau_{C_{12}i}} \geq 0.2 \\ \left(1 - \dfrac{1}{2} \dfrac{\Delta t^n}{a_T \tau_{C_{12}i}} + \dfrac{1}{6} \left(\dfrac{\Delta t^n}{a_T \tau_{C_{12}i}} \right)^2 \right) & \dfrac{\Delta t^n}{a_T \tau_{C_{12}i}} \leq 0.2 \end{cases}, \quad \textbf{(B-249)}$$

$$i = 1,2 \ldots, N_{C_{12}}$$

$$q_{C_{22}i}^{22}(t^n)$$

$$= e^{-\frac{\Delta t^n}{a_T \tau_{C_{22}i}}} q_{C_{22}i}^{22}(t^{n-1})$$

$$+ a_F C_{22_i} \Delta\epsilon_{22}{}^n \begin{cases} \left(\dfrac{1 - e^{-\frac{\Delta t^n}{a_T \tau_{C_{22}i}}}}{\dfrac{\Delta t^n}{a_T \tau_{C_{22}i}}} \right) & \dfrac{\Delta t^n}{a_T \tau_{C_{22}i}} \geq 0.2 \\ \left(1 - \dfrac{1}{2} \dfrac{\Delta t^n}{a_T \tau_{C_{22}i}} + \dfrac{1}{6} \left(\dfrac{\Delta t^n}{a_T \tau_{C_{22}i}} \right)^2 \right) & \dfrac{\Delta t^n}{a_T \tau_{C_{22}i}} \leq 0.2 \end{cases}, \quad \textbf{(B-250)}$$

$$i = 1,2 \ldots, N_{C_{22}}$$

$$q_{C_{23}i}^{33}(t^n)$$

$$= e^{-\frac{\Delta t^n}{a_T \tau_{C_{23}i}}} q_{C_{23}i}^{33}(t^{n-1})$$

$$+ a_F C_{23_i} \Delta\epsilon_{33}{}^n \begin{cases} \left(\dfrac{1 - e^{-\frac{\Delta t^n}{a_T \tau_{C_{23}i}}}}{\dfrac{\Delta t^n}{a_T \tau_{C_{23}i}}} \right) & \dfrac{\Delta t^n}{a_T \tau_{C_{23}i}} \geq 0.2 \\ \left(1 - \dfrac{1}{2} \dfrac{\Delta t^n}{a_T \tau_{C_{23}i}} + \dfrac{1}{6} \left(\dfrac{\Delta t^n}{a_T \tau_{C_{23}i}} \right)^2 \right) & \dfrac{\Delta t^n}{a_T \tau_{C_{23}i}} \leq 0.2 \end{cases}, \quad \textbf{(B-251)}$$

$$i = 1,2 \ldots, N_{C_{23}}$$

$$q_{C_{13}i}^{11}(t^n)$$

$$= e^{-\frac{\Delta t^n}{a_T \tau_{C_{13}i}}} q_{C_{13}i}^{11}(t^{n-1})$$

$$+ a_F C_{13_i} \Delta \epsilon_{11}{}^n \begin{cases} \left(\dfrac{1 - e^{-\frac{\Delta t^n}{a_T \tau_{C_{13}i}}}}{\dfrac{\Delta t^n}{a_T \tau_{C_{13}i}}} \right) & \dfrac{\Delta t^n}{a_T \tau_{C_{13}i}} \geq 0.2 \\ \left(1 - \dfrac{1}{2} \dfrac{\Delta t^n}{a_T \tau_{C_{13}i}} + \dfrac{1}{6} \left(\dfrac{\Delta t^n}{a_T \tau_{C_{13}i}} \right)^2 \right) & \dfrac{\Delta t^n}{a_T \tau_{C_{13}i}} \leq 0.2 \end{cases}, \quad \textbf{(B-252)}$$

$$i = 1,2 \ldots, N_{C_{13}}$$

$$q_{C_{23}i}^{22}(t^n)$$

$$= e^{-\frac{\Delta t^n}{a_T \tau_{C_{23}i}}} q_{C_{23}i}^{22}(t^{n-1})$$

$$+ a_F C_{23_i} \Delta \epsilon_{22}{}^n \begin{cases} \left(\dfrac{1 - e^{-\frac{\Delta t^n}{a_T \tau_{C_{23}i}}}}{\dfrac{\Delta t^n}{a_T \tau_{C_{23}i}}} \right) & \dfrac{\Delta t^n}{a_T \tau_{C_{23}i}} \geq 0.2 \\ \left(1 - \dfrac{1}{2} \dfrac{\Delta t^n}{a_T \tau_{C_{23}i}} + \dfrac{1}{6} \left(\dfrac{\Delta t^n}{a_T \tau_{C_{23}i}} \right)^2 \right) & \dfrac{\Delta t^n}{a_T \tau_{C_{23}i}} \leq 0.2 \end{cases}, \quad \textbf{(B-253)}$$

$$i = 1,2 \ldots, N_{C_{23}}$$

$$q_{C_{33}i}^{33}(t^n)$$

$$= e^{-\frac{\Delta t^n}{a_T \tau_{C_{33}i}}} q_{C_{33}i}^{33}(t^{n-1})$$

$$+ a_F C_{33_i} \Delta \epsilon_{33}{}^n \begin{cases} \left(\dfrac{1 - e^{-\frac{\Delta t^n}{a_T \tau_{C_{33}i}}}}{\dfrac{\Delta t^n}{a_T \tau_{C_{33}i}}} \right) & \dfrac{\Delta t^n}{a_T \tau_{C_{33}i}} \geq 0.2 \\ \left(1 - \dfrac{1}{2} \dfrac{\Delta t^n}{a_T \tau_{C_{33}i}} + \dfrac{1}{6} \left(\dfrac{\Delta t^n}{a_T \tau_{C_{33}i}} \right)^2 \right) & \dfrac{\Delta t^n}{a_T \tau_{C_{33}i}} \leq 0.2 \end{cases}, \quad \textbf{(B-254)}$$

$$i = 1,2 \ldots, N_{C_{33}}$$

$$q_{C_{44}i}^{23}(t^n)$$

$$= e^{-\frac{\Delta t^n}{a_T \tau_{C_{44}i}}} q_{C_{44}i}^{23}(t^{n-1})$$

$$+ a_F C_{44_i} \Delta \gamma_{23}{}^n \begin{cases} \left(\dfrac{1 - e^{-\frac{\Delta t^n}{a_T \tau_{C_{44}i}}}}{\dfrac{\Delta t^n}{a_T \tau_{C_{44}i}}} \right) & \dfrac{\Delta t^n}{a_T \tau_{C_{44}i}} \geq 0.2 \\ \left(1 - \dfrac{1}{2} \dfrac{\Delta t^n}{a_T \tau_{C_{44}i}} + \dfrac{1}{6} \left(\dfrac{\Delta t^n}{a_T \tau_{C_{44}i}} \right)^2 \right) & \dfrac{\Delta t^n}{a_T \tau_{C_{44}i}} \leq 0.2 \end{cases}, \quad \textbf{(B-255)}$$

$$i = 1,2 \ldots, N_{C_{44}}$$

$$q_{C_{55}i}^{13}(t^n)$$

$$= e^{-\frac{\Delta t^n}{a_T \tau_{C_{55}i}}} q_{C_{55}i}^{13}(t^{n-1})$$

$$+ a_F C_{55_i} \Delta\gamma_{13}{}^n \begin{cases} \left(\dfrac{1 - e^{-\frac{\Delta t^n}{a_T \tau_{C_{55}i}}}}{\dfrac{\Delta t^n}{a_T \tau_{C_{55}i}}} \right) & \dfrac{\Delta t^n}{a_T \tau_{C_{55}i}} \geq 0.2 \\ \left(1 - \dfrac{1}{2} \dfrac{\Delta t^n}{a_T \tau_{C_{55}i}} + \dfrac{1}{6} \left(\dfrac{\Delta t^n}{a_T \tau_{C_{55}i}} \right)^2 \right) & \dfrac{\Delta t^n}{a_T \tau_{C_{55}i}} \leq 0.2 \end{cases}, \quad \textbf{(B-256)}$$

$$i = 1,2 \dots, N_{C_{55}}$$

$$q_{C_{66}i}^{12}(t^n)$$

$$= e^{-\frac{\Delta t^n}{a_T \tau_{C_{66}i}}} q_{C_{66}i}^{12}(t^{n-1})$$

$$+ a_F C_{66_i} \Delta\gamma_{12}{}^n \begin{cases} \left(\dfrac{1 - e^{-\frac{\Delta t^n}{a_T \tau_{C_{66}i}}}}{\dfrac{\Delta t^n}{a_T \tau_{C_{66}i}}} \right) & \dfrac{\Delta t^n}{a_T \tau_{C_{66}i}} \geq 0.2 \\ \left(1 - \dfrac{1}{2} \dfrac{\Delta t^n}{a_T \tau_{C_{66}i}} + \dfrac{1}{6} \left(\dfrac{\Delta t^n}{a_T \tau_{C_{66}i}} \right)^2 \right) & \dfrac{\Delta t^n}{a_T \tau_{C_{66}i}} \leq 0.2 \end{cases}, \quad \textbf{(B-257)}$$

$$i = 1,2 \dots, N_{C_{66}}$$

$$q_{\beta_{1_i}}(t^n) = e^{-\frac{\Delta t^n}{a_T \tau_{\beta_1 i}}} q_{\beta_{1_i}}(t^{n-1})$$

$$+ \beta_{1_i} \Delta T^n \begin{cases} \left(\dfrac{1 - e^{-\frac{\Delta t^n}{a_T \tau_{\beta_1 i}}}}{\dfrac{\Delta t^n}{a_T \tau_{\beta_1 i}}} \right) & \dfrac{\Delta t^n}{a_T \tau_{\beta_1 i}} \geq 0.2 \\ \left(1 - \dfrac{1}{2} \dfrac{\Delta t^n}{a_T \tau_{\beta_1 i}} + \dfrac{1}{6} \left(\dfrac{\Delta t^n}{a_T \tau_{\beta_1 i}} \right)^2 \right) & \dfrac{\Delta t^n}{a_T \tau_{\beta_1 i}} \leq 0.2 \end{cases}, \quad \textbf{(B-258)}$$

$$i = 1,2 \dots, N_{\beta_1}$$

$$q_{\beta_{2_i}}(t^n) = e^{-\frac{\Delta t^n}{a_T \tau_{\beta_2 i}}} q_{\beta_{2_i}}(t^{n-1})$$

$$+ \beta_{2_i} \Delta T^n \begin{cases} \left(\dfrac{1 - e^{-\frac{\Delta t^n}{a_T \tau_{\beta_2 i}}}}{\dfrac{\Delta t^n}{a_T \tau_{\beta_2 i}}} \right) & \dfrac{\Delta t^n}{a_T \tau_{\beta_2 i}} \geq 0.2 \\ \left(1 - \dfrac{1}{2} \dfrac{\Delta t^n}{a_T \tau_{\beta_2 i}} + \dfrac{1}{6} \left(\dfrac{\Delta t^n}{a_T \tau_{\beta_2 i}} \right)^2 \right) & \dfrac{\Delta t^n}{a_T \tau_{\beta_2 i}} \leq 0.2 \end{cases} , \quad \textbf{(B-259)}$$

$$i = 1,2 \ldots, N_{\beta_2}$$

$$q_{\beta_{3_i}}(t^n) = e^{-\frac{\Delta t^n}{a_T \tau_{\beta_3 i}}} q_{\beta_{3_i}}(t^{n-1})$$

$$+ \beta_{3_i} \Delta T^n \begin{cases} \left(\dfrac{1 - e^{-\frac{\Delta t^n}{a_T \tau_{\beta_3 i}}}}{\dfrac{\Delta t^n}{a_T \tau_{\beta_3 i}}} \right) & \dfrac{\Delta t^n}{a_T \tau_{\beta_3 i}} \geq 0.2 \\ \left(1 - \dfrac{1}{2} \dfrac{\Delta t^n}{a_T \tau_{\beta_3 i}} + \dfrac{1}{6} \left(\dfrac{\Delta t^n}{a_T \tau_{\beta_3 i}} \right)^2 \right) & \dfrac{\Delta t^n}{a_T \tau_{\beta_3 i}} \leq 0.2 \end{cases} \quad \textbf{(B-260)}$$

$$, \qquad i = 1,2 \ldots, N_{\beta_3}$$

$$q_{\gamma_{1_i}}(t^n) = e^{-\frac{\Delta t^n}{a_T \tau_{\gamma_1 i}}} q_{\gamma_{1_i}}(t^{n-1})$$

$$+ \gamma_{1_i} \Delta T^n \begin{cases} \left(\dfrac{1 - e^{-\frac{\Delta t^n}{a_T \tau_{\gamma_1 i}}}}{\dfrac{\Delta t^n}{a_T \tau_{\gamma_1 i}}} \right) & \dfrac{\Delta t^n}{a_T \tau_{\gamma_1 i}} \geq 0.2 \\ \left(1 - \dfrac{1}{2} \dfrac{\Delta t^n}{a_T \tau_{\gamma_1 i}} + \dfrac{1}{6} \left(\dfrac{\Delta t^n}{a_T \tau_{\gamma_1 i}} \right)^2 \right) & \dfrac{\Delta t^n}{a_T \tau_{\gamma_1 i}} \leq 0.2 \end{cases} , \quad \textbf{(B-261)}$$

$$i = 1,2 \ldots, N_{\gamma_1}$$

$$q_{\gamma_{2_i}}(t^n) = e^{-\frac{\Delta t^n}{a_T \tau_{\gamma_2 i}}} q_{\gamma_{2_i}}(t^{n-1})$$

$$+ \gamma_{2_i} \Delta T^n \begin{cases} \left(\dfrac{1 - e^{-\frac{\Delta t^n}{a_T \tau_{\gamma_2 i}}}}{\dfrac{\Delta t^n}{a_T \tau_{\gamma_2 i}}} \right) & \dfrac{\Delta t^n}{a_T \tau_{\gamma_2 i}} \geq 0.2 \\ \left(1 - \dfrac{1}{2} \dfrac{\Delta t^n}{a_T \tau_{\gamma_2 i}} + \dfrac{1}{6} \left(\dfrac{\Delta t^n}{a_T \tau_{\gamma_2 i}} \right)^2 \right) & \dfrac{\Delta t^n}{a_T \tau_{\gamma_2 i}} \leq 0.2 \end{cases}, \qquad \textbf{(B-262)}$$

$$i = 1,2 \ldots, N_{\gamma_2}$$

$$q_{\gamma_{3_i}}(t^n) = e^{-\frac{\Delta t^n}{a_T \tau_{\gamma_3 i}}} q_{\gamma_{3_i}}(t^{n-1})$$

$$+ \gamma_{3_i} \Delta T^n \begin{cases} \left(\dfrac{1 - e^{-\frac{\Delta t^n}{a_T \tau_{\gamma_3 i}}}}{\dfrac{\Delta t^n}{a_T \tau_{\gamma_3 i}}} \right) & \dfrac{\Delta t^n}{a_T \tau_{\gamma_3 i}} \geq 0.2 \\ \left(1 - \dfrac{1}{2} \dfrac{\Delta t^n}{a_T \tau_{\gamma_3 i}} + \dfrac{1}{6} \left(\dfrac{\Delta t^n}{a_T \tau_{\gamma_3 i}} \right)^2 \right) & \dfrac{\Delta t^n}{a_T \tau_{\gamma_3 i}} \leq 0.2 \end{cases}, \qquad \textbf{(B-263)}$$

$$i = 1,2 \ldots, N_{\gamma_3}$$

Using Equations (B-234) to (B-239), we evaluate each stress component at each time step in terms of its value at the previous time step, state variables and other parameters. In turn, the values of state variables are obtained using Equations (B-246) to (B-263).